Année 2021

N° d'ordre: ----------

Présentée pour l'obtention du titre de

DOCTEUR EN CHIMIE DES MATERIAUX

Présentée et soutenue par

Muhammad Hassan Rafe

Advanced electrospun composite for wastewater treatment

Sous la direction de: Pr. Christelle DELAITE, Dr. Bénédicte LEBEAU et Pr. Dominique C. ADOLPHE

Soutenue le **26 Novembre 2021** devant la commission d'examen

Dr. Ahsan NAZIR	National Textile University Faisalabad-Pakistan	Rapporteur
Pr. Jean-Luc BLIN	Université de Lorraine Nancy-France	Rapporteur
Pr. Leonard ATANASE	Université Apollonia Iasi-Roumanie	Examinateur
Dr. Elham MOHSENZADE	Junia HEI-Hautes Etudes d'Ingenieur-France	Examinatrice

Dedication

This modest effort is dedicated to my parents, beloved wife Uzma Hassan and my lovely kids Abdullah Hassan and Huda Hassan.

Acknowledgment

First and foremost, I would like to thank God for his countless blessing and mercy to complete this project. I have experienced your guidance day by day through all the challenges. I will keep on trusting you for whole of my life.

Secondly, I would like to acknowledge and give my warmest thanks to my supervisor Pr. Christelle DELAITE and co-supervisor Dr. Bénédicte LEBEAU for their continuous guidance, advice, encouragement and facilitations during all the stages of this study. Their presentation, inspiration and motivation have always played a key role in the success of any venture in this work. I am also obliged to my second co-supervisor Pr. Dominique ADOLPHE for being so kind and helpful throughout these years. It was his invaluable feedback and guidance that enlightened my way.

A debt of gratitude is also owed to Dr. Nabyl KHENOUSSI for his intellectual contribution in this progressive topic and paved my beginnings with his technical advice. I would like to extend my heartfelt appreciation to Dr. Magali BONNE and Dr. Elham MOHSENZADEH for their unconditional support.

Last but not least, I am truly thankful to all my colleagues from LPIM, IS2M and LPMT for their kindness and cooperation.

Abbreviations

MB : Methylene blue

NR : Neutral red

CR : Congo red

OMS : Ordered mesoporous silica

SBA-15 : Santa Barbara Amorphous-15

PAN : Polyacrylonitrile

DMSO : Dimethyl sulphoxide

pH : Hydrogen potential

UV : Ultra-violet

OMCs : Ordered mesoporous carbon

RB : Rhodamine blue

TiO_2 : Titanium dioxide

CV : Crystal violet

MCM-22: Mobil Crystalline Material-22

SF : Safranin

RR2 : Reactive red 2

BCB : Brilliant cresyl blue

MMWCNT : Magnetic multi wall carbon nanotubes

MCNFs : Mesoporous carbon nanofibers

Fe-NTA : Ferric-nitrilotriacetate

CNCs : Cellulose nanocrystals

DMP : Dimethyl phthalate

JGB : Janus green B

ZnO : Zinc oxide

ECNFs : Electrospun carbon nanofibers

O-ECNF : Oxidized electrospun carbon nanofibers

DA : Deacetylate

PDA : Polydopamide

DMF : Dimethyl formamide

Sn : Tin

Wt% : Weight percentage

w.r.t : With respect to

SEM : Scanning electron microscope

TGA : Thermogravimetric analysis

SD : Standard deviation

CV : Coefficient of variation

Nm : Nanometers

Table of Contents

Introduction……..11

1.Bibliography survey……17

1.1 Objectives……....18

1.2 Wastewater……..18

1.2.1 Dyes……....18

1.2.2 Adsorption technique……..19

1.2.3 SBA-15 as dye adsorbent……22

1.2.4 Nanofibers as dye adsorbents……..25

1.3 Electrospinning process……27

1.3.1 Types of electrospinning……..28

1.3.2 Jet formation in electrospinning process……..31

1.4 Electrospinning parameters……...33

1.4.1 Polymer solution parameters……33

1.4.1.1 Polymer solution concentration or viscosity……..33

1.4.1.2 Solution Conductivity……36

1.4.1.3 Polymer solution temperature……37

1.4.1.4 Nature and solvent properties……38

1.4.2 Process parameters……..38

1.4.2.1 Solution flow rate……..39

1.4.2.2 Applied voltage……39

1.4.2.3 Collecting distance……42

1.4.3 Environment parameters……43

1.4.3.1 Relative humidity……..44

1.4.3.2 Temperature……...45

1.4.4 Conclusion……...45

1.5 Polymer used for electrospinning……46

1.5.1 Polyacrylonitrile (PAN)……...46

1.5.2 PAN electrospinning……47

1.5.3 PAN nanofibers stabilization and carbonization……48

1.6 Electrospun composite nanofibers……52
1.6.1 Synthesis and properties of SBA-15 ordered mesoporous silica…….54
1.6.2 Morphology of electrospun PAN/SBA-15 composite nanofibers……...57
1.6.3 Dispersion of silica nanoparticles in solvent……...58
1.6.3.1 Mechanical dispersion……...59
1.6.3.2 Chemical dispersion of fillers……61
1.7 Conclusion……61
2. Materials and Methods……63
Introduction……..64
2.1 Materials……...64
2.1.1 Polymer and solvent……....64
2.1.2 Mesoporous silica type SBA-15……..65
2.1.3 Dispersing agents……68
2.1.4 Dyes……68
2.2 Methods……..70
2.2.1 Preparation of formulations for electrospinning……..70
2.2.1.1 PAN/SBA-15/DMSO formulations preparation……....71
2.2.1.2 Viscosity measurement……..72
2.2.1.3 Electrospinning conditions……73
2.2.1.4 Electrospinning of PAN solutions ……75
2.2.1.5 Electrospinning of PAN+SBA-15 formulations……75
2.2.2 Suspensions preparation of dispersing agent ……..76
2.2.3 Zetasizer and Mastersizer……77
2.3 Characterizations of materials……78
2.3.1 Scanning electron microscopy (SEM) of SBA-15, PAN+SBA-15 electrospun composite nanofibers……..78
2.3.2 X-rays diffraction (XRD) analysis of SBA-15…….79
2.3.3 Thermogravimetric analysis (TGA) of electrospun composite nanofibers……..79
2.3.4 Micromeritics specific surface analysis and porosity (BET & BJH)……80

2.3.5 Tensile strength testing of pristine PAN and PAN/SBA-15 nanofibers……...82
2.3.6 Fourier-Transform Infrared spectroscopy 2.4 UV/Visible Spectrophotometer……83
2.3.7 Energy dispersive X-ray spectroscopy analysis (EDX)……84
2.4 UV/Visible Spectrophotometer……...84
2.5 Dyes solution preparation……...85
2.6 Mechanism of dyes adsorption……...86
2.6.1 Langmuir isotherm model……87
2.6.2 Freundlich isotherm model……...88
2.7 Adsorption kinetics……88
2.8 Desorption study of MB, NR and CR with recyclability of adsorbents……90
2.9 Conclusion……..90
3. Preparation of nanocomposites by electrospinning……..91
Introduction……..92
3.1 Synthesis of SBA-15……...92
3.1.1 Accessibility of pores and BET surface area of SBA-15……..92
3.1.2 Structural analysis of SBA-15……..93
3.1.3 Particle size measurement and optimization of dispersing agent (Zetasizer)……..94
3.1.4 Particle size measurement and optimization of dispersing agent (Mastersizer)……..96
3.1.5 Impact of stirring and dispersing agent on deagglomeration of SBA-15 in DMSO…..97
3.1.6 Conclusion……99
3.2 Electrospinning of PAN nanofibers……...99
3.2.1 Rheological analysis of pure PAN solution……99
3.2.2 Preparation of PAN nanofibers……....101
3.2.3 Structural analysis of pristine PAN nanofibers……105
3.2.4 Optimization parameters of PAN/DMSO solution……..107
3.2.5 Conclusion……...108
3.3 Electrospinning of PAN/SBA-15 composite nanofibers……...108

3.3.1 Rheological analysis of PAN/SBA-15 formulations……...109

3.3.2 Preparation of nanofibers composites……..111

3.3.3 Effect of incorporation of SBA-15 on morphology of composite nanofibers…….117

3.3.4 Effect of incorporation of BYK W-9010 on morphology of composite nanofibers……119

3.3.5 Optimization of the parameters for electrospinning……122

3.3.6 Analysis of thermal stability by incorporation of SBA-15 and BYK W-9010 in PAN nanofibers…….123

3.3.7 Conclusion……125

3.4 Characterization of electrospun nanofibers……...126

3.4.1 Accessibility of pores and BET surface area of PAN/SBA-15 composite nanofibers….126

3.4.2 Chemical analysis of PAN, PAN nanofibers and PAN/SBA-15 nanofibers……127

3.4.3 Elemental composition analysis of PAN and PAN/SBA-15 nanofibers……..129

3.4.4 Analysis of mechanical strength of pristine PAN and PAN/SBA-15 composite nanofibers……130

3.5 Conclusion…….131

4. Efficiency of PAN nanofibers loaded with SBA-15 for dye removal from aqueous solution
Introduction……132

4.1 Types of dyes…….133

4.1.1 Cationic dyes…….133

4.1.2 Anionic dyes…….....133

4.2 Methylene Blue adsorption……134

4.2.1 Effect of dye concentration……...134

4.2.2 Adsorption kinetics.……..136

4.2.3 Adsorption isotherm...……...139

4.2.4 Effect of pH……...141

4.2.5 Effect of temperature……142

4.2.6 Batch screening test of Methylene Blue (MB)…….145
4.2.7 Conclusion……146
4.3 Neutral Red adsorption……..147
4.3.1 Effect of dye concentration…….147
4.3.2 Adsorption kinetics…..……149
4.3.3 Adsorption isotherm..…….152
4.3.4 Effect of pH……154
4.3.5 Effect of temperature……..156
4.3.6 Batch screening test of Neutral red (NR)……...158
4.3.7 Conclusion……..159
4.4 Congo Red adsorption……...160
4.4.1 Effect of dye concentration…….160
4.4.2 Adsorption kinetics.……162
4.4.3 Adsorption isotherm...…….165
4.4.4 Effect of pH…….167
4.4.5 Effect of temperature……..169
4.4.6 Batch screening test……171
4.4.7 Conclusion……..172
4.5 Adsorption mechanism of Methylene Blue, Neutral Red and Congo Red dyes……172
4.6 Desorption study of MB, NR and CR recyclability of adsorbent……...…….……..176
4.7 FTIR analysis of adsorbates/adsorbents…….180
4.8 Conclusion…….186
Conclusion and future prospects……..187
References……...190

General Introduction

Introduction

Organic dyes are the essential part of many industrial effluents. Approximately 100,000 different dyes are produced annually and their quantity is more than 7×10^5 tons worldwide [1]. The discharge of these dyes in environment is problematic for toxicological and esthetical reasons as these dyes impede light penetration, damage the quality of receiving streams and also are toxic to food chain organism. Methylene blue (MB), Neutral red (NR) and Congo red (CR) are (selected dyes) used for coloring the products like textile, leather, paper, plastic, etc. These dyes can cause eye burn and if swallowed they can cause irritation to the gastrointestinal tract with the symptoms of nausea, vomiting and diarrhea [2, 3]. For the treatment or purification of dye waste water, there are many physical, chemical and biological methods developed such as ozonation, filtration, adsorption, electrochemical process, annihilation, ion exchange, precipitation, flocculation, etc [3, 4, 5]. Among all these techniques, physical adsorption is the most effective one and it is suitable for industries due to ease, ability to treat dilute solutions, insensitivity to toxic substances and effectiveness. So physical adsorption is the most commonly used process for non-biodegradable dye removal and yields high quality water from wastewater due to its cheep, simple and effective treatment [4, 5, 6].

Nanotechnology is having a large impact in manufactured products in most major industry sectors including electronics, cosmetics, automotive, filtration and healthcare sectors. According to a survey, over 1300 nanotechnology related products are currently in market [7]. For the purpose of filtration many types of nanoparticles, organic materials, agriculture waste, biomass and nanofibers are used. But among all these materials nanofibers mat or membranes have gained a wide and great attention due to presence of considerable microporosity and specific area, small pore size and good mechanical characteristics [7, 8, 9]. Nanofibers are the objects who have slender and elongated structure and whose diameter is less than 100 nm [10]. There are a lot of nanofibers fabrication techniques including jet blowing, melt blowing, co-extrusion, interfacial polymerization, electrospinning and many others. Among these techniques, electrospinning has been widely used due to most feasible and simple technique to produce nanofibers of customized properties, at much higher rate of different polymers and polymers/filler blends. Electrospinning process also has the potential to produce nanofibers on bulk scale [11, 12].

The principle of electrospinning is utilization of electrostatic force to draw polymer solutions into nanofibers as they are released by ejection electrode. In the process of electrospinning a polymer is dissolved in a suitable solvent and a fundamental setup consists of nozzle or syringe containing prepared polymer solution, a high voltage source and a collector is used. When a sufficient voltage is applied between the two electrodes, the polymer solution gets charged and a coulombic repulsion force is developed within it. When the coulombic repulsion force overcomes the surface tension of the solution, it results in production of jet, this jet moves towards the collector under the electrostatic forces and the solvent evaporates simultaneously and finally the jet solidifies into a nonwoven of sub-micron fibers.

The process of electrospinning can be classified according to the fibers generator. Basically, there are two types of electrospinning process; one is with needle electrospinning and other nozzle or needleless electrospinning. Many different setups have been developed, that employ fibers generators other than needle (such as cylinder, wire, disc etc) and the process is called needleless electrospinning, which is mostly used for production of large quantities [13].

Properties of nanofibers depend on many electrospinning parameters. These parameters include solution concentration and solution viscosity, diameter of nozzle or needle, solution flow rate, distance between the electrodes, applied voltage and some ambient parameters like temperature and humidity. These mentioned parameters affect strongly the properties of electrospun nanowebs and also the applications of these nanowebs. There are several applications for which electrospun nanofibers have been studied and it is found that their results are quite promising. There are some important applications areas that are mentioned here, which include energy generation and its storage, environmental protection, electronics, drug delivery, sensors, tissue engineering, filtration and carriers for catalyst and enzymes [13, 14].

The electrospun materials have shown very good potential in many fields and attracted the researchers to carry out extensive studies on electrospun materials. Nevertheless, use of electrospun materials in different fields can be explored better if the process is well understood. These nanofibers are used in many applications like tissue engineering, filtration, wound dressing, fuel cell, capacitors, sensors, etc. For the above mentioned applications, some specific tailoring properties are required regarding hydrophobicity, conductivity, chemical composition, porosity, selectivity etc. From decades, properties tailoring have been used to fulfill specific applications requirements of traditional bulk polymeric products. Among many other properties

tailoring techniques, physical blending of polymer/filler has been widely used due to an easy and effective way of introduction of functional moieties into the bulk polymers.

The main objective of this work is the formation of composite nanofibers by incorporation of mesoporous inorganic fillers in it, so that specific surface area of composite nanofibers may be increased for better adsorption of cationic dyes. Ordered mesoporous silica (OMS) alone is very good for dye removal, but they are obtained as micro-particles, which are difficult to handle and remove from solution. Therefore ordered mesoporous silica (OMS) have been added in PAN polymer sub-micron fibers as filler. Mat composite PAN+SBA-15 nanofibers are expected to have good adsorption properties for dye due to SBA-15 and easy to handle for dye adsorption process and recovery procedure. These mat composites also have other great advantages, which includes large surface area, uniform pore size and controlled surface chemistry. SBA-15 is very high ordered material which possesses a regular 2 dimensional hexagonal array of channels and has a pore diameter of the order 4-14nm range [15]. But during the addition of silica particles in the sub-micron fibers, they form aggregates and as a result of these aggregates the diameter of nanofibers become non uniform therefore it is necessary to remove these aggregates. To remove the aggregates of silica particles in composite nanofibers, a dispersing agent whose name will be introduced in this work. Technically, our goal is the manufacturing of polyacrylonitrile (PAN) nanofibers by the process of electrospinning and the usage of nanofibers as carrier of inorganic fillers that caused porosity, roughness and increased in surface area of composite nanofibers for better adsorption of cationic dyes. The polymeric material selected for this study is polyacrylonitrile (PAN) due to these reasons; (1) this polymer is suitable for the process of electrospinning [16], (2) As its nature is polar, so it is easily soluble in polar solvent like dimethyl sulphoxide (DMSO) that resulted in high dielectric constant favoring the production of non-bedded nanofibers.

The mechanism and limitations of adsorption process will be analyzed by isotherm and kinetic models. These models are valuable plots which explain the mobility of adsorbate from solution to the adsorbent surface at specific pH and temperature. Two different isotherm models like Langmuir and Freundlich has been used for some basic approaches. In Kinetic approach the adsorption equilibrium is defined on a dynamic equilibrium basis while considering the adsorption and desorption rates.

Finally the thesis is divided in four main chapters:

Chapter 1 covers the introduction of cationic and anionic dyes; their toxic effects in water and on human beings and methods of adsorption. Later it describes the process of electrospinning and its parameters influencing the process outcome. These electrospinning parameters are classified into three different categories: parameters of polymer solution, parameters of electrospinning process and ambient parameters. It also presents the functionalization of electrospun composite nanofibers with ordered mesoporous silica. It also describes the synthesis of these fillers, their properties, dispersion methods of fillers aggregates and the influence of incorporating these fillers on the properties of electrospun composite nanofibers.

Chapter 2 explains the materials and methods used in the synthesis of SBA-15, the mechanical and chemical treatment for dispersing silica particles in DMSO and the preparation of PAN/SBA-15 solution in DMSO and conditions used for electrospinning. The characterization techniques of composite nanofibers include the observation of surface morphology of nanofibers, structure, thermal stability, mechanical properties, FTIR analysis and textural properties and dye adsorption characterization are also presented.

In chapter 3, the results and discussions are given which explains the following items: the optimization of electrospinning parameters, the optimization of the mechanical treatment conditions for filler dispersing in DMSO, the effect of incorporation of silica nanoparticles on the morphology of composite nanofibers, on the thermal and textural properties of their composite nanofibers with PAN matrix and the accessibility of SBA-15 mesoporous within the composite nanofibers. The characterization results like structural analysis of fillers and fibers, chemical, mechanical and elemental composition analysis of fibers.

Chapter 4 explains the adsorption behavior of Methylene blue, Neutral red and Congo red dyes on different samples of fillers, composite nanofibers and pristine PAN nanofibers. It also explains the impact of pH, dye concentration, contact time and temperature on adsorption of all presented dyes. The results of adsorption kinetics, adsorption isotherm will also be presented here. And at the end to reduce the process cost, recyclability of the fibers by desorption of all dyes will be discussed.

The last part explains the conclusion of the whole work and future prospects. The suggested outlook covers the uses of the coaxial electrospinning, further characterization of mechanical properties of the composite nanofibers; the impact of adding mesoporous of SBA-15 within the composite nanofibers was studied to increase its surface area for better adsorption of cationic dyes. The adsorption properties of all the dyes by the impact of different parameters and at the end, their desorption and recyclability were explained.

Chapter I

Bibliography survey

Chapter I
Bibliography survey

1.1 Objectives

The main objective of this study is development of PAN/SBA-15 composite nanofibers for cationic/anionic dyes removal by adsorption process. To check the deagglomeration of silica particles, a dispersing agent named BYK W-9010 was successfully introduced in composite nanofibers. Another objective is to increase the accessible percentage of mesopores from 50% to produce more active sites for adsorption of dye molecules. To study the adsorption mechanism of cationic, anionic and neutral dyes, isotherms and kinetics models were used. And at the end desorption and mechanism of recyclability has to be checked to reduce the initial cost of product.

1.2 Wastewater

There are many types of wastes that make ground water pollutant which include municipal wastes, petrochemical and chemical wastes, pulp, paper, tannery and textile wastes etc. Among them, dyes used in textile, paper, leather and pulp industry are the important pollutant in water that will be discussed in this thesis [17, 18].

1.2.1 Dyes

Dyes are the chemical substances that are extensively used to color many products in textile, leather, paper industries and many other materials via absorption, dispersion and synthetic reaction process [4]. In recent days there are more than 100,000 different commercial dyes available in the market with a rough estimated production of 1 million tons per year. It is also estimated that 10-15% of these used dyes are entered in the environment through wastes [19]. These waste waters which are polluted with harmful and toxic dyes are not strongly accepted worldwide under the respective environmental regulations. The dye molecules stay in the aquatic environment due to their less biodegradability, stability to light and temperature and stability to photolysis and oxidizing agents [20, 21].

The major dye classes which are mostly used are basic, acidic, reactive and direct dyes. After studying the detailed literature, it is revealed that cationic and anionic dyes are the mostly used and studied for adsorption. These dyes are mostly used for cotton, silk, acrylic, wool, nylon, plastic leather and paper dyeing industries [22, 23]. It has been observed that, this water soluble dyes can penetrate inside the living body easily and these are more harmful and produces

carcinogenic effects even their concentrations are very small. Dyes like methylene blue, Neutral red and Congo red etc. are very toxic and it is reported that they cause allergic, dermatitis, skin irritation, cancer, mutation, eye burns, permanent injury to human and animals, increase in heart rate, shock, Heinz body formation, cyanosis, jaundice, etc and many others diseases [24, 25]. Even a small quantity of dye can cause breathing difficulty after inhaling while by its oral ingestion it may cause irritation, vomiting, nausea, mental confusion, profuse sweating and methemoglobinemia [26].

For the removal of dyes present in wastewater of textile or other industries, many technological efforts have been made which include chemical, biological and physical techniques. The chemical oxidation technique is applied mostly for the color wastewater treatment which includes chlorine, hydrogen peroxide, Fenton's reagent, potassium permanganate or ozone and UV assisted activation [19, 27]. For the removal of dyes, generally the used chemical techniques are much expensive and the accumulation of concentrated sludge after the decolonization of wastewater results in disposal problem. Although, the chemical techniques are one of the robust ways for removal of dyes. Beside it, another pollution problem may arise which is due to excessive chemical use. There are some biological methods that are also used for dyes wastewater treatment which involve the application of bacteria, fungi and algae. This technique offers some advantages like low operation cost and final product is completely mineralized. However for biological treatment a large land area is required and less flexibility in design and operation are the constraints in this type of treatment [19, 28, 29, 30, 31]. The use of photocatalytic technique for degradation of dyes which has some advantages over the other techniques like no generation of sludge and has the potential of usage of solar light. But there are some drawbacks which are associated with this technique like light penetration, catalyst fouling and separation from treated water [19]. All these techniques are comparatively expensive and can't be afforded easily. Therefore, it is recommended to look for cheaper treatment of dye polluted water and adsorption by composite sub-micron fibers can be a good and cheap option for dye removal.

1.2.2 Adsorption Technique

Adsorption technique or adsorption process is referred as adhesion of ions, molecules or atoms from the dissolved liquid, solid or gas onto some specific surface. In the adsorption process, on

the surface of adsorbent, a film of adsorbate is created. Adsorption and absorption are clearly two different techniques. In the process of absorption the adsorbate is completely dissolved by absorbent (a solid or liquid). The absorption process involves the entire volume of material whereas adsorption is a surface driven process. The adsorption process involves the surface energy and may occur as a result of ion-exchange, precipitation, chemisorptions (covalent bonding) or physisorption (hydrogen bonding or weak Van der Wall's forces) [4].

For the treatment of wastewater from textile, adsorption has gained much attraction because adsorbents are available in bulk quantity, these are cheaper in price, have high pollutant uptake capabilities, robustness and economical desorption cycles and have excellent resistance towards degenerative action of targeted components [32, 33]. There are some materials described below which show adsorption of cationic dyes.

Researchers worked on activated carbon prepared by oil palm shell for the removal of cationic dyes from aqueous solutions through batch and column process. Batch experiments were carried out to study the adsorption kinetics and isotherm at 30^{o}C and solution pH was kept at 6.5 with different concentrations. The results showed that the prepared activated carbon was a promising adsorbent for the removal of dye from aqueous solutions over a wide range of concentrations [37]. A work was focused on synthesis of ordered mesoporous carbon (OMCs) with varying pore size by using SBA-15 as hard template [34]. The resultant synthesized ordered mesoporous carbon (OMC) has abundance of mesopores and narrow mesopore size. Methylene blue dye was used to investigate the adsorption behavior on OMCs. The kinetic studies of adsorption show the following adsorption rate of methylene blue onto OMC, OMC-70>OMC-40>OMC-100 [34]. The adsorption behavior of two cationic dyes methylene blue (MB) and rhodamine blue (RB) was studied onto mesoporous silica-titania materials. The effect of dye structure, particles size of adsorbent, presence of TiO_2, and temperature on adsorption was investigated. Adsorption increased due to the presence of TiO_2 and decreased by increasing temperature. MB is more adsorbed as compared to RB due to its smaller size. Increase in surface area of adsorbent increases the adsorption rate [35]. Another research work describes the adsorption behavior of different basic dyes which include methylene blue, crystal violet (CV) and rhodamine B by the employment of zeolite MCM-22. The adsorption behavior of all three dyes follows the following order MB>CV~RB. Adsorption of basic dyes on Zeolite MCM-22 was endothermic [36].

A research work of anionic dye Congo red adsorbed on electrospun mat of polyacrylonitrile nanofibers was realized by Jadoo *et al*. The results revealed that by increasing pH decreases the adsorption capacity and the optimized parameters for CR adsorption were included; adsorbent dosage 0.006g, initial concentration 25 mg/L and contact time 150 min respectively [8]. Adsorption behavior of two cationic dyes, Neutral red (NR), Safranin O (SF) and two anionic dyes, Reactive red 2 (RR2), Congo red (CR) on SBA-15 was studied and it was observed that adsorption capacity of SBA-15 was greater for NR and SF as compared to RR2 and CR due to strong electrostatic attraction between negative charge surface of SBA-15 and positive charge of dyes and as well as hydrogen bonding. Adsorption kinetics follows the pseudo second order model and adsorption equilibrium data can be well described with Langmuir model [3].

Highly ordered mesoporous silica materials were synthesized under strong acidic conditions using non-ionic surfactant as structure directing agent. For adsorption performance it was observed that SBA-15 exhibited an excellent adsorption capability for the cationic dyes but in the case of anionic and neutral dyes it showed almost no adsorption which is due to the negative charge on the surface of silica nanoparticles. Thermodynamic calculations of the process indicated that cationic dyes adsorption on SBA-15 was exothermic and spontaneous [5]. SBA-15 nanoparticles were also synthesized for adsorption of methylene blue (MB) from synthetic wastewater in batch system. The process showed that removal percentage of methylene blue increases with increase in contact time, pH and SBA-15 dosage and decreases with increase in initial dye concentration [38].

For the better adsorption of cationic dyes like methylene blue (MB), neutral red (NR) and brilliant cresyl blue (BCB), magnetic multi wall carbon nanotubes (MMWCNT) were prepared. The results suggested that adsorption capacity of all three dyes on the surface of MMWCNT increases with temperature and also with pH due to electrostatic attraction between the negatively charged MMWCNT adsorbent surface and cationic dyes having positive charge [39]. Electrospun PAN nanofibers were synthesized by using electrospinning technique from polyacrylonitrile and then were carbonized and oxidized via H_2SO_4/HNO_3 mixture to obtain carbon nanofibers. It was concluded that oxidized electrospun carbon nanofibers can be used as effective adsorbent for cationic dye removal from aqueous solutions. Thermodynamic study showed that adsorption of methylene blue on oxidized electrospun carbon nanofibers was spontaneous and endothermic reaction [40]. In this study mesoporous carbon nanofibers

(MCNFs) were synthesized by using ferric-nitrilotriacetate (Fe-NTA) nanofibers as precursors via annealing technique under enclosed conditions of high temperature of 500 ^{o}C. The results indicated that the samples of mesoporous carbon nanofibers obtained have long fibrous morphology, high surface area and mesoporous structure. Due to this high surface area, the obtained MCNFs exhibited excellent performance for adsorption of methylene blue and methyl orange dyes from aqueous solution [41].

Cellulose nanocrystals (CNCs) were prepared from cellulose fibers via sulfuric acid hydrolysis which adsorbed the cationic organic dye. Cellulose nanocrystals were further activated by TEMPO (2, 2, 6, 6-tetramethylpiperidine 1-oxyl, >98 %) oxidation which further enhanced the adsorption potential of these materials. Pristine and modified cellulosic nanocrystals can be used to adsorb various types of dyes due to their excellent surface area and charge density [42]. Batch or column modes are used to carry out the adsorption studies of dyes. To find the adsorption capacity of an adsorbent, batch studies are the best under optimized conditions of pH, contact time, particles size and adsorbent dose. Batch mode is performed in a fixed shaker where temperature is controlled. Whereas fixed bed columns are considered as better practical approach for assessment the adsorbent capacity under the optimized conditions of flow rate, particles size and bed height [43]. The adsorption capacity of the adsorbent is the adsorbate quantity which is predicted and calculated by using adsorption kinetics and adsorption isotherms. Adsorption kinetics and isotherms can also be used to analyze the mechanism and limitations of the adsorption processes. Adsorption isotherms are valuable plotting that describes the mobility mechanism of the adsorbate from the dye solution and its retention to the surface of adsorbent at fixed conditions of pH and temperature. Typically, these are mathematically correlations which enable displaying the design of operation of adsorptions systems [19, 44].

1.2.3 SBA-15 as dye adsorbent

As we have discussed earlier the removal of dye from colored effluents is very important and essential and various physical, chemical and biological dye removal techniques from aqueous solutions are developed. Among all, physical adsorption has been shown to be an effective method for the dye removal from process or waste effluents due to simplicity of design and operation, the possibility to operate at very low concentration and insensitivity of toxic substances [45]. There are many available adsorbents which have been tested for removing of

dye, like activated carbon, fly ash, clays, alumina, silica gel and zeolite. Among all, zeolites were treated with special attention in the adsorption process. However, zeolites have inherent small pore sizes which are the key limitations for their applications because large molecules are not able to access these pores [46]. Therefore, to overcome these limitations, silica nanoparticles are developed. Silica nanoparticles have many advantages over other adsorbent as these materials have large surface area, uniform pores size and their surface chemistry is controlled. These materials are highly ordered and possess a regular two dimensional hexagonal array of channels. This pore material typically has a pore diameter of the order of 4-14 nm [15]. The adsorption of the most common dyes on silica particles at different pH range are mentioned in table I.1.

Table I.1: Adsorption of common dyes on silica particles at different pH range [3, 5]

Name of dye	**Charged behavior**	**pH range**
Methylene blue (MB)	Cationic	5.51-5.71
Neutral red (NR)	Cationic	7
Congo red (CR)	Anionic	4
Dimethyl Phthalate (DMP)	Neutral	6.04-6.64

The chemical structures of most common dyes are shown below in figure I.1 [3, 5].

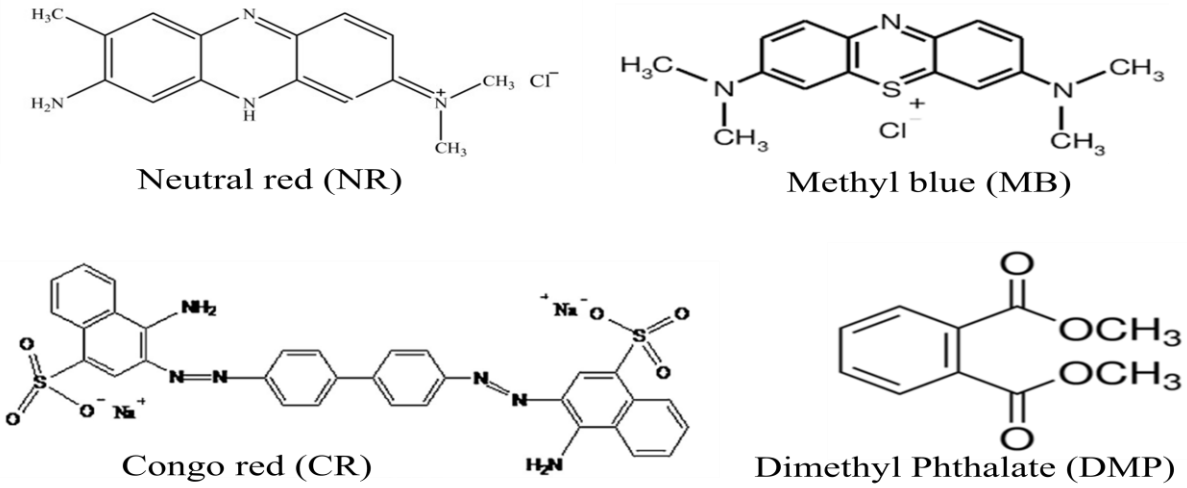


Figure I.1: Chemical structures of different dyes [3, 5]

The SBA-15 has a negative surface when pH value is above 2 and negative charge value decreases with the increasing pH value at constant temperature. Therefore, the negative charged surface of SBA-15 favors the adsorption of cationic species by electrostatic attraction, so

methylene blue and neutral red show better adsorption than CR and DMP [3, 5]. The influence on the adsorption capacities can be explained by charge nature of dyes and zeta potential of SBA-15. The removal of cationic and anionic dyes strongly depends on the pH value of the dye solution. The maximum removal efficiency for the cationic dyes is observed at pH close to 2 whereas for anionic dyes it is observed close to pH 9. The dye removal efficiency for cationic dyes increased in acidic pH range and in the basic pH range it remained almost constant whereas in the case of anionic dyes desorption increased in basic medium and remained almost constant in acidic medium. The reason of low adsorption of cationic dyes below pH 7 and anionic dyes above pH 7 is due to the presence of H^+/OH^- ions which are competing with cationic/anionic dyes for adsorption sites which results in decreasing the adsorption of dyes [4, 38, 40, 42]. If the molecular size of dyes is taken into consideration with charge density, then it is observed that adsorption capacities of Methylene Blue are higher than another cationic dye named Janus Green B (JGB) over SBA-15 at equilibrium. The reason of MB higher adsorption than JGB is due to its small molecular size and strong cationic behavior, as it has less aromatic rings, so it enters easily the inner pores of SBA-15, whereas JGB molecule occupies more active sites on SBA-15, which may hinder other adsorbate from contact with active sites. The adsorption of MB and JGB on SBA-15 is an exothermic reaction, which means a rising temperature led to a lower adsorption capacity of SBA-15 at equilibrium [5, 34].The adsorption mechanism of dyes depends upon the adsorbent structure, on the dye molecular structure, charge and on the temperature. As discussed earlier, MB is a smaller molecule and has higher charge density with a size of 7.03Å as compared to JGB, which has 14.3Å size, so MB has high adsorption as compared to JGB, because when large molecule is adsorbed, the dispersion forces energy is greater than the electrostatic interaction energy. So for the better adsorption of JGB big molecules, large pore diameter of adsorbent is required. The high adsorption enthalpy values result of number of chemical interactions involving, electrostatic attraction, covalent bonding, non polar interaction, water bridging and hydrogen bonding between the dye adsorbent structure, due to positive charged dye molecule and negative charge Si-O adsorbent. Additionally, there are possibilities of formation of H-bonding and water bridges between the dye molecule and adsorbent, increasing the total interaction energy leading to high enthalpy of adsorption [35].

Now, impact of contact time on adsorption of cationic dye on silica nanoparticles is discussed and it is observed that the removal efficiency is rapid in the initial minutes of contact time and

after a few minutes, the removal of dye is not significant. This is because a large number of surface sites are available on silica nanoparticles for adsorption in the beginning and strong attractive forces occurred between the sorbent and dye. By increasing the contact time, the remaining vacant surface sites are difficult for occupation due to occurrence of saturation and as a result, removal efficiency remained almost constant [35, 36, 37, 38]. Some studies explain that dyes removal efficiency was increased by increasing sorbent amount. This dye removal efficiency is attributed to the availability of greater surface area with pore volume and large number of adsorption sites. Whereas, on the other hand, by increasing the concentration of dyes the removal efficiency is decreased. This is because the ratio of dyes to the dosage of the adsorbent increases and numbers of active sites for adsorption decreases and as a result, the removal efficiency also decreases [37, 38].

1.2.4 Nanofibers as dye adsorbent

Many types of nano particles like SBA-15, titania-silica, TiO_2, ZnO etc. have been used for the adsorption/ filtration of water [4, 5, 35, 47]. But these nanoparticles are likely to enter the aquatic environment in all stages of nanomaterials life cycle (production, processing, usage, recycling and disposal). These particles can persist in natural bodies and are not fully removed by drinking water treatment systems, thereby posing a potential public health concern [7, 47]. Therefore, the development of new barrier material is needed to reduce the potential risks related to human and environmental exposure to nanomaterials [7]. In nanofiber webs, due to presence of porosity, small pore size and comparative good specific surface area, have been shown to improve the efficiency of conventional materials used for the filtration and separation of particulate materials [6, 7, 8, 48, 49, 50]. A study was investigated which explains the adsorption of Congo red dye on electrospun nanofibers mat of Polyacrylonitrile. The results confirm that the increase in pH will decrease the adsorption capacity due to the electrostatic repulsion between anionic dye and PAN nanofibers. The study also explains the increase in adsorption quantity by increasing contact time and adsorbent weight but by increasing the dye concentration, initially adsorbed quantity increases but after sometimes it decreases due to completion of active sites [8]. Figure I.2 shows the adsorption behavior of CR dye on pristine PAN nanofibers at different concentration, time interval and pH.

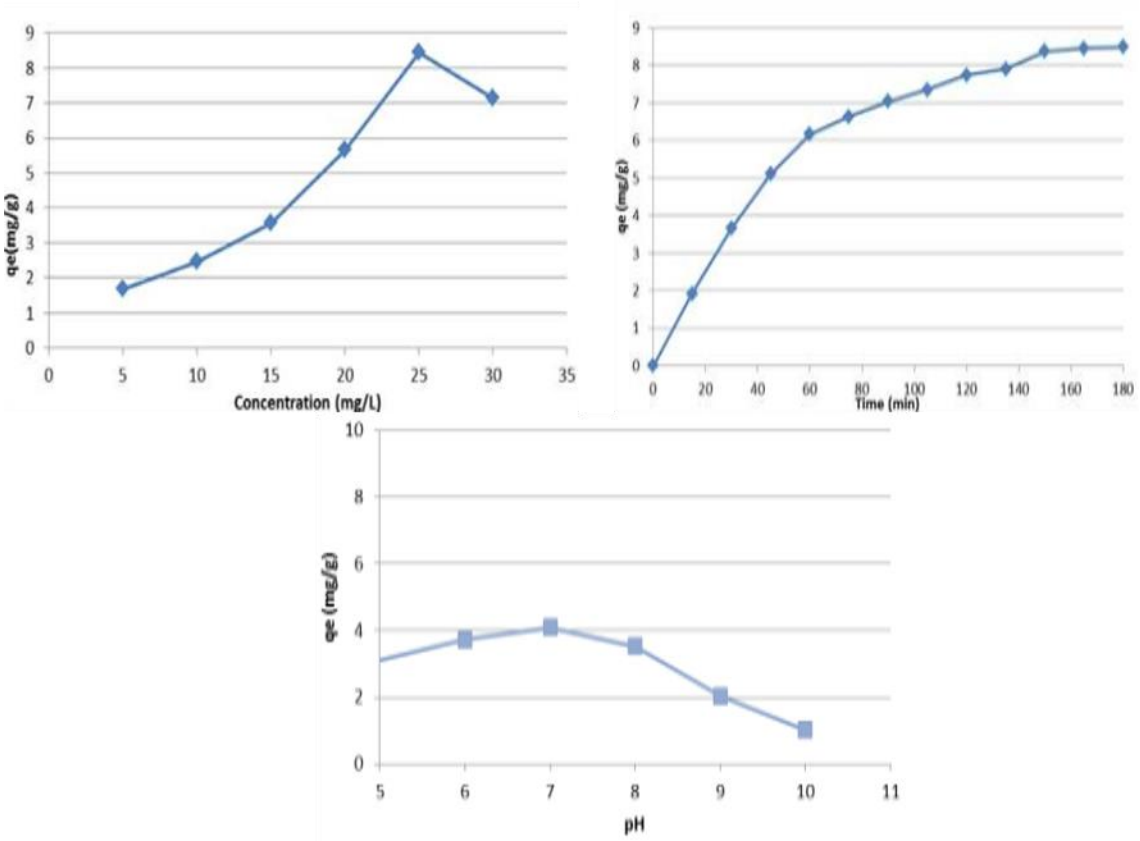


Figure I.2: Impact of Concentration, time and pH on adsorption of CR by PAN nanofibers [8]

Another study explained the adsorption capacity of Congo red and neutral red on pristine PAN nanofibers and composite nanofibers of Calixarene (8)-15/PAN, Easter-Calixarene (8)-15/PAN and amide-Calixarene (8)-15/PAN. The results showed that static adsorption behavior was studied for both dyes which increased the adsorbed quantity in composite nanofibers as compared to pristine PAN nanofibers [50]. Another work explained the fabrication of electrospun carbon nanofibers (ECNFs) from polyacrylonitrile using an electrospinning technique followed by carbonization and oxidation via treatment with a H_2SO_4/HNO_3 mixture that produced functional group on the surface of electrospun carbon nanofibers (ECNF). The adsorption capacity of methylene blue dye on the surface of oxidized electrospun carbon nanofibers (O-ECNFs) is high compared to electrospun carbon nanofibers (ECNFs) due to presence of functional groups on the surface of (O-ECNFs) and methylene blue [6]. One research work explained the adsorption of Congo red (CR) on the surface of polyacrylonitrile functionalized with Fe_3O_4 nanoparticles. The functionalized nanofibers appeared appreciable efficiency to CR adsorption from aqueous solution. The dye adsorbed amount was increased by

increasing initial dye concentration and contact time till the equilibrium reached. Adsorption of dye capacity decreased by increasing temperature refers to the exothermic nature of adsorption system. The desorption of CR dye was found better in basic medium due to repulsive electrostatic forces [51]. A research work explained the production of flexible keratin-based nanofibers membranes by electrospinning process which had nanofibers mean diameter of 220 nm and specific surface area of 13.59 m^2/g. The nanofibers membrane was used for the adsorption of Methylene blue dye, whose adsorption capacity was increased by increasing the initial dye concentration and pH while it decreased with increasing adsorbent dosage. MB adsorption decreased by increasing the temperature of the system and the negative value of enthalpy change indicated the adsorption process was exothermic in nature. The research also showed that very large surface area and high porosity confer high adsorption performance to the keratin nanofibrous membranes [52]. In this research work a new type of deacetylate cellulose acetate (DA) and polydopamine (PDA) composite nanofibers membrane was fabricated by electrospinning and surface modification that was applied as adsorbent for removing cationic methylene blue dye from aqueous solution. The DA@PDA composite nanofibers had an excellent adsorption capacity of MB as compared to DA nanofibers, which is almost 8.6 times higher than the pristine DA nanofibers because of electrostatic and π- π stacking interactions between MB and DA@PDA due to the existence of large amount of phenolic O-H and aromatic rings in the PDA coating layer [53].

1.3 Electrospinning process

Nanofibers can be produced by many different methods like jet blowing, melt blowing, co-extrusion, interfacial polymerization, template synthesis, CO_2 laser supersonic drawing, electrospinning and many others [11]. Among these techniques electrospinning is mostly used due to its simplicity, repeatability and ability to be scaled up, i.e from laboratory scale to the industrial mass production [12]. The process of electrospinning works out by drawing out the jet from the polymer/solvent solution through a needle or spinneret. The polymer jet after leaving the spinneret or needle moves towards the collector. At the needle tip, meniscus has a stress due to its surface tension that allows it to oppose the drawing force exerted by electric force. To draw out the polymer jet, the electric force must be greater than the capillary stress. So the

electrospinning parameters can be estimated by balancing the capillary stress and electrical stress [54].

During the process of electrospinning, normally six forces are exerted, i-e, (i) for transmission of jet from nanofibers generator to collector, electrostatic force is exerted, (ii) gravitational force on jet, (iii) coulombic forces that stretches the jet during the flight towards collector, (iv) surface tension of the solution that opposes the stretching of jet, (v) viscoelastic forces that inhibit the stretching of jet, (vi) friction that is produced due to jet and air particles, opposes the movement of jet flight [55]. So it is clear from above discussion that jet experiences a number of forces and due to these forces jet follows a 3 dimensional path with bending, spiraling and winding paths and it is termed as "bending instability". Due to these involved forces, these bending instabilities reduce the diameter of the jet and as a result fiber is changed into nanofibers range. The drawing rate of final fiber may be up to 1,000,000 nanometers per second and resulted in reduced diameter by increasing the macromolecules orientation [56]. The diameter of electrospun submicron fibers is ranging from 50 nanometers to 10 micrometers (at 10-30 kV and 10-15 cm) [54].

1.3.1 Types of electrospinning

Electrospinning can be classified according to the types of liquid used, the direction of nanofibers production or types of fibers generator. Different types of liquids are used for production of nanofibers in the process of electrospinning; such solutions may be polymer in the solvents, emulsions and melts. So the electrospinning process can be divided according to the type of liquids used for this process. According to this qualification, technique can be categorized as solution electrospinning, melt electrospinning and emulsion electrospinning [57]. Electrospinning process can be divided according to the fiber generation direction; it may be in horizontal direction or may be in vertical direction. In most electrospinning setups the fiber generator is placed at the top and nanofibers collector is put at the bottom and the setup is named as downward electrospinning. Whereas in some cases nanofibers generator is kept on the bottom and collector is hanged upward, so this type of system is termed as upward electrospinning. Whereas in the third system of electrospinning, nanofibers generator and collector is kept parallel to each other and this system is called horizontal electrospinning [58, 59]. Figure I.3 represents all mentioned electrospinning setups.

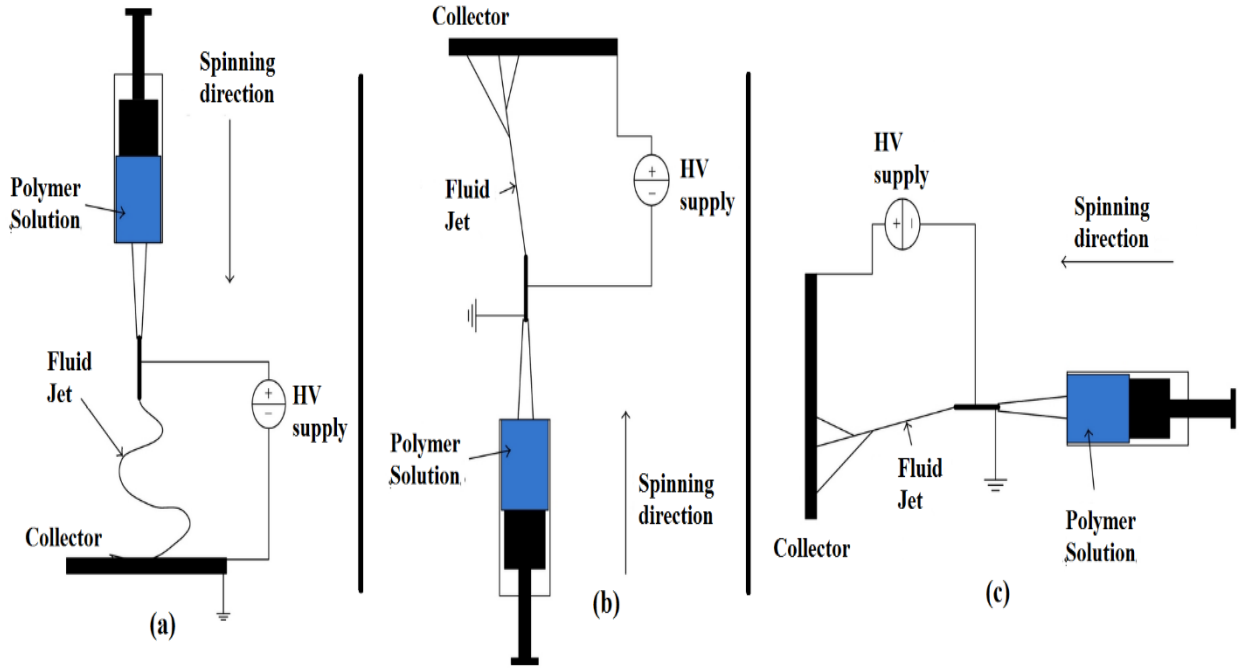


Figure I.3: Types of electrospinning setups showing spinning directions (a) downward, (b) upward, (c) horizontal electrospinning [12]

The upper mentioned classification of electrospinning was based on the direction of nanofibers formation. Now here, another electrospinning classification is discussed, which is based on types of fibers generators and can be divided into needle electrospinning and needleless electrospinning. As the name indicates, in needle electrospinning, a needle is used for the formation of nanofibers and this setup is basic electrospinning setup and mostly used for lab scale and research purpose due to easy handling and less production, whereas for large scale production multiple needle electrospinning machines have also been developed [12]. In needle electrospinning, modification options are limited as compared to needleless electrospinning. Many researchers have developed different needleless electrospinning setups. Needleless electrospinning setups can be subdivided according to rotating nanofibers generators and stationary nanofibers generators [13, 60, 61, 62]. Different needleless electrospinning setups are shown in figure I.4.

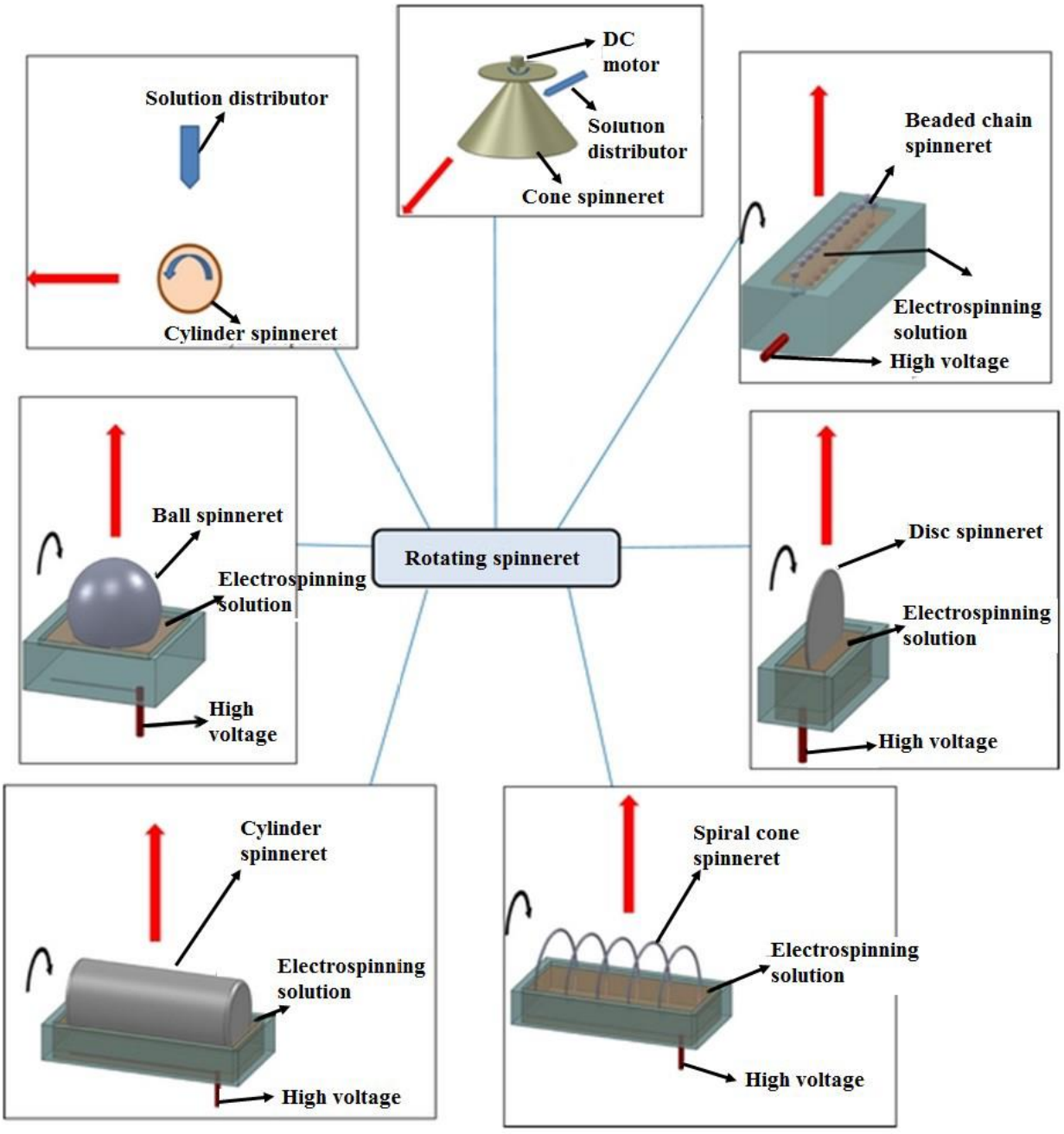


Figure I.4: Rotating fibers generators for electrospinning [12]

In the rotating fiber generator systems of needleless electrospinning, the polymer solution is distributed over the rotating surface which produces nanofibers as the electrostatic force is applied to them. Each of these systems produces nanofibers of its own properties, which includes high production on bulk scale. One of such system includes Nanospider ^{TM} by Elmarco, which provides two sets of wires electrodes: one wire is at bottom that is coated with polymer solution and moves in the solution nozzle having a small orifice and on applying high voltage it produces

nanofibers and the other wire is on the top of cabin, which works as collector of nanofibers. This setup is mostly used for commercial setup and is selected to perform a part of current study. The diagram of wire electrospinning is shown below in figure I.5.

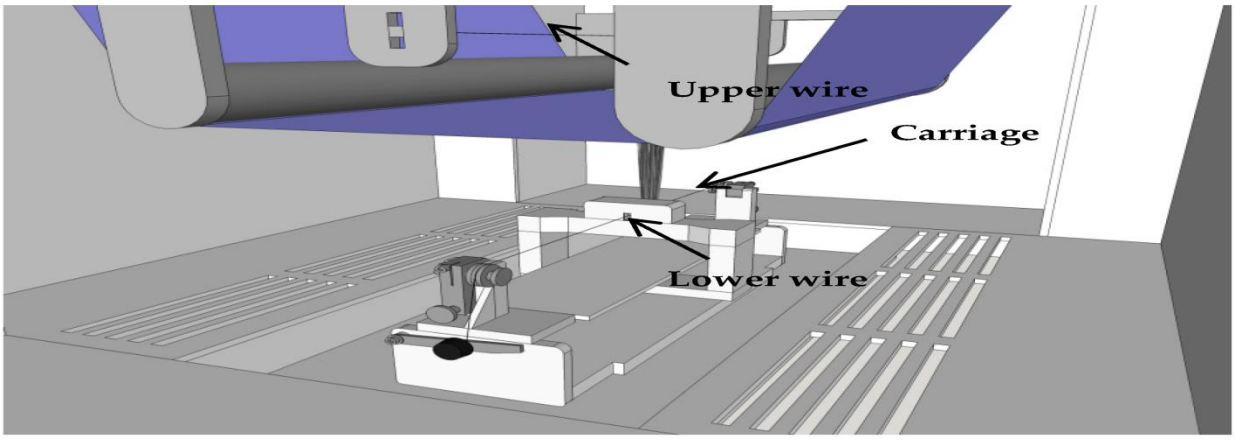


Figure I.5: Wire electrospinning technique

1.3.2 Jet formation in electrospinning process

The electrospinning principle is relies the stretching of electrically charged polymer droplet into very fine filament in the range of nano scale under the action of external applied force. In this process the polymer solution is fed through a capillary (may be nozzle or wire) into a high electric field tension area. This high electric field tension is controlled according to the characteristics required in the product. As the solution droplet is formed on the top of wire and electric field is applied due to which charges accumulate on the droplet surface and leading the droplet into a conical shape known as Taylor cone. When the applied voltage reaches some critical values, the electrostatic forces due to accumulated charges overcome the surface tension of the solution, leading to pull a thin jet out, which in turn travels towards the collector electrode under the action of the external field. During this process the solvent evaporates and the jet is solidified into the form of nanofibers which are deposited on the collector electrode with randomly oriented nanofilaments, depending upon the collector geometry or on the process conditions [63, 64]. Typical electro-hydrodynamic path of jet is composed of main three parts; Taylor cone segment, straight segment and bending instabilities portion as shown in figure I.6 [65, 66].

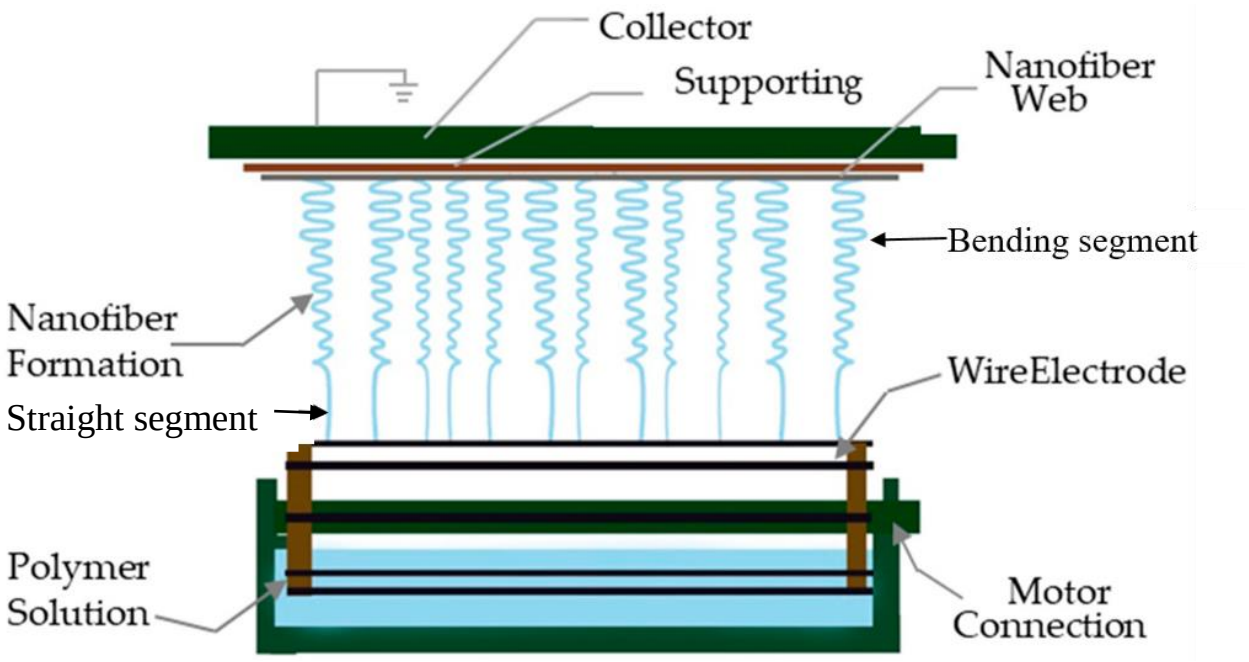


Figure I.6: Typical electrospinning jet formations [66]

When the Coulomb repulsive forces acting on the charges carried on polymer jet overcome the viscoelastic forces and surface tension of the polymer solution, the Taylor cone portion of the jet is pulled outward of the polymer droplet on the surface of charged wire. The next segment is essentially straight and its length is measured along its own axis. The straightness of jet depends on the intensity of driving Coulomb forces. Due to influence of repulsive forces, the bending perturbations start over and grow which results in the jet to coil or to wipe [67]. As the jet has to cover more distance to reach the collector, the turns of coils of jet become larger in diameter due to repulsive forces action on the charges carried on adjacent segments. This process of jet formation is taken place in very small time interval, may be in tens of milliseconds. In the process of jet formation, excess charges carried along the jet, force the jet segments to elongate and results in reduction in diameter as long as they supply enough repulsive forces. It is thought that jet coiling is the cause of jet thinning because if the jet does not undergo coil path, a much higher kinetic energy would be required to elongate the jet [66]. On the other hand, jet travelling implies evaporation of solvent. So, with the jet being dried and as the repulsive forces are not enough strong to elongate the higher bending instability coils, stresses of viscosity become dominant and solidification of the jet starts.

1.4 Electrospinning parameters

Various parameters affect on the production of bead free nanofibers by electrospinning process. In general these parameters are divided in three main categories; polymer solution parameters, process parameters and ambient parameters. The solution parameters include, solution concentration, viscosity, surface tension of solution, types of solvent used to dissolve the polymer, solution dielectric constant, temperature of polymer solution. Process parameters include, voltage applied, distance between the electrodes, called as collecting distance and solution feed rate. At the end, ambient parameters include temperature and humidity of the surrounding environment. So, in this section effect of upper mentioned parameters on the nanofibers morphology and diameter is discussed.

1.4.1 Polymer solution parameters

For the synthesis of nanofibers, obtained by electrospinning, polymer solution is considered to be the strongest factor that affects the morphology and diameter of nanofibers. Suitable polymer solution preparation for nanofibers depends upon different factors that solution should fulfill like, polymer molar mass, surface tension of solution, concentration or viscosity of solution, solution conductivity, solution temperature, solubility of polymer in solvent (solubility parameters of both polymer and solvent) and solvent properties etc. In next paragraphs the extensive approach about the influence of different solution parameters are introduced.

1.4.1.1 Polymer solution concentration or viscosity

The most important factor in electrospinning is solution concentration that affects the morphology and other properties of electrospun nanofibers and the major impact is on nanofibers diameter, in terms of magnitude and quality of fibers [57, 68]. The solution viscosity is controlled by polymer concentration, although there are some other factors playing a major role in solution viscosity, including polymer average molar mass, solvent and environmental conditions [69, 70]. There is a relation between solution concentration and viscosity by a power relationship i-e $\eta = C^{\delta}$ [71]; where η is the symbol of solution viscosity, C is polymer concentration and δ denotes scaling constant. This equation explains that solution viscosity increases exponentially with increasing concentration [71]. However an optimum polymer concentration and viscosity in a solvent has to be defined for every kind of polymer with

different sets of parameters being employed. At concentration lower than that critical value, the jet of polymer is dispersed in the form of droplets or in easy words is electro sprayed due to the less entanglements of polymer molecular chains. Whereas the beads are formed on fibers due to chains relaxation in the presence of solvent because of its higher quantity, resulting in longer evaporation time and as a result of surface tension the chance of molecules relaxation is increased [72]. Generally, in diluted solutions which have concentration< 4 wt/v%, only beads and beads assemblies are obtained due to lack of viscosity. The numbers of chain entanglements are lower than the critical value. Due to this lack of viscosity, the solvent surface tension becomes dominant and as a result the polymer jet is broken up into individual droplets and in this case there is electrospraying rather than electrospinning [73]. This phenomenon is shown in figure I.7a. By increasing the polymer concentration from (4.5-6.5% wt/v) the beads were turned into beads on string morphology. By increasing the viscosity, influence of higher viscoelastic forces arose, the electrostatic forces acting on charges carried on jet are not able to break the jet into individual sections anymore and the jet is still composed of a successive droplets or beads. However these forces can elongate the links between these droplets into thin longitudinal sections and can reduce the size of the droplets as shown in figure (I.7b-d). Further increase in solution concentration (> 7% wt/v) yields higher number of chains entanglement which are high enough to resist the jet breakage and also to withstand further elongation along with solvent evaporation. Thus bead free nanofibers are obtained which is shown in figure (I.7e-f).

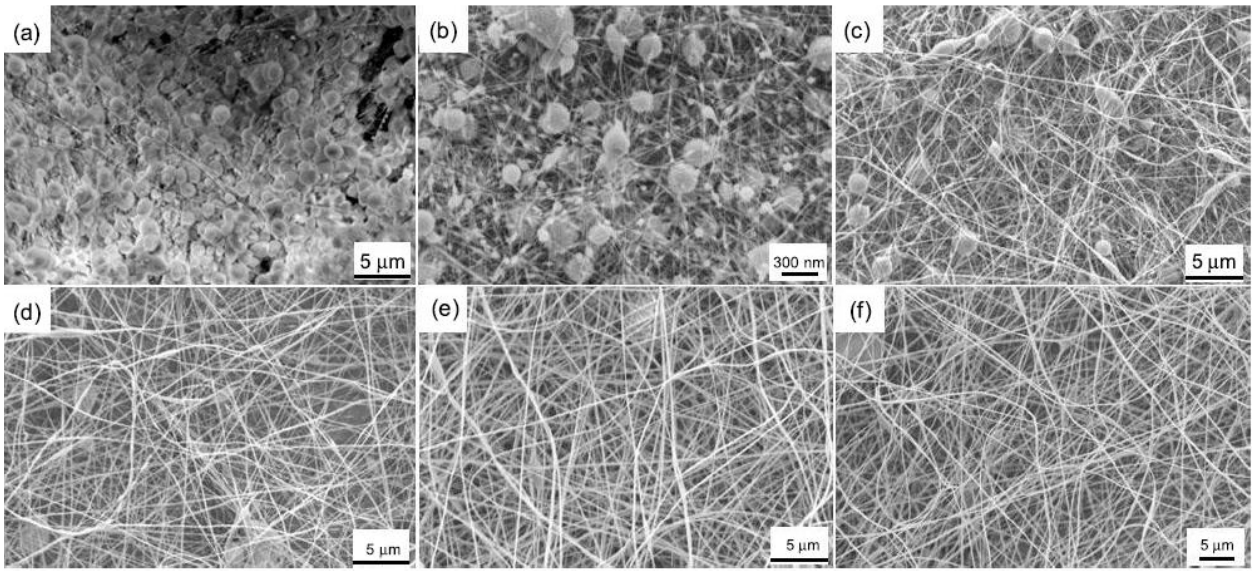


Figure I.7: Outcomes of PAN/DMF solution electrospinning at different concentration of (a) 2wt%, (b) 3wt%, (c) 4wt% (d) 5wt% (e) 6wt% and (f) 7wt% [74]

The observation of these morphologies is also predicted in figure I.8, which gives the relationship between PAN concentration in DMF with the viscosity of its solution and the average diameter of the nanofibers electrospun under the same conditions. The viscosity of the polymer solution increases exponentially or following a power law with the increase of polymer concentration. Moreover, by increasing the polymer concentration or viscosity, the nanofibers with bigger diameter are obtained [75].

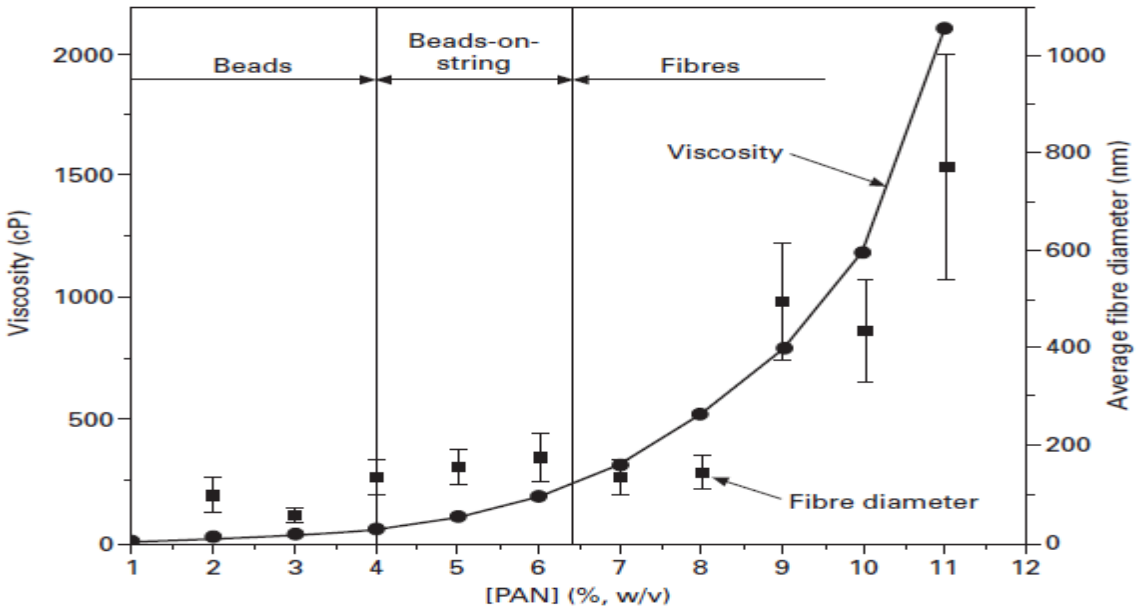


Figure I.8: Relationship of PAN/DMF concentrations with viscosity of solution and electrospun nanofibers diameter [76]

Specific viscosity of the solutions is the incremental viscosity due to the presence of polymer in the solution and it was measured by the formula mentioned in equation 1,

$$\eta_{sp} = \eta - \eta_0 / \eta_0 \qquad (1)$$

η_{sp} denotes the specific viscosity, η_0 is the solvent viscosity [77]. From the previous studies it has been concluded that there are four regimes of polymer solutions of specific viscosity. First regime is dilute regime where viscosity is very low so 1-2wt% of polymer solutions falls in this range and value of specific viscosity $\eta_{sp} \approx C^1$. The second regime is semi dilute unentangled regime where viscosity is higher than first regime but not good enough for electrospinning as polymer chains will not entangle to each other to make nanofibers so up to 7wt% of PAN polymer solutions are considered in this range and specific viscosity is $\eta_{sp} \approx C^{1.25}$. The third regime of specific viscosity is in the range of semi dilute entangled regime where there are enough entanglements of polymer chains so resulted in electrospun nanofibers and value of

specific viscosity is $\eta_{sp} \approx C^{3.6}$. The last regime is concentrated regime whose viscosity is quite higher than all other regimes and has specific viscosity $\eta_{sp} \approx C^{4.8}$ [78, 79]. Figure I.9 gives the graphical representation of different specific viscosity regimes.

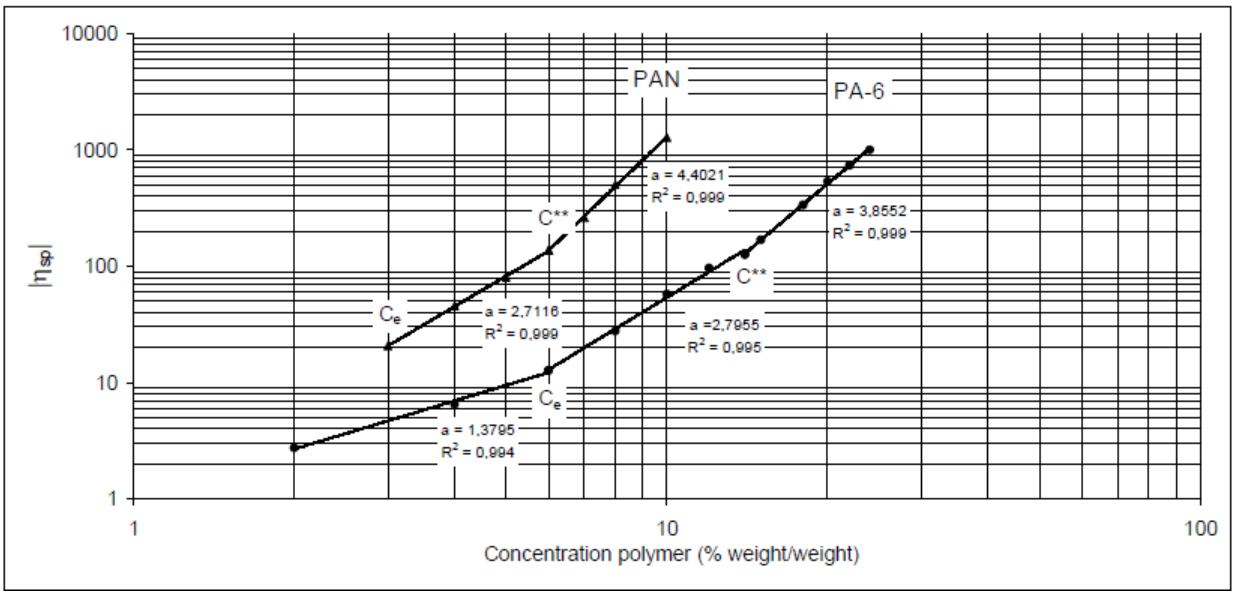


Figure I.9: Specific Viscosity of PAN/DMF and PA-6/Formic acid in ambient condition depending on the polymer concentration [79]

In the graph, the two curves are separated in different parts and these parts have different coefficient of direction. The coefficient of direction is linked to the macromolecular conformation of the polymer chains.

1.4.1.2 Solution conductivity

Solution conductivity governs the effect of electrostatic forces acting on it. Mostly the conductivity of solutions is governed by the properties of solvent employed. Solutions having higher conductivity are pulled easily towards the collector as compared to low conductive solutions due to higher charge density in them. Therefore morphology and properties of nanofibers are also affected by it. It is found that fibers diameter is inversely related to cube root of polymer solution conductivity [80, 81, 82]. Electrospinning solution conductivity can be modified by varying the amount of polymer used or using electrolytes, adding surfactant or appropriate solvent [70, 72, 81]. This modification of conductivity might be helpful in getting the desired morphology and defect free nanofibers. For example nanofibers beaded free structure can

be obtained by addition of specific electrolytes and surfactant in polymer solution [81, 83]. Conductivity can also be modified by increasing the polymer concentration; due to higher solution concentration the result is expected decreased conductivity (due to lower amount of solvent) and thus pose a significant impact on fibers morphology [70, 81]. As described earlier that by increasing concentration, conductivity decreases, so it may be noted that increase in conductivity may lead in decreasing the diameter of nanofibers because of increase of electrostatic pull on polymer. If we compare the nanofibers diameter of 8wt%PAN nanofibers with 10wt% of PAN nanofibers, the conductivity of less concentrated solution is high and its diameter is smaller as can be seen in figure I.10. Moreover it is also observed that increase in conductivity will increase the instability in electrospinning process [84].

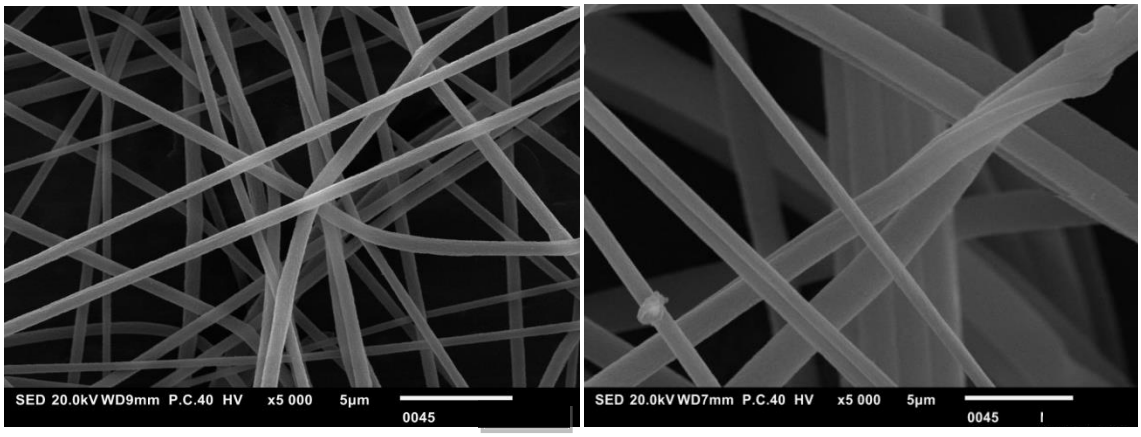


Figure I.10 (a): Thickness of 8wt%PAN nanofibers I.**10 (b):** Thickness of 10wt%PAN nanofibers in DMSO [84]

1.4.1.3 Polymer solution temperature

As discussed earlier the viscosity of the electrospun solution is the most important factor that impacts on the surface morphology of electrospinning nanofibers. It is observed that at some specific polymer concentration, by increasing the solution temperature the solution conductivity is increased whereas solution surface tension and solution viscosity are decreased [16]. Whereas electrospinning of high temperature solution produces thinner nanofibers due to the enhanced solution properties including lower surface tension, higher conductivity and lower viscosity. It is also observed that when electrospinning PAN solution at higher solution temperature, a high voltage is required to carry out the electrospinning process than that needed for the same solution at room temperature [16].

1.4.1.4 Nature and solvent properties

The selection of a good solvent is the most important factor for the transition from electrospraying to electrospinning and to obtain electrospun filaments with diameter in nano scale. Solvent dissolves the polymer and evaporates when nanofibers pass between the needle/wire and collector electrode. Solvent type also determines the surface tension of the solution. Those solvents that have high solubility for polymer are found to produce droplets electrospraying therefore polymer concentration can be increased to overcome this problem [85]. The selection of solvent depends upon the factors like its volatility and the solubility of polymer in it. The solvent that has higher density and higher boiling point with maintaining all other solution and process parameters constant leads to thinner fibers [55]. The solvent that has appropriate volatility will evaporate completely before arriving the collector, which is desirable. Whereas the solvent which has high volatility, it will create problems by drying the polymer away at the tip of the nozzle and thus resulting in failure of the electrostatic force to pull the polymer towards the collector and electrospinning needle will blocked. On the other hand if the volatility of solvent is too low, it will not evaporate before the arriving to the collector, the polymer will not dry away, wet and beaded nanofibers will be obtained. The porosity of the nanofibers also depends upon the evaporation profile of solvents at surface of polymer [86, 87]. If the mixture of different solvents is used they also affect the morphology of the nanofibers by modifying the spinning solution viscosity, conductivity and surface tension of the solution. These mixtures of solvents are used to produce versatile morphologies and to obtain fibers with elliptical, flat-ribbon like and core sheath structures [70].

1.4.2 Process parameters

Process parameters is a class of variables, which implies operating parameters including highly impacting ones, like applied voltage between the two electrodes, distance between the capillary tip and collector electrode, solution feed rate or nozzle size [84, 88, 89, 90] and many other like the type or geometry of collector, polarity of the tip, etc. Nevertheless the influence of the process parameters is quite important, but they are less important as compared to solution variables. The most influencing process parameters on electrospinning jet are explained in the following paragraphs and they will also describe the effect of these parameters on morphology of nanofibers and their diameter as well.

1.4.2.1 Solution flow rate

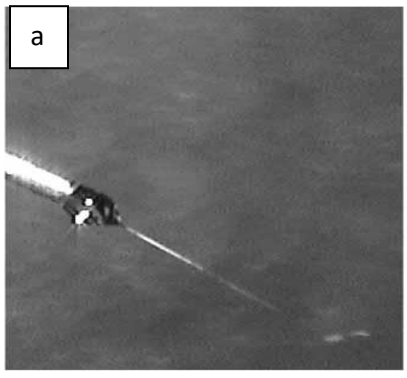
Polymer solution volume or solution feed rate in Taylor cone depends upon the rate at which the polymer solution flows out of the capillary and arrives at the tip of the needle/wire and there is a magnitude of electrostatic force that pulls it towards the collector. Feed rate has a direct impact on the stability of Taylor cone. With maintaining the voltage and collector distance constant, the flow rate has to be optimized. If the solution feed rate is lower than the rate at which it is taken out, then the electrostatic forces will get the solution from inside the capillary or before making the Taylor cone and the droplet will be drawn faster into very thin jet which will be broken up with high probability under the influence of surface tension and results will be the development of beads in the structure [82, 91]. The nanofibers characteristics are badly affected by the improper flow rate of solution. It includes non-uniform diameter, geometry and porosity in the structure of nanofibers. If the flow rate is quite high, the diameter of nanofibers may increase and it may also result in improper drying of nanofibers as it reaches to the collector. The reason is that with high flow rate, electrostatic force has to take a large amount of available polymer towards collector. High flow rate will also increase the number of beads defects and the diameter of beads. The beads defects are the reasons of incomplete drying of nanofibers on the surface of collector. At high flow rates, ribbon like cross section was also observed due to incomplete drying [92, 93]. At the feed rate that is convenient with the electric field tension, the droplet suspended at the needle tip is drawn away with an equilibrium mass balance and as consequence nanofibers with uniform diameter are produced [16].

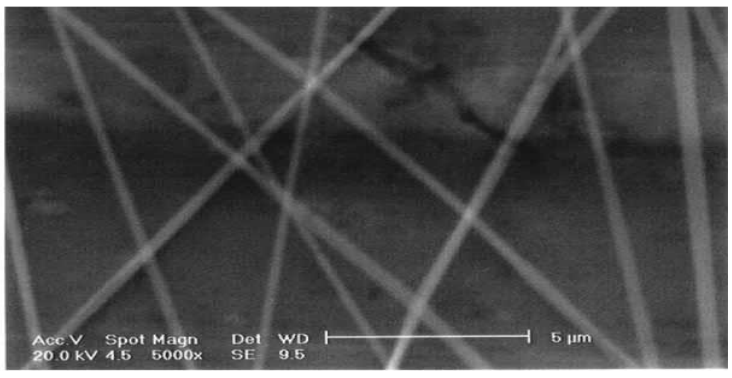
1.4.2.2 Applied voltage

In a neutral solution there are positive and negative charges equally distributed. When the solution is subjected to an external electrical field, the ions present in the solution move in opposite direction, where negative ions present in solution move towards the cathode and positive ions of solution move towards the anode. Consequently, the difference in the number of negative and positive ions in a volume element of the solution is referred to “excess charges” whose electric field acting on a long distance is not negligible or cancelled by other counter ions. These charges are carried along the jet and cause it to experience electrical instabilities which force the jet to stretch and to fight towards the counter electrode where it deposits in the form of a nonwoven filament whose diameter is in nano to sub micrometer scale. The application of high

enough voltage is crucial in electrospinning in order to eject the jet when the magnitude of the generated electric field overcomes the solution surface tension [16].

The main stretching force is electrostatic charge in electrospinning process that decreases the diameter of fibers to nano scale. Voltage is applied across the nozzle/needle and collector to develop and control this charge and it affects the properties of nanofibers very strongly. A value of applied voltage and resulted electrostatic charges, high or low from a certain critical value may produce nanofibers of undesirable characteristics. When the applied voltage magnitude is less than the critical value, no electrospinning occurs and droplets have semi spherical shape. By increasing the voltage close to the critical limit, it initiates the jet to some extent to form the vertex of the droplet whose shape is turned into conical type and cylindrical nanofibers are obtained (figure I.11a). On the other hand, as the voltage is increased from the critical level, Taylor cone shape of droplet is taken place and the defect free cylindrical nanofibers are obtained (figure I.11b). With the further increase of applied voltage, the size of Taylor cone is reduced and the jet seems to be ejected from the tip of the needle and in these cases, beads on sting are produced (figure I.11c). Whereas when too high voltage is applied, Taylor cone is reduced in the needle and no protrusion is visible and drawing of solution drops is faster than the feeding and as a result big amount of beads are observed (figure I.11d) and electrospinning process is not continuous. However, these beads which are formed at higher voltage have smaller diameter but there density is greater and the shape of beads is more spherical as compared to those beads which are formed at voltage below the critical range [92]. It is also observed that nanofibers production is increased at higher electric field [94]. Many studies explained the influence of applied voltage on the diameter of nanofibers [95, 96].





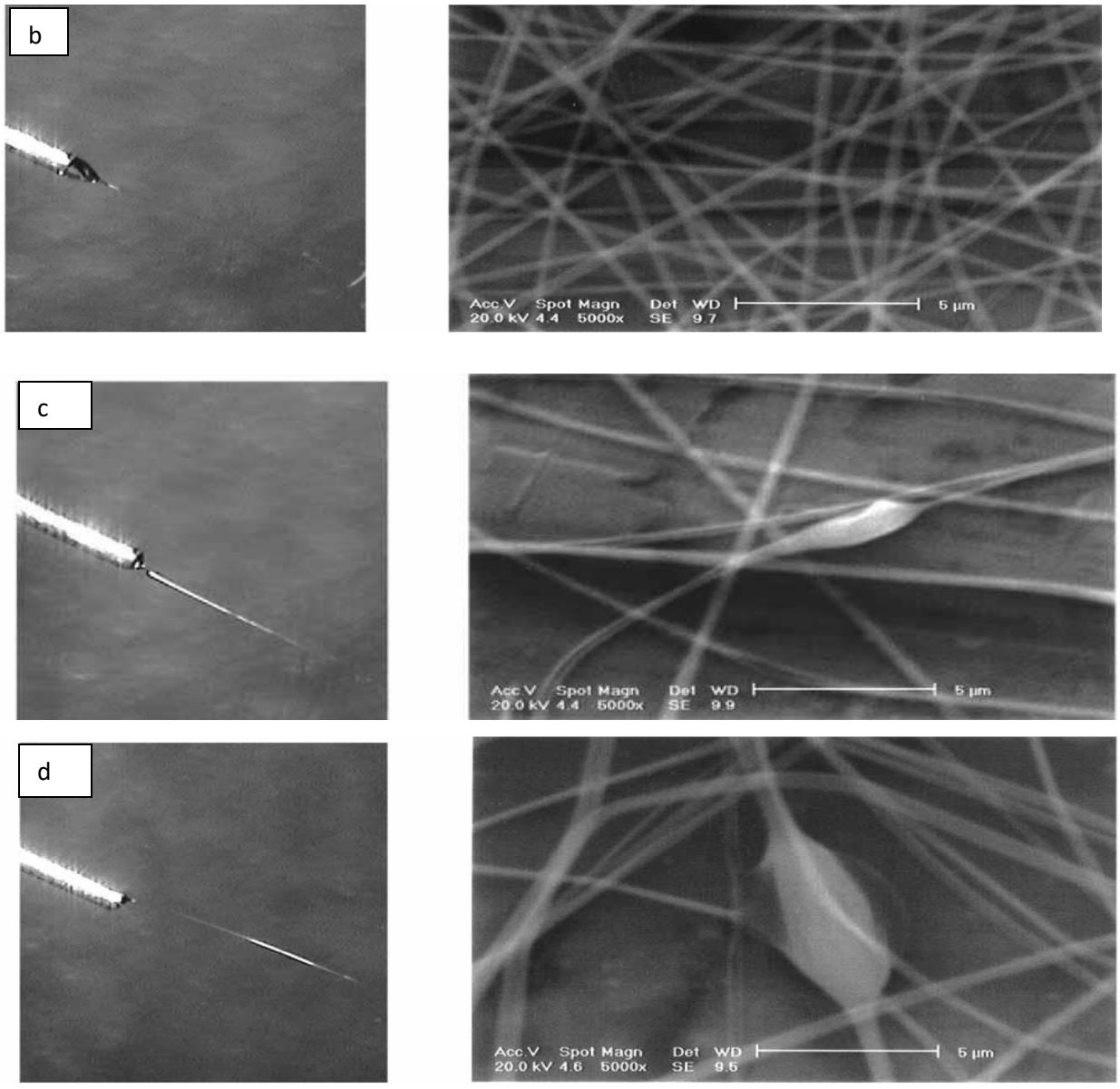


Figure I.11: Jet ejection images and SEM images of 15wt% PAN/DMF nanofibers produced at 15cm and 2ml/h at different voltages (a) 9kV, (b) 10kV, (c) 11kV and (d) 12kV [97]

It has been found that impact of voltage is different on nanofibers diameter, sometimes nanofibers diameter increases [98, 99] by increasing voltage and sometime diameter decreases [97, 100] by increasing the voltage. When the diameter of nanofibers decreases by increasing the applied voltage, it is predicted that higher electric field increases the electric force which pulls and stretches the jet and as a result thin nanofibers are obtained. Whereas, when the nanofibers diameter increases by increasing the voltage, it is explained by the flight time of the jet; higher voltage will accelerate the jet and the flight time is reduced. As the flight time is

shorter, so there will be less time for stretching and elongation of nanofibers. Synergistically, higher voltage may accelerate solvent evaporation rate and resultant nanofibers are coarser.

1.4.2.3 Collecting distance

Electrospun nanofibers morphology and properties are strongly affected by varying the distance between the nozzle and collector because it has direct impact on the jet flight time and electric field gradient (kV/cm) that affect the diameter of nanofibers. If the ambient, solution and process parameters are kept constant, only the collecting distance are varied, then longer collecting distance will offer longer flight time of the jet due to which jet will stretch further and there will be enough time available for the complete evaporation of solvent and as a result finer nanofibers are obtained [84, 94]. Another reason of decreasing the nanofibers diameter is increased electrostatic repulsion at larger distance that also allows the polymer solution to have increased flight time so nanofibers with smaller diameter are obtained [101]. Whereas longer electrode distance shows better molecular orientation due to longer stretching and flight time [102]. When the electrode distance is smaller, it results in formation of larger fibers diameter, however dripping may be observed for low viscosity solutions, particularly at lower voltages [94]. It has been observed in some studies that decreasing the collecting distance has an equal effect on nanofibers diameter as increasing the applied voltage. But this observation is valid to some extent. To find out the optimal condition for the production of PAN nanofibers [103], it has been observed that PAN nanofibers diameter decreases as the collecting distance decreases till a critical point is reached, beyond which the nanofibers diameter has tendency to increase. Reduction in nanofibers diameter when the collecting distance is lower than critical value is discussed earlier, i.e. lower distance yields higher electrostatic forces and resulted in finer nanofibers. The diameter increases when the collecting distance is longer than critical value is thought to be the result of reducing the electrostatic forces. In this case viscoelastic forces are dominant and coarser nanofibers are obtained [103].

Another observation has been taken into consideration during the investigation of influence of electric field on the diameter of electrospun PAN nanofibers by two different approaches, either by putting the applied voltage constant and varying the electrode distance between the nozzle and nanofibers collector (E_d), or by holding the collecting distance fixed and varying the applied voltage (E_v). It was found that by increasing the electric field intensity by decreasing the

collecting distance, the diameter of nanofibers diminishes; while by increasing the electric field intensity by increasing the applied voltage, there is no significant change in diameter, i.e. nanofibers diameter exhibits no dependence on (Ev) [104].

The variation in the collecting distance has an impact on the morphology of nanofibers. Small electrode distance increases the electric instability that the jet experiences and a subsequent formation of beads are observed [105] as shown in figure I.12.

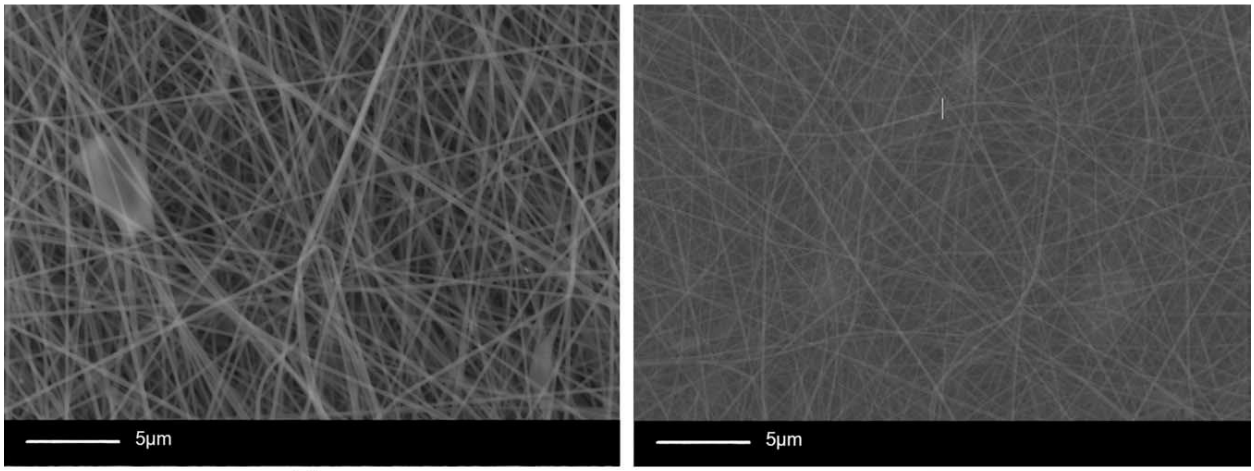


Figure I.12: PAN/DMF nanofibers produced at (30kV and 10wt %) at different collecting distance (a) 5cm, (b) 15cm [103]

1.4.3 Environmental parameters

The environment of electrospinning process plays an important role in determining the properties of nanofibers. These environment parameters are called as ambient parameters which include humidity, vapor content and temperature inside the electrospinning booth [106]. By varying these parameters, nanofibers of different structures and properties can be obtained. These ambient parameters are discussed below.

1.4.3.1 Relative humidity

Humidity is a very important factor among the ambient parameters which surrounds the polymer jet. The effect of relative humidity on the morphology of nanofibers depends upon the nature of polymer, whether it is hydrophobic or hydrophilic. If the humidity of the chamber is low, then evaporation of solvent will be quite high and as a result of decreased stretching of polymer jet, thicker nanofibers will be produced. If the humidity is higher, it will also disturb the nanofibers

morphology due to condensation of water on the surface of nanofibers, water acts as non solvent. Due to solvent evaporation, a dry polymer film is formed around the polymer jet. Consequently, pores are formed to enable the evaporation of the trapped solvent and complete nanofibers solidification [107]. This effect varies from different polymers and mostly depends on the electrospinning solution composition which defines the parameters like evaporation rate and hydrophobicity [107]. A study concerning electrospinning of polyacrylonitrile (PAN) in dimethyl formamide (DMF) was done at room temperature in different relative humidity conditions [108]. It shows that PAN nanofibers produced at 30% relative humidity are smooth as compared to those nanofibers which were produced at 60% relative humidity which had rough surface [108]. This phenomenon is shown in figure I.13.

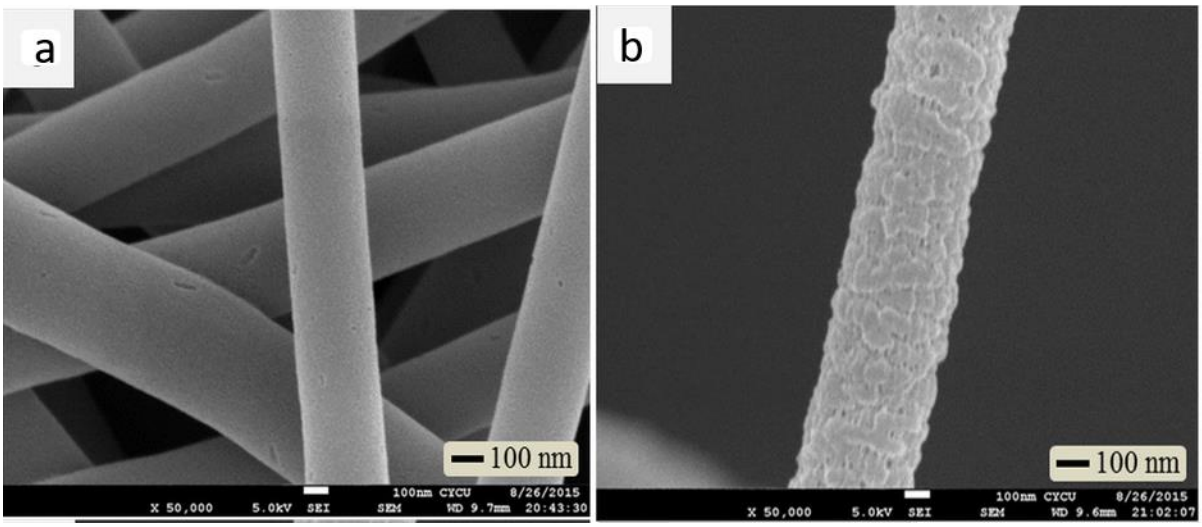


Figure I.13: PAN/DMF nanofibers electrospun at (a) 30% RH and (b) 60% RH [108]

1.4.3.2 Temperature

Temperature is also an important factor in ambient parameters as it can change the viscosity of solution and also solvent evaporation rate [109]. Increasing the surrounding temperature results in viscosity decrease of polymer solution and the resulting nanofibers will be thinner due to high extension. So to get the good nanofibers, optimization of the temperature is required inside electrospinning chamber [109].

1.2.4 Conclusion

The above discussion explains that selection of best parameters for electrospinning is crucial for the production of bead free fibers with the diameter in the range of submicron to nano scale. Electrospinning parameters depend upon different conditions in which the process is being carried out. Three types of morphologies can be observed by varying these electrospinning conditions: electrospraying, beads on string and bead free nanofibers. For the production of desired morphology of nanofibers, the balancing of three sets of electrospinning parameters is required; (i) solution parameters such as concentration of solution or viscosity, solution conductivity, solvent type, dielectric constant of solvent, etc. (ii) process parameters which includes applied voltage, electrode distance, feed rate, etc. (iii) ambient parameters, which include environment temperature and relative humidity. From the literature review, it is concluded that solution parameters are the most important parameters among all others which have significantly impact on morphology of nanofibers. For bead free nanofibers, the increase in polymer concentration or viscosity will increase the diameter of nanofibers, while diameter decreases when using solvents of higher boiling point, higher dielectric constant and higher solution conductivity. Whereas increase in applied voltage has mixed effect on nanofibers diameter; sometimes increases and sometimes decreases. Inverse effect is observed while varying the collecting distance, i.e. decreasing the collecting distance gives finer and coarser nanofibers. Increase in feed rate gives the coarser or thicker nanofibers. Ambient parameters were found an effective tool to control the electrospun nanofibers morphology, ranging from non-porous morphology, passing through wrinkled nanofibers and ending in porous nanofibers.

1.5 Polymers used for electrospinning

The electrospun materials have unique properties which encouraged the researchers to study more about electrospinning materials and their applications as nanofibrous webs alone in composite shape with any other materials. These electrospun polymers are classified broadly as natural and synthetic polymers. Some important natural polymers which are used in electrospinning include Chitin [110], bombyx mori silk fibroin [111], chitosan [112], fibrinogen [113], gelatin [114], collagen [115], myoglobin and hemoglobin [116], pullulan [117], lecithin [118] and starch [119]. Beside these natural polymers, there are a large number of synthetic polymers, which have also been electrospun. They include polyamide 6 [72], polyamide 6-6

[120], polyacrylonitrile [121], polyacrylic acid [122], polycarbonate [123], polyetherimide [124], polyurethane [125], polyvinyl acetate [126], polyvinyl chloride [127], polysulfone [128], polyvinyl butyral [129] and polyvinylidene fluoride [130]. If we see the class of manmade polymers, there are some biodegradable polymers which have been electrospun. Among them some notable include polyhydroxystyrene [12], polyethylene glycol [131], poly (ϵ-caprolactone [132], poly (lactic acid) and poly (lactic acid-co-glycolic acid) [133].

Our study does focus only on one synthetic polymer i.e. Polyacrylonitrile (PAN). The properties offered by this material, that encouraged its selection for current work is discussed in following section.

1.5.1 Polyacrylonitrile (PAN)

From synthetic class of polymers, one of the most valuable polymers is PAN due to its specific advantages for electrospinning such as, easy for electrospinning, low cost and most viable precursors for carbon nanofibers with much high percentage of carbon, easily surface modification for further processes [134, 135]. PAN polymer is relatively stable polymer and has high melting point of 317 ^{o}C, glass transition temperature is also high 95 ^{o}C. The molecular structure of PAN is mentioned below in figure I.14.

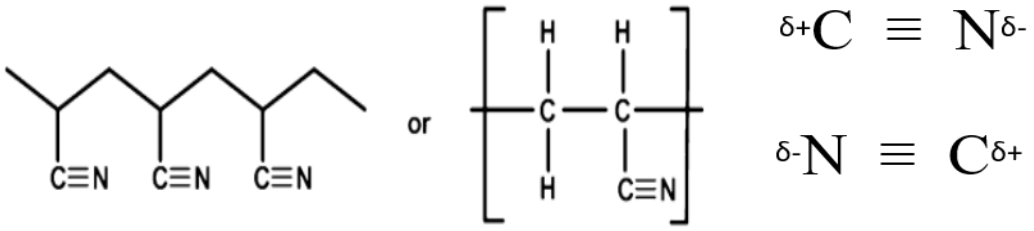


Figure I.14: PAN molecular structure [134]

PAN polymer has more electrostatic forces which are the reasons of good mechanical strength [134]. PAN is widely used in electrospinning process for the manufacturing of fibers from nano to submicron scale. Among many reasons of selecting PAN, the one most suitable reason is that it is precursors for carbon fibers which offers a yield of more than 50% and can be used for production of carbon nanofibers through electrospinning and other techniques [136]. For the production of carbon fibers, different types of precursors can be used which may be cellulose, PAN or pitch, but PAN is the most commonly used material (for the production of about 90%

carbon fibers). PAN is mostly used due to some of its advantages over other precursors, which include higher yield and better mechanical properties [137, 138].

For the production of carbon nanofibers (CNF) and their composites, normally vapor growth or electrospinning techniques are mostly used. Carbon nanofibers obtained by vapor growth are produced by gases which contain carbon in the presence of metallic catalysts. Fibers produced by this technique however are shorter in length and their alignment with some added shortcomings are not well, such as complicated processing, lower yield and higher production cost [56]. Whereas electrospinning is the technique that has been successfully utilized to produce continuous strong carbon fibers in nanometer length dimension.

1.5.2 PAN Electrospinning

PAN (typical molecular weight 150,000 g/mol) is a semi crystalline polar polymer that can be electrospun by dissolving it in some suitable polar solvents like dimethyl sulphoxide (DMSO), dimethyl formamide (DMF), dimethylacetamide, dimethylsulfone, teramethylsulfide and ethylene carbonate (in aqueous form); Dimethyl sulphoxide (DMSO) as solvent is considered quite suitable for electrospinning process because it has good dissolving capability for PAN, appropriate volatility and high dielectric constant [94, 134, 139, 140]. PAN polymer may also be dissolved in ionic liquids but for this purpose, process should be controlled and optimized by increasing spinning solution temperature [93]. If some special nanofibers structures are required like porous nanofibers, liquid additives can be used with original solvents [94].

For uniform electrospinning of PAN solutions, normally 6-14wt% of PAN solution is employed and the solution is given some suitable time (normally 24-30 hours), so that solution may become homogeneous at room temperature. It has been found that diameter of nanofibers increases linearly by increasing the solution concentration [81, 94, 48, 141]. For concentration below than 6wt% of PAN polymer, beaded fibers are produced till the concentration low as 2wt%, where only droplets of polymer solutions are obtained [34, 57]. In the case of PAN nanofibers and many other polymers, the most pronounced effect on nanofibers diameter is produced by the concentration, while the other factors like voltage and electrode distance have less significant effect [97, 98]. Nanofibers properties are also affected by the addition of different additives, which includes surfactant, electrolytes, nanoparticles and different polymers. It has

been studied that different salts are also added as additives in electrospinning solutions and the salts increase the conductivity of solutions which influences the electrospinning parameters. The sequence of increase in solution conductivity of different salts have been found as LiCl>$NaNO_3$> $CaCl_2$>NaCl; therefore the obtained diameters by these solutions would be like LiCl>$NaNO_3$> $CaCl_2$>NaCl, in the descending order [142].

1.5.3 PAN nanofibers stabilization and carbonization

The stabilization of PAN nanofibers is necessary before the process of carbonization to maintain their stability. In the process of stabilization, the crystalline and amorphous phases of the polymer are stabilized by converting a thermoplastic polymer to non thermoplastic polymer with weight loss more than 10% and their diameter is also decreased a little [136, 143]. The process of stabilization (more specifically called oxidative stabilization) is carried out by controlled heating process, whereas the fibers are kept under pressure and heated up to 300 ºC for one hour in the condition of air [56, 143, 144]. In the process of stabilization, many chemical reactions take place within the polymer structure; they include cyclization, aromatization, dehydrogenation, oxidation and cross linking. And the resultant structure is crosslinked ladder ring structure as shown in figure I.15 [136].

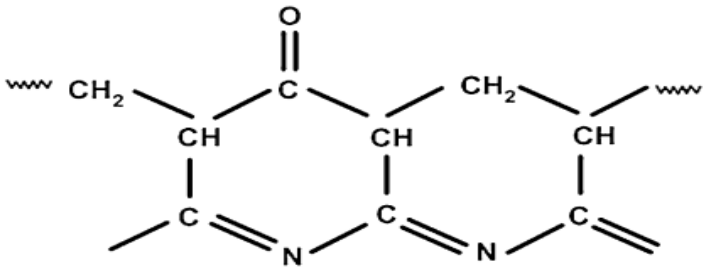


Figure I.15: Ladder structure of PAN polymer [136]

In this process, PAN nanofibers shrink up to 25-35% from their original dimensions and for maintaining their dimensions, they must be held in support. It has been found that addition of fillers like SBA-15 decreases the thermal shrinkage [145]. For thermal stabilized PAN, different researchers suggested different structures of polymer. These structures include cyclic heteroaromatics [146], cyclic polyamine [147] and many different crosslinked structures [148, 149]. From these studies, it is suggested that in the process of stabilization, C≡N (nitrile group)

containing structure is converted to C=N conjugated structure, that may results in cyclization (in the case of intramolecular) or crosslinking (in the case of intermolecular). Due to the dehydrogenation and oxidation process in stabilization, some conjugated C=C structures and carbonyl groups may also be produced. Chemical changes that occur during carbonization are shown in figure I.16 [136].

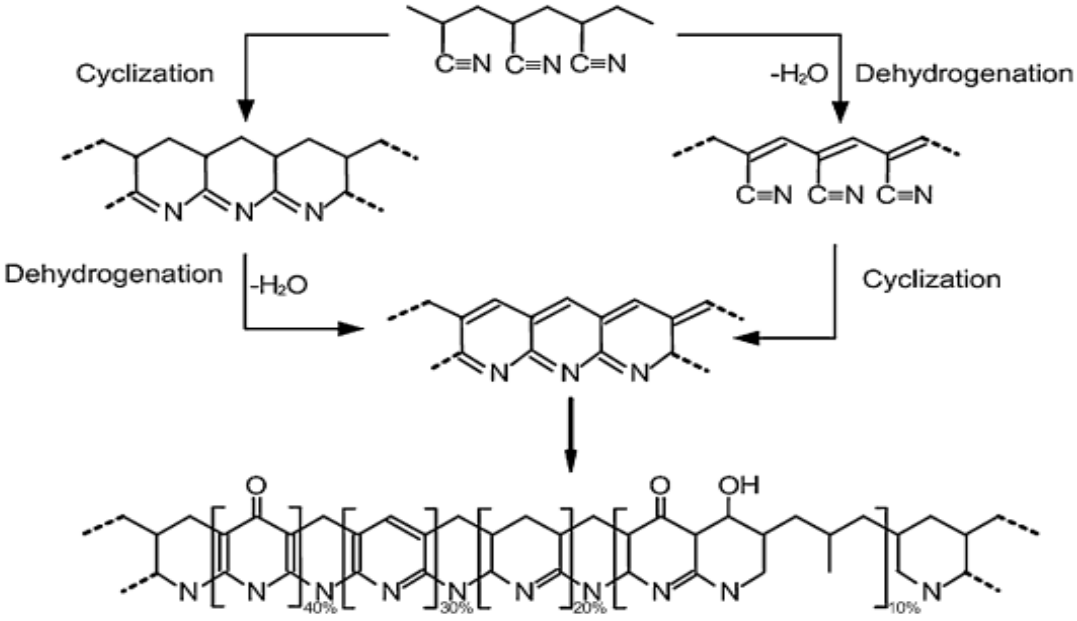


Figure I.16: Chemical reactions during PAN stabilization [136]

During the process of thermal treatment, the PAN nanofibers are under tension and this heating process stabilizes both the crystalline and amorphous phases and it helps to maintain the molecular orientation in the whole bulk of orientation [150]. To increase the density of PAN nanofibers a hot-pressing pretreatment can also be carried out. Due to these pretreatments the conductivity of carbon webs can be increased. The conductivity increase of PAN nanofibers may be due to increased number of crosslinks between the fibers, due to temperature and pressure and it is increased with increase in treatment time [151].

The process of carbonization is done to convert the contents of PAN to pure carbon or at least close to pure carbon. During this process, considerable weight loss of PAN nanofibers is observed and their diameter is also decreased [143, 144]. These results are achieved by high thermal treatment in the inert environment that leads in polymerization and further in aromatic

growth of molecular chains. The fibers obtained after this process can have exceptionally high modulus depending upon the context of carbonization.

The carbonization process is carried out between 800-3000 ^{o}C temperatures in an inert environment depending upon the degree of carbonization required. By increasing the temperature up to 600 ^{o}C, dehydrogenation in already cyclized structures allows for crosslinking in lateral direction which results in graphite like structure [136]. As the temperature is increased above 600 ^{o}C, the network of carbon is increased by the elimination of N group from the structure and structure becomes highly crosslinked; this process continuous to the temperature as high as 1300 ^{o}C. The change that occurs during carbonization of stabilized structure is shown in figure I.17 [152].

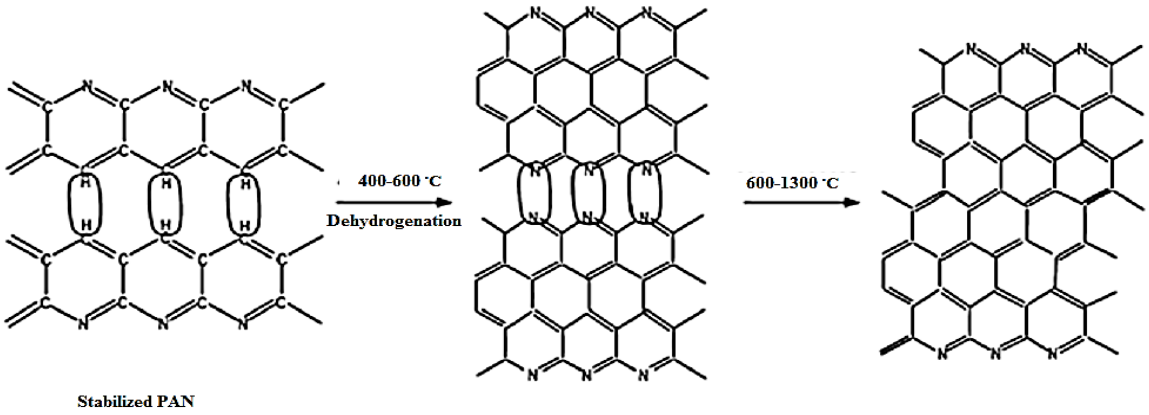


Figure I.17: Change of structure during PAN carbonization [152]

In the process of carbonization by increasing the temperature above 400 ^{o}C, the contents other than carbon start to leave the structure, due to which many different gases which includes H_2, CO, CH_4, H_2O, N_2, NH_3 and HCN are evolved from the system. Above 800 ^{o}C, mostly HCN and N_2 are the dominant impurities which re-expelled [152]. The networking in the structure is increased due to the evolution of these gases and different reactions. Further increase in temperature will increase the carbonization and results in graphitization. The fibers of graphene have better molecular alignment and crystallized structure; which is the main reason of improved properties. Higher the temperature of process, growth of graphitic crystal will be more that will result in larger crystallites [153]. In graphitized fibers, the layers of graphene are pileup with each other to form a structure like ribbon, which is not visible in normal carbonized fibers having randomly arranged molecules [154]. The TEM images of two types of fibers are shown in figure I.18.

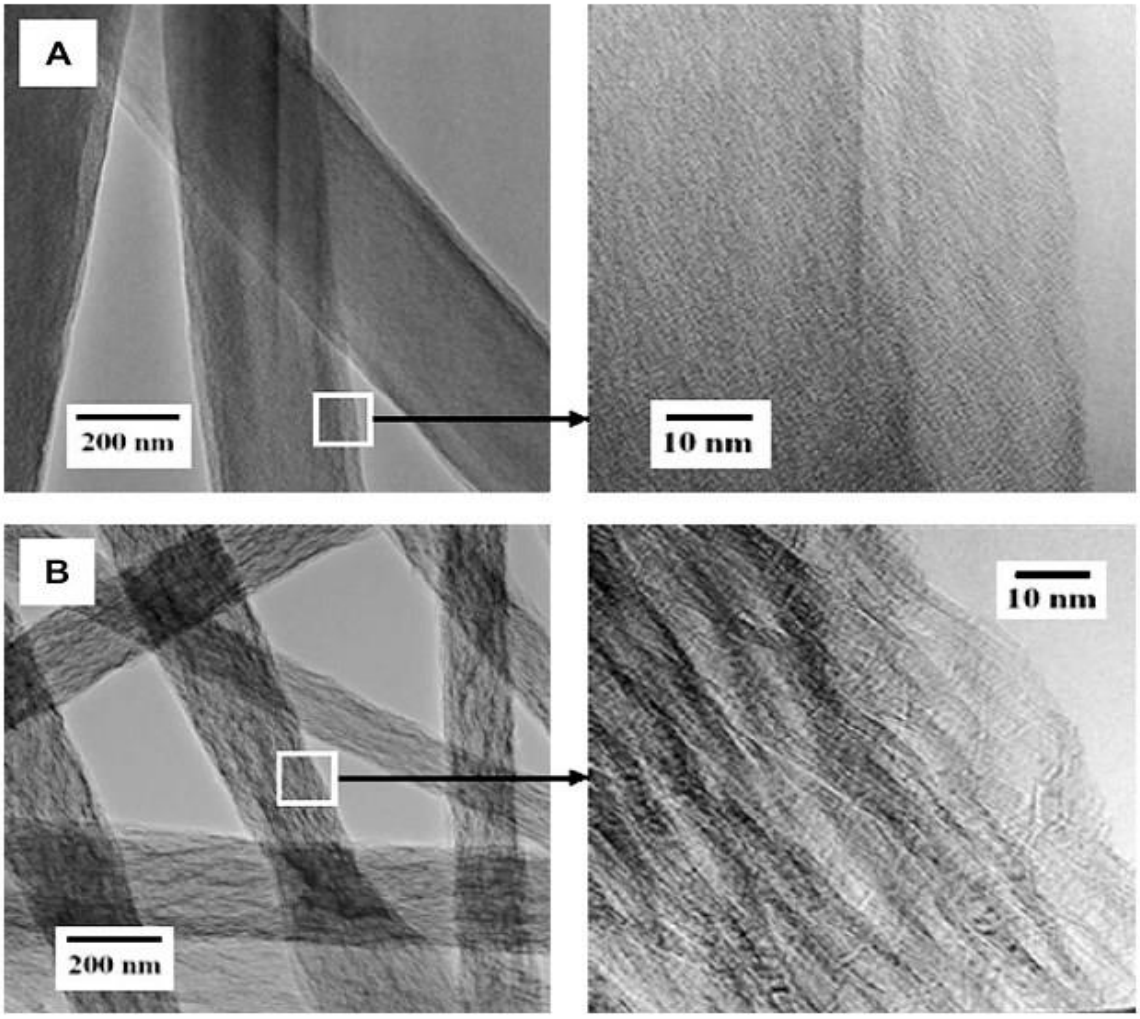


Figure I.18: Heat treated TEM images of carbonized fibers at (a) 1000 ^{o}C (b) 2200 ^{o}C [154]

Increase rate of temperature is very important parameter for both process including stabilization and carbonization that describes the properties of final web. During this process, temperature is increased progressively to control the dimensional shrinkage and weight loss of web. Some studies explain the effect of different heating rates to reach the carbonization temperature. One study explains that progressive stabilization and carbonization was performed by increasing the temperature rate at 5 ^{o}C/min to reach the temperature level of 230 ^{o}C, then the rate of temperature was decreased to 1 ^{o}C/min until 270 ^{o}C was obtained and then again it was increased to 5 ^{o}C/min to get the temperature level of 800 ^{o}C. It was observed that by this process higher yield with lower dimensional shrinkage was obtained as compared to one without progressive heating treatment [155]. During the process of thermal analysis, the density of nanofibers increases (due to compaction) up to the 1000 ^{o}C and later it decreases; the reason behind this

sudden decrease in density is due to the fact that open pores are converted to closed pores at 1000 ^{o}C [156,157]. At lower temperature ranges close to 1000 ^{o}C, the strength obtained of carbon fibers is quite low and content of carbon normally reaches closed to 95% and by increasing the temperature above 1500 ^{o}C, high modulus of carbon fibers are achieved [136]. Because the carbon atoms are bounded together in crystals that are aligned parallel to the long axis of the fibers, as the crystal alignment gives the fiber high strength to volume ratio [158].

1.6 Electrospun composite nanofibers

Electrospun composite nanofibers are used in a wide range of applications, like tissue engineering, sensors, filtration, wound dressing, fuel cells, capacitors, etc. To get these applications, some tailoring specific properties are required regarding chemical composition, hydrophobicity, conductivity, porosity, selectivity and many others. Generally, most of nanofibers produced of chemically stable and mechanically strong polymers do not have such properties. On the other hand, those nanofibers which are issued from active polymers (those can actuate/change shape in response to an environmental stimuli i.e. heat, light, pH etc.) very often do not have excellent mechanical properties or even cannot electrospun alone [159, 160].

Addition of nanoparticles provides modification in the morphology of nanofibers by producing large fiber diameters and due to agglomeration of fillers some beads shaped structures are also observed, whereas high surface area of composite nanofibers allows enhancing the functionality of incorporated nanoparticles due to their accessibility. For efficient way of using of fillers, they are immobilized on some supports and for that supports nanofibers are one of the best option. Immobilization of nanoparticles on nanofibers not only increases the efficiency of nanoparticles but also allows their extended and repeated usability [161, 162]. Nanofibers morphology is modified by adding the nanoparticles which produces larger fiber diameter, possible with some bead shaped structures due to agglomeration of particles that makes the surface of nanofibers rougher. Especially in the case of PAN nanofibers, thermal properties are also modified thus affecting the stabilization and carbonization stages for the development of carbon nanofibers [162].

Tailoring in the polymers or nanofibers has been used for many decades to get specific application requirements. Therefore, in the field of composite nanofibers, this technique has been applied to create some innovative nanofibers for specific applications which are mentioned

above. There are many techniques which are used for tailoring properties of electrospun nanofibers including physical blending [58] or coating [163], surface grafting polymerization [164], plasma treatment [165], layer to layer deposition [166], wet chemical method [167], microwave irradiation [168] and others. To get the good tailoring properties among all these, physical blending is a widely used technique due to its effective and easy way of introducing fillers/functional molecules into the bulk polymer. There are some fillers described below which are mostly used to functionalize polyacrylonitrile for different potential applications.

A work was focused on adding bismuth oxichloride nano-sheets in PAN nanofibers for the purification of waste water that showed excellent efficiency for degradation of rhodamine B with UV irradiation [169]. Whereas some good result have also been achieved by the addition of TiO_2 in PAN nanofibers [170]. For photocatalysis, PAN/Ag_3O_4 has been electrospun from a PAN/DMF/Ag_3O_4 solution [171]. To get improved magnetic properties, nanoparticles of Fe_3O_4 have been added in PAN nanofibers for the production of magnetic PAN/Fe_3O_4 nanocomposites [172]. In PAN nanofibers, silica nanoparticles have also been introduced by adding these fillers directly in polymer solution in the presence of efficient dispersing setup (strong mechanical stirring for 24 hours). This technique has been used for energy storage by developing PAN/poly (L-lactic acid)/Si and PAN/SiO_2 nanofibers [173-138]. It has been found that introduction of hollow graphitic carbon nano-spheres in carbon nanofibers by electrospinning, improves the storage capacity, ions diffusion and electrons collection in lithium ion batteries [174].

The addition of silver salt in the electrospinning solution for the *in-situ* development of silver nanoparticles, results in good evenly dispersion of silver nanoparticles in PAN nanofibers and smoothness of electrospinning process. Composite like this shows a very good antimicrobial activity [175]. Another research explains the development of hollow carbon nanofibers by adding tetraethoxy orthosilicate in PAN nanofibers and these were converted into silica by heating treatment for carbonization along with various gases were emitted by producing micropores in carbon fibers. These composites exhibited good performance for using as super capacitors [176]. Sn nanoparticles were incorporated in PAN nanofibers by in-situ reduction of $SnCl_2$ and the resultant nanofibers composite was employed for energy storage [177]. Some nanofibrous composites of PAN/TiO_2 for anode material of lithium ion batteries have been developed by in-situ development of TiO_2 nanoparticles [178]. There is another study which explains the development of iron oxide nanoparticles in PAN nanofibers for utilization in

capacitors [179]. In another work, some nanoparticles of gold were attached to PAN nanofibers by electrospinning a PAN solution in the presence of reducing agent. The obtained nanofibers were treated with hydrogen tetrachloroaurate (III) trihydrate to attach gold nanoparticles on fiber surfaces and it showed excellent sensing capability [180]. In another similar work, gold particles were developed and doped in PAN/polyaniline nanofibers for their applications in transistors [181].

In this context of thesis, the focus of our research is on functionalizing electrospun PAN nanofibers by adding SBA-15 fillers by direct physical blending. Here the methods of SBA-15 synthesis, approaches used to disperse them in solvents, their influences on the polymer/filler dispersion and on the morphology of produced nano composite are explained.

1.6.1 Synthesis and properties of SBA-15 ordered mesoporous silica

First time, mesoporous silica nano particles (MSNs) were synthesized in Japan and later on the Stucky group introduced the Santa Barbra Amorphous (SBA) materials ranging from 2-50nm in 1998 in university of California, Santa Barbra [182]. This material consists of a silicon oxide matrix, whose main characteristics are (i) pore size between 2 and 15 nm, (ii) cylindrical mesoporous having a hexagonal arrangement, (iii) presence of micropores (pore size <2nm), mesopores channel are interconnected through micropores, (iv) significant surface chemical activity. This activity depends on concentration and distribution on the solid surface of different silanol (Si-OH) and siloxan (Si-O-Si) groups, as silanol groups enable the anchor of various chemical compounds and thus may modify the surface of solid for specific applications [183]. The structure of SBA-15 is shown in figure I.19.

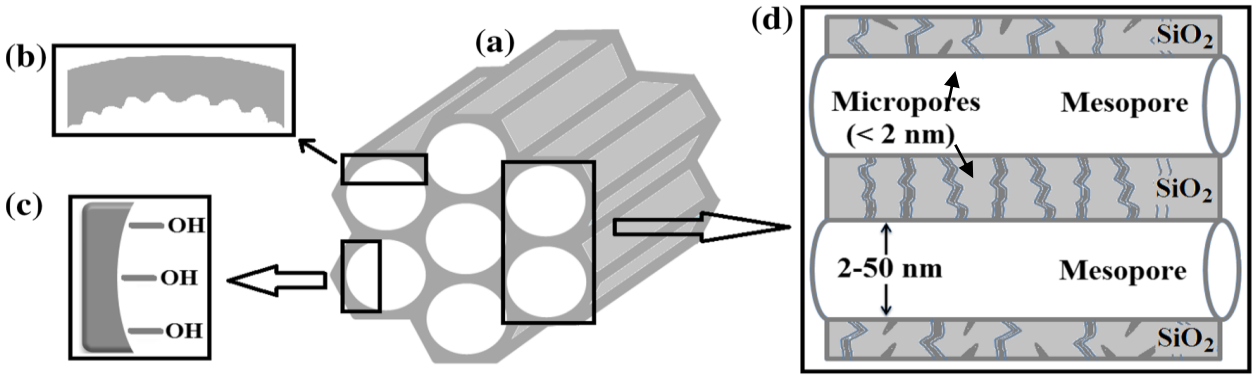


Figure I.19: The main SBA-15 characteristics [183]

(a) Hexagonal arrangement of cylindrical Mesoporous, (b) pore surface roughness, (c) superficial silanol groups (d) Mesoporous interconnected by micropores

SBA-15 was first synthesized by Zhao et al. in 1998 [184]. The synthesis of this material combined the sol-gel chemistry and use of assemblies of surfactant molecules as framework templates. The self-assembly mechanism is widely employed by using poly(ethylene glycol)-poly(propylene glycol)-poly(ethylene glycol) triblock copolymer (known as Pluronic P123) as structure directing agent and tetraethyl orthosilicate (TEOS) as silica source. The formation mechanism of SBA-15 is summarized in figure I.20.

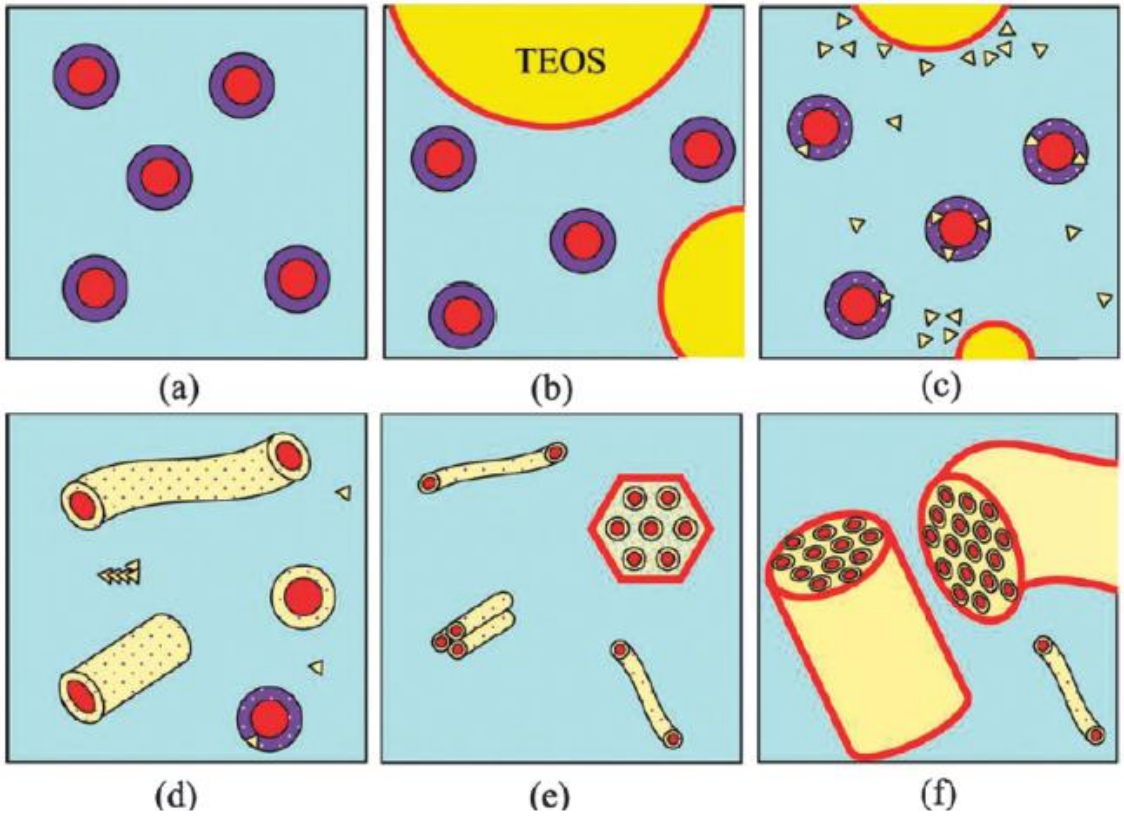


Figure I.20: Synthesis mechanism of 2D-hexagonal SBA-15. (a) Initial solution of P123, (b) Addition of TEOS silica precursor (c) Hydrolysis step and beginning of condensation (d) Shape transformation of the hybrid organic-inorganic micelles from spherical to rod-like (e) Nucleation of the 2D-hexagonal phase (f) Growth of the 2-D hexagonal phase [185]

The main finding is that the micelles in solution undergo a sphere to rod shape transition prior to the formation of 2D-hexagonal mesophases and that this phenomenon is linked to the fact that silica oligomers are present within the shell of the micelles. The methodology to synthesize SBA-15 materials involves three main stages, (i) During the hydrolysis of silica precursors (TEOS in this case), no modification of the spherical micelles occurs. (ii)- Then the condensation of the silica starts and some oligomers begin to interact with the EO groups at the surface of the

micelles. (iii)- Upon further silica condensation, a sphere to rod shape transition of the micelles occurs. When a sufficient amount of silica oligomers are present within the shell, the precipitation of the 2D-hexagonal mesophases is observed. It can also be explained by fact that the attractive van der Waal's interaction between the hydrophobic cores of the micelles becomes the dominant interaction, including the formation of micelles aggregates [185, 186].

The synthesis conditions such as, hydrothermal treatment temperature and duration, the quantity of silica source or pH play a key role to get a well defined structure with control of both the morphology and the pore diameter. For example, hexagonal ordering of SBA-15 materials can be improved by adjustment of the pH during hydrothermal treatment. Hydrothermal treatment conditions have also a great influence on the structure, the porosity and also the stability of the materials.

SBA-15 is nanostructure silica materials having following characteristics:

- Highly ordered hexagonal array of unidimensional cylindrical mesopores interconnected by micropores [188]. Structure is shown in figure I.21
- Chemically and mechanically stable and tunable structure [188]
- Tunable pore size (i-e between 5 and 30 nm depending upon the synthesis conditions) [16]
- Narrow pore size distribution [188]
- High BET specific surface area (order of magnitude of 2000 m^2/g) [188]
- High pore volume [16]
- Thick walls of amorphous silica which confers SBA-15 materials a good hydrothermal stability [16]



Figure I.21: Hexagonal porous structure of SBA-15 [183]

It should be noted that ordered mesoporous silica are composed of amorphous silica framework, i.e theoretically, amorphous structures do not scatter X-rays. The regular arrangement of pores

can be considered as a kind of super structure with long range ordering. This long range ordering of SBA-15 can be evidenced by X-ray diffraction and basal reflection (gives d-spacing of the basel layer which represents the thickness of silicate layers) can be detected by low 2θ angles [187].

1.6.2 Morphology of electrospun PAN/SBA-15 composite nanofibers

Electrospun pristine PAN/DMSO nanofibers, obtained under optimal conditions are smooth and bead free [16]. Whereas the addition of mesoporous silica nanoparticles in PAN nanofibers results in non-uniform and wrinkled nanofibers with a rough surface. Moreover, depending upon the dispersion quality of the silica nanoparticles within the polymer solution, increase in the content of silica nanoparticles, increases the roughness of the composite nanofibers and nano-scale protrusions or aggregates of the nanoparticles appear on the outside surface of the composite nanofibers [162, 189, 190]. The impact of adding silica nanoparticles in pristine PAN nanofibers is shown in figure I.22.

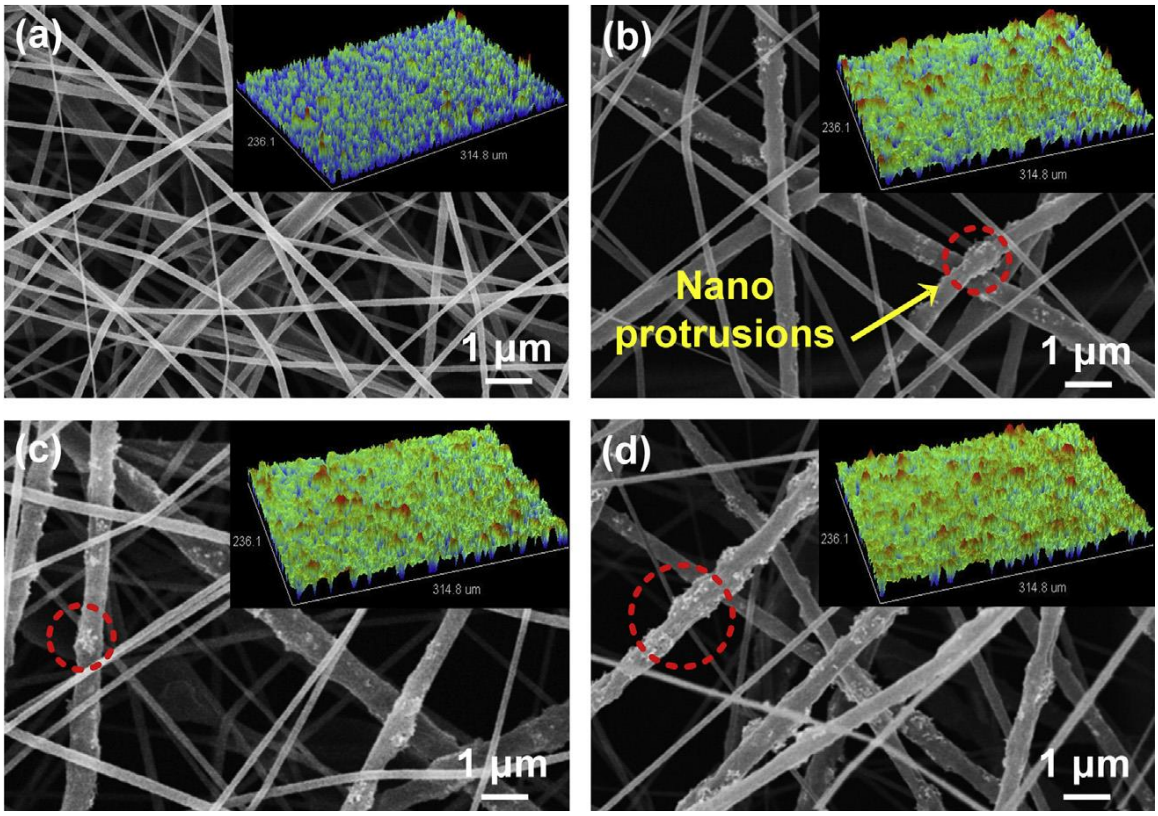


Figure I.22: SEM images of (a) pristine PAN and PAN/SBA-15 (b) with 4wt% of silica, (c) with 8wt% of silica (d) with 12wt% of silica [189]

It has been revealed from experimental results that mesoporous silica nanoparticles maintain their mesoporous structure even after being incorporated within the electrospun hybrid nanofibers and their mesopores are still accessible [190]. The specific surface area, average pore size and pore volume of the mesoporous silica nanoparticles incorporated nanofibers are smaller than those of pristine mesoporous silica nanoparticles and limited percent of mesoporous within the composite nanofibers are still accessible (less than 50% of the total mesopores) [138]. However the specific surface area of the composite nanofibers is higher than that of pristine nanofibers [138,189, 191].

1.6.3 Dispersion of silica nanoparticles in solvent

The silica nanoparticles when dissolved in solvent are physically associated with each other. The reason behind such a phenomenon of aggregation or forming bundles is that SBA-15 are attracted to each other by molecular forces (Van der Waal's forces + Hydrogen bonding) and most importantly, they have an extreme high aspect ratio, which favors the agglomeration of nanoparticles. Whereas, it is requirement of most applications that silica nanoparticles in composite nanofibers to be individual and well dispersed for preferred orientation along the fibers axis. Usually the goal of silica nanoparticles orientation within the nanofibers composite is to get benefit from their high aspect ratio in reinforcing, increasing surface area and other characteristics, along with the need of keeping the nanofibers as much thinner as possible to increase the interface with the target environment. This is the reason why the dispersion of silica nanoparticles in the target medium is of great importance. The aggregates of silica nanoparticles in PAN film is shown in figure I.23.

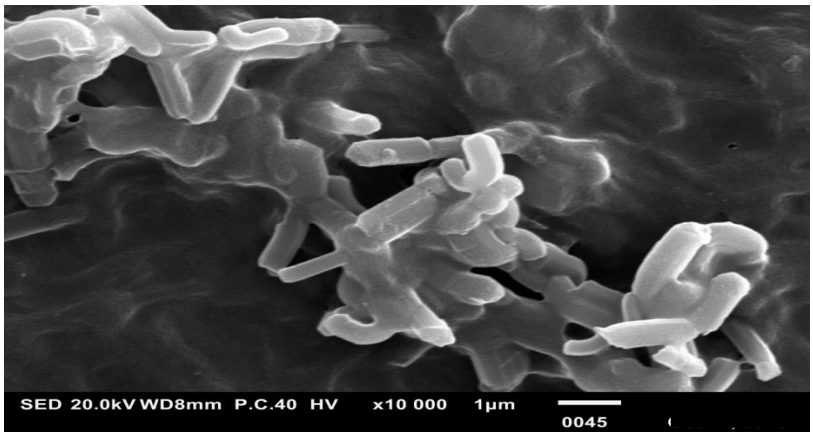


Figure I.23: SEM image of SBA-15 aggregates

For dispersion of silica nanoparticles from their aggregates, there are two main approaches; first is mechanical methods like ultrasonication, high shear mixing, high impact mixing, grinding and mixing, etc. and second is chemical methods by using surfactant, dispersing agent or surface modification of silica nanoparticles by chemical functionalization [16]. To the best of our knowledge and intensive literature research, there is not any scientific work published on dispersion of SBA-15 ordered mesoporous silica in a polymer solution by mechanical or chemical methods. The both methods are discussed below.

1.6.3.1 Mechanical dispersion

The mechanical dispersion of fillers implies the application of high shear stress to separate the fillers from their aggregates. Such stress can be obtained by ultrasonication or high shear mixing. The act of applying sound energy to agitate particles in a sample or solution is ultrasonication. It uses the principle of bubble cavitation which is followed by a sequence implosion to yield a high local shear needed for separation for individual fillers from their aggregates. Bubble cavitation and implosion are yielded from a successive production of compression and vacuum waves. There are four successive phases of cavitation and implosion phenomenon [192] as shown in figure I.24 [193].

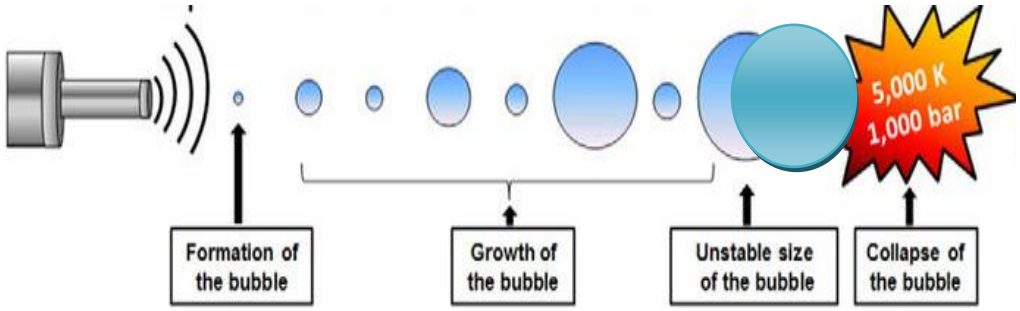


Figure I.24: Illustration of ultrasonic bath principle [193]

In phase 1, bubble nucleation takes place where numerous gaseous bubbles are formed and enlarged, to form microscopic gaseous cavities in the liquid solvent. In phase 2, a high pressure is exerted on the newly expended bubbles compresses them which cause a very high increase in the gas temperature inside the bubble until it collapses on itself which is phase 3 and implodes. In phase 4, when the bubble implodes, it releases a certain amount of energy which impacts, in turn, the surface of fillers aggregates. This leads to exfoliate or peel off the fillers aggregates, resulting in individualizing the sub-micron particles.

The size of the cavitation bubbles strongly depends on the frequency of the propagated ultrasonic waves, the higher the frequency applied the size the bubbles will be smaller. Big size bubbles having low frequency releases higher energy than small ones. However, higher frequencies produce more bubbles in unit time and enables better cavitation distribution per surface unit. Ultrasonication technique is very common tool used to disperse carbon nanotubes in low viscosity liquids [194, 195]. Nevertheless ultrasonication is also widely used in dispersing nanoparticles; aggressive and prolonged sonication may shorten the carbon nanotubes [196].

Another mechanical method of fillers dispersion is high shear mixing in either low viscosity fluids like organic solvents or high viscosity matrix like polymer solution. This process generates high shear stress, which impacts the aggregates of fillers and reduces their size consequently. Rotor/stator is the most common system that is used for high shear generation, which is shown in figure I.25.

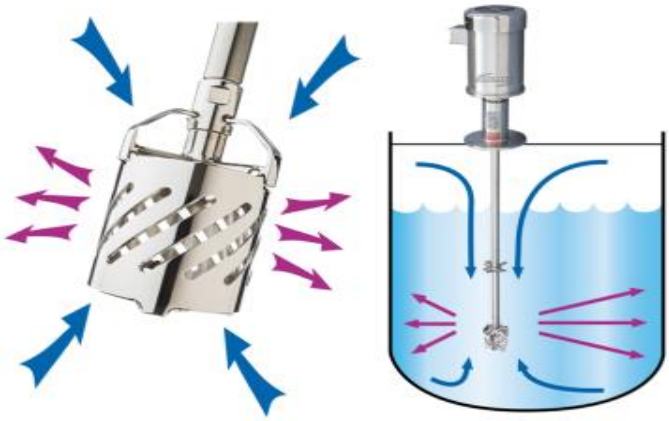


Figure I.25: High shear mixing in rotor-stator system [193]

Due to high speed of rotor, the aggregates of fillers present in the solvent medium are drawn in the axial direction into the head of dispersion and then pressed in the radial direction through the gaps of rotor-stator system, so that the material is subjected to high shear forces. In addition, in the interstice between the rotor and stator, a high turbulence is developed which gives an optimal mixing of the dispersion. High shear mixing has been used for a dry powder of raw multi wall nano tubes of carbon at 24000 rpm for 5 minutes and it was found that the average size of aggregates was reduced 5 times of their original size [194]. High shear mixing was also found a very effective method for the dispersion of purified single walled carbon nanotubes in super acid

dope (120% H_2SO_4 of which 20% excess SO_3) [197]. In this work a high shear mixing for 72 hours at 3500 rpm, using a rotor/stator homogenizer and as a result higher shear mixing gave stable and homogeneous dispersion of single wall nanotubes in super acid medium.

1.6.3.2 Chemical dispersion of fillers

Dispersion of fillers in a solvent or polymer solution by the chemical process implies the modification of surface energy of the nanoparticles to enhance the wetability or the physical affinity of the particles. Such modification in surface energy has the tendency to disrupt the Van der Wall's forces and Hydrogen bonding that attracts the nanoparticles to each other and thus results in hindering the nano fillers to reaggregate. Dispersion of nanoparticles by non-covalent or physical treatment can be achieved by adding some type of dispersing agent or surfactant into a suspension of nanoparticles of filler in a solvent pretreated by some type of mechanical dispersion.

Here, an example is explained to clarify the mechanism of the synergetic effect of ultrasonication or shear mixing followed by adding a dispersing agent in yielding uniform dispersion of fillers in an aqueous medium [198]. As discussed before, the mechanical dispersion has the role of creating high local shear stress that promotes the exfoliation of the fillers from their aggregates. (i) once the tiny gaps are formed, (ii) the dispersing agent diffuses into those gaps and starts to deaggregate the nanoparticles by steric or electrostatic repulsions and as a result the previously formed gaps propagate (iii) leading to ultimately separating nanoparticles from their aggregates.

1.7 Conclusion

Dyes are some chemicals which are used in many industries like textile, paper, leather, etc. The removal of dyes from the waste water is necessary as these are very harmful for aquatic life and as well as for human life. There are many techniques for removal of dyes which include chemical, biological and physical. Among all these techniques, adsorption is very popular technique due to its simple design and operation, insensitivity of toxic substances and possibility to operate at very low concentration. There are many types of nanoparticles adsorbents used but these nanoparticles have some limitations as they are likely to enter the aquatic environment in all stages of nanomaterials life cycle and are toxic for human bodies. Therefore, the development of new barrier materials like nanofibers web are needed which have very large specific surface

area, very small pore size and high porosity and have been shown to improve the efficiency of conventional materials used for the filtration and separation of particulate materials. Mesoporous silica materials are highly ordered hexagonal unidimensional cylindrical mesopores which are chemically and mechanically stable. They have high BET surface area, high pore volume and narrow pores size distribution. The addition of silica nanoparticles in polymer nanofibers increased their surface area and made the surface rough. Silica nanoparticles can be deagglomerated in the composite by using some chemical or mechanical methods.

Next chapter will present in details the preparation of PAN and PAN/filler solutions in DMSO, the electrospinning conditions and techniques used to characterize the electrospun composite and pristine PAN nanofibers. These techniques include SEM, TGA, viscosity measurement, nanoparticles sizes, X-ray diffraction, EDX, FTIR, BET surface area measurement and tensile strength measurement. Here solution making of different dyes in distilled water will also be studied and later on, their adsorption of these dyes on fillers, composite nanofibers and pristine PAN nanofibers will be mentioned. Different parameters on which adsorption depends like pH, temperature, concentration, impact of time and adsorption models including pseudo 1^{st} and 2^{nd} order kinetics, Langmuir and Freundlich isotherm will also be described. At the end desorption and recyclability of adsorbate will be checked to reduce the product cost.

Chapter II

Materials and methods

Chapter II

Materials and Methods

Introduction

This chapter will discuss the selection of raw materials and the methods used to prepare composite sub-micron fibers of PAN/filler by electrospinning process. The produced nanofibers are constituted of mainly two components: polyacrylonitrile polymer as matrix and SBA-15 as additive phase. The description of SBA-15 synthesis and production of polymer solution, polymer/filler solution with and without BYK as dispersing agent is mentioned. Three different dyes, Methylene blue (MB), Neutral red (NR) and Congo red (CR) are selected as adsorbates and their solution preparation of different concentrations are mentioned whereas the mechanism of adsorption and the adsorption parameters are also explained in this chapter.

2.1 Materials

2.1.1 Polymer and Solvent

Polyacrylonitrile (PAN) has been selected in this study as a carrier of filler due to its excellent electrospinnability, low cost and good mechanical properties [94, 140]. PAN is a semi-crystalline [16] polymer of an average molecular weight (Mw) of 150,000 g/mol and it has a density of 1.184 g/ml at 25^{o}C. PAN was purchased from Sigma Aldrich (France).

Dimethyl sulphoxide (DMSO) with purity of 99.8% was purchased from Sigma-Aldrich (France). It has a molecular weight of 78.13 g/mol and a density at 20^{o}C of 1.1g/cm^{3}. PAN powder and DMSO are used as received without any further purification. Figure II.1 gives the formula of PAN and DMSO.

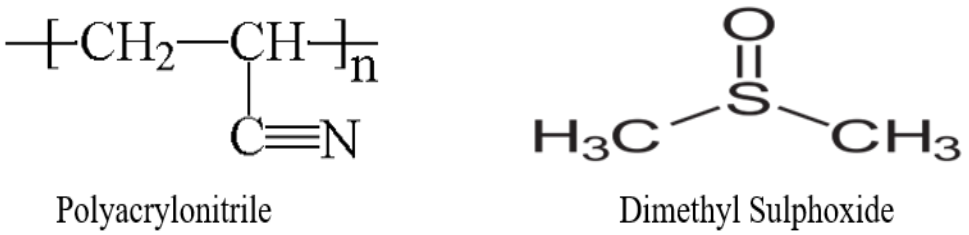


Figure II.1: Formulas of PAN and DMSO [199]

The strength of physical bonding of the material is represented by solubility parameter (δ) which is sum of the dispersion (δ_d), polar (δ_p) and hydrogen bonding (δ_h) contributions ($\delta^2 = \delta_d^2 + \delta_p^2 +$

δ_h^2). DMSO has the overall solubility parameters close to PAN, these overall solubility parameters at 25°C are mentioned in table II.1.

Table II.1: Overall and individual solubility parameters of PAN and DMSO at 25 °C [199]

Solubility parameter ($MPa^{1/2}$)				
Material	**δ**	**δ_d**	**δ_p**	**δ_h**
PAN	25.3	18.2	16.2	6.8
DMSO	26.6	18.4	16.4	10.2

The results indicate that DMSO has strong and more consistent polarization of molecules which produces PAN solution more stable and tolerable to the environmental conditions.

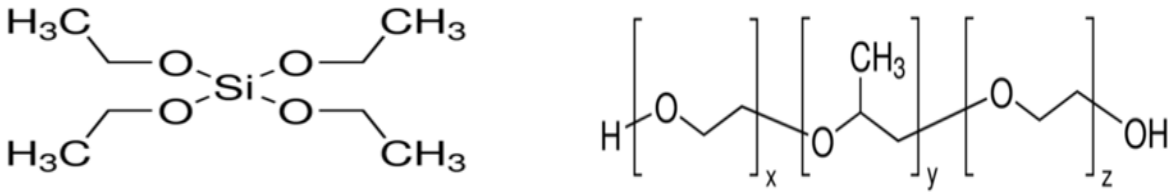
2.1.2 Mesoporous silica type SBA-15

The filler used in this study is rod-like SBA-15 type ordered mesoporous silica particles synthesized via sol-gel method and in the presence of P123 an amphiphilic triblock copolymer. SBA-15 materials were prepared according to Zhao *et al.* [184] procedure as follows:

- **Constituents molar ratio:** 1.0 TEOS: 0.017 P_{123}: 5.6 HCl: 197 H_2O
- **Reagents sources:**
  - ✓ Pluronic P_{123} ($[(PEO)_{20}(PO)_{70}(PEO)_{20}]$, Aldrich) as porogen agent
  - ✓ Tetraethyl orthosilicate (TEOS, Aldrich, 98%) as silica source
  - ✓ Hydrochloric acid (HCl) 37%
  - ✓ Distilled water (H_2O)
- **Gel preparation**

1. In a polypropylene bottle, 3.5 g of P_{123} was dissolved in 16.5 mL of HCL 12M and 111.75 mL of H_2O. The solution was heated at 40°C and maintained under vigorous stirring for 3 hours.
2. After complete dissolution of $P_{123,}$ TEOS (7.427g) was rapidly added to P_{123} acidic solution and the mixture was ripened at 40 °C for 2 hours without stirring.
3. The mixture was then transferred to oven for further condensation at 90 °C under static conditions for 24 hours.

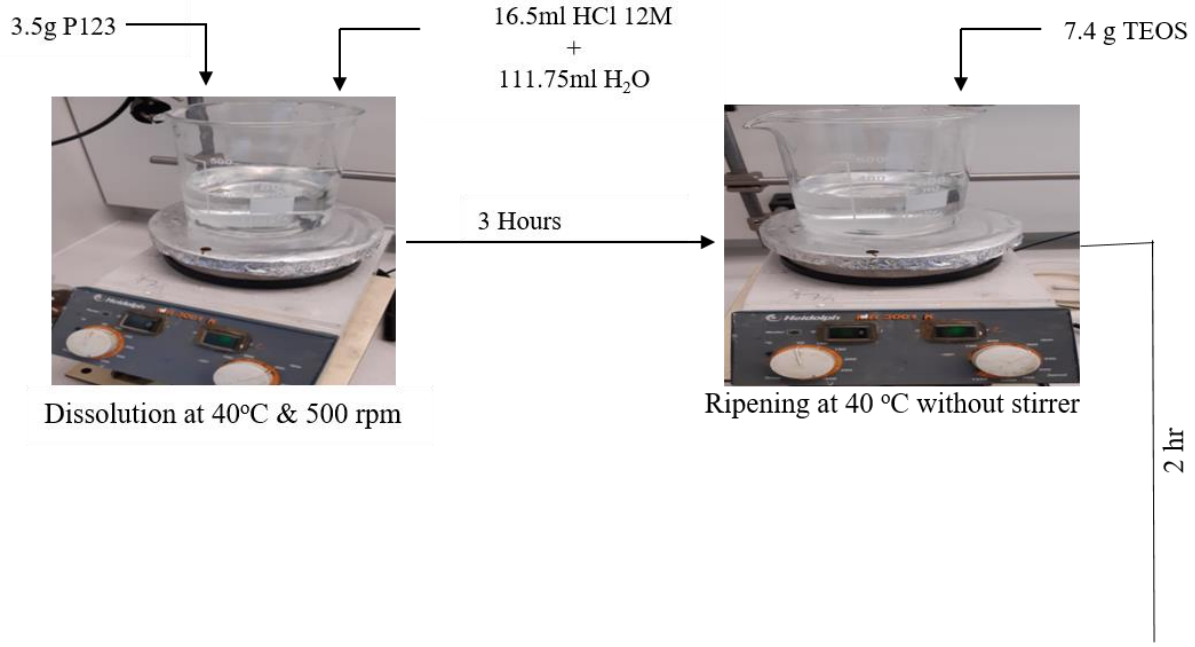
4. Finally, the product was recovered by filtration, washed with distilled water and dried at 70 °C for 48 hours.
5. To remove P_{123} and liberate the porosity, the as-synthesized materials were calcined at 500 °C under air for 4 hours in muffle furnace. The formulas of TEOS and Pluronic P_{123} are displayed in figure II.2.



Tetraethylorthosilicate Pluronic P123

Figure II.2: Formulas of TEOS and Pluronic P_{123} [200]

In figure II.2, X=Z=20 and Y=70 denote degrees of polymerization. Figure II.3 illustrates the followed procedure for the synthesis of SBA-15 powder.



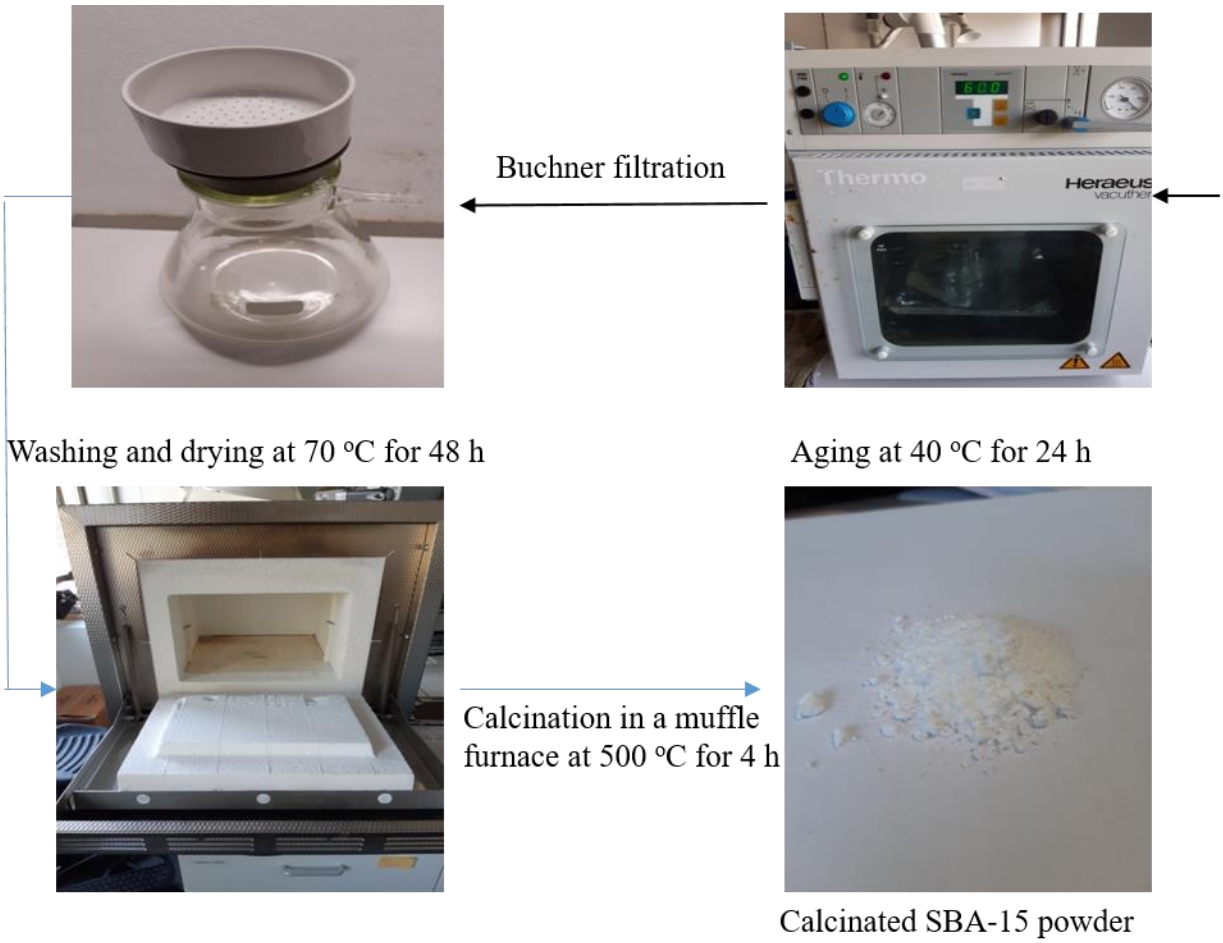


Figure II.3: Synthesis of SBA-15 according to Zhao *et al*. [184]

Table II.2 gives the theoretical composition of reagents used for the synthesis of SBA-15 type mesoporous silica.

Table II.2: Summary sheet of SBA-15 mesoporous silica particles synthesis

Theoretical composition	**P_{123}**	**H_2O**	**HCl**	**TEOS**
Molecular wt. (g/mol)	5800	18	36.5	208.3
Molar composition (mol)	0.017	197	5.6	1
Theoretical quantity (g)	4	126.8	19.4	9.1
Experimental quantity (g)	4.046	127	19.5	9.1

2.1.3 Dispersing agent

In this study, different dispersing agents are used for better deagglomeration of fillers present in polymer solution. Three different types of dispersing agents were introduced and their quantity was optimized and the best was used for further deagglomeration. Their names are mentioned below,

- BYK W 9010
- BYK W 980
- BYK W 966

These all dispersing agents were kindly given by BYK Company (Germany). All These dispersing agents prevent particles agglomeration by steric effects. The addition of these dispersing agents results in a fine and homogeneous distribution of solid particles in liquid media that insures the long-term stability of this system. The sample of BYK W 9010 was analyzed and its formula is given in figure II.4,

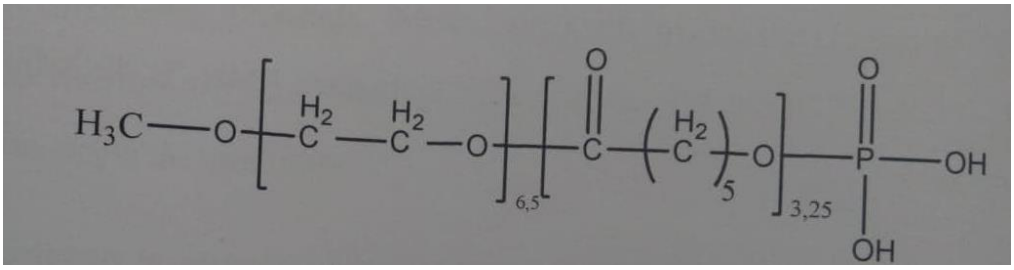


Figure II.4: Formula of BYK W-9010

2.1.4 Dyes

In this study Methylene Blue (MB), Neutral Red (NR) and Congo Red (CR) has been used. All the dyes were purchased by Sigma-Aldrich. Some properties of dyes are mentioned in table II.3 and in figure II.5 chemical formulas are given. These dyes are selected in this study for adsorption because these are most commonly used in acrylic, silk, cotton, nylon, wool, leather, plastic and paper dyeing. Due to their large consumption, there is a large possibility of bulk release of these dyes as wastewater. 28.8 mg of MB dye, 26 mg of NR and 62.7 mg of CR dye were dissolved in 1000 mL of deionized water for preparing 90µM stock solution for MB and NR dyes and 45 µM stock solution for CR dye. All experimental solutions were prepared by subsequently dilution required of the stock solution with deionized water.

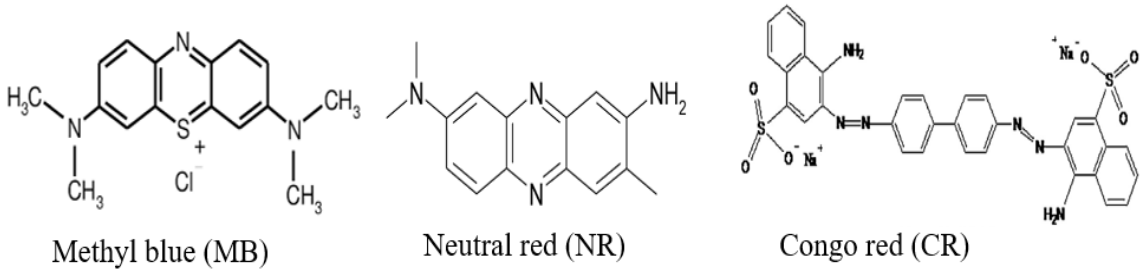


Figure II.5: Structural formula of methylene blue, Neutral red and Congo red [3, 5]

Table II.3: Properties of MB, NR and CR dyes [3, 5]

Molecular formula	**Molecular weight (g/mol)**	**Wavelength of the maximum UV-Vis absorption λ_{max} (in water)**
$C_{16}H_{18}ClN_3S$	319.8	668 nm
$C_{15}H_{17}N_4$	288.8	529 nm
$C_{32}H_{22}N_6Na_2O_6S_2$	696.6	499 nm

Screening criteria was used for the selection and categorization of the collected adsorbents [9]. These criterias are based on adsorption or removal efficiency (S %) of all selected dyes. From this categorization as shown in figure II.6, the best adsorbent was optimized and can be used further in batch or column reactor.

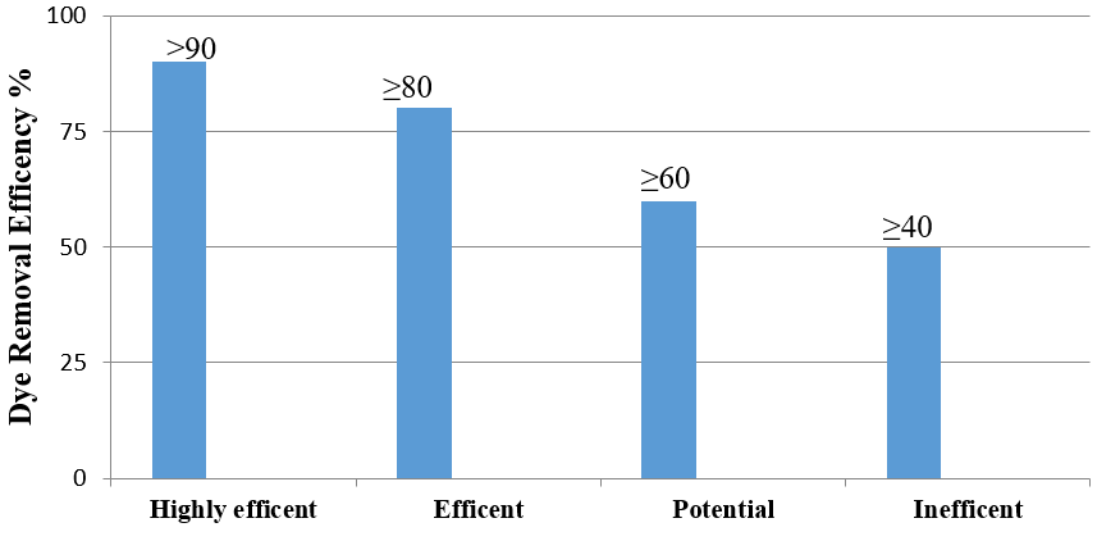


Figure II.6: Adsorbent performance criteria [9]

2.2 Methods

This part of chapter describes the detail process of preparation of PAN solution, PAN+SBA-15 solution and PAN+SBA-15+ dispersing agent solution in dimethyl sulphoxide (DMSO). In this section, electrospinning conditions of needleless electrospinning machine and techniques used to characterize the resultant electrospun composite nanofibers are explained. These techniques include SBA-15 particles size measurement in solvent by Zetasizer and Mastersizer, viscosity measurement by Rheometer, Scanning electron microscope for observing the nanofibers and SBA-15 particles morphology, small angle X-ray diffraction for the structural analysis of SBA-15 particles, thermo-gravimetric analysis (TGA) for investigating the thermal stability of pristine PAN and composite nanofibers, FTIR Fourier Transform Infrared (spectroscopy) for analysis of different functional groups present in polymer and composite nanofibers, tensile strength measurement of nanofibers, EDX energy-dispersive X-ray spectroscopy coupled with SEM was used for elemental analysis or chemical characterization of the composite nanofibers and volumetric nitrogen adsorption/desorption analysis to investigate the textural properties of SBA-15 and composite nanofibers with and without dispersing agent. At the end, the composite nanofibers were characterized by batch screening of adsorbents. The equilibrium, kinetic and dynamic behaviors of the adsorption process was then evaluated to study the adsorption of methylene blue, neutral red and congo red molecules onto the prepared composite nanofibers with and without dispersing agent.

2.2.1 Preparation of formulations for electrospinning

Here the preparation of PAN solutions in DMSO is introduced and the dispersion of used filler in DMSO by introduction of a dispersing agent followed by a mechanical treatment is explained.
To study the effect of polymer concentration on the electrospinning of PAN solution, eight solutions with concentration 5, 6, 7, 8, 9, 10, 11 and 12 wt% were prepared. The prepared solution is 25 g and the ratio of PAN and solvent is mentioned in table II.4.

Table II.4: PAN solution composition in DMSO

Sr No.	**PAN Concentration (wt %)**	**PAN wt (g)**	**DMSO wt (g)**
1	5	1.25	23.75
2	6	1.5	23.5

3	7	1.75	23.25
4	8	2.0	23
5	9	2.25	22.75
6	10	2.5	22.5
7	11	2.75	22.25
8	12	3.0	22

Ultra Turrax stirs the solutions at room temperature at 1000 rpm for 40 minutes. After Ultra Turrax, shear stirring, magnetic stirrer at 300 rpm stirred the solution again for 24 hours at room temperature.

2.2.1.1 PAN/SBA-15/DMSO formulations

Two sets of PAN/SBA-15 solutions in DMSO were prepared having total weight 25 g, one with dispersing agent and other without dispersing agent. Each set consists of eight solutions having PAN from 5 to 12 wt%. In each solution, the ratio of SBA-15 with PAN is 1:5 w/w and the solutions having dispersing agent BYK W9010, have 1wt% of BYK W9010 with respect to weight of SBA-15. For adding 1wt% (w.r.t SBA-15 wt.) dispersing agent in PAN/SBA-15 suspension, 10wt% of BYK W-9010 solution in DMSO was prepared.

Table II.5 gives the exact amount of SBA-15 and dispersing agent in 25 g of solution for different concentrations.

Table II.5: Amount of SBA-15 and dispersing agent in DMSO

PAN Concentration %	**PAN (g)**	**SBA-15 (g)**	**BYK W-9010/DMSO solution (µg)**	**DMSO (g)**
5	1.25	0.25	22.5	23.5
6	1.5	0.3	27	23.2
7	1.75	0.35	31.5	22.9
8	2.0	0.4	36	22.6
9	2.25	0.45	40.5	22.3
10	2.50	0.5	45	22
11	2.75	0.55	49.5	21.7

12	3.0	0.6	54	21.4

For making PAN/SBA-15/BYK W9010 solutions in DMSO, each time calculated amount of dispersing agent was added before the addition of filler. After incorporation of BYK W9010, calculated amount of SBA-15 was inserted and for this suspension high shear homogenizer (Ultra-Turrax T-25-IKA-France) at 1000 r.p.m for 20 minutes is used. This step has a goal of breaking down the aggregates of silica particles. Calculated quantity of PAN (grams) was then added to the prepared suspensions to obtain the required PAN concentration (wt %) in each electrospinning solutions. The resulting solution was stirred again by Ultra-Turrax at 1000 r.p.m for 40 minutes at room temperature. After the high shear mixing for 40 minutes, the solution was put on magnetic stirrer for 24 hours at 300 r.p.m at room temperature, so that solution may become homogenous and stable before electrospinning.

2.2.1.2 Viscosity measurement

Viscosity of polymer solution is very important parameter for manufacturing of electrospun nanofibers. Viscosity gives the idea about the structural properties of resultant nanofibers. It also helps in prediction about the behavior of polymer solution during electrospinning process. In general, a solution is electrospinnable if the polymer jet remains unbroken until dry fibers are formed. To measure the viscosity, Anton Paar MCR 302 model of Rheometer (as shown in figure II.7) with “Plan Plan mode” was used. Shear rate of the process was varied between 1-200/sec and the temperature was fixed at 20 ^{o}C. Each sample was run for 320 seconds. Specific viscosity was also measured, which is incremental viscosity due to presence of polymer in the solvent.

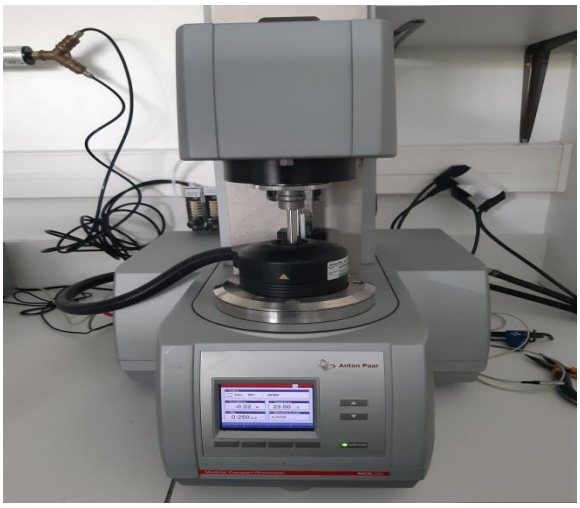


Figure II.7: Rheometer MCR 302

2.2.1.3 Electrospinning conditions

The prepared PAN and PAN/Filler solutions in DMSO with and without dispersing agent are electrospun directly by needleless electrospinning machine, named Nanospider^{TM} delivered by Elmarco Company Czech Republic shown in Figure II.8.



Figure II.8: Elmarco Nanospider

This set up is consisting of closed cylindrical cabin and that cabin is composed of cylindrical base frame, metallic feed system, carriage and its linear slide drive. The carriage is driven by pneumatic system: compressed air must be connected after the carriage module is connected. The carriage module of spinning utilizes a stationary spinning electrode wire on which continuous spinning solution is deposited by a special carriage. The carriage works as moving reservoir of polymer solution that has a calibrated metal orifice inserted through which wire is drawn. The

spinning solution flows out slowly from the orifice during movement of carriage and is applied on the wire surface. During this wetting process of wire, neither the evaporation of the spinning solution from the free surface, nor the drying of the polymer on the wire occurs, nor is the wire continuously rewound. Due to the high applied voltage on the solution wire and collector wire that is at the top of electrospinning cabin, nanofibers are formed and they move upward towards the collector wire. Figure II.9 shows the parts of inner portion of electrospinning cabin.

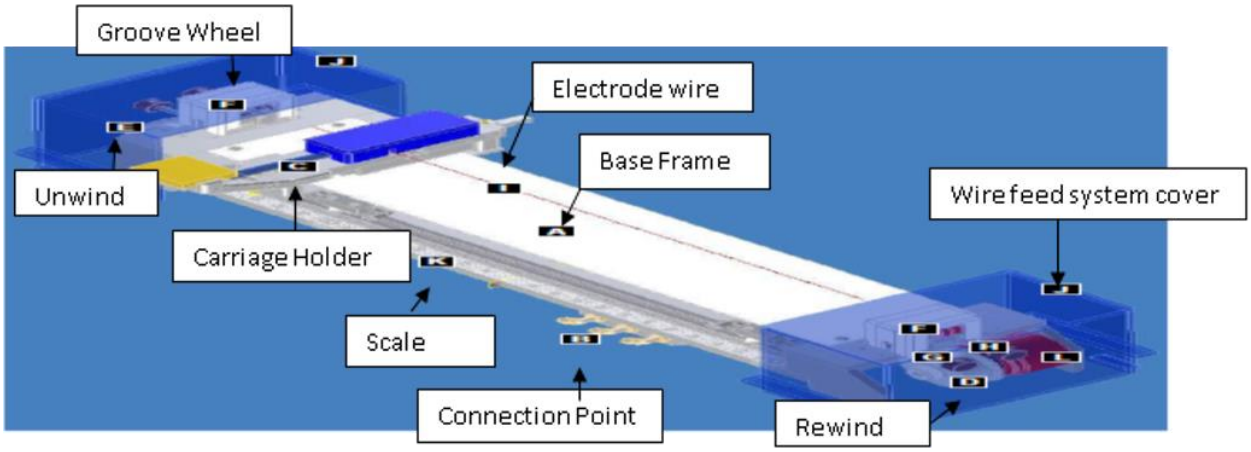


Figure II.9: needleless electrospinning cabins

The most important part of needleless electrospinning cabin is carriage that is shown in figure II.10 and it delivers fresh spinning solution on the surface of grounded wire.

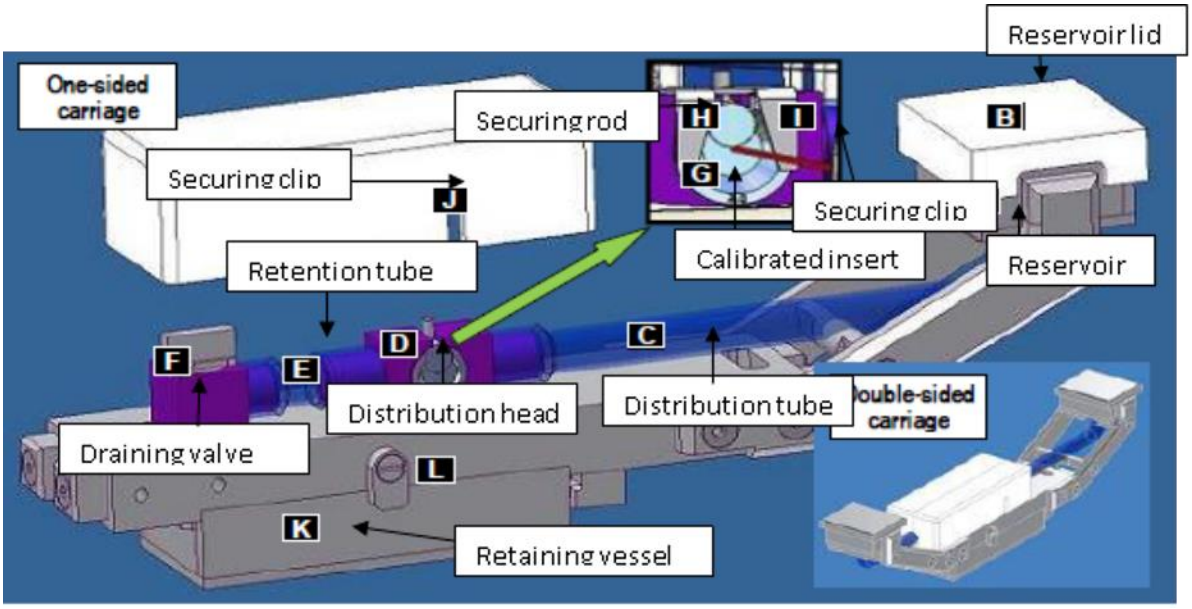


Figure II.10: Parts of carriage

Tube is the main part of carriage and it is connected to the fresh spinning solution reservoir, a calibrated metal insert and a tub connected to the solution outlet with the draining valve. The spinning solution flows through the tube and leaks partially from the calibrated insert through which bottom wire is led. Coating of the wire with the spinning solution is accomplished by movement of the carriage forwards and backwards. A homogeneous layer of the solution is achieved by the precisely designed calibrated insert and proper setting of wire position in the insert orifice. Used solution is collected in the retaining vessel.

2.2.1.4 Electrospinning of PAN solution

PAN solutions mentioned in table II.4 were electrospun with maintaining the nozzle size 0.8 mm and varying the applied voltage 30, 50, 70 kV. The collecting distance (distance between the bottom wire and collector wire) also varied between 12.5, 15 and 20 cm. All the electrospinning parameters of needleless electrospinning machine are mentioned in tableII.6.

Table II.6: Electrospinning parameters

PAN concentration (wt %)	5 to 12
Voltage (kV)	30, 50, 70
Collecting distance (cm)	12.5, 15, 20
Nozzle size (mm)	0.8
Relative Humidity (RH%)	33±2
Temperature ^{o}C	21±2
Wire speed (mm/sec)	0.5
Carriage speed (mm/sec)	180
Time of sampling (min)	15

2.2.1.5 Electrospinning of PAN+SBA-15 formulations

PAN+SBA-15 solutions (mentioned in table II.5) with and without dispersing agent were electrospun in two trials: In the first trial collecting distance was fixed at 12.5, 15 and 20 cm alternatively with nozzle size 0.8 mm and applied voltage was varied between 30, 50 and 70 kV for 15 minutes of each sample. The other parameters like temperature, wire speed, relative humidity and carriage speed remained constant as in table II.6. The second trial was executed by

fixing applied voltage at 30, 50 and 70 kV alternatively and varying the collecting distance at 12.5, 15 and 20 cm. The other parameters remained constant. Figure II.11 illustrates the procedure of preparing PAN/filler solution and electrospinning setup.

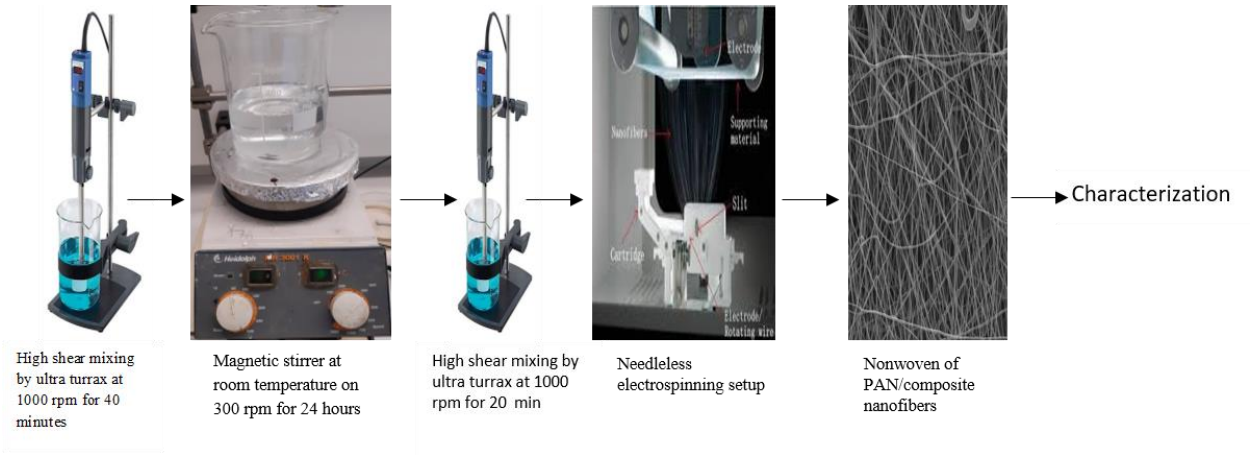


Figure II.11: Schematic representations of PAN/Filler composite nanofibers elaboration

2.2.2 Suspensions preparation of dispersing agents

Three types of dispersing agents were used in this study. The best dispersing agent was selected by measuring the particles size of SBA-15 suspensions in DMSO with 1 wt% compared to SBA-15 particles. The optimal amount of the selected dispersing agent was also determined from particles size measurements of SBA-15/DMSO suspensions containing from 0.5 to 2 wt% of dispersing agent. SBA-15 was dispersed in DMSO in the presence of dispersing agents, whose quantity is measured (as mentioned in 2.2.1.1) with respect to the weight of fillers and used ultra Turrax for 10 minutes at 1000 r.p.m before measuring the particles size in Zetasizer at room temperature. Table II.7 gives the exact weight of all types of dispersing agents used, as compared to the weight of fillers.

Table II.7: Weight of all dispersing agent w.r.t. fillers weight

BYK Type	Wt.% of BYK	Weight of BYK solution	Weight of SBA-15	Weight of DMSO
BYK W9010	0.5	11.25µg	0.25g	0.8271g
BYK W980				
BYK W966				
BYK W9010	1	22.5µg		
BYK W980				

BYK W966				
BYK W9010	1.5	33.75µg		
BYK W980				
BYK W966				
BYK W9010	2	45µg		
BYK W980				
BYK W966				

2.2.3 Zetasizer and Mastersizer

The dynamic light of diffusion in Zetasizer nanoseries (from Malvern Company) makes it possible to measure the sizes of colloidal particles suspended in a liquid from sub-nanometer to several micrometers in diameter (fields of applications are paints, pastes, cosmetics, food industry etc,). Its principal is based on the measurement of the diffusion speeds of particles subjected to Brownian movement. In solution, particles move under the effect of thermal agitation and interparticle collisions, which generate fluctuations in the intensity of the scattered light. These fluctuations can then be correlated with hydrodynamic diameter of the particles, comprising the particle and its solvation layer. The essential point in the quality measurement of the size of the particle is the capacity to present in front of the optical part of the instrument like a well dispersed sample at an appropriate concentration. In Zetasizer, the mono chromatic light of a He-Ne laser of wavelength equal to 632.8nm is used.

The Mastersizer 3000 (from Malvern Company) uses the technique of laser diffraction to measure the particle size and particle size distribution of materials. It does this by measuring the intensity of light scattered as a laser beam that passes through a dispersed particulate sample. Then this data is analyzed to calculate the size of the particles that created the scattering pattern. Mastersizer can deliver the measurements of different particles in the range of 10 nm to 3.5 mm. For the diffusion speed measurement, the speckle pattern produced by illuminating the particles with a laser is observed. The scattering intensity at a specific angle will fluctuate with time and this is detected using a sensitive avalanche photodiode detector. The intensity changes are analyzed with a digital auto correlator, which generates a correlation function. This curve is analyzed to give the size and size distribution. This distribution can be defined by different values: dv10, dv50 and dv90 which

correspond respectively to 10%, 50% and 90% cumulative volume of particles over the particle size distribution in percentage cumulative.

2.3 Characterization of materials

Nanofibers obtained after electrospinning process, were analyzed for many structural and performance properties. A brief description of different tools used for these characterizations is mentioned below.

2.3.1 Scanning Electron microscopy (SEM) of SBA-15, PAN/SBA-15 electrospun composite nanofibers (SEM)

The morphology of pristine PAN nanofibers and PAN/SBA-15 composite nanofibers with and without dispersing agent was characterized by scanning electron microscope (SEM) (JEOL JSM-IT 100) as shown in figure II.12 (a). All the samples were analyzed at three different magnifications, i-e x500, x5000 and x20000. Prior to analysis, the nonwovens of the nanofibers are gold-coated (figure II.12 (b) in order to render their surface conductive for SEM purpose. Upon the acquired SEM images, diameters of 100 different nanofibers of each nonwoven were measured using Image J 1.45S software. Diameter is measured along the nanofibers axis where there are no obvious aggregates. The average diameter, standard deviation and coefficient of variation of each sample are calculated and results are plotted using Microsoft Excel.



Figure II.12 (a): SEM JEOL JSM-IT 100



Figure II.12 (b): Sample for SEM

2.3.2 X-rays diffraction (XRD) analysis of SBA-15

The structure of SBA-15 was analyzed by small angle PANalytical X'Pert PRO MPD X-ray diffractometer as shown in figure II.13. XRD analysis is carried out by using X-ray diffractometer at a step of 0.02^{O} in a 2θ range of 0.5-10^{o} for SBA-15 particles. The wavelength of the X-ray beam is 0.15418 nm (Cu kα radiation). XRD analysis is based on constructive interference of monochromatic X-rays and a crystalline sample. X-rays are generated by cathode rays tube, filtered to produce monochromatic radiation, collimated to concentrate and directed toward the sample. The interaction of incident rays with the sample produces constructive interference and a diffracted ray, when conditions satisfy Bragg's law ($\lambda=2d\sin\theta$). This law relates the wavelength of electromagnetic radiation to the diffraction angle and the lattice spacing in a crystalline sample.



Figure II.13: PANalytical X'Pert PRO MPD X-ray diffraction

2.3.3 **Thermogravimetric analysis (TGA) of electrospun composite nanofibers**

Thermal stability of pristine PAN nanofibers and PAN/SBA-15 composite nanofibers with and without dispersing agent was studied using thermogravimetric analysis (TGA-DTA). Thermo-gravimetric analyses of SBA-15, pure PAN powder, pristine PAN nanofibers, PAN/SBA-15 composite nanofibers and PAN/SBA-15+BYK W-9010 composite nanofibers were performed by using a TG Q500 apparatus (figure II.14). Each sample from 5 to 10 mg approximately was heated under air or under nitrogen (60mL/min air flow rate or 40mL/min N_2 flow rate) from 25 ^{o}C to 800 ^{o}C. The heating rate was set at 10^{o}C/min.

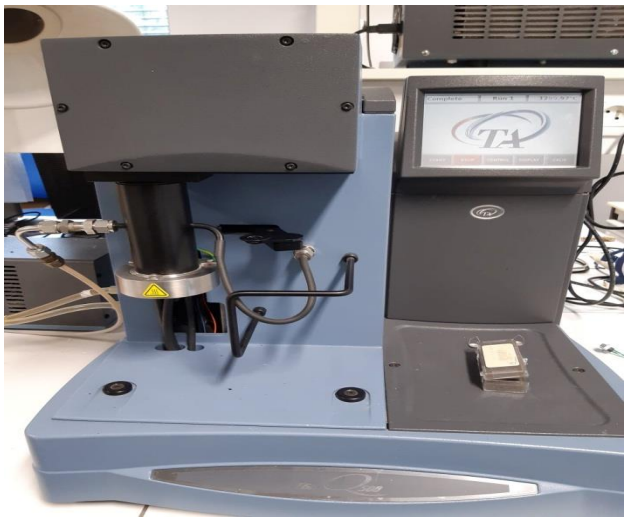


Figure II.14: TG Q 500

2.3.4 **Specific surface analysis and porosity (BET and BJH)**

The textural properties of SBA-15 sub-micron particles, PAN/SBA-15 and PAN/SBA-15+BYK W-9010 nanofibers were characterized by means of volumetric nitrogen adsorption/desorption analyses performed on a Tristar (Micrometritics) apparatus (figure II.15 a) at -195 ^{o}C. Before the measurement, all the samples including silica sub-micron particles were out gassed at 80 ^{o}C in vacuum and heated at 150 ^{o}C for 20 hours under the pressure of 0.99 Pa (figure II.15 b). The process of degassing results in the removal of physisorbed water without dehydroxylation. The specific surface area (SBET), pores volume and pores size of the pristine SBA-15 particles and those incorporated into the composite nanofibers were determined by applying BET (Brunauer-Emmett-Teller), KJS (Kruk-Jaroniec-Sayari) and BJH (Barrett, Joyner and Halenda) methods [201, 202].

The specific surface area (S_{BET}) is measured in m^2/g and it can also be calculated by applying the transformed BET equation (2) that is mentioned below, using nitrogen as adsorptive gas [10]:

$$S_{BET} = 4.35\ (V_m/m) \qquad (2)$$

Where:

- V_m is the volume of adsorptive (in cm^3) required to cover the surface of the solid with a monolayer
- m is the adsorbent mass in gram

Pore size is determined by applying BdB equation (3) and using nitrogen as adsorptive gas [16]:

$$r_p - t_e = \frac{-4.15}{\log(\frac{P}{Po})} - \frac{28\left[\left(\frac{r_p}{t_e}\right)-1-Ln\left(\frac{r_p}{te}\right)\right]-0.034(r_p-t_e)2}{(r_p-t_e)\log(\frac{P}{Po})} \quad (3)$$

Where:

- r_p is the pore radius
- t_e is the thickness of the multilayer covering the pore wall at equilibrium.
- (P/P^O) is the relative pressure of equilibrium

Pore volume (V_p) is obtained by applying BJH equation (4) on the desorption branch of the isotherm [10]:

$$Vp\ (i) = \left(\frac{r_{p(i)}}{r_{k(i)+\Delta t_{(i)}}}\right)[\Delta V(i) - \Delta t(i)\sum_{i=0}^{n-1} a_{p(i)} + \Delta t(i)\sum_{i=1}^{n-1}\frac{t_{(i)}}{r_{p(i)}}\, a_{p\ (i)} \quad (4)$$

Where:

- $V_{p(i)}$ is the pore volume
- $r_{p(i)}$ is the pore average radius
- $r_{k(i)}$ is the average Kelvin radius of meniscus
- $\Delta t(i) = t_{(i-1)}$-$t_{(i)}$ is the reduction in the multilayer thickness that covers the empty pores whose radius $r_p > r_{p(i)}$
- $\Delta V(i)$ is the variation in the volume of the adsorbed gas due to the reduction in the pressure
- $a_{p(i)}$ is the surface of pore
- $t_{(i)}$ is the average thickness of the multilayer of adsorbed gas

Pore size distribution is obtained by tracing the ratio $\Delta V(i)/\Delta rp(i)$ as a function of $r_{p(i)}$



Figure II.15 (a): Tristar **(Micrometritics)**



Figure II.15 (b): Degassing process

2.3.5 Tensile strength testing of pristine PAN and PAN/SBA-15 nanofibers

Tensile strength tests of all the nanofibers were performed on MTS 20/M tensile testing machine (figure II.16a) equipped with a pair of pneumatic gripes. To prepare specimens for mechanical characterization, electrospun nanowebs were cut 1×4 cm^2 (figure II.16b) from different area of nanowebs collection surface, then samples were sandwiched between two cardboard layers which functioned as templates. The specimen was placed between the grips of tensile testing machine and before test the template was cut from cutting lines. All the tests were conducted using a 10N load cell with the following parameters: 20mm/min extension rate, 2 cm distance between gripes and without any pre-tension. All tests were performed under textile standard conditions of 20±2 ºC and 65±2% R.H. The thickness of all the samples was measured by electronic micrometer (figure II.17). For each test of tensile strength and thickness, 5 samples were used and then calculated the average value of tensile strength in MPa and thickness in µm.



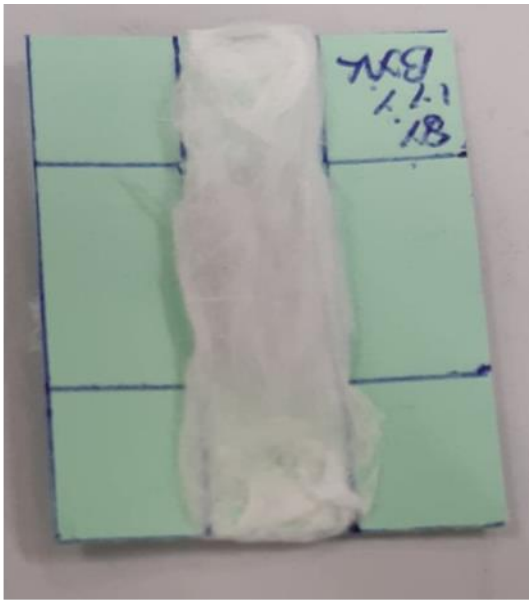


Figure II.16 (a): Tensile testing machine

Figure II.16 (b): Specimen for tensile testing



Figure II.17: Electronic micrometer

2.3.6 Fourier-transform infrared spectroscopy (FTIR)

Fourier-transform infrared Platinum ATR VERTEX 70 spectrometer (shown in figure II.18) was used to analyze the samples of PAN powder, pristine PAN nanofibers and PAN/SBA-15 composite nanofibers with and without dispersing agent. OPUS 7.5software was used for analysis in FTIR. Attenuated total reflectance (ATR) range used was 400-4000 cm^{-1} and sample was scanned for 50 times at room temperature.



Figure II.18: Fourier-transform infrared spectrometer

2.3.7 Energy-dispersive X-ray spectroscopy (EDX)

EDX is a powerful technique that enables the user to analyze the elemental composition of a desired sample. The major operating principal that allows EDX to function is the capacity of high energy electromagnet radiation (X-rays) to eject core electrons from an atom. Removing these electrons from the system will leave behind a hole that a higher energy electron can fill it and it will release energy as it relaxes. The energy released during this relaxation process is unique to each element on the periodic table and as a result sample with X-rays can be used to identify which elements are present, as well as what proportion they are present in. Elemental mapping of PAN/SBA-15 and PAN/SBA-15+BYK W-9010 composite nanofibers was recorded on a JEOL JSM-7900F.

2.4 UV/Visible Spectrophotometer

Spectrophotometer is an optical instrument that can measure intensity of light in relationship with the wavelength. In spectrophotometer, a prism or grating is used for the incident beam to split into different wavelengths. The waves of particular wavelength can be adjusted to fall on the test solution. The main components of spectrophotometer are light source, a device that separates the light into component wavelengths, a sample holder and a detector. A tungsten lamp is used in visible light spectrophotometer but in UV/Visible spectrophotometer a second lamp is used that can measure wavelength up to 1100 nm. In this study 8453 UV/Visible

spectrophotometer of Agilent company (America) is used for the determination of the dye concentration by measuring the UV-Vis absorbance of the supernatant during the adsorption process on all used adsorbents. To measure the UV-vis absorbance bands, 3 mL solution of each dye separately was poured in a cuvette and required quantity (mentioned in 2.5 section) of adsorbent was added to cuvette. After every 10 minutes the maximum of absorbance of MB (λ_{max} = 668 nm), NR (λ_{max} = 529 nm) was measured and after every 25 minutes in the case of CR (λ_{max} = 499 nm). Extra time for adsorption of CR was given due to very slow adsorption rate. The molar attenuation coefficient (is a measure of how strongly a chemical species or substance absorbs light at a particular wavelength) of each dye was measured as "ε = A/cL". Where ε is molar attenuation coefficient, A (a.u) is absorbance of pure dye in solution, c is concentration of dye and L is the length of the cuvette that is 1 cm. The calculated values of molar extinction coefficients for MB, NR and CR are 32020, 11770 and 38170 $mol^{-1}.cm^{-1}$, respectively.

2.5 Dyes solutions preparation

Six different molarity solutions (15, 30, 45, 60, 75, 90 µM) by following equation 5 of methylene blue, Neutral red and for Congo red six solutions (7.5, 15, 22.5, 30, 37.5 and 45 µM) were prepared in flask containing 100 mL of dye solution and were placed in room temperature condition.

$$\text{Molarity (M)} = \frac{\text{mass of solute (g)}}{\text{molar mass of solute } \left(\frac{\text{g}}{\text{mol}}\right) \times \text{volume of solution (L)}} \quad (5)$$

All the solutions were wrapped in aluminum foil to avoid light contact and degradation. For all experiments, 1 mg of SBA-15 particles, 5.72 mg for each PAN/SBA-15 composite with and without BYK W-9010 and 4.72 mg of pristine PAN nanofibers was added in 1 mL of each dye solution and the dye concentration in the supernatant was followed through UV-visible spectrophotometer. In composite nanofibers, filler/polymer ratio is 1: 4.72, therefore quantity of SBA-15 and PAN (mg) is constant in all absorbent samples. The adsorption capacity (q_e) and adsorption efficiency (S %) of the adsorbent were calculated by following equations 6 and 7 respectively,

$$q_e = [(C_0 - C_t)]V/m \quad (6)$$

$$S\% = [(C_0 - C_t)/C_0] \times 100 \quad (7)$$

Where q_e is the dye adsorbed or distributed on the adsorbent surface in mg/g (mg for adsorbent and g for adsorbate), C_0 and C_t are initial and final concentration (g/L) of adsorbate respectively. m and V are the mass of adsorbent (g) and volume of solution (L) respectively. Both adsorption capacity (q_e) and adsorption efficiency (S %) are very important parameters in comparing performance of different adsorbents. q_e gives us an idea about the contaminant amount, that can be adsorbed onto unit mass adsorbent from waste stream. The sorption efficiency is just the removal efficiency of adsorbent irrespective of its amount.

The effects of operational and environmental parameters on dye removal capacity of the adsorbent were examined till equilibrium time, which was established for the respective adsorbent.

2.6 Mechanism of dye adsorption

Dye adsorption is mostly studied in batch reactors where the concentration of dye is kept constant and there is no inflow and outflow stream. In adsorption process, the molecules of dye are adsorbed on the surface of adsorbent till the equilibrium get established between liquid solution and adsorbing surface. Therefore, in batch adsorption, the surrounding fluids and adsorbent approach a dynamic equilibrium after an adequately longer contact time. At this point, the adsorbate is distributed in a defined manner between the adsorbent and solution. The partition ratio indicates the concentration of adsorbate, adsorbed per weight unit of total mass of adsorbent in solution.

The isotherm models depict the primary evidence about the adsorption mechanism. Adsorption data of MB and NR dyes with variable initial concentrations (30 to 90 µM) and for CR dye (7.5 to 45 µM) for different adsorbents was subjected to two different isotherm models. The reaction parameters, i-e temperature (20 ^oC), pH 7, contact time 120 min for cationic dyes and 275 min for anionic dye and adsorbent dose 1mg were kept constant. Among the isotherm models, Langmuir (1918) and Freundlich (1906) were applied.

Equilibrium time is the state of adsorption process, where maximum or removal of dye is attained at given conditions. The samples were prepared by considering the dye solution volume 100mL, dye concentration of 15, 30, 45, 60, 75, 90 µM. The adsorbent was added as mentioned before at room temperature. The samples were withdrawn for analysis at predetermined time intervals. The equilibrium time was established for each adsorbent and the rest of the parameters were investigated till equilibrium.

The dye solution pH is a crucial factor, which can influence directly the adsorption process. The variation in pH can affect the adsorbent surface by increasing, decreasing or neutralizing the positive or negative charges. The change in the surface negativity or positivity respectively, enhances or hinders the adsorption of dye molecules on the surface of adsorbent. Different pH values (2, 5, 7 and 10) were used to assess the effect of pH variation on cationic dye uptake by selected adsorbent. pH was determined with pH paper.

The dye adsorption process can be endothermic or exothermic which depends upon the temperature of the system. The adsorption reaction for any specific adsorbate can be endothermic if q_e of the adsorbent is raised with rise in temperature and exothermic if the conditions are reversed. The quantitative effect of the temperature can vary for adsorbent. Different temperatures (20, 35 and 50 ^oC) were used to find the relationship for varying temperatures on dye removal by respective adsorbent. Different thermodynamics parameters including Gibbs free energy (ΔG^0), enthalpy (ΔH^0) and entropy (ΔS^0) were calculated from equations 8 and 9 respectively.

$$\ln (q_e/C_e) = \Delta S^0/R - \Delta H^0/RT \quad (8)$$

$$\Delta G^0 = -R \times T \times \ln K_L \quad (9)$$

R is the gas constant (8.314 J $K^{-1}mol^{-1}$). Ce and qe are the concentration and adsorbed quantity of dye at equilibrium, respectively. The values of ΔH^0 and ΔS^0 were calculated from the plot and intercept on the plot of $\ln K_L$ and 1/T as described in equation 10.

$$K_L = q_e/C_e \quad (10)$$

Different concentrations of cationic dyes (15, 30, 45, 60, 75, 90µM) and anionic dye (7.5, 15, 22.5, 30, 37.5, 45µM) were used to study the dye removal efficiency and capacity of the studied adsorbent at constant conditions of the adsorbent dose, pH and temperature.

2.6.1 Langmuir isotherm model

The adsorbents which follow the Langmuir isotherm models are assumed having fixed specific sites, each of which adsorbs single dye molecule, making monolayer or single layer to the thickness of individual molecule. The constants calculated by Langmuir model (equation 11) have firmly defined the physical meanings in comparison to that of Freundlich equation [5, 34, 36, 41].

$$q_e = \frac{q_{max} K_L C_e}{1 + K_L C_e} \quad (11)$$

q_e is the adsorption capacity (mg/g) of the adsorbent at equilibrium. q_{max} (mg/g) is maximum adsorption capacity which forms a monolayer on the adsorbent surface, C_e (mg/L) is the equilibrium concentration of dye in solution phase and K_L (L/mg) is the constant associated to likeliness of binding sites and is calculated by slope and intercept. The linear form of Langmuir equation 12 is as follows [5, 34, 36, 41],

$$\frac{C_e}{q_e} = \frac{C_e}{q_{max}} + \frac{1}{q_{max} K_L} \quad (12)$$

The validity of Langmuir model can also be proved through a constant, called equilibrium parameter or dimensionless factor, i-e. $R_L = 1/ (1+K_L C_0)$, which measures the suitability of the adsorbent for dye adsorption. The value of R_L shows the favorability of the adsorption reaction as well as of the Langmuir isotherm model, i-e it is irreversible if $R_L = 0$, favorable of $0<R_L<1$, linear if $R_L=1$ or unfavorable if $R_L>1$ [5, 34].

2.6.2 Freundlich isotherm model

This isotherm model describes the heterogeneous surface of the adsorbent with sites having dissimilar adsorbing potential and each site is supposed to participate in the process of adsorption. The widely used Freundlich equation 13 is mentioned as below [5, 34, 36, 41]:

$$q_e = K_F C_e^{1/n} \quad (13)$$

The linear form of this equation is,

$$\ln q_e = \ln K_F + 1/n \ln C_e \quad (14)$$

q_e denotes the adsorption capacity of adsorbent at equilibrium and C_e is the dye concentration in liquid phase at equilibrium. K_F is Freundlich constant which shows heterogeneity factor of adsorption that are determined by the slope and intercept of Freundlich isotherm [5, 34].

2.7 Adsorption kinetics

Adsorption kinetics represents the rate of adsorption of adsorbate controlled by the time at the solid liquid interface and it is the main characteristics that define the sorption efficiency. Adsorption

kinetics can be defined as the rate at which equilibrium of dye adsorption is approached. The adsorption rate is limited by the mechanism of mass transport and depends on the properties of the adsorbent and the dye as adsorbate. The mechanism of mass transport of the dye to the adsorbent surface is categorized as: (i) transportation of bulk solution in which dye molecules from bulk solution are transported to boundary layer or liquid film surrounding the adsorbent. (ii) Liquid film diffusion that is the transport of the dye across the stationary liquid layer on the adsorbent surface. The mass transport from this layer is governed by the concentration gradient. (iii) Intra-particle diffusion that involves the transport of the dye molecules from adsorbent surface to binding sites within the particle. The intra-particle diffusion is dependent on the size and the porous structure of the adsorbent particles. This phenomenon can occur due to the pore diffusion, which is the diffusion of the dye molecules in the fluid filled pores, or solid or surface diffusion, which is the diffusion of dye molecules along adsorbent surface after adsorption has taken place. (iv) Binding, after transportation of dye molecules to the vacant sites, formation of adsorption bond occurs. In physical adsorption case, the "attachment" of dye molecule to the adsorbent surface occurs rapidly. Therefore, preceding the diffusion is slowest step and termed as rate limiting step which controls the removal rate of the dye from solution. However, if the adsorption is the instance of chemical reaction that changes the dye molecule nature, chemical reaction will be the slowest step which limits the rate of dye removal. The rate limiting steps for the adsorption process are used to be defined by the expression of kinetic adsorption models. Most widely used models in literature [5, 34, 36, 41] are pseudo first order kinetics and pseudo second order kinetics which is applied to analysis the dye adsorption data. Pseudo first order kinetics assumes that diffusion steps are involved in rate controlling for the dye removal from the solution. Whereas pseudo second order assumes chemisorptions as the rate controlling step of dye removal process.

The effect of reaction time on the dye adsorption capacity of adsorbent was determined by the kinetic models at C_0 15, 30, 45, 60, 75 and 90µM. The kinetic models are explained in following equations 15 and 16 [5, 34, 36, 41]:

$$\text{Pseudo first order: } \log (q_e - q_t) = \log q_e - K_1 t/2.303 \quad (15)$$

$$\text{Pseudo second order: } t/q_t = 1/K_2 q_e^2 + 1/q_e\, t \quad (16)$$

q_e and q_t (mg/g) are the concentration of adsorbed dye at equilibrium, at any time t (min) respectively. K_1 (min^{-1}) is the pseudo first order and K_2 (g/mg.min) is the pseudo second order rate constants. The kinetic constants and correlation coefficients were calculated from the slope and intercept of both the models.

2.8 Desorption study of MB, NR and CR with recyclability of adsorbents

An efficient adsorbent should possess qualities of high adsorption capacities and as well as excellent desorption characteristics. To determine the reusability of all the adsorbents, including SBA-15 particles, pristine PAN nanofibers and PAN+SBA-15 composite nanofibers with and without dispersing agent for MB, NR and CR, five simultaneously desorption-adsorption cycles were performed on UV/Vis spectrophotometer. Desorption was performed at pH 2, 7 and 10 for all dye adsorbed samples in distilled water for 24 hours at room temperature whereas adsorption was performed at 30 µM solution concentrations for cationic MB and NR dyes and 15 µM solution concentrations for anionic CR dye till equilibrium (150 min for MB, 120 min for NR and 275 min for CR) at neutral pH and room temperature. After each desorption, all the adsorbents were dried at room temperature for 16-20 hours for next adsorption.

2.9 Conclusion

In this chapter, the details of used materials and methods for the synthesis of SBA-15 particles, pristine PAN and PAN/SBA-15 nanofibers are mentioned. In addition the techniques used for the characterizations of fillers and nanofibers are explained.

Next chapter will describe the optimization of electrospinning parameters, optimization of dispersing agent for fillers dispersion in DMSO, the effect of incorporation of SBA-15 on the morphology of PAN nanofibers. It will also explain the influence of embedding SBA-15 on thermal and textural properties of their composite nanofibers with PAN matrix, and the accessibility of mesoporous of SBA-15 and composite nanofibers.

Chapter III

Preparation of nanocomposites by electrospinning

Chapter III

Preparation of nanocomposites by electrospinning

Introduction

In this chapter, PAN and PAN/SBA-15 composite nanofibers have been obtained by needleless electrospinning process. Here, studies of polymer/filler formulations in solvent, optimization of electrospinning parameters, the effect of incorporation of fillers on the morphology, thermal stability, structure and mechanical properties of composite nanofibers are described. Later on the composition of pristine PAN and composite nanofibers was studied graphically by FTIR and EDX, whereas the accessibility of mesopores of SBA-15 within PAN/SBA-15 composite nanofibers with and without dispersing agent was measured.

3.1 Synthesis of SBA-15

SBA-15 silica particles have been synthesized according to Y. Belmoujahid et al procedure [195], as explained in previous chapter (section 2.1.2). The obtained SBA-15 sub-micron particles have a length ranged from 1 to 2 µm and a width ranged from 0.4 to 0.5 µm. SEM images of synthesized SBA-15 are shown in figure III.1.

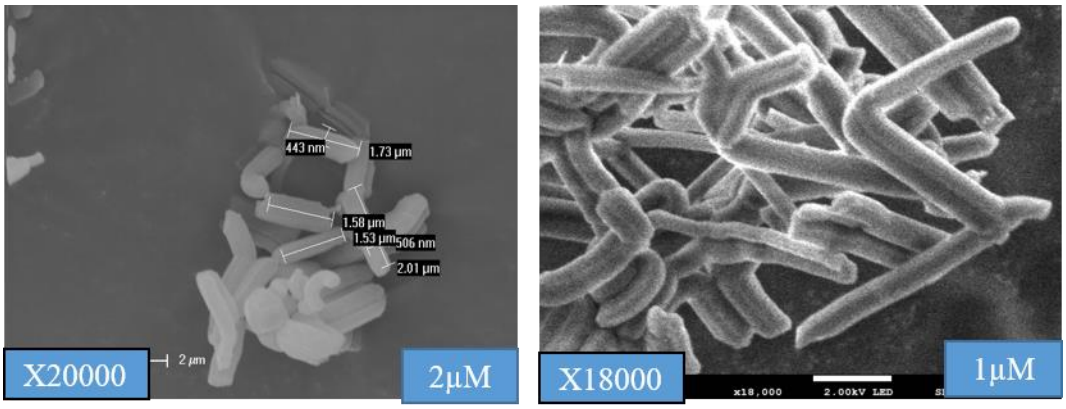


Figure III.1: SEM images of synthesized SBA-15

3.1.1 Accessibility of pores and BET surface area of SBA-15

N_2 adsorption/desorption isotherms with BJH desorption pore size distribution of silica SBA-15 is displayed in figure III.2.

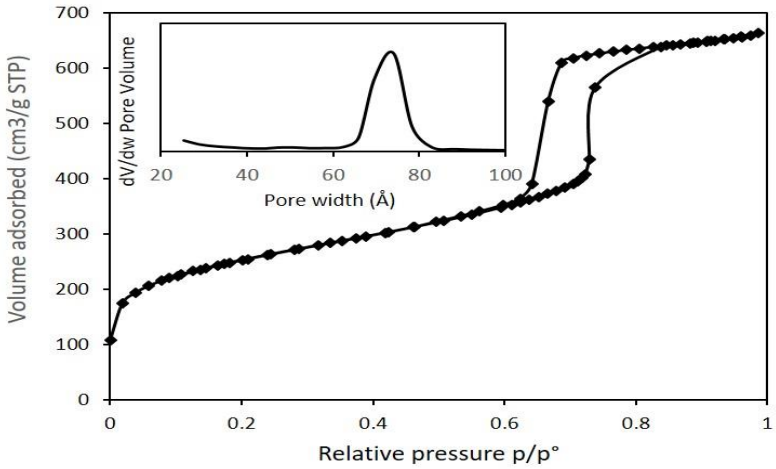


Figure III.2: N_2 adsorption/desorption isotherms of raw SBA-15 Insets: BJH desorption pore size distributions.

The N_2 adsorption/desorption isotherm of raw SBA-15 is a mixture of type I and type IV with an H1-type hysteresis loop according to IUPAC classification [201]. Type I at low relative pressure indicates the presence of micropores. The type IV with a capillary condensation step is characteristic of mesoporous solids. Indeed, SBA-15 silica is characterized by the presence of mesopores arranged in an ordered hexagonal array (about 7.2 nm of diameter) connected through micropores. In H1 type hysteresis loop, the adsorption and desorption branches are parallel and quasi-vertical: it is characteristic of capillary condensation and evaporation process in the cylindrical pore open at both ends and this is observed with adsorbents that have a very narrow size distribution of cylindrical mesopores. This is confirmed with the mono-modal pore size distribution (PSD) plot with mesopores diameter of SBA-15 particles in the range of 6.5-8 nm and a maximum at 7.2 nm. Specific surface areas, pore volumes and pore sizes determined from the N_2 adsorption/desorption isotherms are reported in table III.1.

Table III.1: SBA-15 Textural characteristics determined by N_2 adsorption/desorption isotherms.

Sample	S_{BET} (m^2/g)	Pore volume[a] (cm^3/g)	Micropore volume[b] (cm^3/g)	Pore width[c] (nm)
SBA-15	917	1.02	0.163	7.2

[a]determined at p/p0 =0.9, [b]determined by t-plot method, [c]value corresponding to the maximum of PSD

3.1.2 Structural analysis of SBA-15

The structure of SBA-15 was characterized by using X-ray diffraction (XRD) (figure III.3).

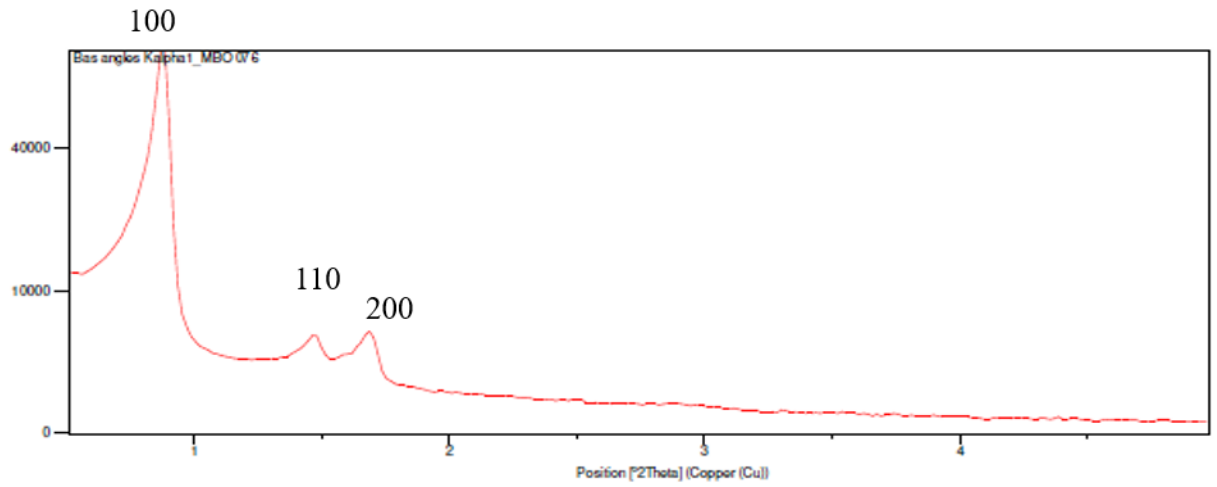


Figure III.3: XRD of SBA-15 particles

Figure III.3 gives diffractograms of SBA-15 powder that exhibits three peaks at 2θ values of 0.9°, 1.5° and 1.7° indexed as (100), (110) and (200) reflections respectively. Such crystallography is consistent with a well ordered 2-D hexagonal pore arrangement that is characteristic of SBA-15 type materials [16].

3.1.3 Particle size measurement and optimization of dispersing agent (Zetasizer nano series)

As discussed earlier that three different types of dispersing agents were used in this study and the best dispersing agent was chosen. For this purpose, two different apparatus were used: Zetasizer nano series and Mastersizer 3000, so that the impact of dispersion agent on deagglomeration of SBA-15 may be counter tested.

Particle size measurement of fillers is very essential to determine the impact of dispersing agent on dispersion of silica sub-micron particles. Technique used for this purpose is dynamic light scattering which reveals the size of elementary particles. Four suspensions of 2wt% of SBA-15 in DMSO for each dispersing agent (mentioned in 2.1.3 section) were prepared and 0.5, 1, 1.5 and 2 wt% (w.r.t. weight of SBA-15) of each dispersing agent was added in solvent before the incorporation of SBA-15. Prior to analysis, each suspension was stirred with Ultra Turrax homogenizer at 1000 r.p.m for 20 minutes. An average value of particle size was determined from the measurements realized on three identical formulations. Average diameter and Polydispersity index of particles are mentioned in table III.2.

Table III.2: Impact of dispersing agents on diameter and PDI of SBA-15 particles in Zetasizer

Sr. No	Sample Name	PDI	Avg. Diameter nm
1	SBA-15	0.115	596±90
2	0.5wt% BYK W-9010	0.834	632±98
3	0.5wt% BYK W-980	0.413	562±70
4	0.5wt% BYK W-966	0.758	561±70
5	1wt% BYK W-9010	0.621	120±18
6	1wt% BYK W-980	0.931	326±35
7	1wt% BYK W-966	1	337±48
8	1.5wt% BYK W-9010	0.909	301±36
9	1.5wt% BYK W-980	1	300±35
10	1.5wt% BYK W-966	0.844	310±41
11	2wt% BYK W-9010	1	383±55
12	2wt% BYK W-980	1	333±44
13	2wt% BYK W-966	1	417±52

Solvent: DMSO

The results show that for each concentration of dispersing agents, the diameter of particles is different and the best deagglomeration with average particle size of 120±18 nm is resulted in the case of 1wt% of BYK W-9010 which is due to H-bonding between the silanol of SBA-15 and dispersing agent resulting in steric repulsion between the silica particles. The phenomena of dispersing can be seen in figure III.4.

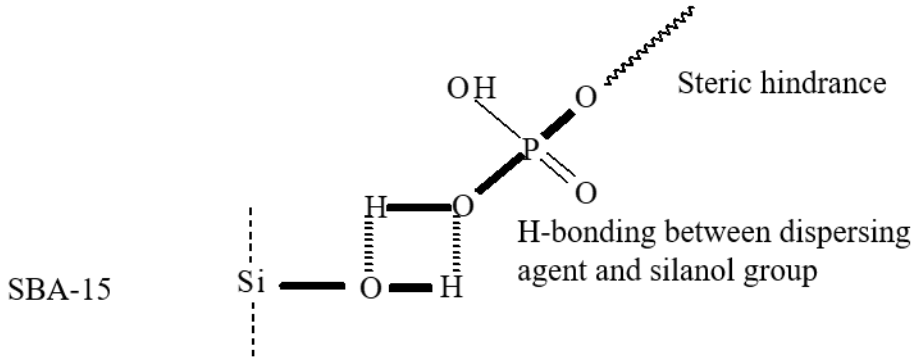


Figure III.4: Deagglomeration phenomena of SBA-15 by dispersing agent (BYK W-9010)

3.1.4 Particle size measurement and optimization of dispersing agent (Mastersizer)

Another technique to measure the dispersion or distribution of the particles was carried out by laser granulometry in Mastersizer. This distribution can be defined by different values like Dv10, Dv50 and Dv90, which corresponds respectively to 10%, 50% and 90% cumulative volume of particles over particle size distribution in percentage cumulative. Dv stands for Median of size distribution volume. Like process in Zetasizer, again four suspensions of 2wt% of SBA-15 in DMSO for each dispersing agent (as mentioned in 2.1.3 section) were prepared and 0.5, 1, 1.5 and 2 wt% (w.r.t. weight of SBA-15) of each dispersing agent was added in solvent before the incorporation of SBA-15. Prior to analysis, each suspension was stirred with Ultra Turrax homogenizer at 1000 r.p.m for 20 minutes. The impact of concentration of BYK W-9010 is displayed in figure III.5 whereas the impact of nature of dispersing agents is displayed in figure III.6. The all results of dispersion are displayed in table III.3.

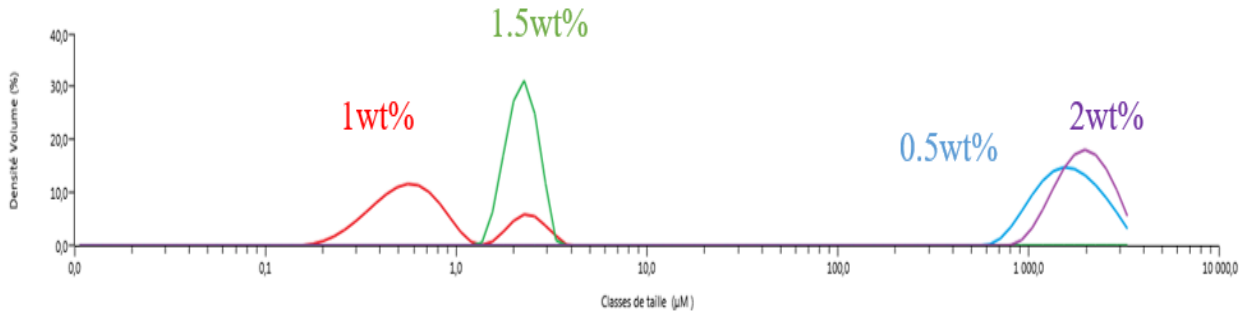


Figure III.5: Impact of BYK W-9010 concentration on SBA-15 deagglomeration (1.7wt%SBA-15/DMSO)

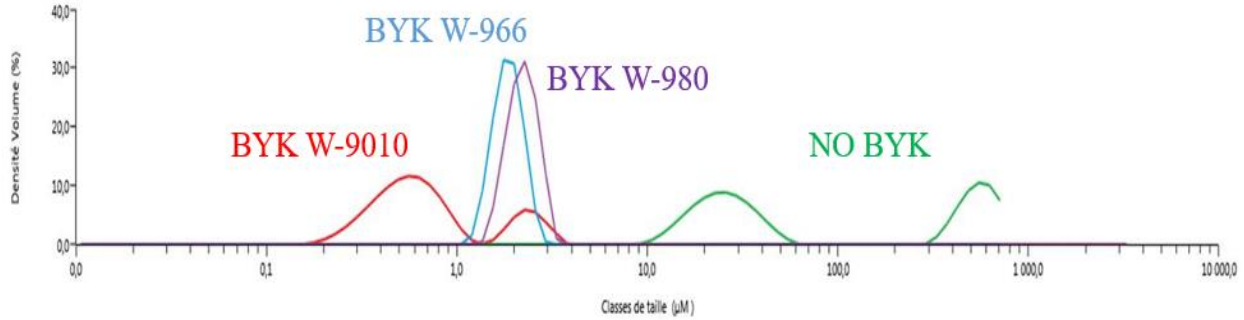


Figure III.6: Impact of nature of dispersing agents on SBA-15 deagglomeration (1.7wt% SBA-15/DMSO)

Table III.3: Impact of dispersing agents on diameter of SBA-15 particles in Mastersizer

Sr. No	Sample name	Dv (10) µm	Dv (50) µm	Dv (90) µm
1	2wt%SBA-15/DMSO	16.8	36.8	633
2	0.5wt% BYK W-9010	987	1600	2620
3	0.5wt% BYK W-980	1290	1800	2520
4	0.5wt% BYK W-966	1300	1960	2870
5	1wt% BYK W-9010	0.327	0.616	2.38
6	1wt% BYK W-980	1.47	1.85	2.31
7	1wt% BYK W-966	1.73	2.21	2.75
8	1.5wt% BYK W-9010	2.93	3.87	5.25
9	1.5wt% BYK W-980	790	1620	2660
10	1.5wt% BYK W-966	1680	2460	3200
11	2wt% BYK W-9010	1280	1930	2850
12	2wt% BYK W-980	1380	1990	2860
13	2wt% BYK W-966	1080	1800	2740

The results show that dispersion of silica particles are best in the case of 1wt% of all dispersing agent and particularly for 1wt% of BYK W-9010 that shows very small median of size distribution volume as compared to other dispersing agent. In explanation it can be said that 10% of SBA-15 particles are under 0.327 µm, 50% of SBA-15 particles are under 0.616 µm and 90% particles are under 2.38 µm. Therefore 1wt% of BYK W-9010 is optimized quantity for dispersion of SBA-15 particles due to hydrogen bonding and electrostatic repulsion.

3.1.5 Impact of stirring and dispersing agent on deagglomeration of SBA-15 in DMSO

Dispersing is the mixing of at least two substances that do not dissolve in each other or do not chemically react each other. The goal of dispersing process was the production of SBA-15 suspension in DMSO and during suspension production; solid particles were smoothly distributed in the liquid. Ika T25 Ultra-Turrax was used for dispersion process of SBA-15 aggregates. A DMSO suspension having 0.02wt% of SBA-15 was prepared and prior the addition of silica sub-micron particles 1wt% (w.r.t) of dispersing agent was added in DMSO. In Ultra Turrax, rotor/stator high shear generation system of was used (as shown in figure III.7), in

which rotor moved with high circumferential speed of 1000 r.p.m for 20 minutes, which produced suction and the aggregates of SBA-15 within the DMSO medium were drawn in the axial direction into the head of dispersion and then pressed in the radial direction through the gaps of rotor-stator system due to which the aggregates of silica particles subjected to high shear forces.

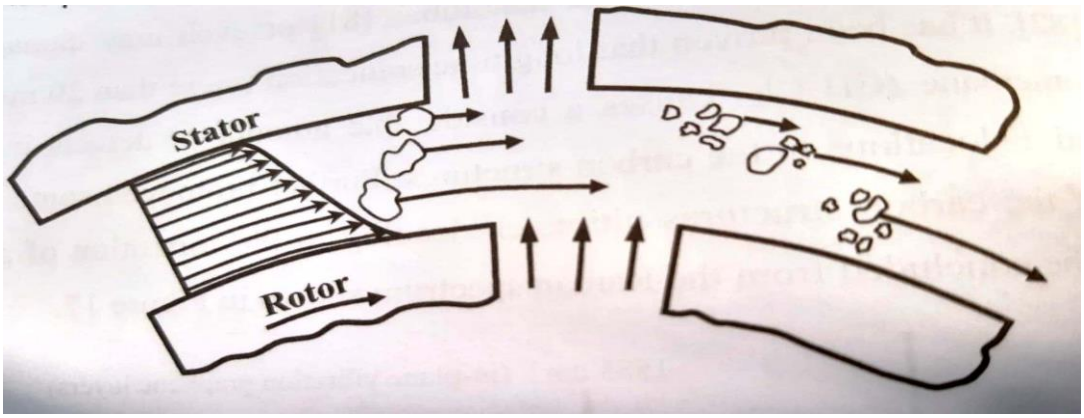


Figure III.7: Principle of high shearing mixing in rotor/stator system

In addition, in the interstice between the rotor and the stator, a high turbulence was also developed which promoted the exfoliation of the fillers from their aggregates. As the tiny gaps were formed, the dispersing agent diffused into those gaps and started to deaggregate the silica sub-micron particles by steric or electrostatic repulsions and as a result the previously formed gaps propagated in leading to ultimately separating the fillers from their aggregates. The phenomenon of deagglomeration is shown in figure III.8.

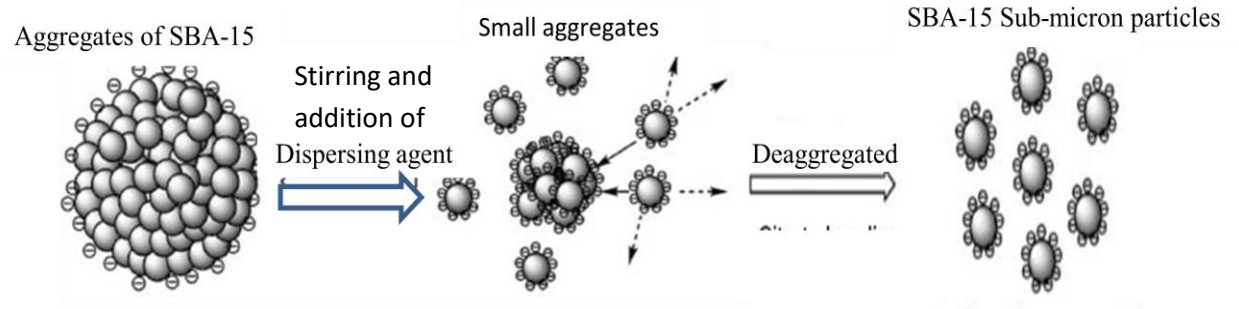


Figure III.8: Deagglomeration phenomena of SBA-15 particles by stirring and dispersing agent

High shearing of SBA-15 powder at 1000 r.p.m for 20 minutes and impact of 1wt% BYK W-9010 was found to reduce the average size of their aggregates from 596 nm to 120 nm.

3.1.6 Conclusion

SBA-15 sub-micron particles were successfully synthesized by the method of Zhao *et al*, and the SEM images of obtained particles are of cylindrical or rod shape having 1 to 2µm length and their width is 400 to 600 nm. Three peaks in XRD show that silica particles are well ordered and have 2-D hexagonal pore arrangement. They have 917 m^2/g of surface area, 1.02 cm^3/g pore volume and 0.165 cm^3/g micro pore volume. Two dispersion techniques (chemical and mechanical) and three dispersing agents of different concentrations were used and optimized for the deagglomeration of silica particles in DMSO suspension. All the suspensions were stirred mechanically for 20 minutes. As a result of optimization, 1wt% of BYK W-9010 was selected for better deagglomeration of particles.

3.2 Electrospinning of PAN nanofibers

3.2.1 Rheological analysis of pure PAN solution

PAN/DMSO solutions of different concentrations from 5 to 12 wt % were prepared in DMSO for viscosity study in order to identify the better concentration in term of viscosity for electrospinning process. Each PAN/DMSO formulation was stirred for 40 minutes at 1000 r.p.m by IKA T18 digital Ultra Turrax to make the solution homogeneous. The formulations were further stirred at room temperature with magnetic stirrer at 300 r.p.m for 24 hours to make the mixtures stable. The viscosity of PAN/DMSO solutions were measured by using Anton Paar Modular Compact Rheometer 502 on “plan-plan mode” at 20 ^oC. An average value of viscosity was determined from five measurements realized on each formulation. The average viscosities of DMSO formulations of PAN from 5 to 12 wt% concentrations are reported in figure III.9.

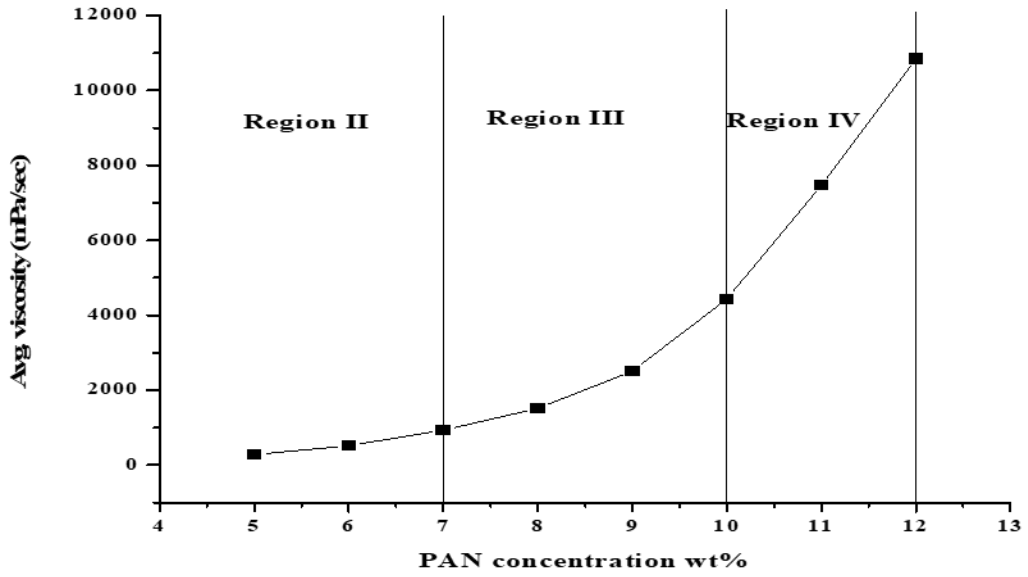


Figure III.9: Average viscosities of PAN solutions in DMSO

The results show that increase in concentration of PAN in DMSO increases the viscosity. The increase in viscosity is ascribed to the increase of intermolecular interactions and increase in hydrodynamic volume of independent macromolecular coils [199]. In the same way, dispersion, strong polarization and hydrogen bonding between the solvent and the polymer affect the viscosity [199]. From previous studies, it has been concluded that there are four regimes of specific viscosity. Regime I (not observed) is diluted regime where viscosity is very low, so usually 1-2 wt% of polymer solutions fall in this range. The regime II corresponds to semi-dilute unentangled regime, where viscosity is higher than the ones of the region I but not high enough for electrospinning, since polymer chains will not entangle to each other to make nanofibers: from 5 to 7wt% of PAN, polymer solutions are considered in this range. The regime III corresponds to semi dilute entangled regime, where there is enough entanglement of polymer chains for electrospinning. In this study specific viscosity values of 8wt% and 10wt% of PAN fall in this regime, which are favorable for good electrospinning nanofibers. Whereas the regime IV (here up to 10wt% of PAN) is concentrated regime whose viscosity is quite higher than all other regimes [200]. The best suitable solutions for electrospinning and their viscosities are mentioned in Table III.4.

Table III.4: Viscosities and specific viscosities of electrospinning solutions.

Sr. No	Sample Name	Viscosity* (mPa/sec)	Specific viscosity (mPa/sec)
1	8wt% PAN	1516 ± 63	757±32
2	10wt% PAN	4442 ± 27	2220±13

*Average values from five measurements at 20 ^{o}C

The viscosity of the solution has a great impact on the electrospinnability and on the morphology of the resulting nanofibers [16]. The viscosity of polymer solution profoundly influences the jet formation and jet stability and is crucial for the successful formation of smooth nanofibers. The solution has to maintain appropriate viscosity in order to survive stretching, acceleration and whipping [75, 203]. In table III.4, specific viscosities of the solutions are also mentioned. Specific viscosity is the incremental viscosity of the solution due to the presence of polymer. It is measured by using equation 17,

$$\eta_{sp} = (\eta - \eta_0) / \eta_0 \qquad (17)$$

Where η is the viscosity of solution and η_0 is the viscosity of solvent. Regardless of the formulation composition, the specific viscosity is more than twice higher for 10 wt% PAN solutions compared to 8 wt% ones. Strong increase of viscosities can be attributed to semi dilute entangled regime (Region III). Between 8-10 wt% the addition of polymer contribute mainly in entanglements of polymer chains resulting in high viscosity. Therefore it is concluded that following study will use 8 and 10wt% PAN solution.

3.2.2 Preparation of PAN nanofibers

PAN/DMSO solutions were electrospun with maintaining the nozzle size (calibrated insert) fixed at 0.8 mm and varying the applied voltage between 30, 50 and 70 kV. The collecting distance (distance between polymer solution wire and collecting aluminum foil) was varied between 12.5, 15 and 20 cm. Table III.5 summaries the electrospinning conditions of PAN solutions in DMSO.

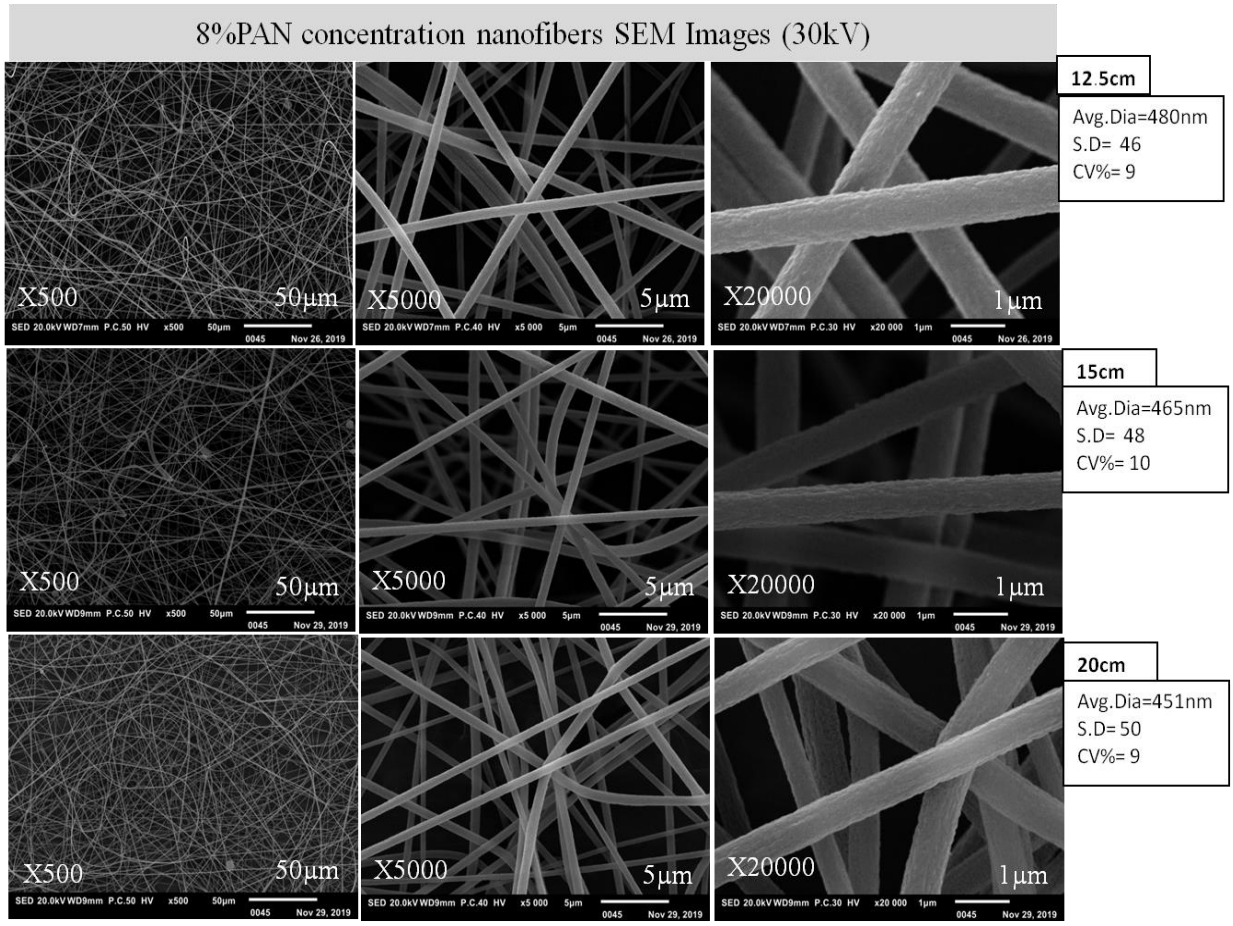
Table III.5: Electrospinning parameters for PAN solutions

PAN Concentrations (wt %)	8 and 10
Voltage (kV)	30, 50 and 70
Collecting distance (cm)	12.5, 15 and 20
nozzle size (calibrated insert) mm	0.8
Relative humidity (%)	33±2

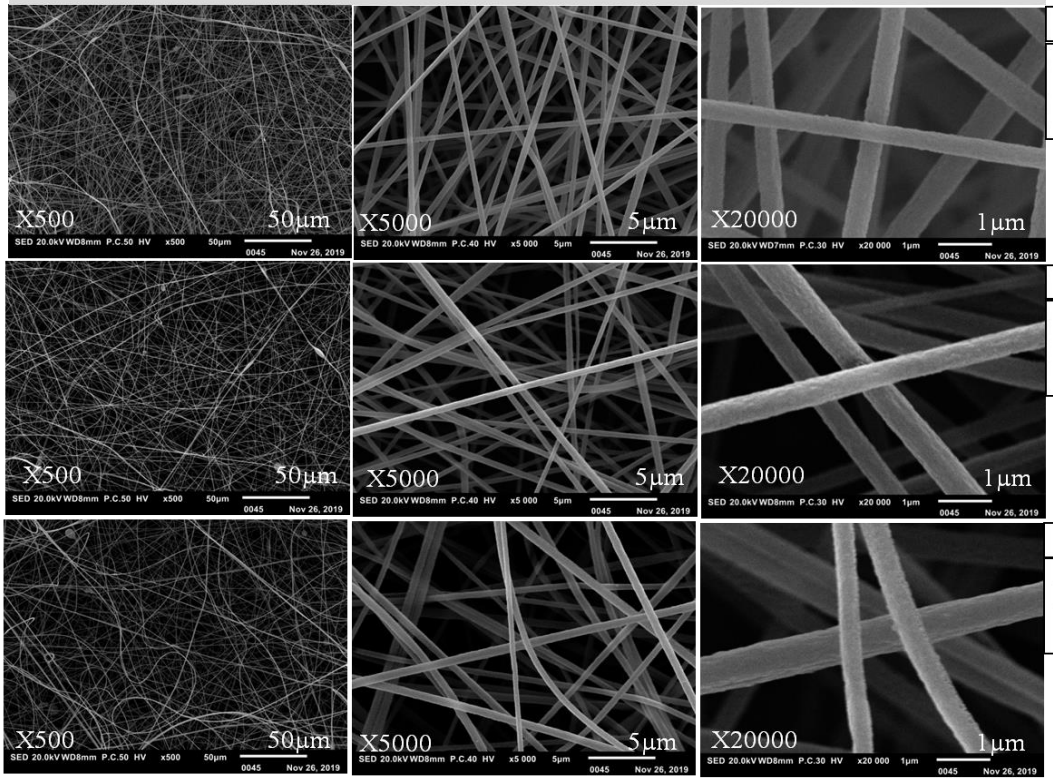
Temperature ^{o}C	20±2

PAN/DMSO solutions were electrospun in three trials:

The first trial was executed by maintaining the collecting distance at 12.5 cm, electrospinning time for 15 minutes and varying the applied voltage between 30, 50 and 70 kV whereas nozzle size was fixed at 0.8ml. In the second and third trial collecting distance was fixed at 15 cm and 20 cm respectively and other parameters like time of electrospinning, applied voltage and nozzle size were changed as in first trial. The obtained nanofibers SEM images from above mentioned parameters are illustrated in figure III.10.



8%PAN concentration nanofibers SEM Images (50kV)



12.5cm

Avg.Dia=495nm
S.D=50
CV%= 10

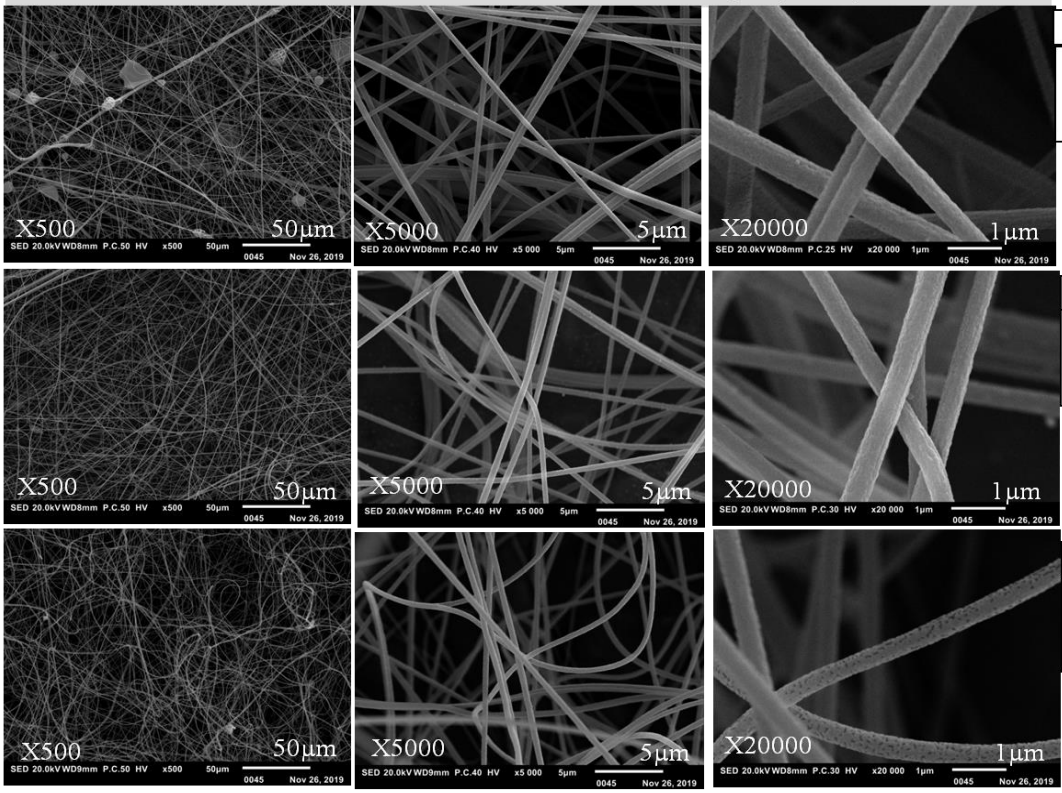
15cm

Avg.Dia=475nm
S.D= 51
CV%= 9

20cm

Avg.Dia=462nm
S.D= 49
CV%= 9

8%PAN concentration nanofibers SEM Images (70kV)



12.5cm

Avg.Dia=474nm
S.D= 89
CV%= 19

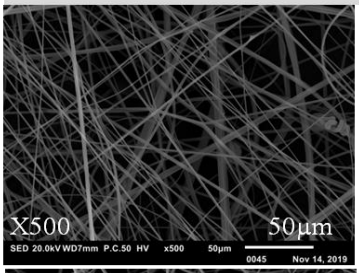
15cm

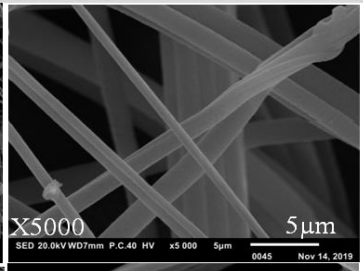
Avg.Dia=413nm
S.D= 63
CV%= 15

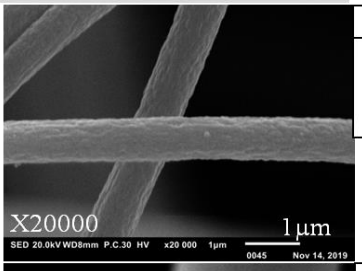
20cm

Avg.Dia=442nm
S.D= 77
CV%= 17

10%PAN concentration nanofibers SEM Images (30kV)

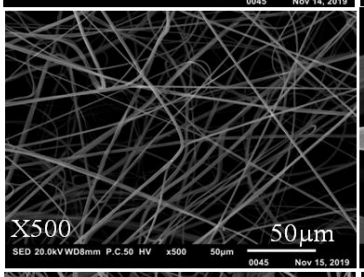


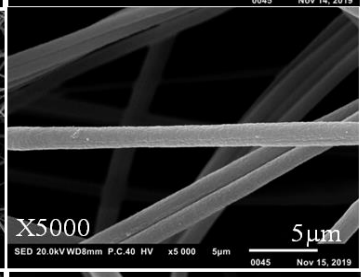


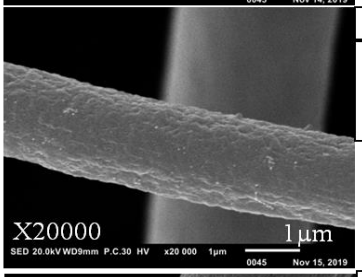


12.5cm

Avg.Dia=564nm
S.D= 53
CV%= 9

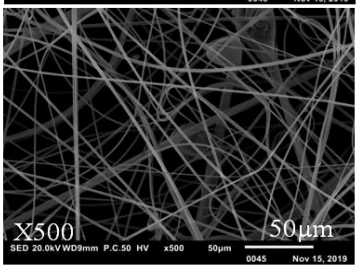


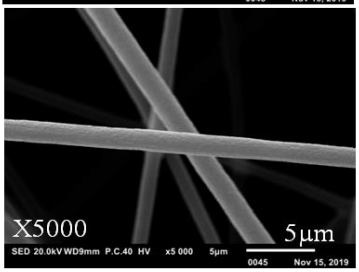


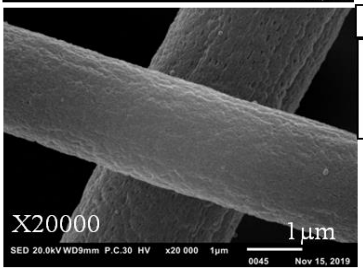


15cm

Avg.Dia=551nm
S.D= 57
CV%= 10



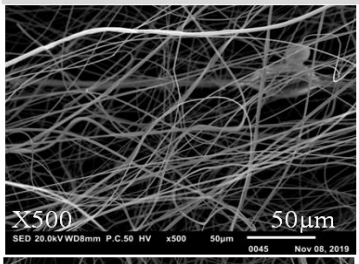


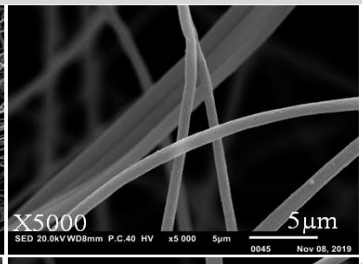


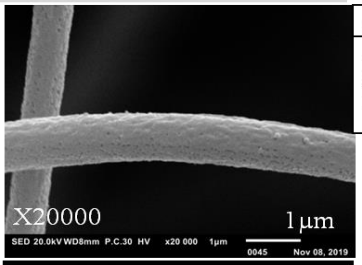
20cm

Avg.Dia=538nm
S.D= 49
CV%= 9

10%PAN concentration nanofibers SEM Images (50kV)

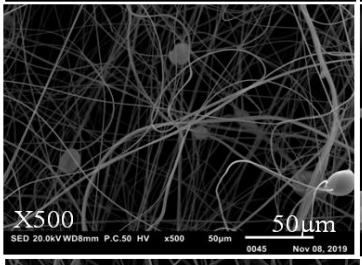


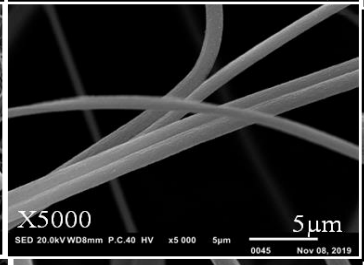


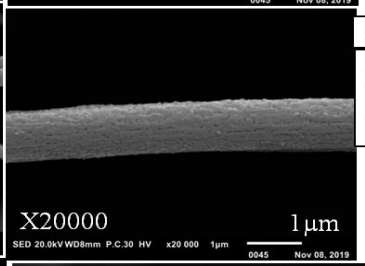


12.5cm

Avg.Dia=570nm
S.D=56
CV%= 10

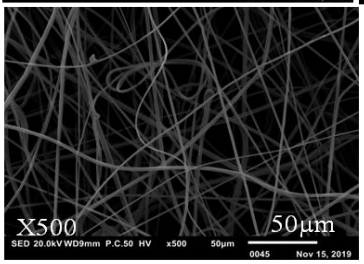


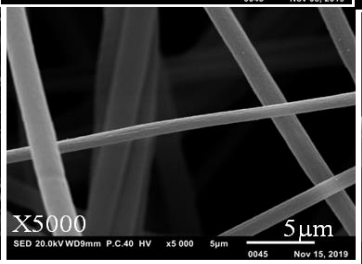


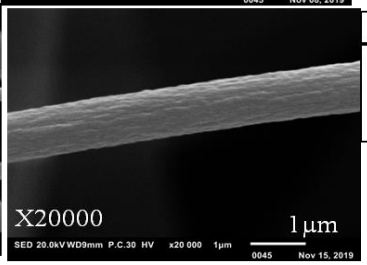


15cm

Avg.Dia=557nm
S.D= 51
CV%= 9







20cm

Avg.Dia=543nm
S.D= 49
CV%= 9

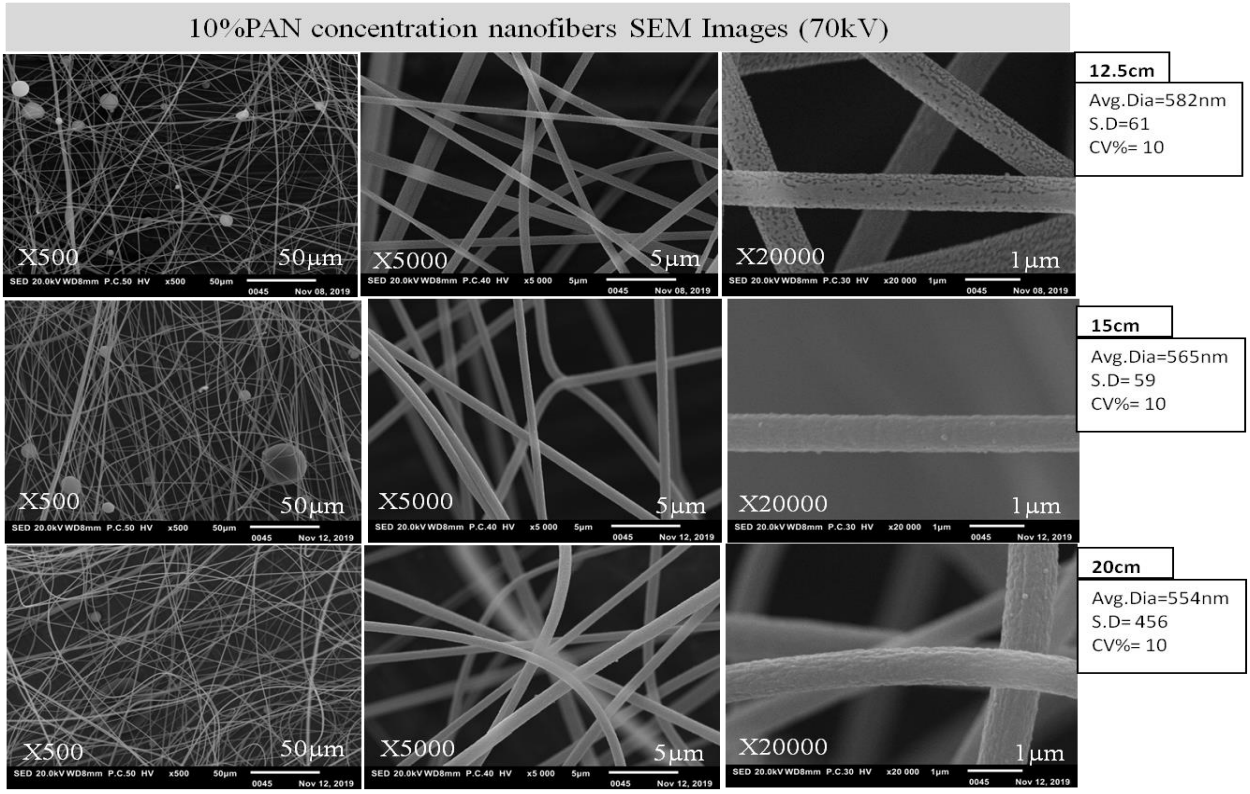


Figure III.10: SEM of pristine PAN nanofibers at 8 and 10wt% PAN concentration in DMSO

3.2.3 Structural analysis of pristine PAN nanofibers

This section explains the structural analysis of pristine PAN nanofibers manufactured by two different solutions of PAN/DMSO, including 8 and 10 wt% of PAN concentrations for electrospinning. The structural analysis of pristine PAN nanofibers was observed by scanning electron microscope and is shown in figure III.10. The variation of the average diameter of PAN nanofibers with electrode distance produced from 8 wt% PAN and 10 wt% PAN solutions at 30, 50 and 70 kV is displayed in figure III.11.

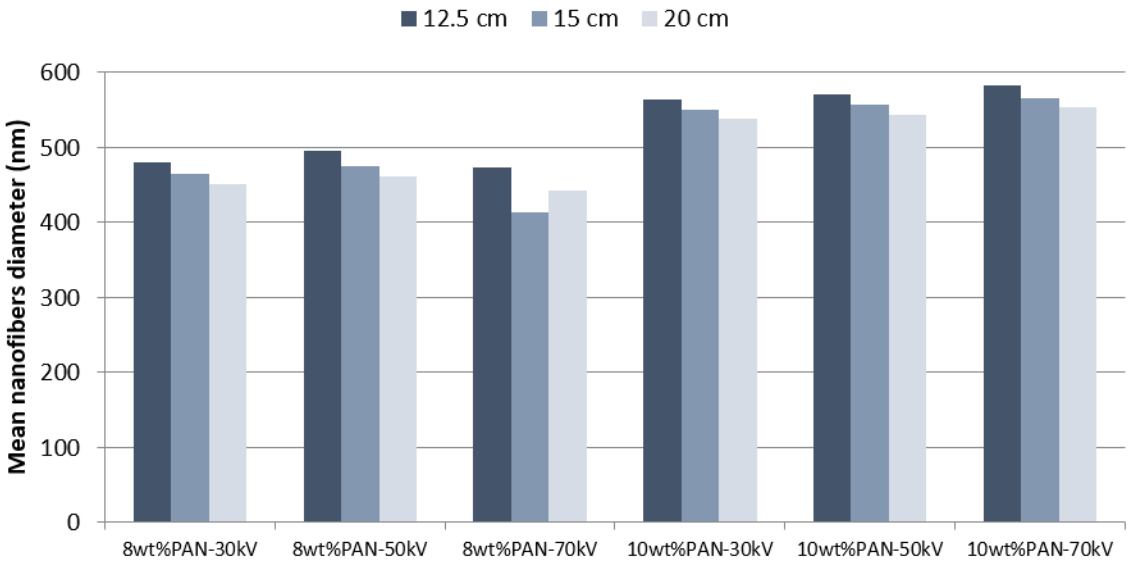


Figure III.11: Variation of the average diameter of PAN nanofibers with voltage and electrode distance.

Whether the voltage is 30, 50 or 70 kV for a given PAN concentration, the diameter of nanofibers decreases with the increase of the electrode distance. The reason behind is that longer collecting distance offers a longer flight time for the jet so the jet is stretched further and there is enough time available for solvent to evaporate, thus finer fibers are produced [97,100]. Nevertheless, this variation is weak since it is in the error domain. By increasing the voltage from 30 to 50 kV, the diameter of nanofibers increased, which is due to the flight time of the jet and further increase in voltage, decreased the nanofibers diameter which is due to the stretching of jet by increase in electric field. Indeed, higher voltage will accelerate the jet and reduce the flight time. Shorter flight time will offer less time for fibers to be stretched and elongated [98]. Synergistically, higher voltage may accelerate the solvent evaporation rate. However, the impact of the PAN concentration on the nanofibers diameter is important (about 100 nm) highlighting the role of the viscosity on the nanofibers diameter. The reason is that by increasing the polymer concentration, viscosity increased as a result of the increase of the number of polymer chain entanglements and thus the viscoelastic forces. SEM images of raw PAN nanofibers with standard deviation (SD) and coefficient of variation (CV %) is displayed in figure III.10 and table III.6.

Table III.6: Electrospinning parameters and average diameters of nanofibers produced from 8 and 10 wt% PAN formulations.

S. No	Sample name	Voltage (kV)	Distance (cm)	Nanofibers diameter (nm)-Standard deviation CV in %
1	PAN 8 wt%	30	12.5	480 ± 46 - CV = 9
2			15	465 ± 48 - CV = 10
3			20	451 ± 50 - CV = 9
4		50	12.5	495 ± 50 - CV = 10
5			15	475 ± 51 - CV = 9
6			20	462 ± 49 - CV = 9
7		70	12.5	474 ± 89 - CV =19
8			15	413 ± 63 - CV = 15
9			20	442 ± 77 - CV =17
10	PAN 10 wt%	30	12.5	564 ± 53 - CV = 9
11			15	551 ± 57 - CV = 10
12			20	538 ± 49 - CV = 9
13		50	12.5	570 ± 56 - CV =10
14			15	557 ± 51 - CV =9
15			20	543 ± 49 - CV =9
16		70	12.5	582 ± 61 - CV = 10
17			15	565 ± 59 - CV = 10
18			20	554 ± 56 - CV =10

In all cases, PAN nanofibers have smooth surface and look quite homogeneous in diameter. However, a close look of nanofibers obtained at 50 and 70 kV reveals the presence of some bulbs, especially in the case of the 10 wt % electrospun PAN with electrode distance of 12.5 and 15 cm (figure III.10).

3.2.4 Optimization parameters of PAN/DMSO solution

The SEM results and the diameters of nanofibers are mentioned in figure III.10, which explains that at 70 kV and on all collecting distances of 12.5, 15 and 20 cm, there are some electrospraying (bulbs) in images, standard deviation (S.D) and coefficient of variation (CV%) are also quite high. Therefore 70 kV is not suitable for further electrospinning in both PAN concentrations of 8 and 10wt%. In the case of 30 and 50 kV, the standard deviation (S.D) and coefficient of variation (CV %) on all collecting distances of 8wt% of PAN nanofibers is almost identical whereas if we compare the same voltages and collecting distances with 10wt% of PAN nanofibers, the values of SD and CV% are higher. It means that the nanofibers obtained at 8wt%

of PAN concentration are smooth and uniform as compared to nanofibers of 10wt% of PAN concentration. The optimized parameters of PAN/DMSO solutions are mentioned in table III.7.

Table III.7: Optimized PAN/DMSO electrospinning parameters

Sample	Viscosity (mPa/sec)	Voltage kV	Distance cm	Nanofibers diameter (nm)
8wt% PAN/DMSO	1516 ± 63	30	12.5	480 ± 46 CV%= 9
			15	465 ± 48 CV% = 10
			20	451 ± 50 CV% = 9
		50	12.5	495 ± 50 CV%= 10
			15	475 ± 51 CV%= 9
			20	462 ± 49 CV%=9

Relative humidity: 33±2% Temperature: 20±2 ^{o}C

Electrospinning conditions pristine PAN nanofibers of this study are compared with electrospinning conditions of literature in table III.8.

Table III.8: Electrospinning conditions of literature [7, 8]

Sample	Voltage kV	Distance cm	Nozzle mm	Nanofibers diameter nm
12wt%PAN/DMSO	40	24	0.6	450 ± 110
14wt%PAN/DMSO	80	24	0.9	350 ± 70

The resultant nanofibers of this study are quite impressive in the terms of their better standard deviation values as compared to the nanofibers in literature.

3.2.5 Conclusion

Viscosity analysis of PAN/DMSO solution shows that polymer solutions that fall in the region of semi dilute entangled regime are suitable for electrospinning, therefore from 8wt% of PAN/DMSO concentrations show electrospinning nanofibers. 8 and 10wt% of PAN concentration in DMSO at 30, 50, 70 kV and 12.5, 15, 20 cm electrode distance were selected for electrospinning and as a result, nanofibers obtained. On the basis of better CV% and S.D 8wt% of PAN at 30, 50 kV and 12.5, 15, 20 cm parameters were optimized for further process.

3.3 Electrospinning of PAN/SBA-15 composite nanofibers

This section will explain the elaboration process of PAN/SBA-15 composite nanofibers with and without dispersing agent.

3.3.1 Rheological analysis of PAN/SBA-15 formulations

PAN/DMSO solutions incorporating SBA-15 particles, with or without dispersing agent were prepared at different PAN concentrations in DMSO (X= 5 to 12 wt %) for rheological study in order to identify the optimal concentration in term of viscosity for electrospinning process. For all SBA-15 formulations, the PAN/SBA-15 weight ratio was fixed to 5. PAN/DMSO formulations are: X wt% PAN, X wt% PAN/ SBA-15 (5:1 PAN/SBA-15 wt ratio) and X wt% PAN/ SBA-15 (5:1 PAN/SBA-15 wt ratio) / (1 wt% dispersing agent compared to SBA-15). Each SBA-15 containing suspension was stirred for 40 minutes by IKA T18 digital Ultra Turrax to make the suspension homogeneous with well deagglomeration of SBA-15 particles. All PAN/SBA-15 formulations were further stirred at room temperature with magnetic stirrer at 300 r.p.m for one day to make the mixtures stable and were stirred again for 15 minutes with Ultra Turrax at 1000 r.p.m just before electrospinning. The viscosity of all PAN+SBA-15/DMSO formulations with and without dispersing agent was measured by using Anton Paar Modular Compact Rheometer 502 on "plan-plan mode" at 20 ^{o}C. An average value of viscosity was determined from five measurements realized on each formulation. The average viscosities of PAN+SBA-15 formulations in DMSO, having PAN from 5 to 12wt% concentration with PAN: SBA-15 of 5:1 wt: wt ratio of SBA-15 and dispersing agent was 1wt% w.r.t silica particles are reported in figure III.12.

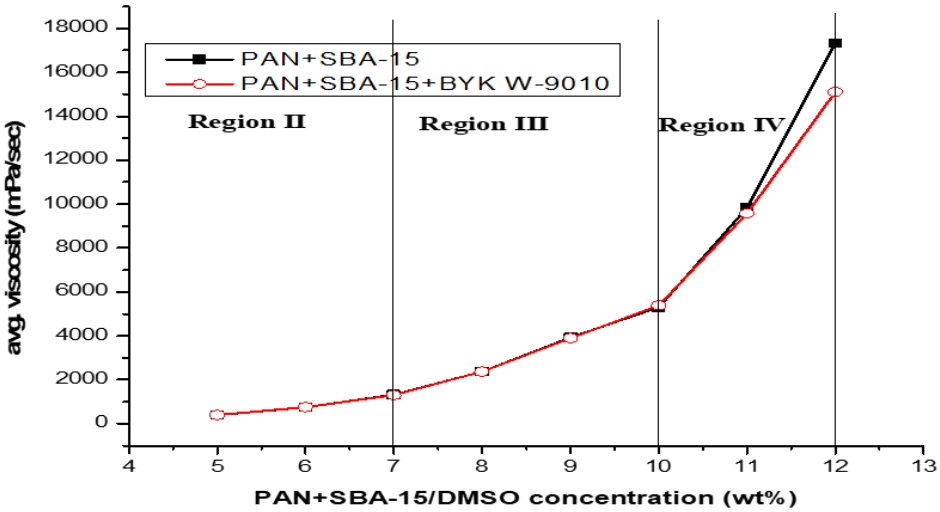


Figure III.12: Average viscosities of PAN+SBA-15/DMSO formulations

The impact of concentration of polymer on viscosity has been discussed earlier in section (3.2.1) which also explains the different regime of specific viscosities. Incorporation of SBA-15 increases the viscosity of solution whereas addition of BYK W-9010 has no effect on viscosity. The addition of fillers in polymer solution resulted in two different interactions, that is polymer-filler interaction and filler-filler interactions. It was found that filler-filler interaction caused an increase of steady shear viscosity whereas between polymer-filler interaction there existed strong coupling effect, storage modulus, higher zero shear viscosity, earlier shear thinning transition and a stronger shear thinning behavior [202]. In table III.9, the specific viscosities of the selected polymer concentrations for electrospinning, 8 and 10wt% with 1.7 and 2 wt% of fillers and 1wt% of dispersing agent w.r.t fillers respectively are mentioned.

Table III.9: Viscosities and specific viscosities of PAN+SBA-15/DMSO formulations

Sr. No	Sample Name	Viscosity* (mPa/sec)	Specific viscosity (mPa/sec)
1	8wt% PAN + 1.7wt% SBA-15	2380 ± 35	1189±17
2	10wt% PAN + 2wt% SBA-15	5302 ± 44	2650±22
3	8wt% PAN + 1.7wt% SBA-15 + 0.017 wt% BYK W-9010	2370 ± 53	1184±26
4	10wt% PAN + 2wt% SBA-15 + 0.02 wt% BYK W-9010	5390 ± 43	2694±21

*Average values from five measurements
** 0.02 and 0.017wt% of BYK W-9010 in the formulations. These values correspond to 1wt% compared to SBA-15.

Specific viscosity expresses the incremental viscosity due to the presence of the polymer in the solution. The graphical form of specific viscosity is shown in figure III.13.

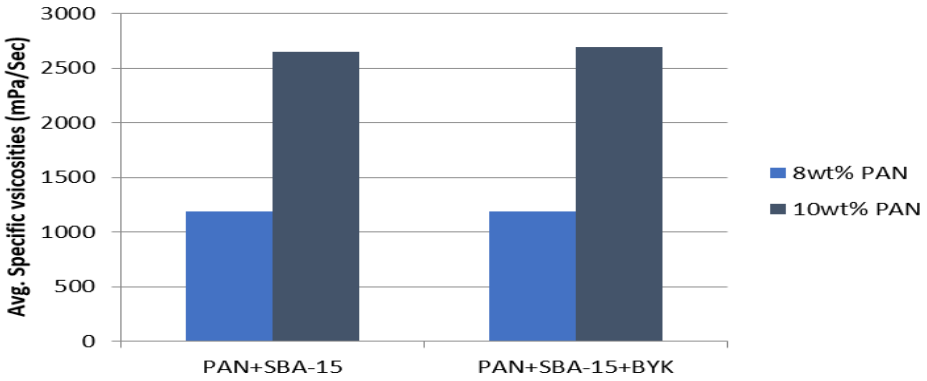


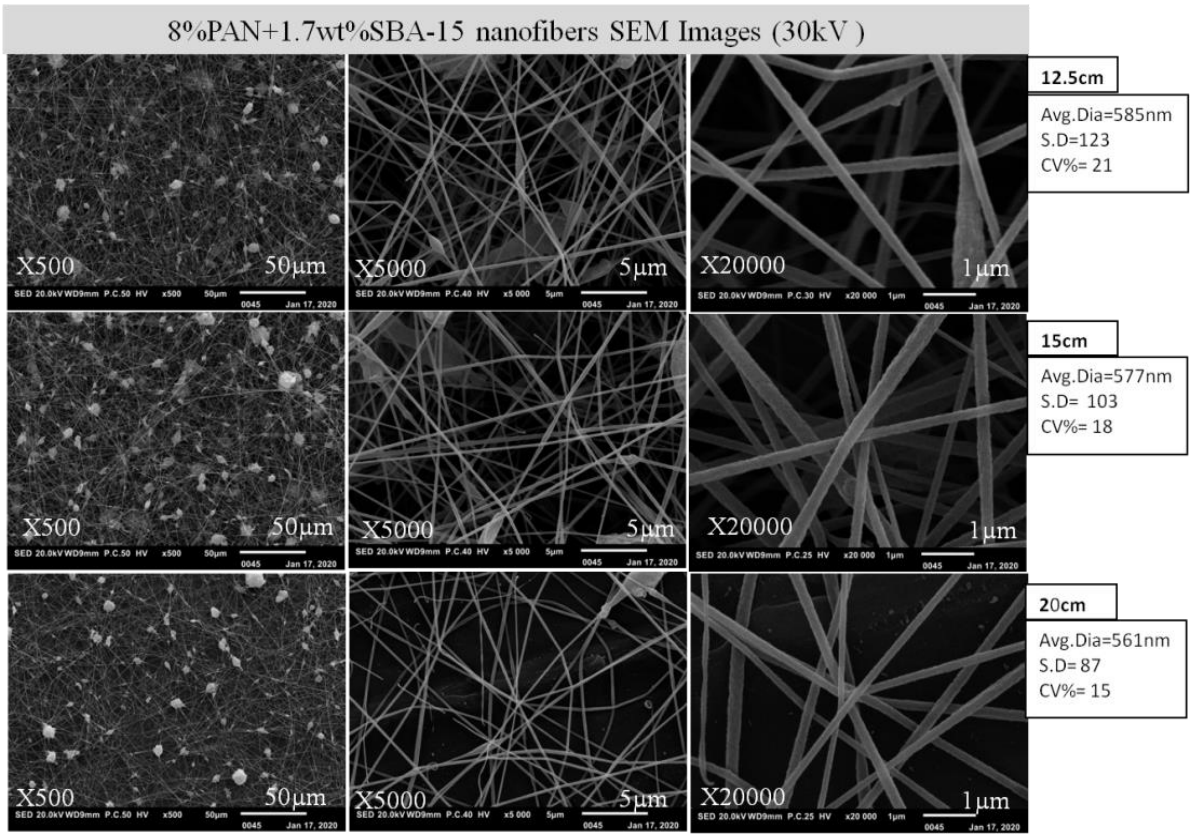
Figure 13: Specific viscosity of 8 and 10 wt% PAN+SBA-15/DMSO formulations.

For both 8 and 10 wt% PAN-based formulations the specific viscosity increases with SBA-15 and with SBA-15+BYK W-9010. However, there is no difference between PAN/SBA-15 and

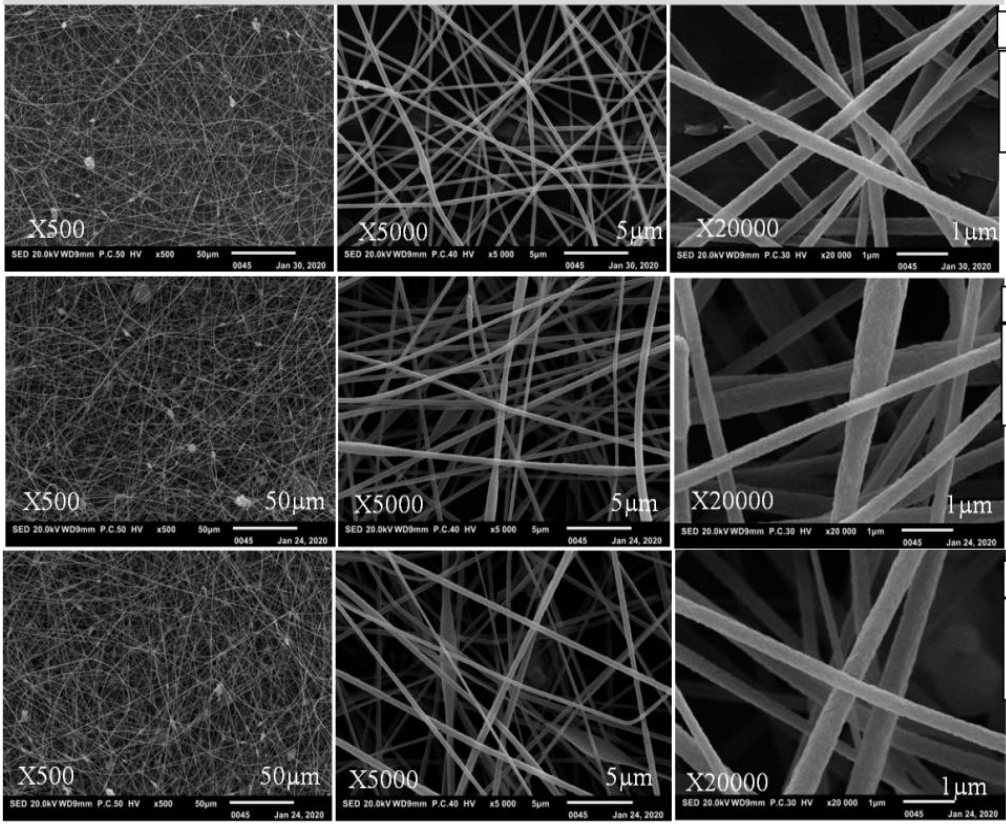
PAN/SBA-15+BYK W-9010. The specific viscosity is mainly impacted by the presence of the SBA-15 in the formulations.

3.3.2 Preparation of nanofibers composites

PAN/SBA-15 and PAN/SBA-15/BYK W-9010 solutions were electrospun under the same process conditions and parameters as mentioned in table III.5 (in the section 3.2.2 preparation the nanofibers), but in this process 2wt% fillers and 1wt% of dispersing agent w.r.t fillers was added in the solution of PAN/DMSO. Selected SEM images of obtained composite nanofibers under all the applied voltages of 30, 50 and 70 kV, collecting distance of 12.5, 15 and 20 cm and fixed nozzle size of 0.8 mm are showed in figure III.14.



8%PAN+1.7wt%SBA-15 +0.017wt% BYK W-9010 nanofibers SEM Images (30kV)

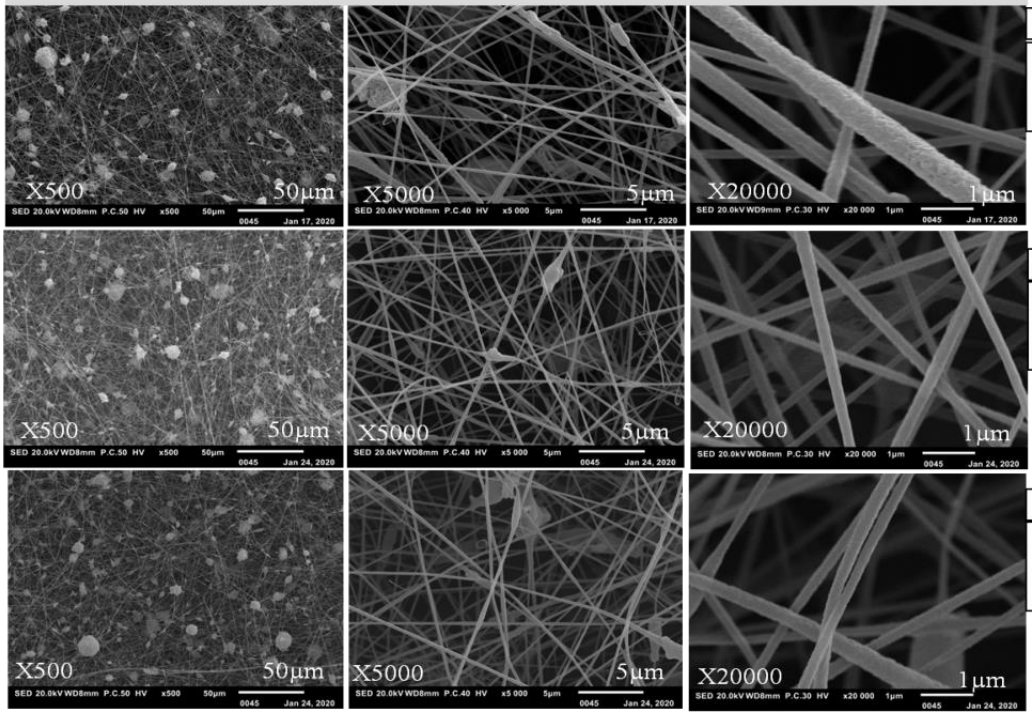


12.5cm
Avg.Dia=548nm
S.D=49
CV%= 9

15cm
Avg.Dia=560nm
S.D= 51
CV%= 9

20cm
Avg.Dia=533nm
S.D= 47
CV%= 9

8%PAN+1.7wt%SBA-15 nanofibers SEM Images (50kV)

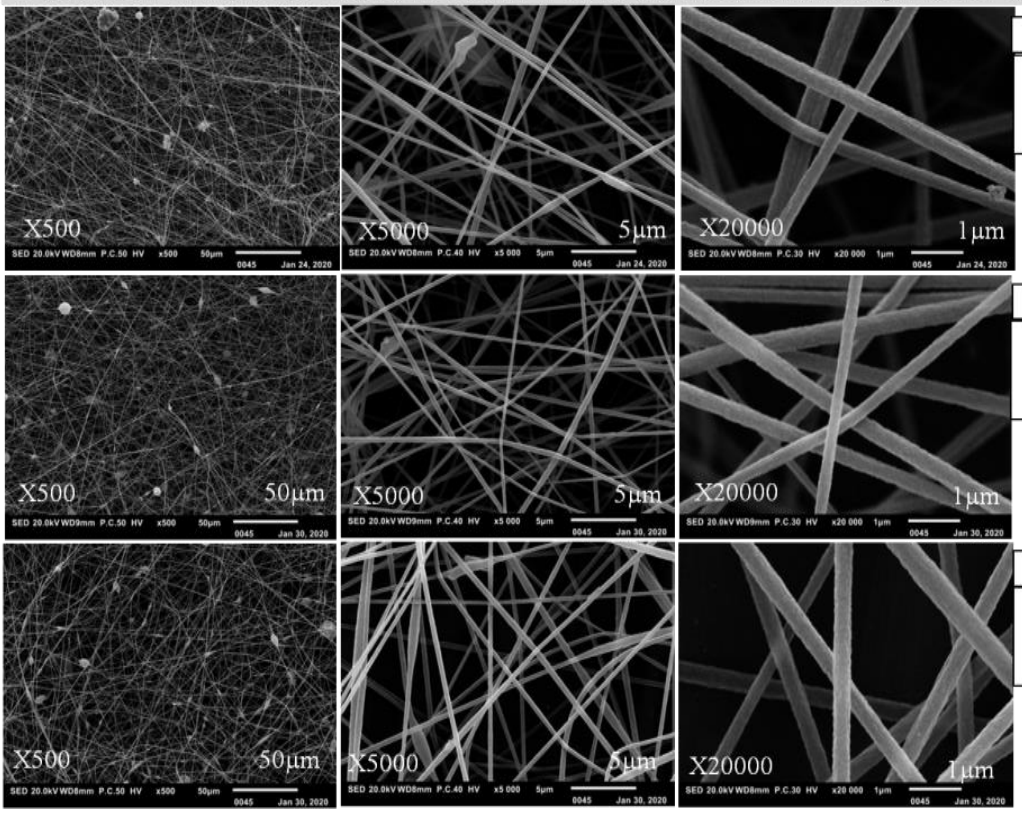


12.5cm
Avg.Dia=587nm
S.D=78
CV%= 13

15cm
Avg.Dia=573nm
S.D= 73
CV%= 13

20cm
Avg.Dia=552nm
S.D= 75
CV%= 14

8%PAN+1.7wt%SBA-15 +0.017wt% BYK W-9010 nanofibers SEM Images (50kV)

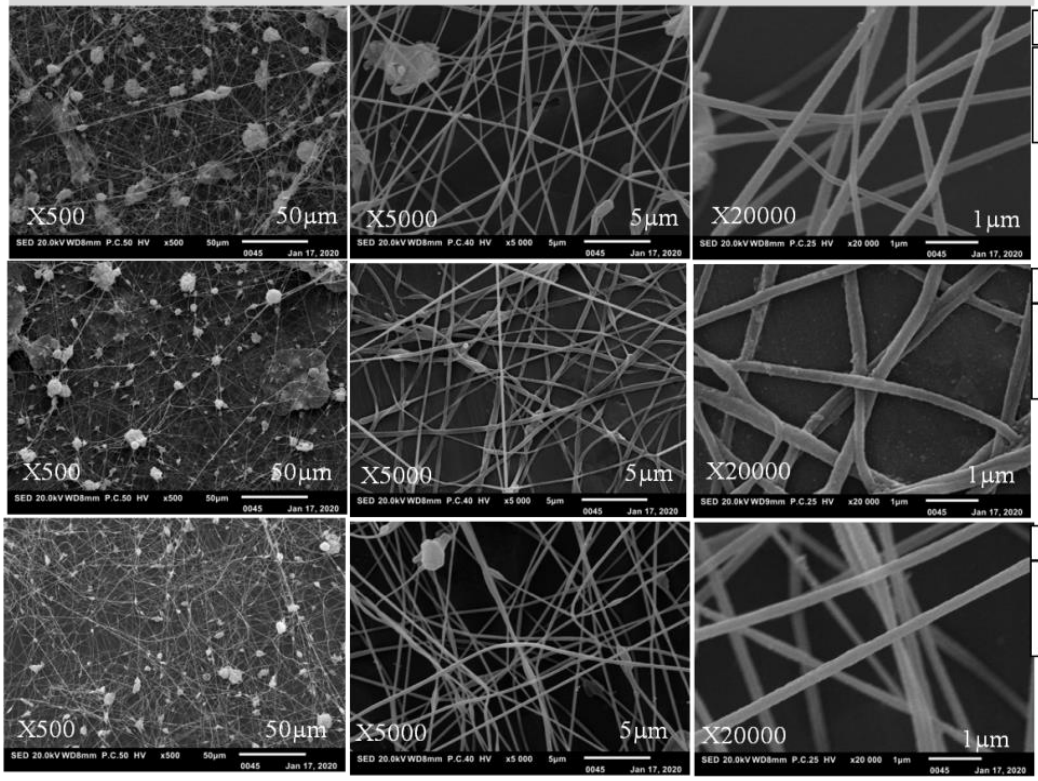


12.5cm
Avg.Dia=575nm
S.D=49
CV%= 8.5

15cm
Avg.Dia=534nm
S.D= 47
CV%= 9

20cm
Avg.Dia=513nm
S.D= 50
CV%= 10

8%PAN+1.7wt%SBA-15 nanofibers SEM Images (70kV)

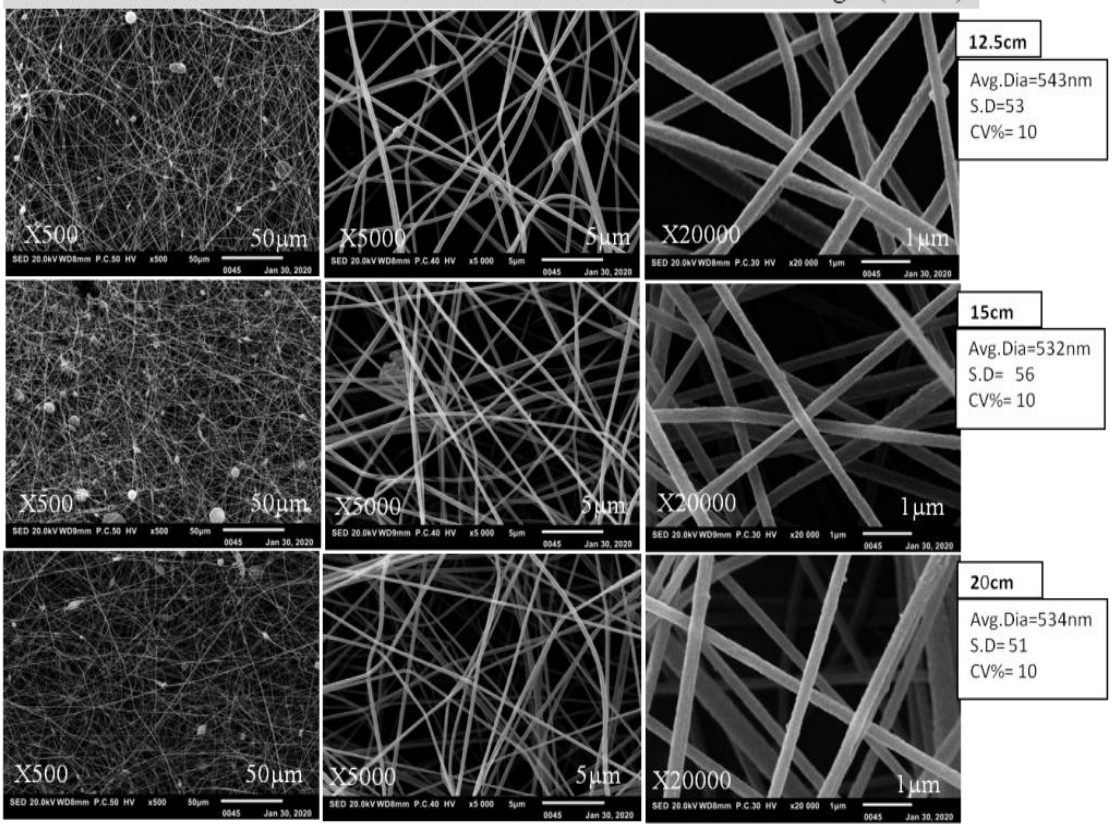


12.5cm
Avg.Dia=590nm
S.D=81
CV%= 14

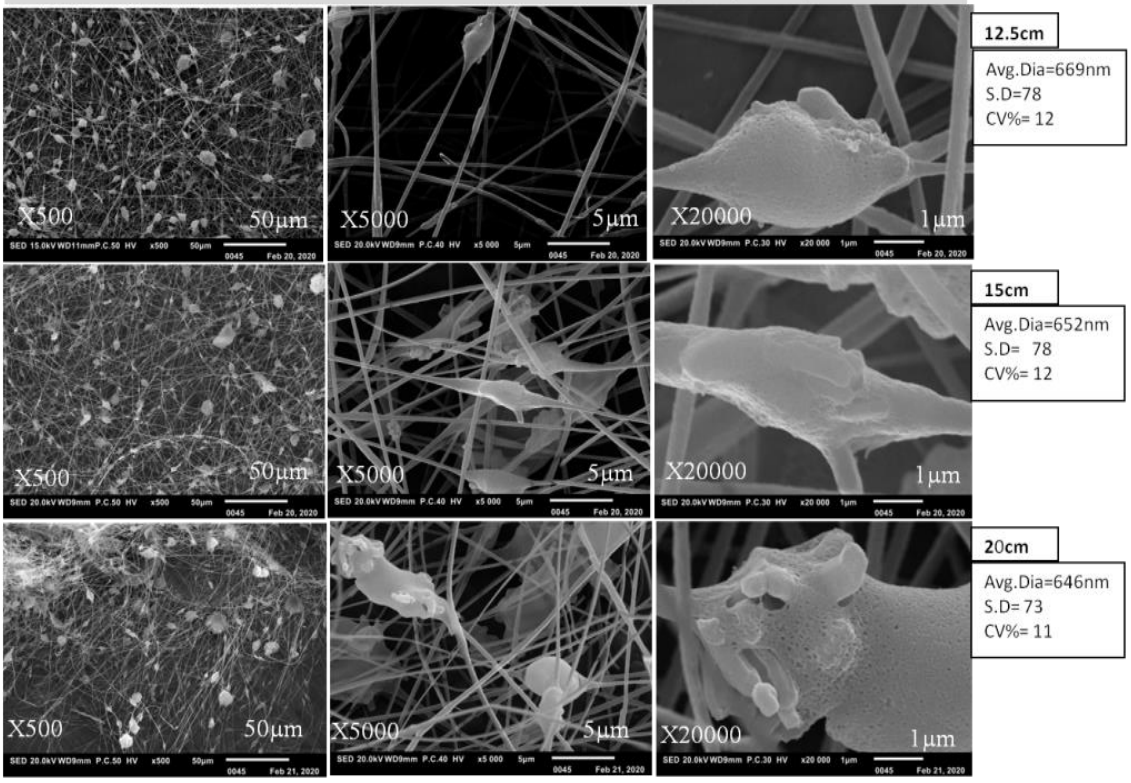
15cm
Avg.Dia=578nm
S.D= 77
CV%= 13

20cm
Avg.Dia=554nm
S.D= 63
CV%= 11

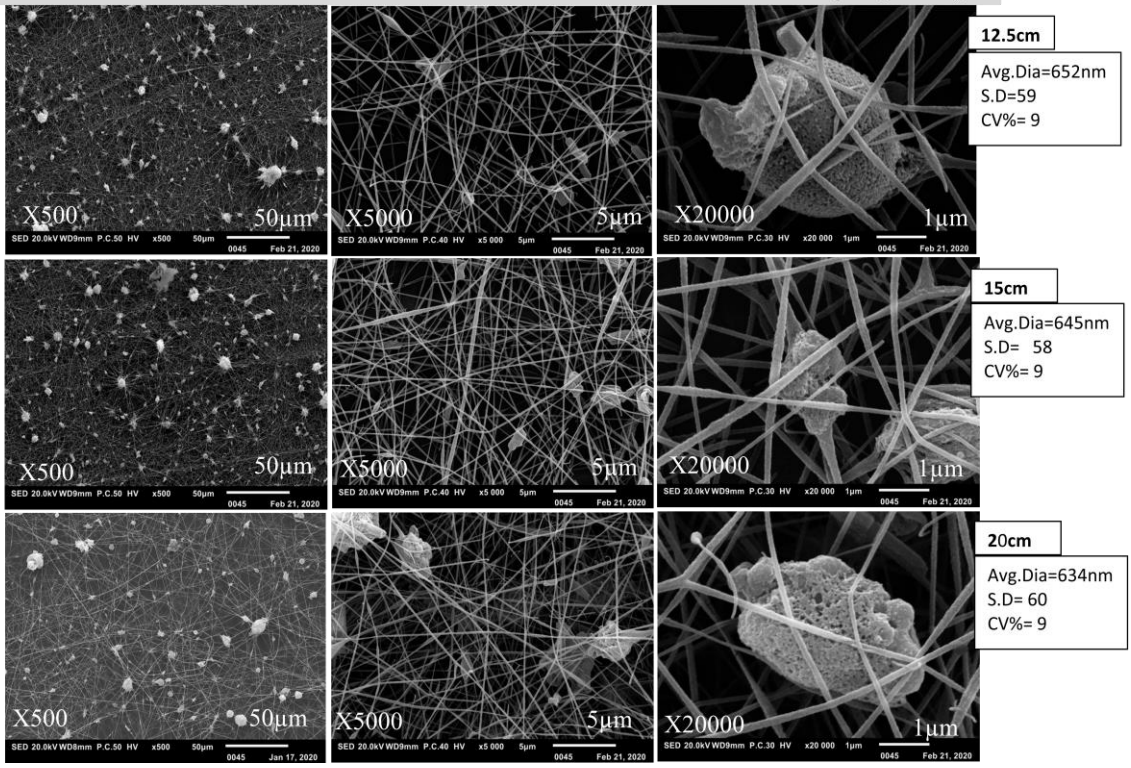
8%PAN+1.7wt%SBA-15 +0.017wt% BYK W-9010 nanofibers SEM Images (70kV)



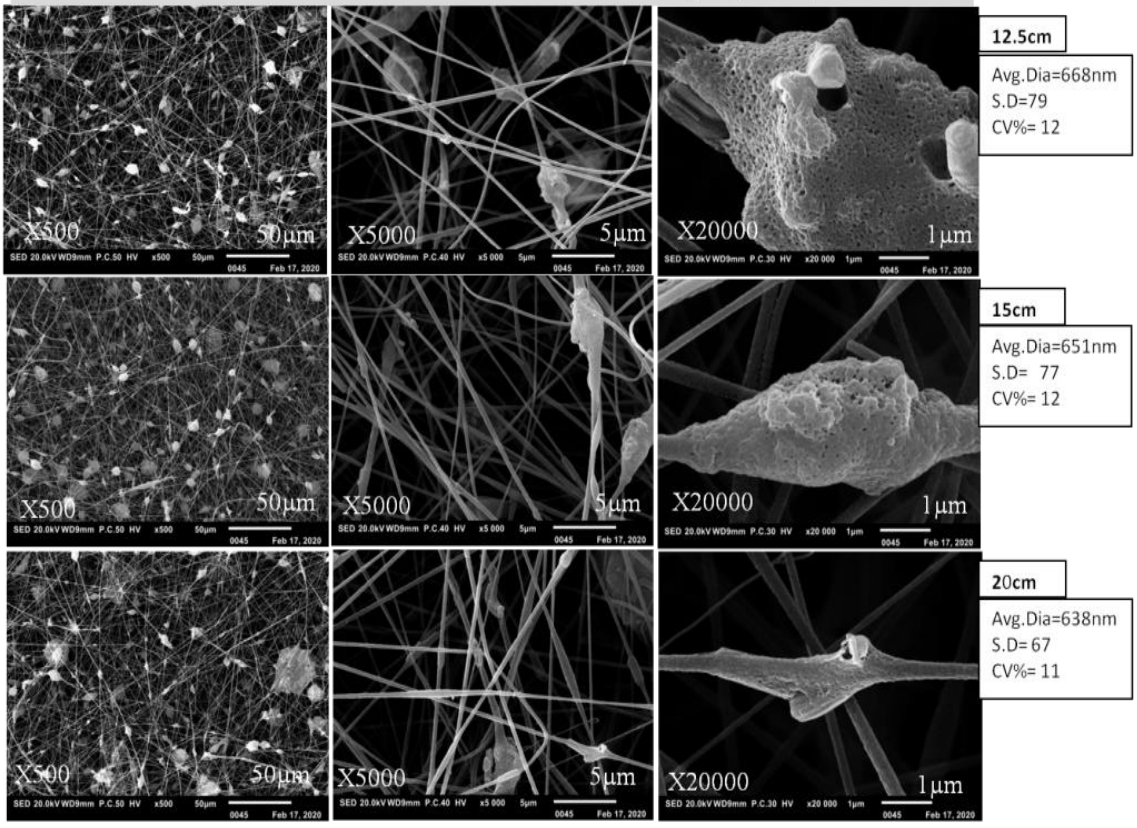
10%PAN+2wt%SBA-15 nanofibers SEM Images (30kV)



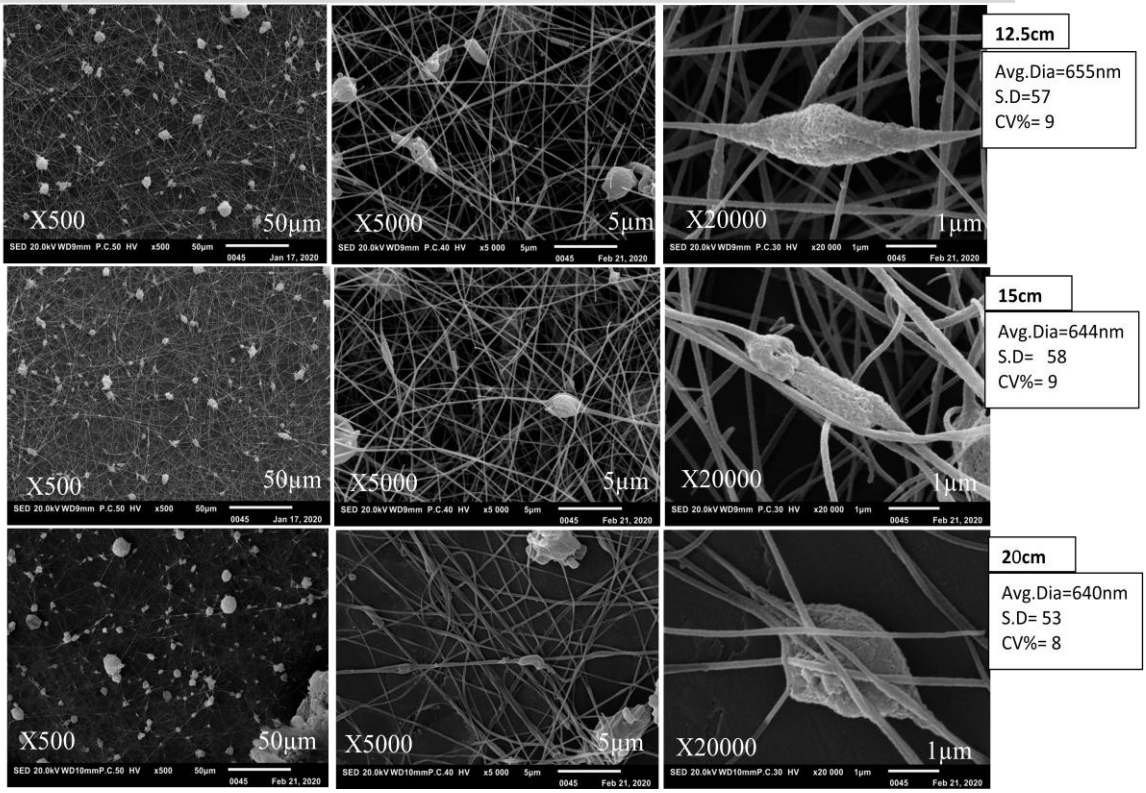
10%PAN+2wt%SBA-15 +0.02wt% BYK W-9010 nanofibers SEM Images (30kV)



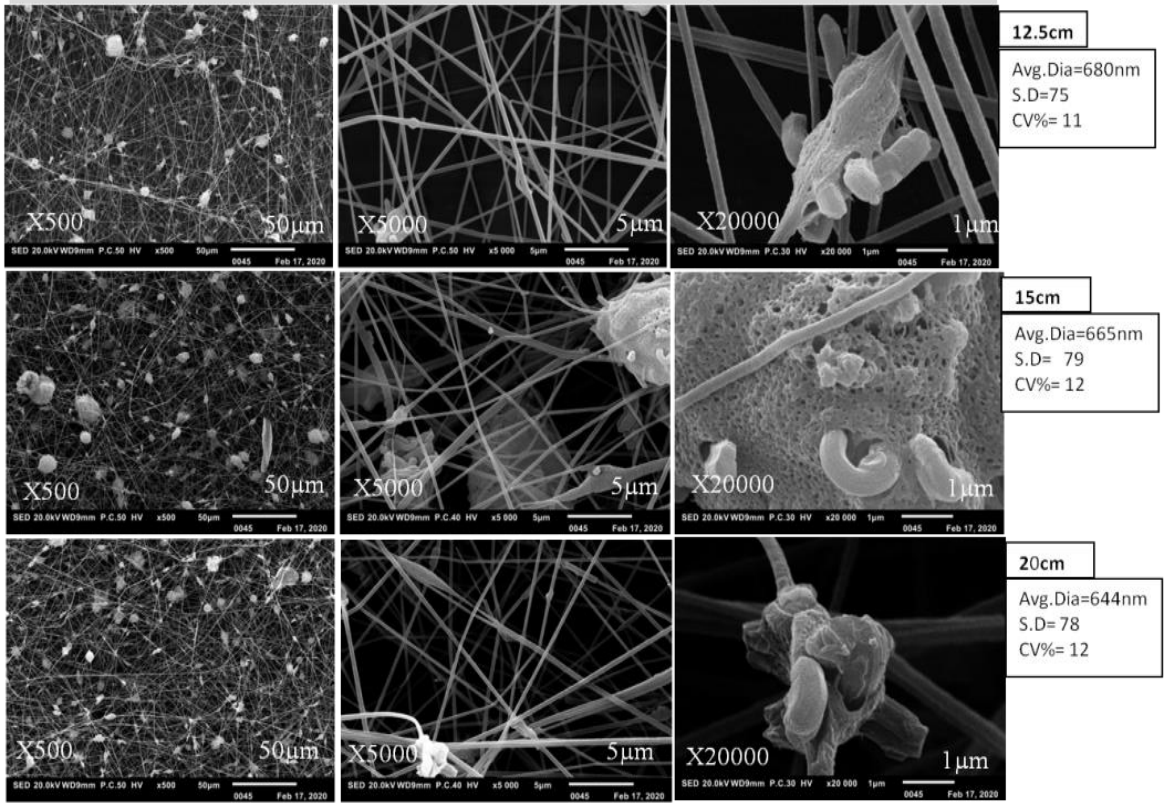
10%PAN+2wt%SBA-15 nanofibers SEM Images (50kV)



10%PAN+2wt%SBA-15 +0.02wt% BYK W-9010 nanofibers SEM Images (50kV)



10%PAN+2wt%SBA-15 nanofibers SEM Images (70kV)



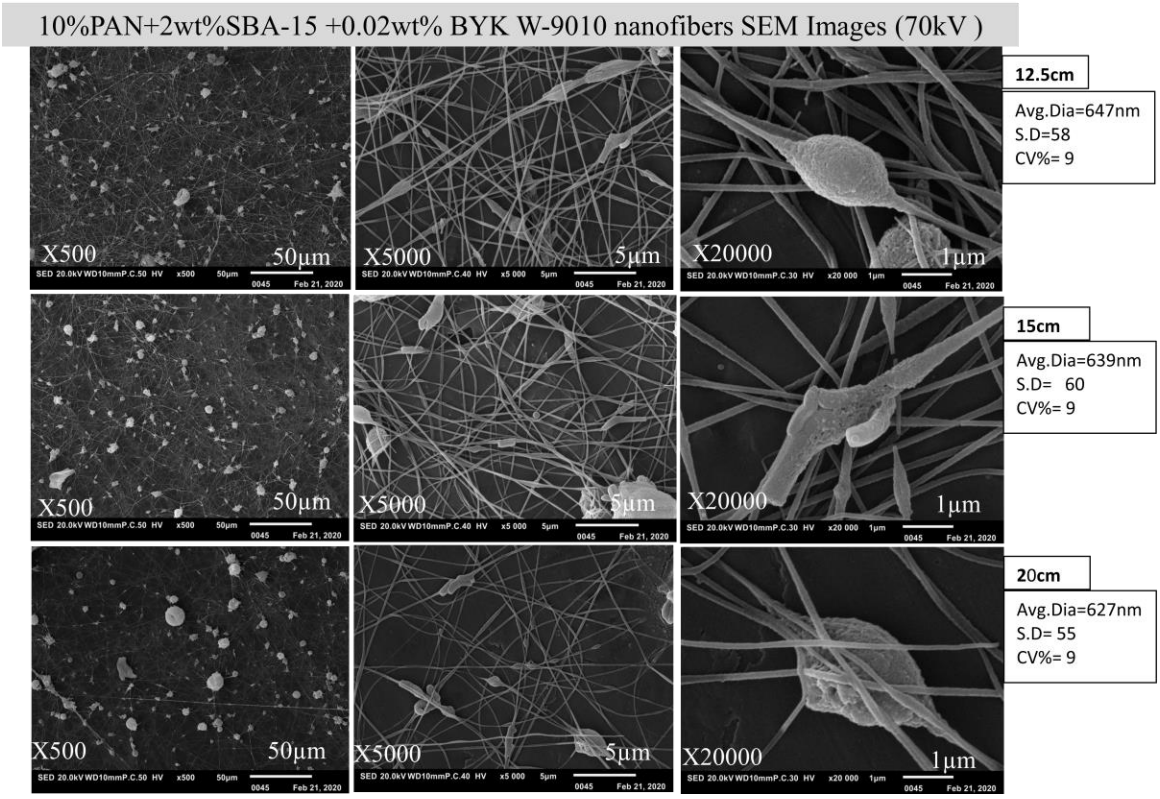


Figure III.14: SEM images of PAN/SBA-15 nanofibers with and without BYK W-9010

3.3.3 Effect of incorporation of SBA-15 on morphology of composite nanofibers

In this section, the morphology of PAN/SBA-15 composite nanofibers is discussed and compared with pristine PAN nanofibers. In the case of PAN 8wt%, 1.7wt% of SBA-15 and in other case of PAN 10wt%, 2wt% of SBA-15 was incorporated in solution and SEM analysis was used for structural analysis. The SEM results in figure III.14 show that the presence of SBA-15 particles leads to non-uniform fibers with very rough surface as compared to pristine PAN nanofibers. In table III.10, there are displayed the standard deviation (SD) and coefficient of variation (CV %) values of PAN/SBA-15 composite nanofibers.

Table III.10: Diameter of PAN/SBA-15 composite nanofibers

S. No	Sample name	Voltage (kV)	Distance (cm)	Nanofibers diameter (nm)- Standard deviation CV in %
1	PAN 8 wt% + 1.7 wt%* SBA-15	30	12.5	585 ± 123 - CV = 21
2			15	577 ± 103 - CV = 18
3			20	561 ± 87 - CV = 15
4		50	12.5	587 ±78 - CV = 13
5			15	573 ± 73 - CV = 12
6			20	552 ± 74 - CV = 14

7		70	12.5	590 ± 81 - CV = 14
8			15	578 ± 77 - CV = 13
9			20	554 ± 63 - CV = 11
10	PAN 10 wt% + 2 wt%* SBA-15	30	12.5	669 ± 78 - CV = 12
11			15	652 ± 78 - CV = 12
12			20	646 ± 73 - CV = 11
13		50	12.5	668 ± 79 - CV = 12
14			15	651 ± 77 - CV = 12
15			20	638 ± 67 - CV = 11
16		70	12.5	680 ± 75 - CV = 11
17			15	665 ± 79 - CV = 12
18			20	644 ± 78 - CV = 12

* wt% compared to PAN and corresponding to 5:1 wt ratio of PAN: SBA-15

By adding SBA-15 particles, the diameter of nanofibers is increased whatever the PAN concentration. The comparison of diameter of PAN and PAN/SBA-15 nanofibers is mentioned in figure III.15.

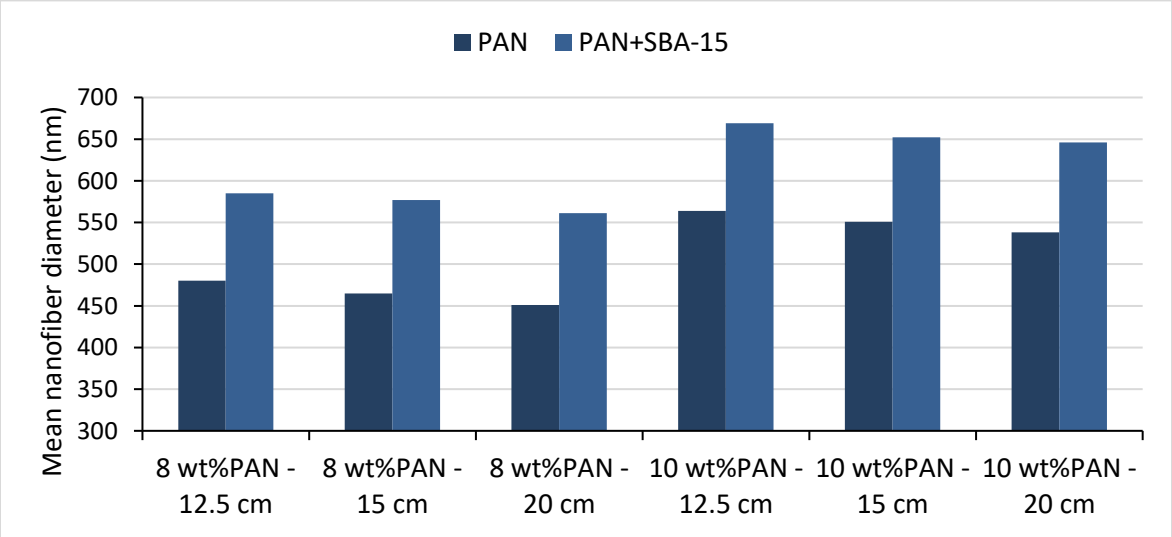


Figure III.15: Impact of SBA-15 addition on PAN diameter

The increase in PAN concentration from 8 to 10 wt % and thus SBA-15 concentration from 1.7 to 2 wt % increased the diameter of nanofibers due to the increase of solution viscosity indicating a better entanglement of polymer chains [75]. More the loading percent of SBA-15, the bigger diameter is and probability of finding more particles closely arranged or aggregated within the nanofibers leading to increase the diameter of the nanofibers. In most of the cases, by increasing electrode distance, the diameter of nanofibers slightly decreased due to extra time of flight jet that resulted in more extension of polymer jet and more time of jet relaxation. The figure III.16

illustrates the effect of the voltage that was varied from 30 to 50 and then 70 kV on the nanofibers diameter.

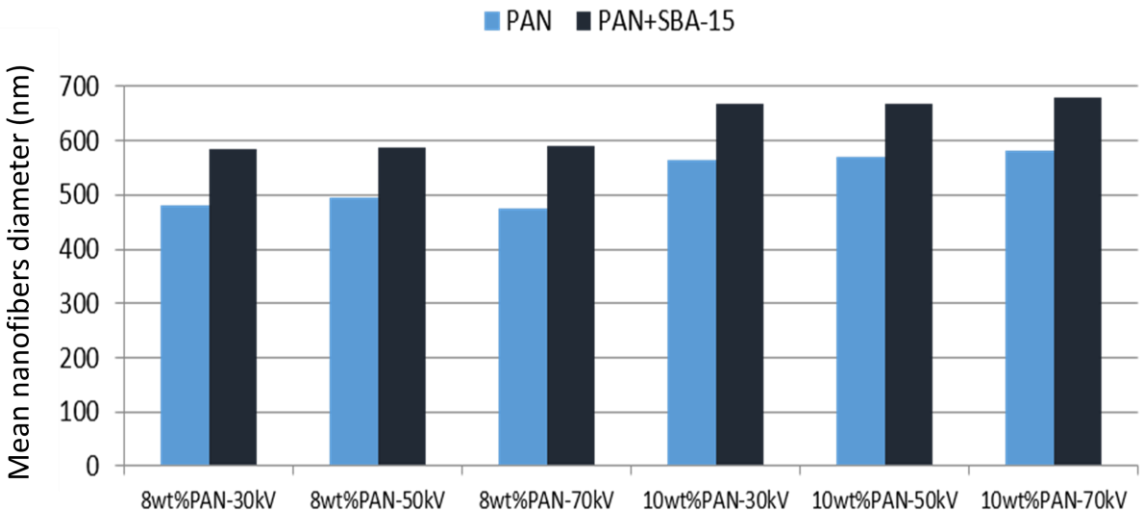


Figure III.16: Variation of the diameter of PAN and PAN/SBA-15 composite nanofibers obtained at 30, 50 and 70 kV for 8 and 10 wt % formulations (electrode distance = 12.5 cm).

For 8 and 10 wt % PAN with and without SBA-15, by increasing voltage, the nanofibers diameter remained almost constant within the experimental error limits.

3.3.4 Effect of incorporation of BYK W-9010 on morphology of composite nanofibers

In this section, the PAN/SBA-15 and PAN/SBA-15+BYK W-9010 composite nanofibers are discussed. The variation of the nanofibers diameter at 30 kV with electrode distance for the 8 and 10 wt % PAN formulations containing SBA-15 and in presence or not of dispersing agent is displayed in figure III.17. By adding dispersing agent in composite nanofibers reduces the diameter of nanofibers and CV% compared to PAN/SBA-15 nanofibers as a result of a better deagglomeration of silica nanoparticles.

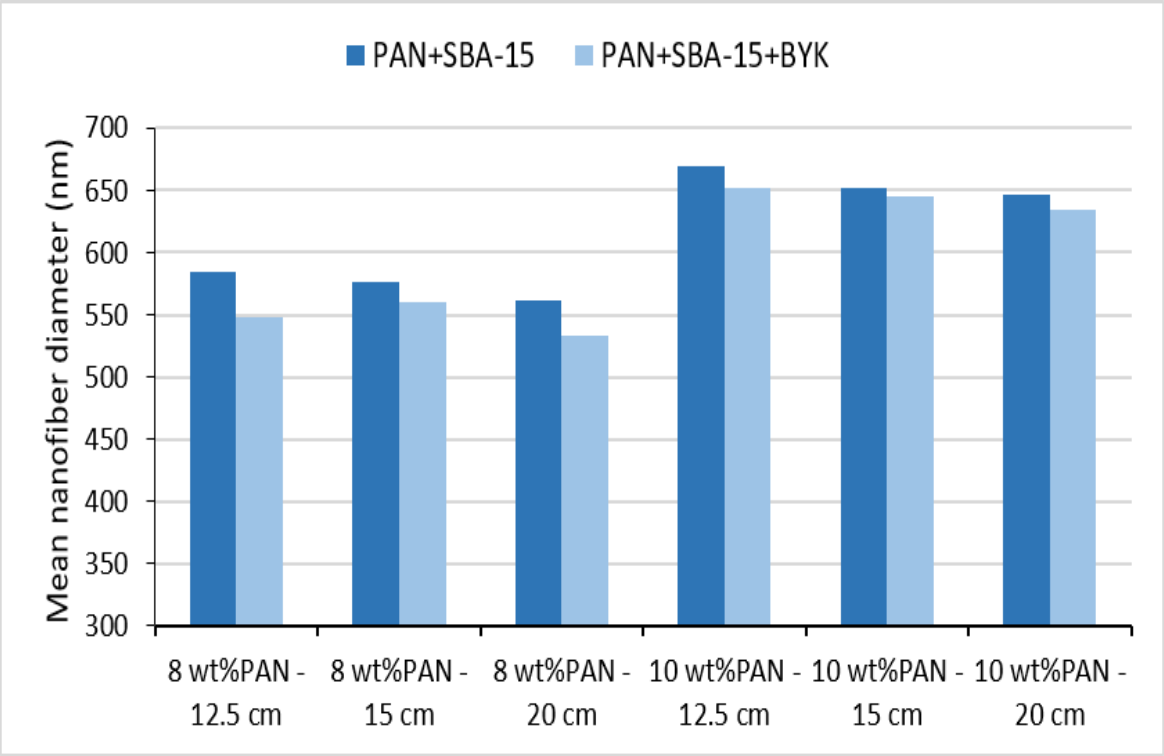


Figure III.17: Variation of diameter of PAN/SBA-15 and PAN/SBA-15+BYK W-9010 composite nanofibers obtained at 30 kV with different electrode distances for 8 wt % and 10 wt % PAN-based formulations.

The impact of concentration of polymer, fillers and applied voltage is similar as discussed earlier in the case of pristine PAN and PAN/SBA-15 nanofibers. In figure III.18, a selection of SEM images of composite nanofibers with and without dispersing agent are displayed and standard deviation (SD) and coefficient of variation (CV %) values are mentioned in table III.11.

Table III.11: Nanofibers diameter, CV%, SD of PAN/SBA-15+BYK W-9010

S. No	Sample name	Voltage (kV)	Distance (cm)	Nanofibers diameter (nm)- Standard deviation CV in %
1	PAN 8 wt% + 1.7 wt%* SBA-15 + 0.017wt%** BYKW9010	30	12.5	548 ± 49 - CV = 9
2			15	560 ± 51 - CV = 9
3			20	533 ± 47 - CV = 9
4		50	12.5	575 ± 49 - CV = 8.5
5			15	534 ± 47 - CV = 9
6			20	513 ± 50 - CV = 10
7		70	12.5	543 ± 53 - CV = 10
8			15	532 ± 56 - CV = 10
9			20	534 ± 51 - CV = 10
10		30	12.5	652 ± 59 - CV = 9
11			15	645 ± 58 - CV = 9

12	PAN 10 wt% + 2 wt%* SBA-15 + 0.02wt%** BYKW9010		20	634 ± 60 - CV = 9
13		50	12.5	655 ± 57 - CV = 9
14			15	644 ± 58 - CV = 9
15			20	640 ± 53 - CV = 8
16		70	12.5	647 ± 58 - CV = 9
17			15	639 ± 60 - CV = 9
18			20	627 ± 55 - CV = 9

* wt% compared to PAN and corresponding to 5:1 wt ratio of PAN: SBA-15

**wt% compared to SBA-15 and corresponding to 100:1 wt ratio of SBA-15: BYK W-9010

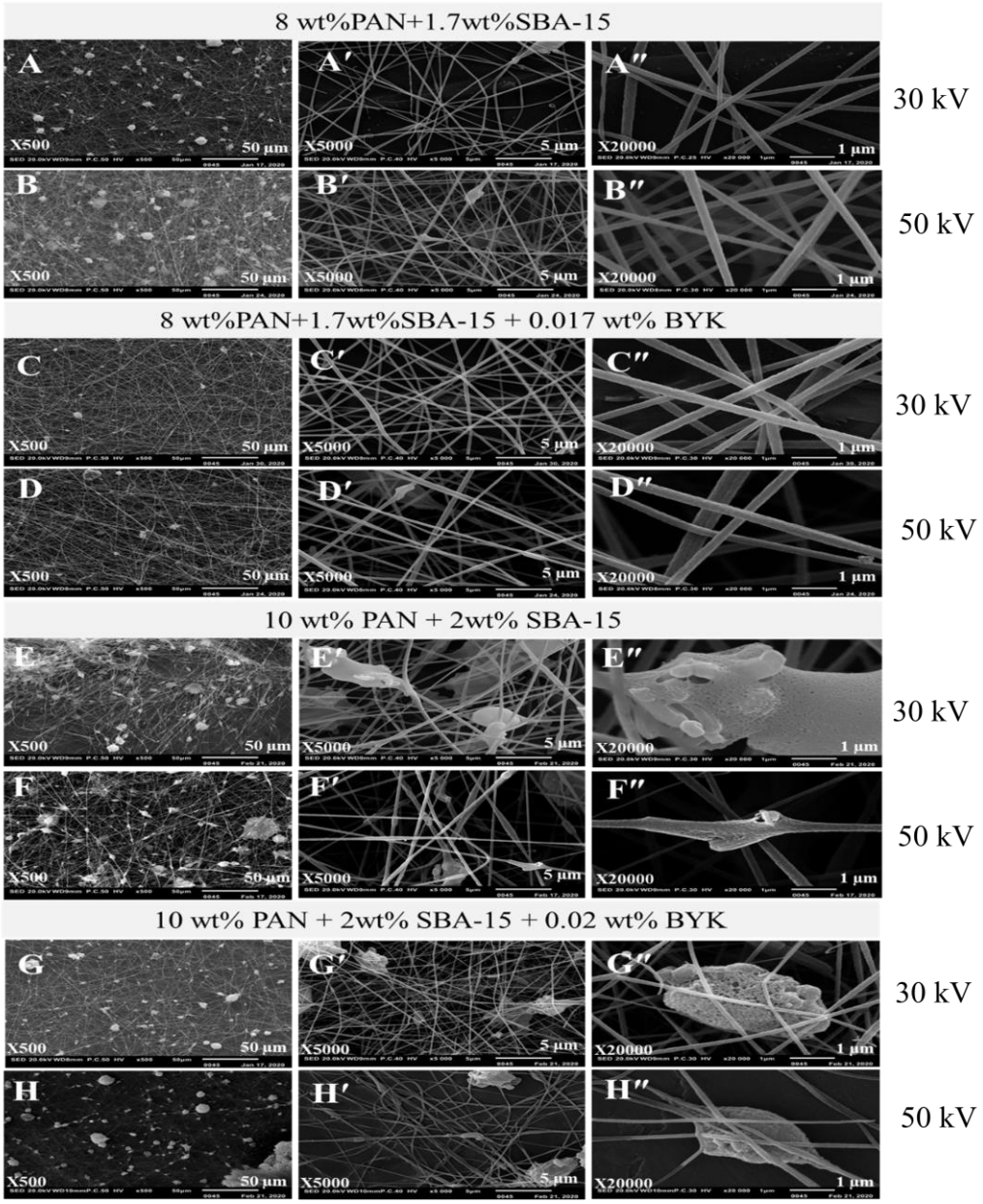


Figure III.18: SEM images of PAN/SBA-15 composite nanofibers produced at 30 and 50 kV (Electrode distance = 12.5 cm).

Whether the PAN concentration is 8 or 10 wt%, for both high voltages 30 and 50 kV, at low magnification, PAN/SBA-15 nanofibers are coexisting with several aggregates that appear sticked to the nanofibers. EDX coupled SEM analyses were realized and confirmed that these aggregates were made of raw PAN (See EDX C and N elemental mappings displayed in section 3.4.2). At higher voltage (50 kV) the aggregates appear more numerous and/or bigger (Figure III.18 A, B, E, F). At high magnification, the presence of rod-shape SBA-15 particles is observed as isolated and glued in nanofibers or glued in the aggregates (Figure III.18 B', E', E', F', F''). The presence of silica particles in the PAN nanofibers and aggregates was confirmed by EDX coupled SEM analyses (See EDX C and N elemental mappings displayed in section 3.4.5). Whatever the voltage, for both 8 and 10 wt% PAN concentrations, the addition of dispersing agent appears to decrease the presence of aggregates (Figure III.18 C, D, G, H). However, the effect of deagglomeration in the presence of dispersing agent appears more beneficial with 8 wt % of PAN. A voltage of 30 kV and a PAN concentration of 8 wt% appear the most suitable conditions to produce PAN/SBA-15 composite nanofibers.

3.3.5 Optimization of the parameters for electrospinning

The SEM images of composite nanofibers with and without dispersing agent and their diameters with standard deviation (S.D) and coefficient of variation (CV %) are displayed in figure III.14. The results show that composite nanofibers without dispersing agent in both PAN concentrations have very high standard deviation and coefficient of variation values, so obtained composite nanofibers are not smooth and uniform. Now, if we compare the composite nanofibers with dispersing agent, they have better uniformity and smoothness as nanofibers without dispersing agent. They have quite impressive results of standard deviation and coefficient of variation. In the case of 8wt%+1.7wt%, among both concentration of PAN/SBA-15, the obtained nanofibers at 30 and 50kV on all collecting distances of 12.5, 15, 20 cm have better results of uniformity. The best optimized parameters in the case of composite nanofibers at are mentioned in table III.12.

Table III.12: Optimized electrospinning parameters for composite nanofibers

Sample	Viscosity (mPa/sec)	Voltage kV	Distance cm	Nanofibers diameter (nm)
8wt% PAN+1.7wt		30	12.5	548±49 CV%= 9
			15	560±51 CV% =9

%SBA-15+0.017wt %BYK W-9010/DMSO	2370 ± 53		20	533±47 CV% = 9
		50	12.5	575±49 CV%=8.5
			15	534±47 CV%= 9
			20	513±50 CV%=10

Relative humidity: 34±2% Temperature: 20±2 °C

Table III.13 describes the electrospinning conditions of PAN/SBA-15 composite nanofibers in literature for comparison of electrospinning condition in this study.

Table III.13: Electrospinning conditions of literature [7, 14]

Sample	**Voltage kV**	**Distance cm**	**Feed rate mL/h**	**Nanofibers diameter nm**
10wt%PAN+3wt%SBA-15/DMF	29	15	2	487 ± 65
15wt%PAN+15wt%SiO_2/DMF	13	15	0.5	709 ± 76

The resultant composite nanofibers of this study are quite impressive in the terms of their better standard deviation values as compared to the nanofibers in literature.

3.3.6 Analysis of thermal stability by incorporation of SBA-15 and BYK W-9010 in PAN nanofibers

To study the thermal degradation of pure PAN nanofibers and PAN/SBA-15 composite nanofibers the process of TGA is commonly used. This process offers a quantifiable analysis of the amount of moisture and volatile compounds present in the nanocomposites fibers, weight loss and thermal breakdown. It is determined that by thermal degradation of polyacrylonitrile: hydrogen cyanide and ammonia are the main constituents of degradation [204]. Figure III.19 shows the thermogravimetric curves recorded under air of pure PAN nanofibers and PAN/SBA-15 composite nanofibers.

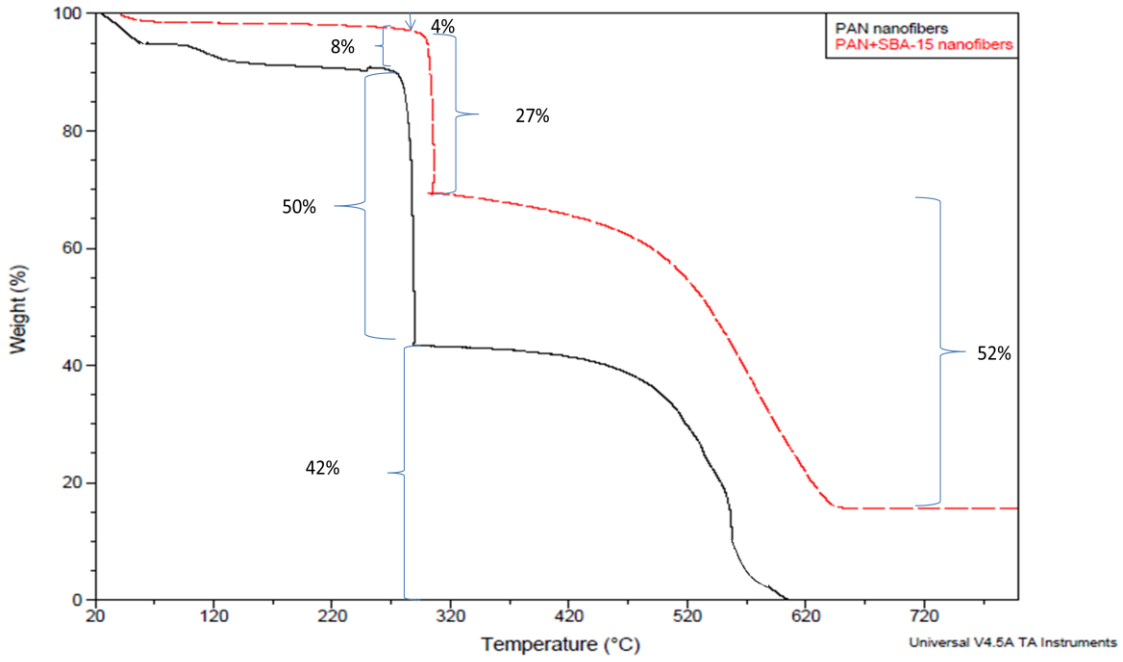


Figure III.19: TGA curves of 8wt% pristine PAN nanofibers (black lines) and 8 wt % PAN/1.7wt % SBA-15 (dotted lines) composite nanofibers.

The heating of PAN produces chemical reactions, such as, cyclization, degradation and cross-linking, so the mechanism of these processes depends on the heating rate, atmosphere, mass of polymer and nature of the filler materials [205]. TGA curves of pure PAN nanofibers and PAN/SBA-15 composite nanofibers show a three-step weight loss. From 20 to 200°C, both pristine PAN and composite PAN/SBA-15 nanofibers exhibits a weight loss, which can be attributed to the desorption of DMSO and physically adsorbed water [218]. The major weight loss observed from 250 to 350°C corresponds to dehydrogenation reactions with maxima at 310 ^{o}C for pure PAN nanofibers and at 298 ^{o}C for PAN/SBA-15 composite nanofibers. The dehydrogenation reactions correspond to the PAN cyclization reaction [206,207]. The corresponding weight losses associated to these reactions are 36 and 26 % for PAN and PAN/SBA-15 composite nanofibers, respectively. These exothermic weight losses are due to the oligomerization of nitrile groups in PAN [208]. The third weight loss observed in the temperature range from 320 ^{o}C to 720°C for pristine PAN and PAN composite nanofibers may be attributed to the evaporation of anhydrous ammonia (NH_3), (HCN), and PAN polymer chain fragments. The thermal decomposition of pristine PAN is complete at 710°C but in the case of composite nanofibers, about 17 wt % of residue is remaining at temperature up to 650°C, which

corresponds to SBA-15. Higher thermal stability is observed due to the presence of SBA-15 in pristine PAN nanofibers. The delay in PAN cyclization is likely due to the strong hydrogen bridges between PAN nitrile groups (-C≡N) and SBA-15 silanol groups (-Si-OH) [16].

TGA and DTA were also realized on PAN/SBA-15/BYK W-9010 composite nanofibers and similar curves were obtained (Figure III.20). From TGA total weight losses; the SBA-15 contents of 15.7 wt% and 16.7 wt% were determined for 8 wt % PAN/1.7 wt % SBA-15 and 8 wt % PAN/1.7 wt % SBA-15/0.017 wt % BYK nanofibers, respectively.

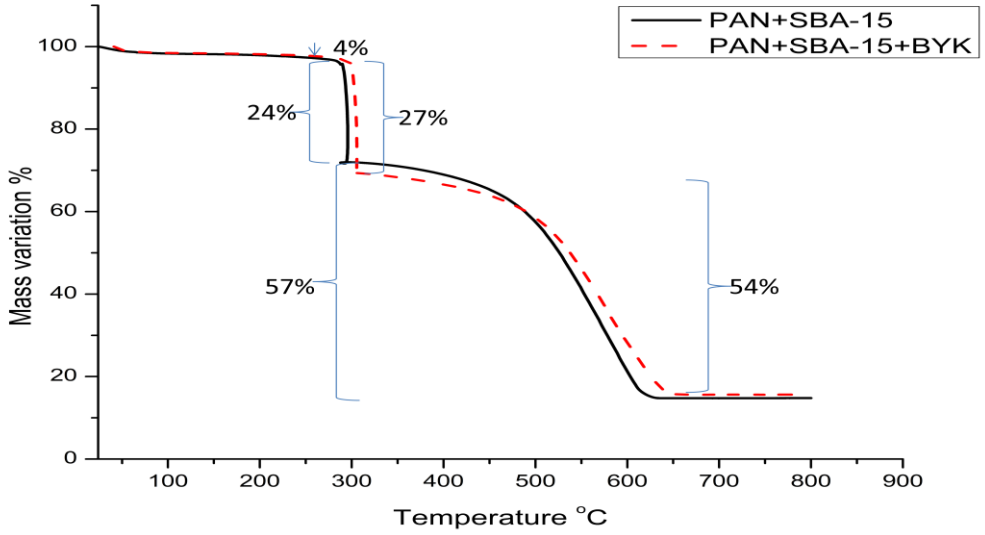


Figure III.20: TGA curves of 8wt% PAN/1.7wt% SBA-15/0.017wt% BYK W-9010 (dotted lines) and 8 wt % PAN/ 1.7wt % SBA-15 (black lines)

3.3.7 Conclusion

Rheological analysis shows that below 7wt% of PAN concentration electrospinning is not possible and addition of silica sub-micron particles increased the viscosity of the suspension whereas dispersing agent does not impact the viscosity. Fabricated composite nanofibers were analyzed and 8wt%of PAN+1.7wt% SBA-15+0.017wt%BYK W-9010 were optimized at 30, 50 kV and 12.5, 15, 20 cm for further process on the basis of CV% and S.D. It was also observed on SEM images of composite nanofibers that some part of silica particles was entrapped into nanofibers surface and other part was on the surface of nanofibers and porosity of the SBA-15 part on the surface can be accessed.

3.4 Characterization of electrospun nanofibers

All the characterizations of pristine PAN and PAN/SBA-15 composite nanofibers are presented here.

3.4.1 Accessibility of pores and BET surface area of PAN/SBA-15 composite nanofibers

N_2 adsorption/desorption isotherms with BJH desorption pore size distribution of electrospun 8 wt % PAN-based composite nanofibers are displayed in figure III.21.

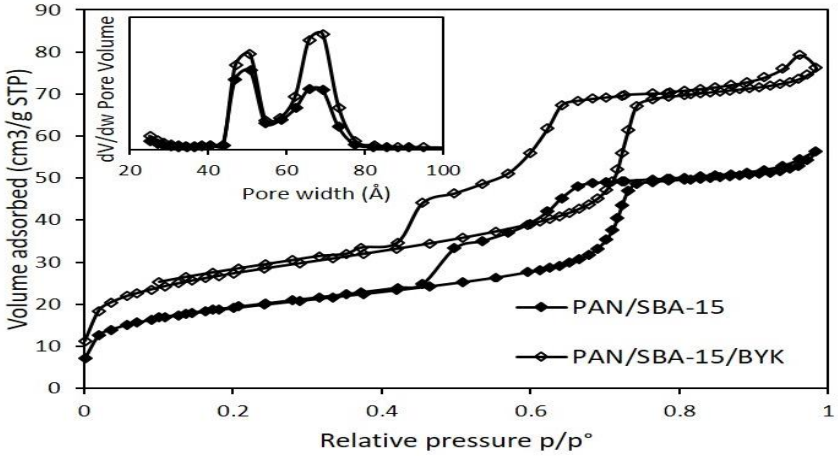


Figure III.21: N_2 adsorption/desorption isotherms of 8 wt % PAN/SBA-15 composites. Insets: BJH desorption pore size distributions.

The isotherms of PAN/SBA-15 with and without BYK W-9010 dispersing agent are also a mixture of type I and type IV. There is also a small increase of the volume adsorbed at high relative pressure indicating textural porosity. However, the hysteresis type H1+H3 is composite and the isotherm looks like the one of plugged hexagonal templated silica (PHTS) material with combined micro- and mesopores. The desorption at higher pressures is associated with the evaporation of liquid from open pores. On the other hand, plugged mesopores remain filled until they empty via cavitation. Consequently, the pore size distribution is bimodal with 2 pore sizes: a small one of about 5 nm due to the cavitation phenomena when plugged mesopores empty, and the larger one of 6.9 nm corresponding to the main mesopores of the raw SBA-15. Pore plugging may be due to the penetration of PAN at the entrance of mesopores. Specific surface areas, pore volumes and pore sizes determined from the N_2 adsorption/desorption isotherms are reported in table III.14.

Table III.14: SBA-15 content (wt %) determined by TGA and textural characteristics determined from N_2 adsorption/desorption isotherms.

Sample	wt% SBA-15[a]	S_{BET} (m^2/g)	Pore volume[b] (cm^3/g)	Micropore volume[c] (cm^3/g)	Pore width[d] (nm)
8 wt% PAN/1.7 wt% SBA-15	15.7	68.7	0.08	0.009	5.4
8 wt% PAN/1.7 wt% SBA-15/0.017 wt% BYK W-9010	16.7	98.5	0.11	0.015	5.5

[a]weight percentage of SBA-15 in composite nanofibers determined by TGA analysis performed under air = mass loss between 200 and 700°C, [b]determined at p/p0 = 0.9, [c]determined by t-plot method, [d]value corresponding to the maximum of the PSD

The specific surface area and pore volumes of composite nanofibers are much smaller than the one of the raw SBA-15 because of the presence of non-porous PAN (83.3 wt % for PAN: SBA-15 wt ratio of 5:1). The TGA realized on composite nanofibers have shown that composite nanofibers without and with BYK W-9010 contain 15.7 wt% and 16.7 wt% of SBA-15, respectively. Since the S_{BET} of raw SBA-15 is 917 m^2/g, the S_{BET} for a physical mixture of PAN/SBA-15 with PAN: SBA-15 wt ratio of 5:1 is expected to be 153 m^2/g in case of 100% accessibility of SBA-15. However, the S_{BET} of nanofibers composites is lower indicating that the porosity of SBA-15 is not totally accessible. For 8 wt % PAN/1.7 wt % SBA-15, the S_{BET} of 68.7 m^2/g would indicate that 45 % of the porosity is accessible. In the case of 8 % wt PAN/1.7 wt % SBA-15/0.017 wt % BYK the S_{BET} is higher with 98.5 m^2/g that corresponds to 64 % of accessible porosity. The higher pore accessibility may be relied to the deagglomeration effect of the dispersing agent.

3.4.2 Chemical analysis of PAN, PAN nanofibers and PAN/SBA-15 nanofibers

The chemical analysis of PAN powder and PAN nanofibers is compared in figure III.22 where FTIR spectra are displayed. The small band for PAN powder at 3650 cm^{-1} is observed due to OH stretching vibration. The bands at 2939cm^{-1}, 2940 cm^{-1} for PAN powder and PAN nanofibers and 1452 cm^{-1} for both samples are due to C-H stretching and CH in C-H_2 bending vibrations. A big band at 2243 cm^{-1} in both samples corresponds to saturated nitrile group of C≡N stretching vibration. The bands at 1628 cm^{-1} and 1630 cm^{-1} for both samples are result of C=C. Bands at 1356 cm^{-1} and 1363 cm^{-1} in both samples are related to bending vibration of CH_3 symmetric to CCH_3. Bands in the range of 793 cm^{-1} are created as a result of =C-H group, 1070 cm^{-1} is

assigned to C-N and 534 cm^{-1} and 538 cm^{-1} for PAN powder and PAN nanofibers are C=O bending and twisting vibrations [206, 209, 210, 211].

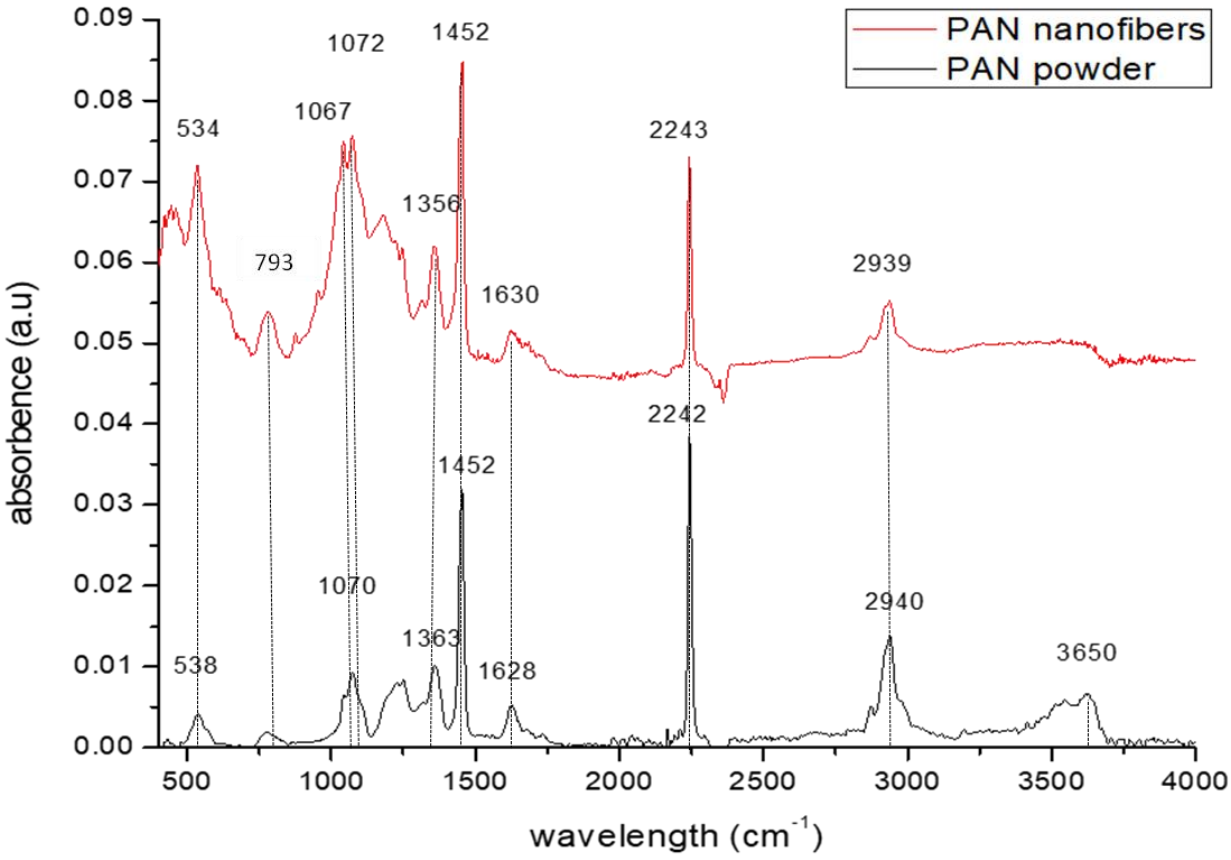


Figure III.22: FTIR spectra comparison of PAN powder and PAN nanofibers

In figure III.23, is presented the FTIR spectra comparison of PAN/SBA-15 composite nanofibers with and without dispersing agent named BYK W-9010. The bands close to 458 cm^{-1}, 801 cm^{-1} and 1083 cm^{-1} in both samples corresponds to the stretching, bending and out of plane Si-O bonds respectively. The peak close to 939 cm^{-1} is the result of Si-OH stretching in both samples. The peaks of PAN are assigned as follows: close to 535 cm^{-1} for C=O twisting vibration, 1241 cm^{-1} for stretching vibration of C-N, 1452 cm^{-1} scissor vibration of C-H in C-H_2, 2242 cm^{-1} stretching vibration of saturated nitrile group C≡N and 2940 cm^{-1} stretching vibration of C-H and 1363 cm^{-1} bending vibration of CH_3 symmetric to CCH_3 . The results of bands of both samples are also identical, because the quantity of dispersing agent was very small no band of P-OH in the range of 2300-2100 cm^{-1} and 2700-2560 cm^{-1} and no band of P=O at 1680 cm^{-1} were detected [206, 209, 210, 211, 212].

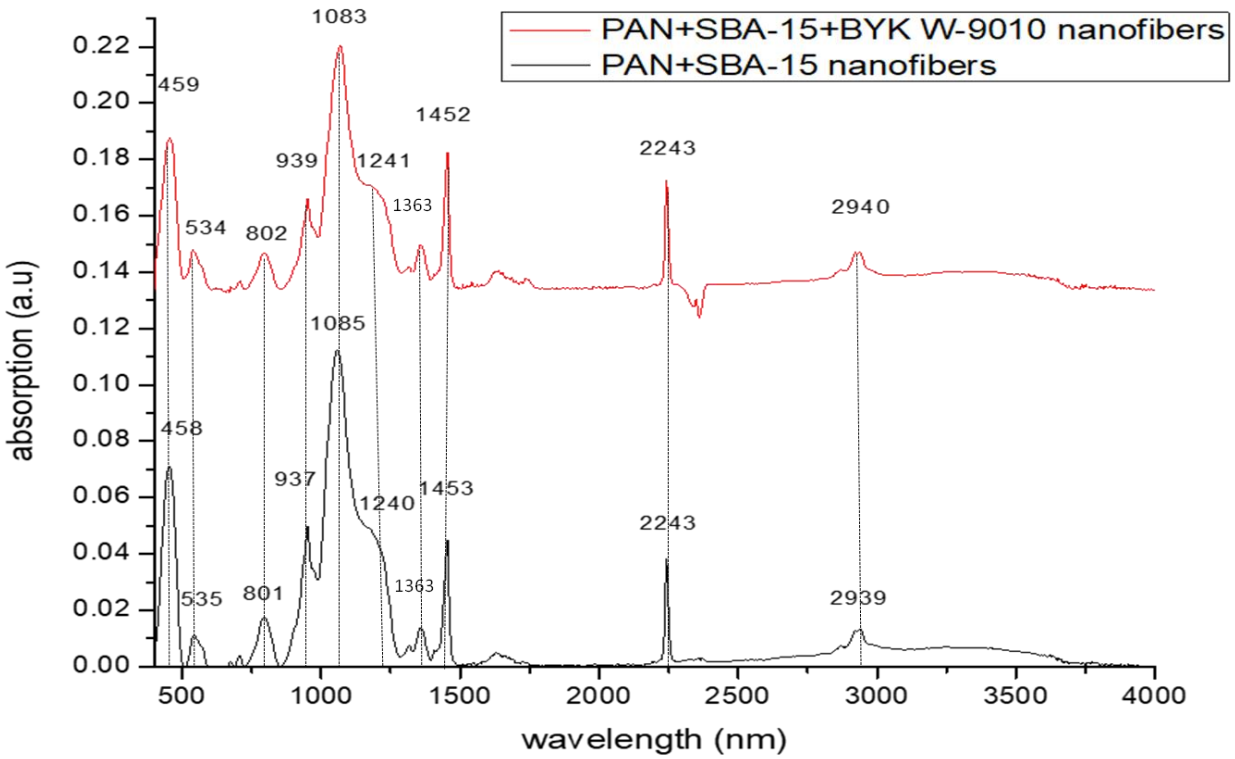


Figure III.23: FTIR spectra comparison of PAN/SBA-15 composite nanofibers with and no BYK W-9010

3.4.2 Elemental composition analysis of PAN and PAN/SBA-15 nanofibers

To investigate the aggregates of elements of pristine PAN and PAN/SBA-15 nanofibers, EDX was performed. Figure III.24 explained the EDX coupled SEM analyses of PAN and composite nanofibers and confirmed the presences of aggregates in pristine PAN nanofibers and these aggregates were made of C and N. Whereas in the case of composite nanofibers, silica aggregates were observed because silica particles were entrapped due to PAN on the surface nanofibers.

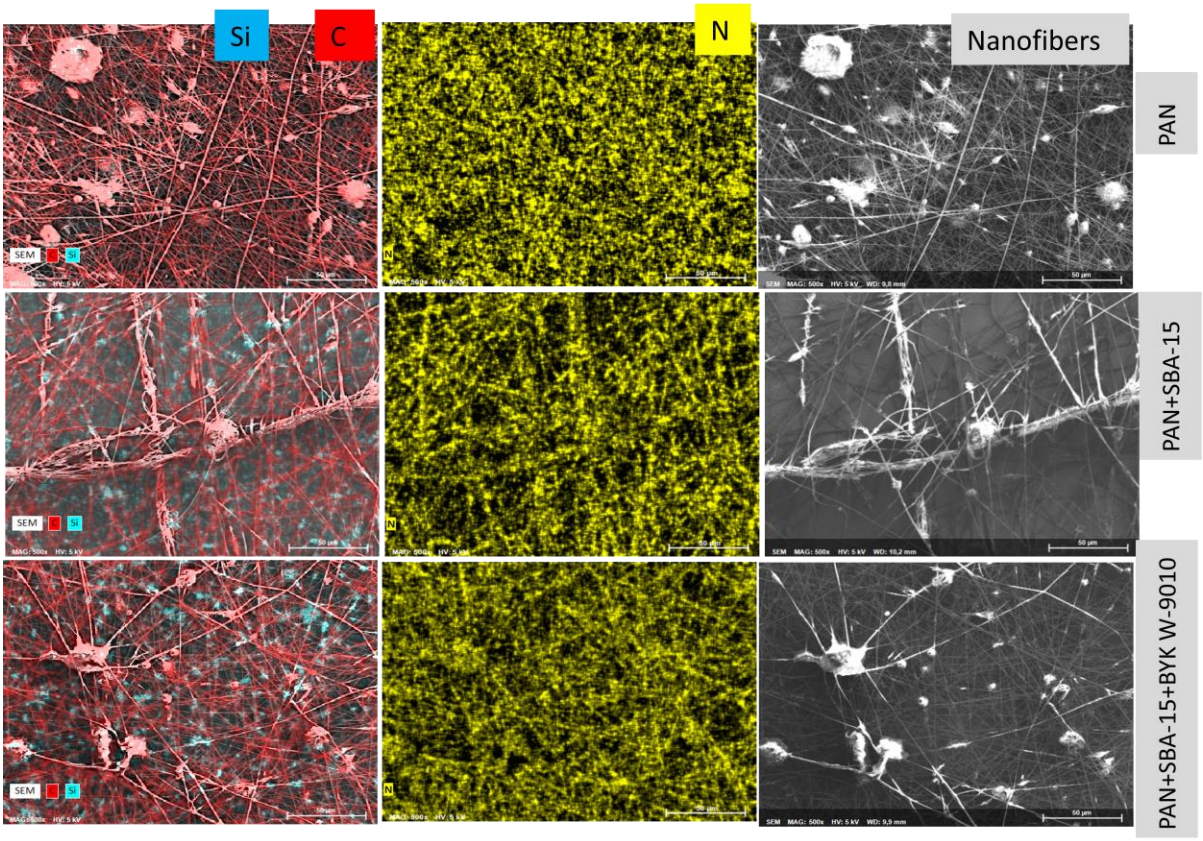


Figure III.24: Elemental mapping images of PAN and composite nanofibers

3.4.4 Analysis of mechanical strength of pristine PAN and PAN/SBA-15 composite nanofibers

Five tensile tests were performed on each 8 wt % PAN-based nanofibers sample produced at 50 kV and the average tensile strength and Young's modulus are reported in table III.15.

Table III.15: Tensile strength and Young's Modulus of samples obtained from 8 wt % PAN formulations at 50 kV with electrode distance of 15 cm.

S. No	Sample name	Avg. Tensile strength (MPa)	Young's Modulus E (MPa)
1	8 wt % PAN	0.61±0.05	0.06±0.004
2	8 wt % PAN + 1.7 wt % SBA-15	1.22±0.05	0.12±0.007
3	8 wt % PAN + 1.7 wt % SBA-15 + 0.017 wt % BYK W-9010	0.92±0.08	0.09±0.006

The results show that the addition of SBA-15 particles in PAN nanofibers increased the tensile strength compared to raw PAN nanofibers because of high storage modulus that increased the

tensile and impact strength due to good stress transfer [202]. However, the deagglomeration of SBA-15 particles with dispersing agent did not improve tensile strength. High strength of PAN/SBA-15 composite nanofibers with or without dispersing agent is also due to interfacial interaction between silica particles and PAN matrix [12].

3.5 Conclusion

Synthesized SBA-15 had surface area of 917 m^2/g and micropores value was 0.165 cm^3/g. Particles size measurement explained that 1wt% of BYK W-9010 with the help of mechanical stirrer is optimized for better deagglomeration of silica particles. Viscosity of PAN/DMSO and PAN+SBA-15/DMSO solution results showed that below 7wt% of polymer concentration there was just electrospraying due to lack of molecular chains interactions. Optimized electrospinning parameters on the basis of coefficient of variation and standard deviation were 8wt% PAN+1.7wt% of SBA-15 at 30, 50 kV and 12.5, 15 and 20 cm electrodes distance. Composite nanofibers with dispersing agent had 98.5 m^2/g surface area and accessible porosity of 64% as compared to no dispersing agent composite nanofibers, which had 68.7 m^2/g surface area, and 45% accessible porosity. Introduction of silica particles increase the diameter and non uniformity of pristine PAN nanofibers whereas dispersing agent reduces the agglomeration and diameter of composite nanofibers. Chemical analysis showed the presence of nitrile group, silanol group bands whereas no peak of BYK W-9010 detected as its quantity was very small. Mechanical strength of composite nanofibers was increased as compared to pristine PAN nanofibers due to strong polymer filler interaction which resulted in higher storage modulus and complex viscosity.

Next chapter will explain the adsorption behavior of Methylene blue, Neutral red and Congo red dyes on different samples including SBA-15, composite nanofibers and pristine PAN nanofibers. It will also explain the impact of pH, dye concentration, contact time and temperature on adsorption of all presented dyes. The results of adsorption kinetics, adsorption isotherm will also be presented here. And at the end to reduce the process cost, recyclability of the fibers by desorption of all dyes will be discussed.

Chapter IV

Efficiency of PAN nanofibers loaded with SBA-15 for dye removal from aqueous solution

Chapter IV

Efficiency of PAN nanofibers loaded with SBA-15 for dye removal from aqueous solution

Introduction

In this chapter, the mechanism of adsorption of three different dyes including Methylene Blue, Neutral Red and Congo Red on SBA-15 particles, PAN+SBA-15 composite nanofibers and pristine PAN nanofibers is investigated. The pseudo 1st and 2nd order kinetics models and the Langmuir and Freundlich isotherm models have been applied on the data sets obtained during the adsorption of dyes to investigate the type of adsorption process. Impact of pH, initial dye concentration and contact time on dye adsorption was also studied. Thermodynamic parameters such as standard Gibb's free energy ($\Delta G°$), standard enthalpy change ($\Delta H°$) and standard entropy change ($\Delta S°$) were evaluated at equilibrium conditions to gain an understanding of the nature of entrapment. Results obtained in such a fundamental study will be useful in manufacturing of PAN based composite entrapment for the treatment of effluents containing cationic and anionic dyes such as those generated in dying industries.

4.1 Types of dyes

Ionic dyes are of two types:

- Cationic dyes
- Anionic dyes

4.1.1 Cationic dyes

The dye level in the textile effluent ranges from 10-50 mg/l and sometimes can be higher [228]. Cationic dyes can be dissociated into positively charged ion in an aqueous solution. They can interact with the negative groups present on the surface of adsorbents. There are many types of cationic dyes such as azo dyes, triarylmethane dyes and anthraquinone dyes. The commonly used is the cationic portion in the dyes having an onium group to form salt during adsorption process. These dyes are water soluble with strong affinity and fastness and also have excellent light resistance and heat resistance [213, 214].

4.1.2 Anionic dyes

The reactive dyes in textile industry are discharged at the concentration of 60 mg/l and sometimes can be increased from 100 to 200 mg/l [228]. These dyes are soluble in water and they possess acidic groups, such as SO_3H and COOH and are mostly applied on wool, silk and nylon when ionic bond is established between protonated $–NH_2$ group of fibers and acid group of dye. Overall washing fastness is poor whereas light fastness is good [213, 214].

4.2 Methylene Blue (MB)

Methylene Blue (MB) is a cationic dye having molecular weight of 319 g/mol and chemical formula is shown in figure IV.1.

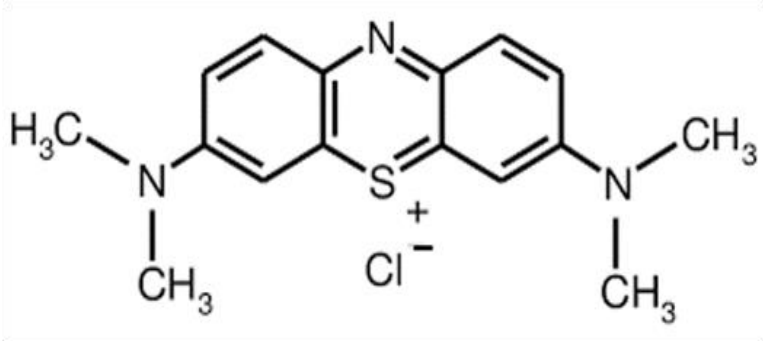


Figure IV.1: Chemical formula of methylene blue (MB)

MB has vast applications in textile, paper, wood, pulp and medical industry [17, 18, 215].

4.2.1 Effect of concentration

The effect of increase in MB concentration (from 15 to 90 µM) and their adsorption rate at equilibrium (15 µM= 100 min, 30 µM=150 min, 45 µM= 170 min, 60 µM= 170 min, 75 µM = 180 min and 90 µM= 200 min) on all adsorbents (SBA-15, PAN nanofibers and PAN composite nanofibers) at neutral pH and room temperature are shown in figure IV.2.

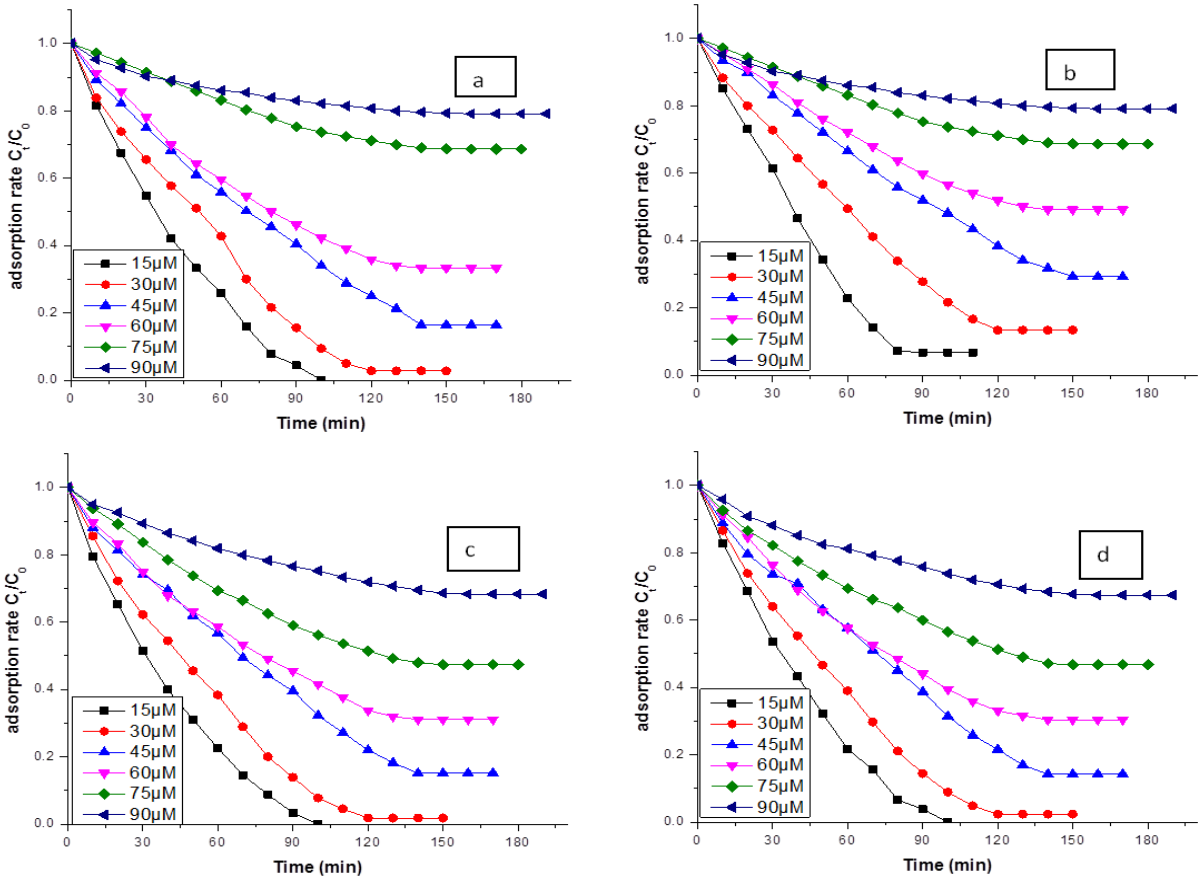


Figure IV.2: Adsorption rate at different concentrations of MB (pH 7 and room temperature) on SBA-15 (a), PAN nanofibers (b), PAN+SBA-15 nanofibers (c) and PAN+SBA-15+BYK nanofibers (d)

Figure IV.2 shows that by increasing MB concentration the adsorption rate decreases, whatever the adsorbent is. This is due to the increase of dye's cations ratio to the dose of the adsorbent and the number of active adsorption sites required to accommodate the remaining adsorbate while the number of adsorbate increases and hence the removal efficiency of MB decreases.

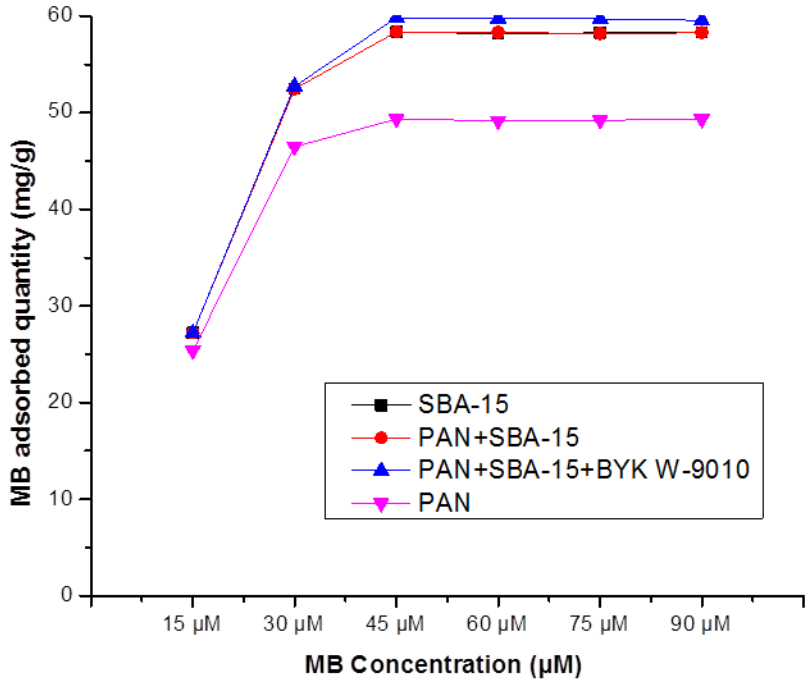


Figure IV.3: MB adsorbed quantity (mg/g) on all adsorbents at different concentrations of MB at neutral pH and room temperature

The figure IV.3 shows that initially MB was adsorbed rapidly and the highest adsorption capacity was observed at 45µM for all adsorbents and at higher concentration the adsorption became constant due to saturation of active sites.

4.2.2 Adsorption kinetics

Adsorption kinetics is the rate of retention of a solute from an aqueous environment to solid-phase interface at a given adsorbent dose, temperature, flow rate and pH. To measure the rate of adsorption, a mother aqueous solution of 90µM was prepared with distilled water at room temperature and was used to prepare daughter solutions of 15, 30, 45, 60 and 75 µM in distilled water whose pH was around 7. All the solutions were prepared in vials that were wrapped in aluminum foil to avoid any decomposition under sunlight. The adsorption mechanism of Methylene Blue onto SBA-15, pristine PAN nanofibers and composite nanofibers with and without dispersing agent was analyzed by two linear kinetic models including pseudo 1^{st} order and pseudo 2^{nd} order [5,34,36,41] and the results at neutral pH and room temperature are described in figure IV.4.

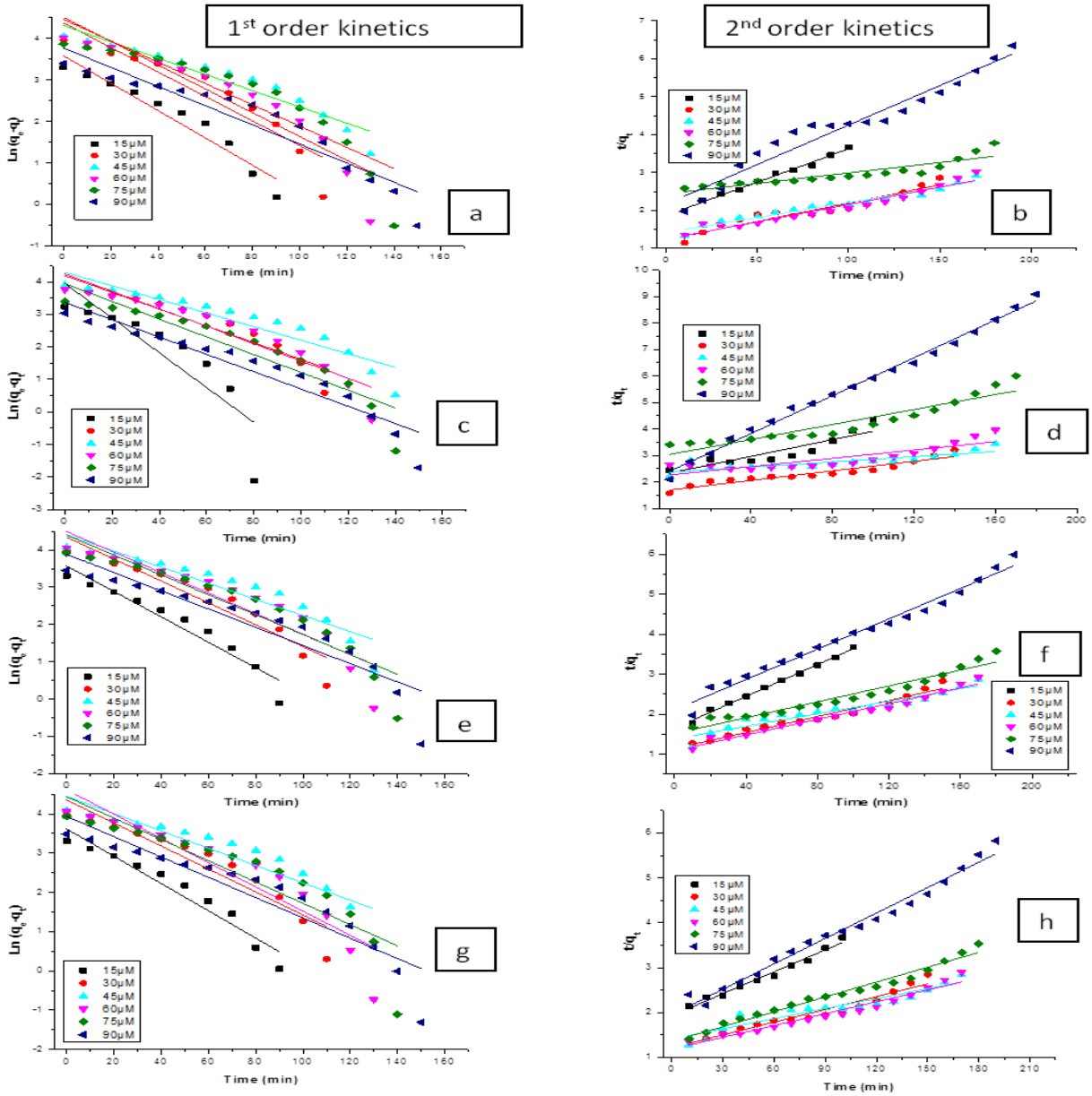


Figure IV.4: Pseudo 1st and 2nd order kinetics models of MB adsorption at neutral pH and room temperature on SBA-15 (a, b), PAN nanofibers (c, d), PAN+SBA-15 nanofibers (e, f) PAN+SBA-15+BYK nanofibers (g, h)

Pseudo 1st and 2nd order kinetics equations 15 and 16, respectively, are described in the second chapter. The parameters values at neutral pH and room temperature of both kinetic models and the correlation coefficients (R^2) were obtained by plotting graphs $Ln(q_e-q_t)$ versus t and t/q_t versus t for 1st and 2nd order kinetics, respectively. These values are listed in tables IV.1 for SBA-15, IV.2 for PAN nanofibers, IV.3 for PAN+SBA-15 composite nanofibers and IV.4 for PAN+SBA-15+BYK W-9010 composite nanofibers.

Table IV.1: Pseudo 1st and 2nd order kinetics parameters of MB adsorption on SBA-15 particles

MB Conc.	Pseudo 1st order kinetics			q_e exp**	Pseudo 2nd order kinetics		
	q_e cal.* mg/g	K_1 min^{-1}	R^2	mg/g	q_e cal.* mg/g	K_2 g/min.mg	R^2
15µM	30.3	0.4×10^{-3}	0.93	**27.2**	27	0.7×10^{-3}	0.99
30µM	59.7	0.4×10^{-3}	0.86	**52.5**	54.9	0.3×10^{-3}	0.92
45µM	62.6	0.2×10^{-3}	0.92	**58.4**	60.6	0.2×10^{-3}	0.96
60µM	67.7	0.3×10^{-3}	0.86	**58.1**	61.3	0.22×10^{-3}	0.94
75µM	68.2	0.3×10^{-3}	0.82	**58.2**	64.5	0.1×10^{-3}	0.82
90µM	49.6	0.2×10^{-3}	0.89	**58.25**	56.1	0.42×10^{-3}	0.97

***qe calculated** obtained from Pseudo 1st and 2nd order kinetics equations (15 and 16)
****qe experimental** data determined from adsorption curves obtained with the UV-Vis spectrophotometer

Table IV.2: Pseudo 1st and 2nd order kinetics parameters of MB adsorption on PAN nanofibers

MB Conc.	Pseudo 1st order kinetics			q_e exp**	Pseudo 2nd order kinetics		
	q_e cal.* mg/g	K_1 min^{-1}	R^2	mg/g	q_e cal.* mg/g	K_2 g/min.mg	R^2
15µM	51.9	0.7×10^{-3}	0.72	**25.4**	36	0.33×10^{-3}	0.81
30µM	56.3	0.3×10^{-3}	0.88	**46.5**	50.3	0.24×10^{-3}	0.91
45µM	59.7	0.3×10^{-3}	0.87	**49.4**	44.3	0.13×10^{-3}	0.87
60µM	56.8	0.4×10^{-3}	0.88	**49.1**	44.5	0.25×10^{-3}	0.88
75µM	44.1	0.3×10^{-3}	0.86	**49.2**	44.6	0.24×10^{-3}	0.88
90µM	45.4	0.3×10^{-3}	0.90	**49.3**	49.1	1.21×10^{-3}	0.99

***qe calculated** obtained from Pseudo 1st and 2nd order kinetics equations (15 and 16)
****qe experimental** data determined from adsorption curves obtained with the UV-Vis spectrophotometer

Table IV.3: Pseudo 1st and 2nd order kinetics of MB adsorption on PAN+SBA-15 nanofibers

MB Conc.	Pseudo 1st order kinetics			q_e exp**	Pseudo 2nd order kinetics		
	q_e cal. * mg/g	K_1 min^{-1}	R^2	mg/g	q_e cal. * mg/g	K_2 g/min.mg	R^2
15µM	29.7	0.4×10^{-3}	0.93	**27.2**	27.2	0.82×10^{-3}	0.81
30µM	58	0.4×10^{-3}	0.89	**52.5**	54.7	0.29×10^{-3}	0.99
45µM	65.6	0.2×10^{-3}	0.87	**58.4**	63.3	0.18×10^{-3}	0.92
60µM	66.4	0.4×10^{-3}	0.85	**58.3**	59.1	0.24×10^{-3}	0.97
75µM	66.3	0.3×10^{-3}	0.87	**58.2**	56.5	0.2×10^{-3}	0.94

90µM	50.1	0.3×10^{-3}	0.84	**58.25**	58.9	0.39×10^{-3}	0.98

***qe calculated** obtained from Pseudo 1st and 2nd order kinetics equations (15 and 16)
****qe experimental** data determined from adsorption curves obtained with the UV-Vis spectrophotometer

Table IV.4: Pseudo 1st and 2nd order kinetics of MB adsorption on PAN+SBA-15+BYK W-9010 nanofibers

MB Conc.	**Pseudo 1st order kinetics**			**q_e exp****	**Pseudo 2nd order kinetics**		
	q_e cal. * mg/g	**K_1 min^{-1}**	**R^2**	**mg/g**	**q_e cal. * mg/g**	**K_2 g/min.mg**	**R^2**
15µM	29.7	0.4×10^{-3}	0.93	**27.2**	27.1	0.71×10^{-3}	0.98
30µM	57.4	0.4×10^{-3}	0.88	**52.7**	54.7	0.27×10^{-3}	0.95
45µM	66	0.3×10^{-3}	0.85	**59.9**	64.5	0.17×10^{-3}	0.88
60µM	70.8	0.4×10^{-3}	0.85	**59.8**	62.5	0.22×10^{-3}	0.95
75µM	57.4	0.3×10^{-3}	0.92	**59.7**	58.4	0.27×10^{-3}	0.98
90µM	54.5	0.3×10^{-3}	0.91	**59.6**	59.1	1.21×10^{-3}	0.99

***qe calculated** obtained from Pseudo 1st and 2nd order kinetics equations (15 and 16)
****qe experimental** data determined from adsorption curves obtained with the UV-Vis spectrophotometer

In all tables of kinetics models, K_1 is the rate constant of the pseudo 1st order adsorption process (min^{-1}) and K_2 is the rate constant of the pseudo 2nd order of adsorption ($g/mg^{-1}min^{-1}$). The theoretical (q_e calculated) values estimated from pseudo 1st order kinetic models showed different values than pseudo 2nd order kinetic values when compared to experimental values (q_e experimental" determined by the data obtained from UV-Vis spectrophotometer adsorption curves) at equilibrium. Moreover, R^2 (coefficient of correlation) values of pseudo 2nd order kinetic model are higher (close to 1) in most of the cases than those of pseudo 1st order kinetics model. Therefore, the pseudo 2nd order kinetic model describes better MB adsorption on silica particles, PAN nanofibers, and composite nanofibers with and without dispersing agent. This suggests that the rate-limiting step may be the chemisorptions involving valence forces through sharing or exchange of electrons between the adsorbent and adsorbate and the dye adsorption is related to the availability of adsorption sites rather than dye concentration in the aqueous solution [3, 6].

4.2.3 Adsorption isotherm

The adsorption isotherms show the relationship between the concentration of adsorbate in solution and the amount of adsorbate adsorbed by the adsorbent at equilibrium. Two adsorption isotherm models, Langmuir and Freundlich [5, 34, 36, 41] were used to analyze whether the adsorption was monolayer over homogeneous sites or heterogeneous system (section 2.6.1 &

2.6.2). The results of both isotherm models at neutral pH and room temperature are displayed in figure IV.5 and table IV.5.

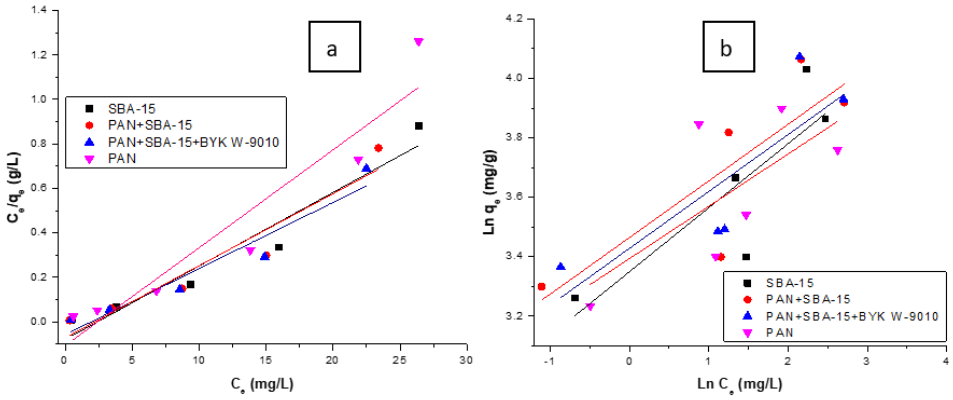


Figure IV.5: Langmuir (a) and Freundlich (b) isotherm models of MB on all adsorbents (pH 7, room temperature)

Table IV.5: Langmuir and Freundlich isotherm data with actual[a] value of adsorbed quantity

S No.	Langmuir isotherm				q_e act.[a]	Freundlich isotherm		
	$q_{e\ max.}$ mg/g	K_L (L/mg)	R_L	R^2	mg/g	1/n	K_f mg/g	R^2
1*	52.6	0.214	0.37	0.91	**58.4**	0.31	83.2	0.43
2*	52.6	0.4	0.37	0.91	**59.3**	0.34	38.9	0.78
3*	52.9	0.5	0.313	0.92	**59.9**	0.15	109.7	0.22
4*	41.7	0.224	0.504	0.89	**49.4**	0.17	104.7	0.31

1*= SBA-15; 2*= PAN+SBA-15; 3*= PAN+SBA-15+BYK; 4*= PAN nanofibers
[a]q_e actual = actual adsorbed quantity of MB (data obtained from curves of spectrophotometer)

According to the results as described in table IV.5, the values of $q_{e\ max.}$ K_L and R_L were calculated from the plot C_e/q_e versus C_e (equation 12, chapter 2). In this study, the adsorption of MB on all adsorbents including silica particles, pristine PAN nanofibers and PAN composite nanofibers is better fitted with Langmuir isotherm model since $q_{e\ max.}$ values are close to actual adsorbed $^a q_e$ act. values and R^2 values are greater in the range of (0.89 to 0.92) close to 1 as compared to Freundlich isotherm model where R^2 values are scattered (0.22 to 0.78). Therefore, the MB adsorption is indicated monolayer onto the homogeneous surface of all adsorbents [5, 34]. The R_L assumes the nature and feasibility of adsorption process and its values are less than unity (in the range of 0.312 to 0.5), and higher than zero, which indicated that adsorption of MB was favorable

on all adsorbents [5, 34]. In Freundlich isotherm, the values of K_f and 1/n were calculated from plot Ln C_e versus Ln q_e (equation 14, chapter 2) which indicated maximum adsorption capacity of adsorbents and linearity of adsorption process, respectively. The 1/n obtained values are in the ranges of (0.15 to 0.34) that are less than 1, therefore the adsorption process is favorable. In table IV.6, the maximum monolayer adsorption of MB on different adsorbents is given for comparison from literature data, with the adsorption of MB in this study.

Table IV.6: Comparison of maximum adsorption of MB onto various adsorbents (pH =7, Room temperature)

Adsorbents	**Adsorbent: adsorbate solution (mg/mL)**	**Adsorbed quantity q_m (mg/g)**
SBA-15	1:1	49.1 [5]
Mesoporous Carbon nanofibers	1:2	59.14 [41]
Multi wall carbon nanotubes	1:1	11.89 [39]
Zeolite MCM-22	1:1	54.3 [36]
SBA-15	1:1	58.4 (In this study)
PAN+SBA-15	5.72:1	59.3 (In this study)
PAN+SBA-15+BYK W-9010	5.72:1	59.9 (In this study)
PAN nanofibers	4.72:1	49.4 (In this study)

The adsorption results of MB on all adsorbents used in this study, particularly composite nanofibers are quite better than the adsorption results of MB on different adsorbents reported in the literature.

4.2.4 Effect of pH

MB removal was studied at different pH of 3, 5, 7 and 9. The pH was adjusted by 0.1M solution of HCl and 0.1M solution of NaOH. As MB is cationic in nature, therefore it exists in aqueous solution in the form of positively charged ion and its degree of adsorption onto the surface of adsorbents used (SBA-15, PAN nanofibers and PAN composite nanofibers) was influenced by the surface charge of (SBA-15 = -40 mV and PAN = -12.5 mV at pH 7), which in turn was affected by the solution pH [5, 216]. MB adsorption efficiency of 30 µM concentrated solution, at room temperature on all used adsorbents at pH mentioned above is displayed in figure IV.6 and adsorbed quantities of MB in (mg/g) are mentioned in table IV.7.

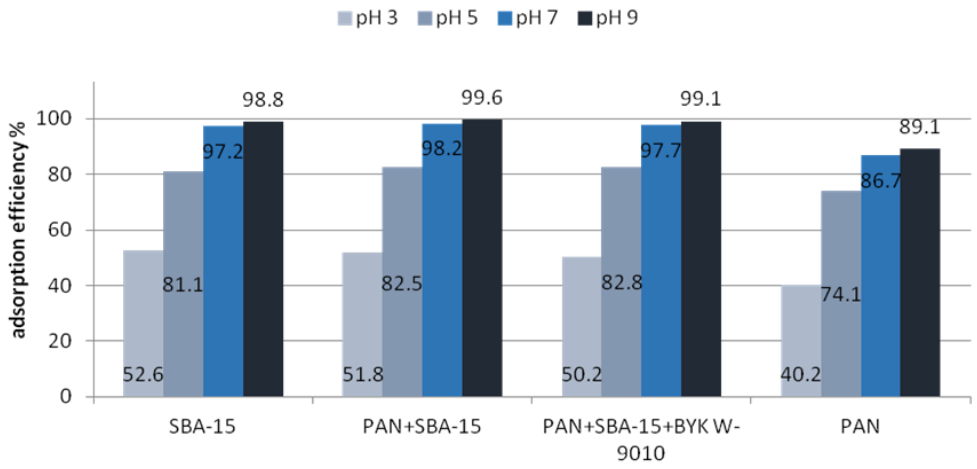


Figure IV.6: MB adsorption efficiency at different pH on different adsorbents at equilibrium (30µM room temperature)

Table IV.7: MB adsorbed quantity (mg/g) at different pH on different adsorbents at equilibrium (30µM, room temperature)

pH	SBA-15	PAN+SBA-15 nanofibers	PAN+SBA-15+BYK W-9010 nanofibers	PAN nanofibers
3	28.4	27.9	27.1	21.7
5	43.8	44.5	44.7	40.0
7	52.5	53.0	52.7	46.8
9	53	53.7	53.5	48.1

30 µM concentrated MB solution was selected randomly to study the effect of pH. The adsorption of MB was significantly lower on all adsorbents at pH 3 than at pH 9 (table IV.7 and figure IV.6). Less adsorption at lower pH can be ascribed to excess of H^+ ions, which may compete on active adsorption sites with the cationic groups of MB dye molecule that resulted in development of repulsive forces between the positively charged adsorbent and cationic dye. Beside it could also be decreased by hydrogen bonding between the adsorbent and dye molecule [1, 3, 6]. Moreover, at high pH, the decrease in positive charges at the solid-liquid interface was observed and the adsorbent surface became negatively charged. That resulted in high adsorption of MB on adsorbents.

4.2.5 Effect of temperature

To investigate the temperature effect on the adsorption of MB by SBA-15 particles, PAN nanofibers, PAN+SBA-15 composite nanofibers with and without dispersing agent, the Gibbs free

energy (ΔG^0), enthalpy (ΔH^0) and entropy (ΔS^0) were calculated from equations 8 and 9 (chapter 2)[3, 5, 6].

The adsorption efficiency of SBA-15, PAN and PAN+SBA-15 composite nanofibers for MB at temperature of 20, 35 and 50 ^oC at pH 7 are shown in figure IV.7.The values of ΔH^0 and ΔS^0 were calculated from the plot of LnK_L vs 1/T (equation 10, chapter 2) as displayed in figure IV.8.

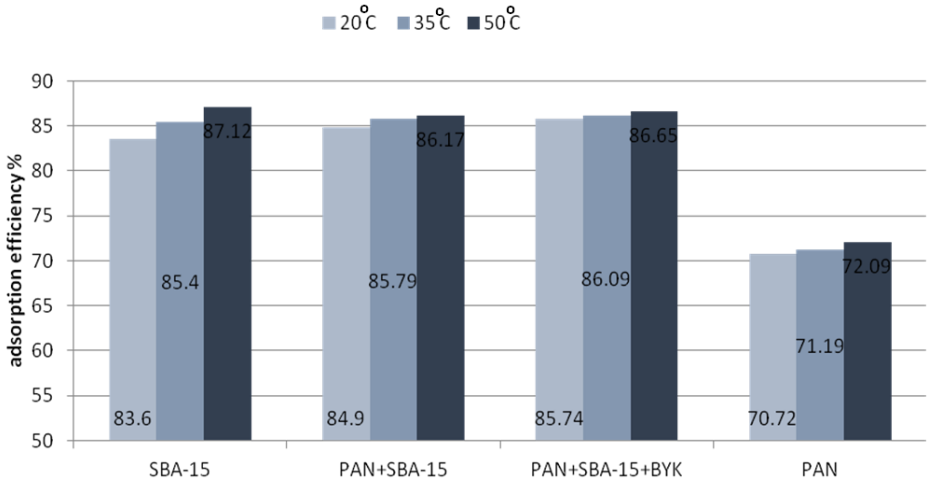


Figure IV.7: MB adsorption efficiency at 20, 35 and 50 ^oC (45µM, all adsorbents)

To study the temperature effect of MB adsorption on all adsorbents, 45µM concentrated solution was selected randomly. The results of figure IV.7 shows that by increasing temperature, adsorption of MB on all adsorbents increased, therefore this adsorption process is endothermic [3,6]. The increase in adsorption capacity was due to the penetration of dye molecules across the external boundary layer and through the internal pores of silica particles and composite nanofibers with increasing temperature [3, 6].

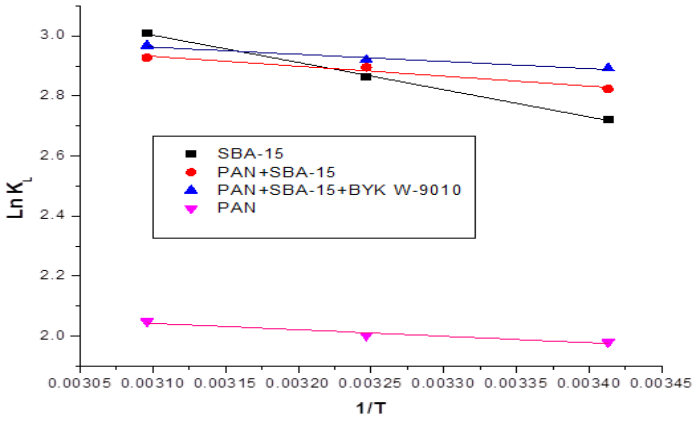


Figure IV.8: Thermodynamic parameters of MB adsorption on all adsorbents (45µM and pH 7)

The thermodynamic properties of MB adsorption on different adsorbents deduced from plots displayed on figure IV.8 are reported in table IV.8.

Table IV.8: Thermodynamic properties of MB adsorption on different adsorbents

Adsorbents	**Temperature (K)**	**K_L (L/g)**	**ΔG^o (KJ/mol)**	**ΔH^o (KJ/mol)**	**ΔS^o (J/K. mol)**	**R^2**
SBA-15	293	15.2	-6.6	7.6	48.4	0.998
	308	17.5	-7.4			
	323	20.3	-8.1			
PAN+SBA-15	293	16.8	-9.8	2.8	32.9	0.93
	308	18.1	-6.9			
	323	18.7	-7.9			
PAN+SBA-15+BYK	293	18	-7.1	2	30.8	0.94
	308	18.5	-7.5			
	323	19.4	-7.9			
PAN	293	7.2	-4.8	1.8	22.5	0.91
	308	7.4	-5.2			
	323	7.8	-5.5			

Generally, it is considered that magnitude of the change in Gibbs free energy is about 0 to -20 KJ/mol for physisorption and -80 to -400 KJ/mol for chemisorption [5]. The negative values of ΔG^o at various temperatures mean that adsorption process of MB on all adsorbents was spontaneous and thermodynamically favorable. The positive ΔH^o values indicated that MB adsorption on all adsorbents was endothermic reaction [3,5], which means rising temperature led to higher adsorption capacity of adsorbents at equilibrium. An adsorption process is considered as physical or chemical, if the absolute magnitude of ΔH^o< 25 KJ/mol or >40 KJ/mol, respectively. Therefore, adsorption of MB on all used adsorbents is further confirmed as physisorption. In the case of ΔS^o, the positive values reveal the affinity of MB towards sorbent and positive values also explain that energy gained and increased randomness at solid/solution interface during adsorption process [5].

4.2.6 Batch screening test of Methylene Blue (MB)

Methylene blue is a strong cationic dye having pKa of 3.8 selected for the adsorption capacity efficiency process due to its vast applications [17, 18, 215]. The adsorption efficiency of the four adsorbents including SBA-15 particles, pristine PAN nanofibers, and PAN + SBA-15 nanofibers with and without dispersing agent has been taken using a UV-Vis spectrophotometer (as explained in section 2.4) at equilibrium, at room temperature and pH 7 and their screening results are shown in figure IV.9.

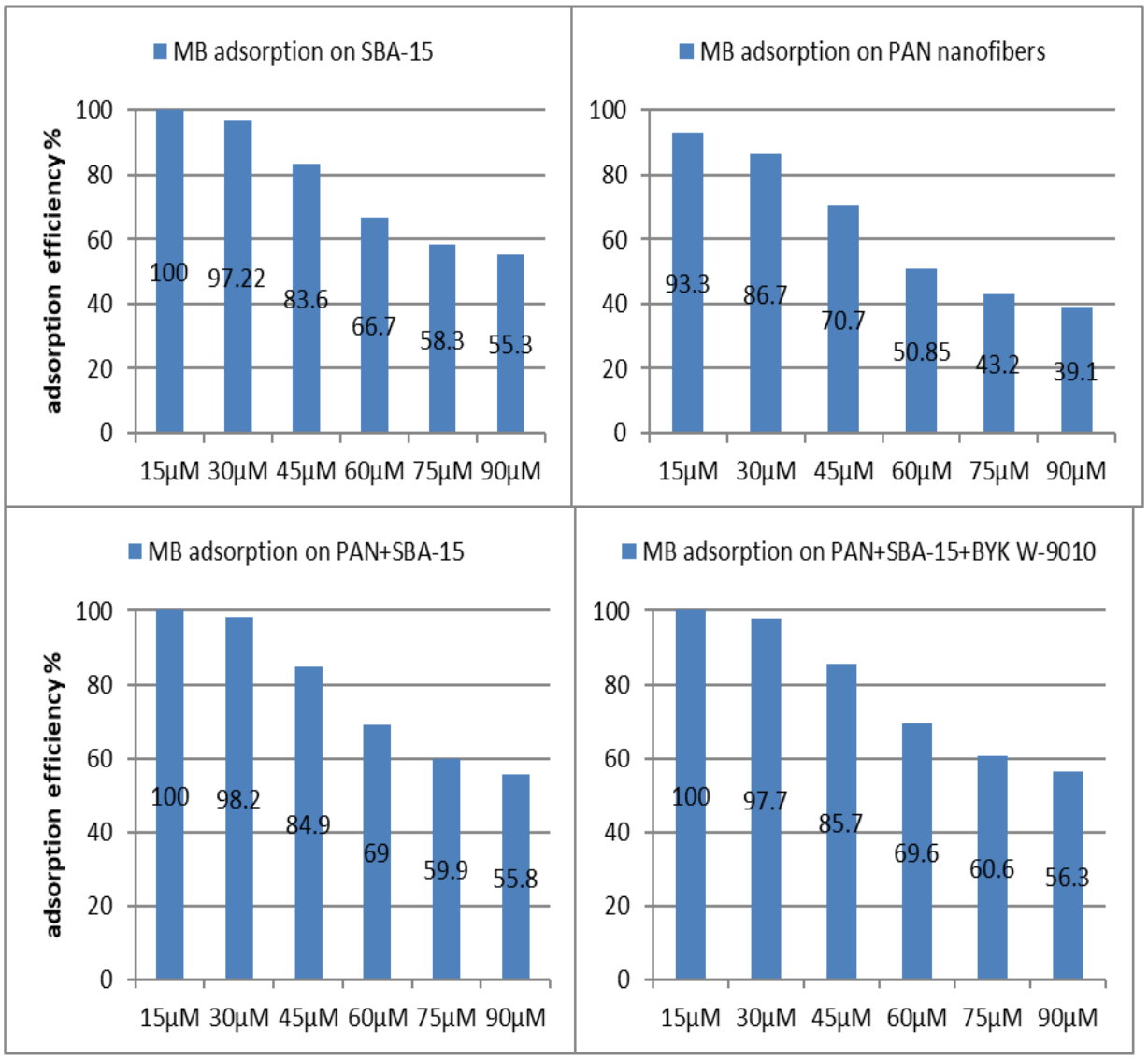


Figure IV.9: MB adsorption efficiency on all used adsorbents at equilibrium (pH 7, room temperature)

It has been observed that all the adsorbents are showing excellent results of adsorption and they are highly efficient ≥ 90% category at ≤ 30 µM for SBA-15 and PAN+SBA-15 composites nanofibers and at ≤ 15 µM for pure PAN nanofibers. SBA-15 particles and PAN+SBA-15 nanofibers show a maximum adsorption efficiency of 100 % at 15µM but pristine PAN shows 93.3 % at the same concentration. The incorporation of silica particles in PAN nanofibers increases the adsorption efficiency from 93.3 to 100% at 15 µM but it is not very significant. Addition of dispersing agent has led to a similar adsorption behavior as composite nanofibers without dispersing agent, whereas increase in dye concentration resulted in decrease of adsorption efficiency. The adsorption process of 15 µM MB solution on all adsorbents at equilibrium, neutral pH and room temperature is displayed in figure IV.10.

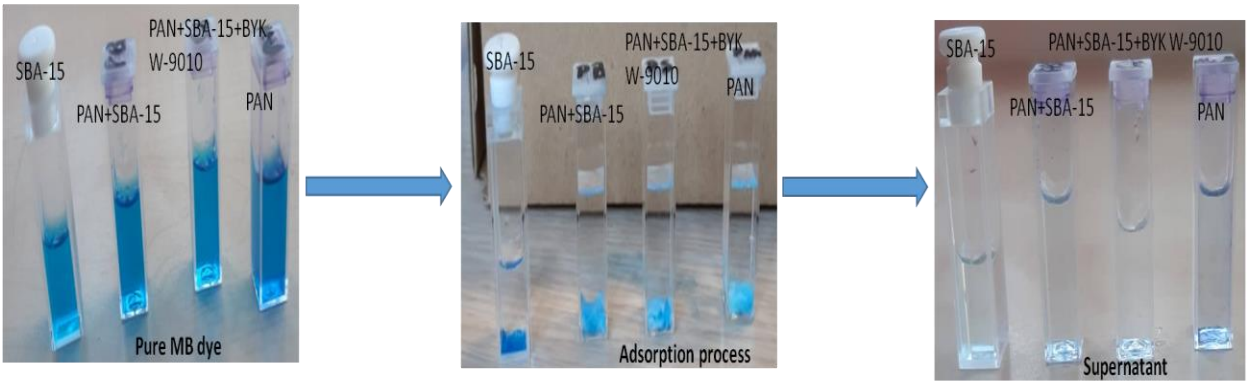


Figure IV.10: MB adsorption on all adsorbents at equilibrium (15 µM, pH 7 and room temperature)

4.2.7 Conclusion

Batch screening test was used for evaluation of MB adsorption on SBA-15 particles, PAN nanofibers and PAN+SBA-15 composite nanofibers with and without BYK dispersing agent. All the adsorbents showed excellent adsorption behavior due to strong positive charge on MB and high negative charge on SBA-15 of -40 mV and -12.5 mV at pH 7 on PAN. Pseudo 2nd order kinetic model was better to fit MB adsorption, whereas in the case of adsorption isotherms, the Langmuir model showed the better result, so the adsorption was homogenous monolayer. By increasing pH of solution, the adsorption increased due to increase in electrostatic force of attraction. Moreover, increase in concentration, increased the adsorption till the saturation point. Thermodynamics calculations indicated that the adsorption of cationic dye molecules on all adsorbents is physisorption and spontaneous. The adsorption results of this study are in agreement with literature results. The main focus of the study was to increase the adsorption of MB (having

zeta potential +18 mV at pH 7) on PAN nanofibers (-12.5 mV at pH 7) after addition of SBA-15 (-40 mV at neutral pH) which increased the surface charge to more anionic [3, 216, 217]. As a result of MB adsorption, low quantity was adsorbed on pristine PAN nanofibers as compared to PAN+SBA-15 composite nanofibers but the difference remained low and improvements with SBA-15 are not noticeable.

4.3 Neutral Red (NR)

Neutral Red (NR) is a weak cationic dye having molar mass of 288 g/mol and chemical formula is shown in figure IV.11.

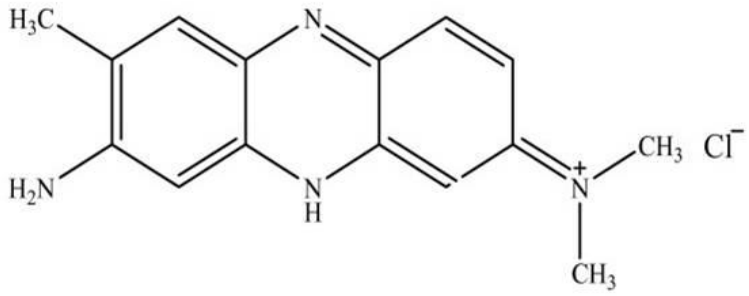


Figure IV.11: Chemical formula of Neutral Red (NR) dye

NR is eurhodin dye which is generally used for staining in histology and also in some grown medium for bacterial and cell culture [3].

4.3.1 Effect of concentration

The effect of increase in NR concentration (from 15 to 90 µM) and their adsorption rate at equilibrium (15 µM= 100 min, 30 µM=120 min, 45 µM= 150 min, 60 µM= 160 min, 75 µM = 160 min and 90 µM= 200 min) on all adsorbents (SBA-15, PAN nanofibers and PAN composite nanofibers) at neutral pH and room temperature are shown in figure IV.12.

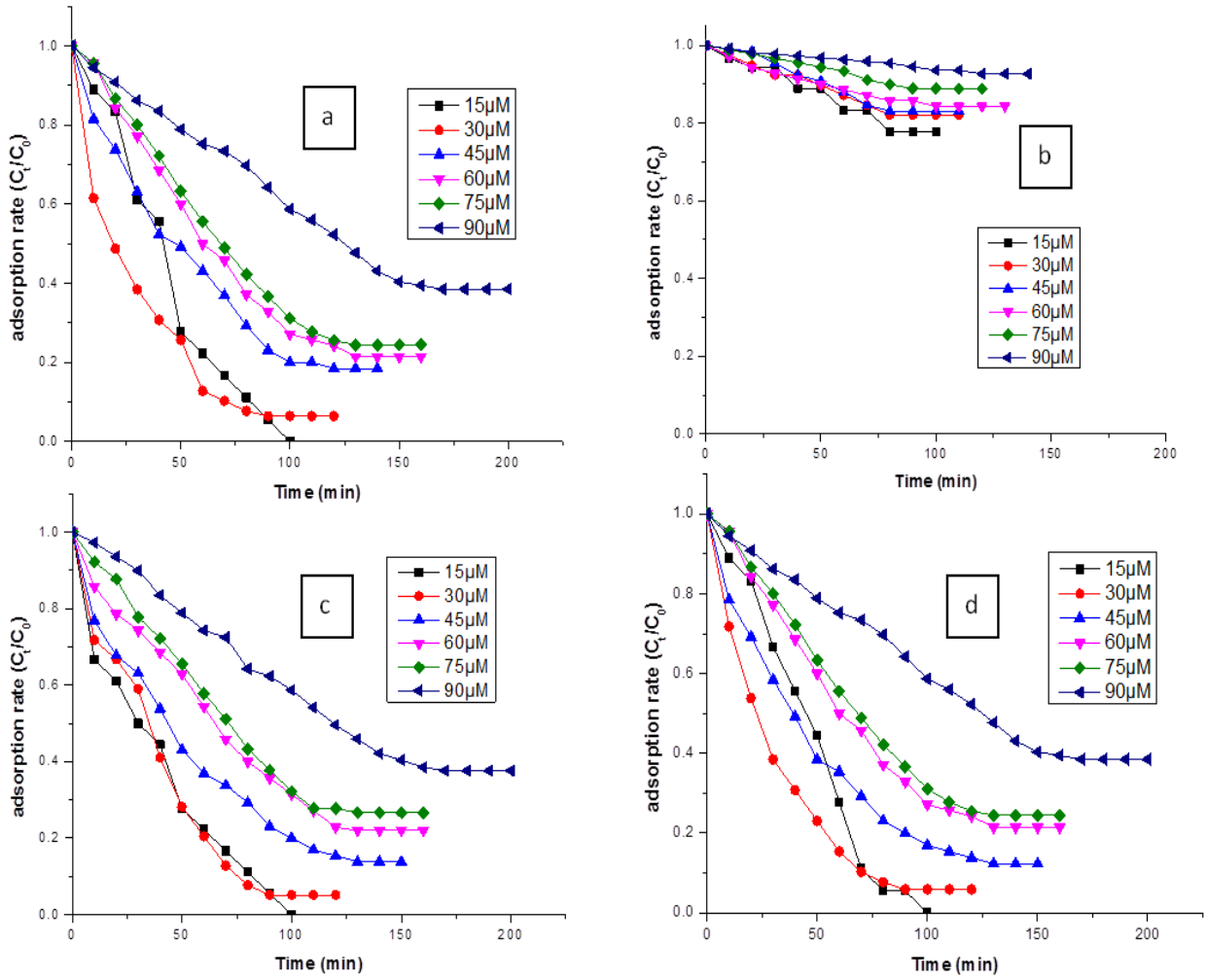


Figure IV.12: Adsorption rate at neutral pH and room temperature of different concentrations of NR on SBA-15 (a), PAN nanofibers (b), PAN+SBA-15 nanofibers (c) and PAN+SBA-15+BYK W-9010 nanofibers (d)

The results presented on figure IV.12 describe that adsorption efficiency on all used adsorbents decreased by increasing the concentration of NR dye. The reason behind is that increase of dye's cations ratio to the dosage of the adsorbent and the number of active adsorption sites required to accommodate the remaining adsorbate. While the number of adsorbate increases and hence the removal efficiency of NR decreases whereas adsorbed quantity (mg/g) remains constant after saturation.

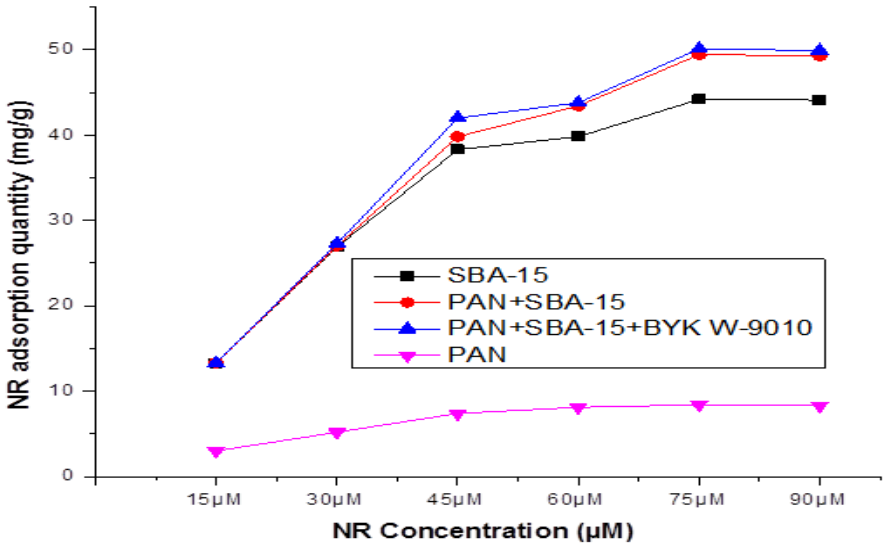


Figure IV.13: NR adsorbed quantity (mg/g) at equilibrium on all adsorbents at different NR concentrations (neutral pH, room temperature)

Above figure IV.13 explained that adsorbed quantity of NR at equilibrium was increased by increasing the initial concentration of dye from 15 to 75 µM and after, the adsorption quantity was constant due to the saturation of active sites. Highest adsorption was observed at 75µM for all adsorbents.

4.3.2 Adsorption kinetics

Like for MB, a 90µM NR mother solution was prepared and further 15, 30, 45, 60 and 75µM daughter solutions were prepared for adsorption and kinetic studies. Pseudo 1st and 2nd order kinetics were used to measure the adsorbate rate of retention at solid phase interface at constant pH and temperature and their results at neutral pH and room temperature are described in figure IV.14.

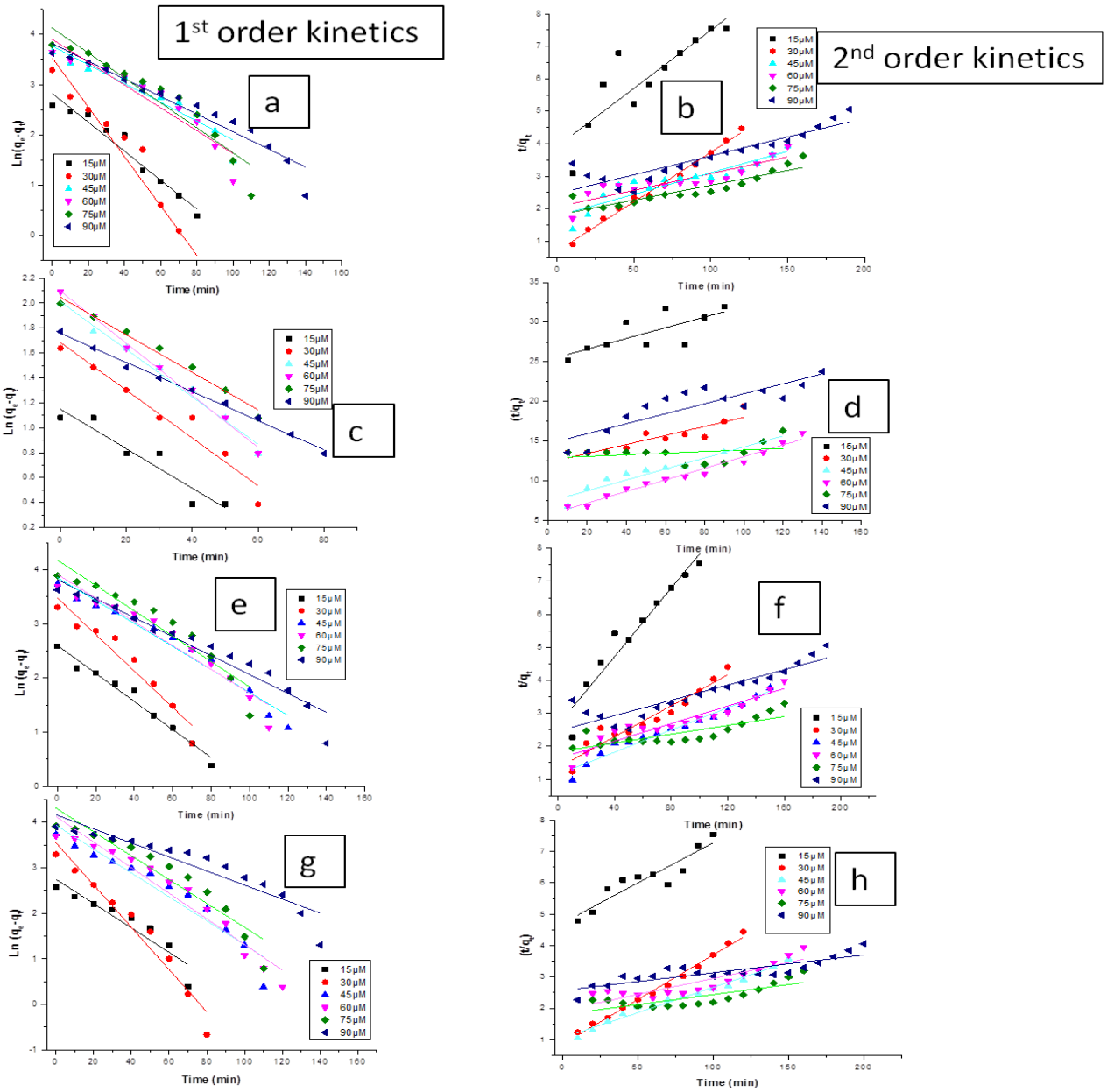


Figure IV.14: Pseudo 1st and 2nd order kinetics (at pH 7 and room temperature) for NR adsorption on SBA-15 (a, b), PAN nanofibers (c, d), PAN+SBA-15 nanofibers (e, f), PAN+SBA-15+BYK W-9010 (g, h)

The parameters values of both kinetic models and their correlation coefficients (R^2) were obtained by plotting graphs Ln (q_e-q_t) versus t and t/q_t versus t for 1st and 2nd order kinetics respectively and are mentioned in table IV.9 for SBA-15, table IV.10 for PAN nanofibers, table IV.11 for PAN+SBA-15 nanofibers and table IV.12 for PAN+SBA-15+BYK W-9010 nanofibers.

Table IV.9: Pseudo 1st and 2nd order kinetics parameters of NR adsorption on SBA-15 particles

NR Conc.	Pseudo 1st order kinetics			q_e exp**	Pseudo 2nd order kinetics		
	q_e cal.* mg/g	K_1 min^{-1}	R^2	mg/g	q_e cal.* mg/g	K_2 g/min.mg	R^2
15µM	15	0.36×10^{-3}	0.95	**13.3**	22.2	0.52×10^{-3}	0.73
30µM	29.5	0.7×10^{-3}	0.92	**26.9**	27	1.97×10^{-3}	0.99
45µM	44.9	0.24×10^{-3}	0.90	**38.3**	47.6	0.25×10^{-3}	0.83
60µM	46.5	0.33×10^{-3}	0.89	**39.8**	49.5	0.2×10^{-3}	0.77
75µM	51.4	0.24×10^{-3}	0.91	**44.2**	53.8	0.19×10^{-3}	0.82
90µM	49.2	0.13×10^{-3}	0.94	**44.1**	46.3	0.19×10^{-3}	0.83

*** q_e calculated** obtained by Pseudo 1st and 2nd order kinetics equations (15 and 16)
****q_e experimental** data determined by adsorption curves from spectrophotometer

Table IV.10: Pseudo 1st and 2nd order kinetics parameters of NR adsorption on PAN nanofibers

NR Conc.	Pseudo 1st order kinetics			q_e exp**	Pseudo 2nd order kinetics		
	q_e cal.* mg/g	K_1 min^{-1}	R^2	mg/g	q_e cal.* mg/g	K_2 g/min.mg	R^2
15µM	3.2	0.2×10^{-3}	0.88	**3**	14.93	0.18×10^{-3}	0.51
30µM	6	0.27×10^{-3}	0.94	**5.2**	17.55	0.27×10^{-3}	0.8
45µM	7.4	0.16×10^{-3}	0.98	**7.4**	14.93	0.65×10^{-3}	0.93
60µM	8.2	0.21×10^{-3}	0.99	**8.1**	13.70	0.93×10^{-3}	0.97
75µM	7.8	0.13×10^{-3}	0.98	**8.4**	102.1	0.05×10^{-3}	0.47
90µM	8.1	0.05×10^{-3}	0.99	**8.3**	15.87	0.27	0.73

*** q_e calculated** obtained by Pseudo 1st and 2nd order kinetics equations (15 and 16)
****q_e experimental** data determined by adsorption curves from spectrophotometer

Table IV.11: Pseudo 1st and 2nd order kinetics parameters of NR adsorption on PAN+SBA-15 nanofibers

NR Conc.	Pseudo 1st order kinetics			q_e exp**	Pseudo 2nd order kinetics		
	q_e cal. mg/g	K_1 min^{-1}	R^2	mg/g	q_e cal. mg/g	K_2 g/min.mg	R^2
15µM	13.5	0.33×10^{-3}	0.97	**13.3**	17.5	1.8×10^{-3}	0.92
30µM	30.6	0.48×10^{-3}	0.93	**27**	29.9	0.83×10^{-3}	0.92
45µM	42.5	0.17×10^{-3}	0.965	**39.8**	48.1	0.38×10^{-3}	0.96
60µM	45.1	0.21×10^{-3}	0.933	**43.4**	50.2	0.11×10^{-3}	0.9

75µM	58.1	0.19×10^{-3}	0.895	**49.4**	75.7	0.09×10^{-3}	0.63
90 µM	52.4	0.13×10^{-3}	0.94	**49.3**	58.2	0.05×10^{-3}	0.83

*** q_e calculated** obtained by Pseudo 1st and 2nd order kinetics equations (15 and 16)
****q_e experimental** data determined by adsorption curves from spectrophotometer

Table IV.12: Pseudo 1st and 2nd order kinetics parameters of NR adsorption on PAN+SBA-15+BYK W-9010 nanofibers

NR Conc.	**Pseudo 1st order kinetics**			**q_e exp****	**Pseudo 2nd order kinetics**		
	q_e cal. mg/g	**K_1 min^{-1}**	**R^2**	**mg/g**	**q_e cal. mg/g**	**K_2 g/min.mg**	**R^2**
15µM	16.6	0.45×10^{-3}	0.86	**13.3**	17.6	0.68×10^{-3}	0.84
30µM	29.4	0.66×10^{-3}	0.95	**27.3**	27.8	1.5×10^{-3}	0.99
45µM	47	0.22×10^{-3}	0.92	**42**	43.3	0.51×10^{-3}	0.98
60µM	48.4	0.28×10^{-3}	0.94	**43.8**	49.5	0.21×10^{-3}	0.77
75µM	55.7	0.22×10^{-3}	0.90	**50.1**	75.7	0.09×10^{-3}	0.59
90 µM	56.8	0.11×10^{-3}	0.87	**49.9**	94.3	0.04×10^{-3}	0.71

*** q_e calculated** obtained by Pseudo 1st and 2nd order kinetics equations (15 and 16)
****q_e experimental** data determined by adsorption curves from spectrophotometer

The results in all tables explained that in most of cases, coefficient of correlation (R^2) values of pseudo 1st order kinetics is greater than pseudo 2nd order kinetics and are close to 1. The q_e experimental values are also in agreement with the q_e calculated values of pseudo 1st order kinetics. Therefore, all the adsorbents of NR follow the pseudo 1st order kinetic model and the adsorption process is physisorption [3, 5].

4.3.3 Adsorption isotherm

Two adsorption isotherm models, Langmuir and Freundlich were used to analyze NR adsorption, and determine whether it was monolayer over homogeneous sites or heterogeneous system. The results of both isotherm models are displayed in figure IV.15 and table IV.13.

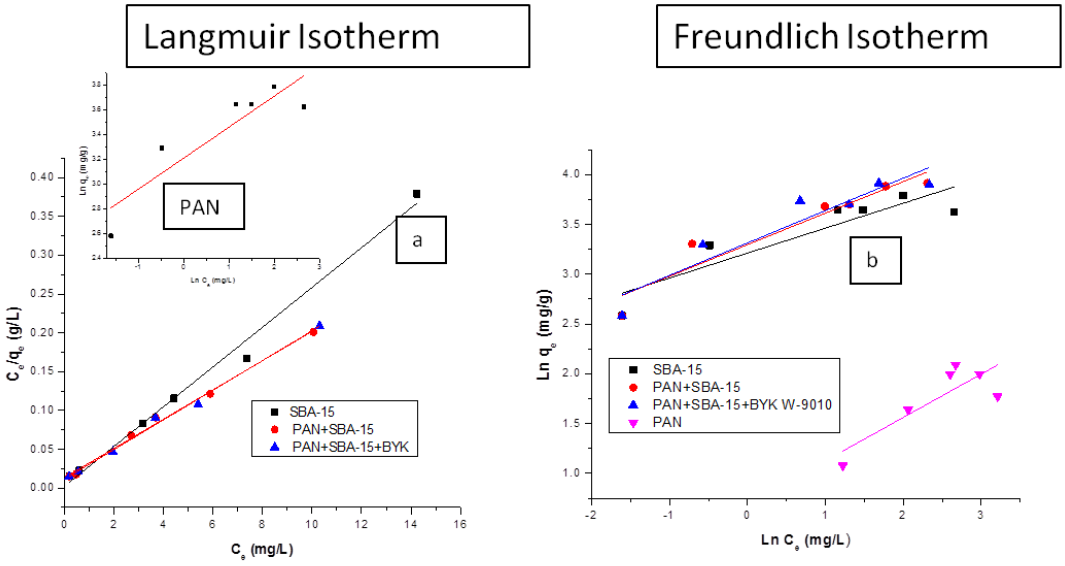


Figure IV.15: NR adsorption isotherm models Langmuir (a) and Freundlich (b) (pH 7 and room temperature)

Table IV.13: Langmuir and Freundlich isotherms data with actual** values of adsorbed quantity

S No.	Langmuir isotherm				q_e act.**	Freundlich isotherm		
	$q_{e\ max.}$ mg/g	K_L L/mg	R_L	R^2	mg/g	1/n	K_f mg/g	R^2
1*	39.1	1.13	0.17	0.988	**44.2**	0.25	16.2	0.77
2*	53.2	1.39	0.14	0.993	**49.4**	0.32	19.8	0.86
3*	52.6	1.58	0.123	0.994	**50.1**	0.33	20.6	0.86
4*	7.6	0.378	0.38	0.82	**8.4**	0.44	4.9	0.63

1*= SBA-15 2*= PAN+SBA-15 3*= PAN+SBA-15+BYK 4*= PAN nanofibers
**q_e actual = actual adsorbed quantity of NR (data obtained from curves of spectrophotometer)

Table IV.13 summarized all the constants and correlation coefficients R^2 of both isotherm models. The Langmuir model yielded the best fit with higher R^2 values, close to 1 as compared to Freundlich model. Conformation of the experimental data into Langmuir isotherm equation indicated the homogeneous nature of all used adsorbents. The results also demonstrated the formation of monolayer coverage of dye molecules at the outer surface of adsorbents [3, 5, 6]. The R_L assumes the nature and feasibility of adsorption process and its values are less than unity (in the range of 0.14 to 0.38) and higher than zero, which indicated that adsorption of NR was favorable on all adsorbents. In Freundlich isotherm the values of K_f and 1/n were calculated from plot Ln C_e versus Ln q_e (equation 14), which indicated maximum adsorption capacity of

adsorbents and linearity of adsorption process respectively. The 1/n obtained values are in the ranges of 0.25-0.44 that are less than 1 therefore the adsorption process is favorable [3, 5, 6]. In table IV.14, the maximum monolayer adsorption of NR on different adsorbents from literature is compared with the adsorption of NR in this study at neutral pH and room temperature.

Table IV.14: Comparison of maximum adsorption of NR onto various adsorbents (pH =7, room temperature)

Adsorbents	**Adsorbent: adsorbate solution (mg/mL)**	**Adsorbed quantity q_m (mg/g)**
Saw dust	3:1	26.7 [218]
Halloysite nanotubes	1:1	50.92 [219]
Natural Sepioloite	10:1	36.32 [220]
Chitosan & activated carbon composite	10:1	30 [221]
SBA-15	1:1	44.2 (In this study)
PAN+SBA-15	5.72:1	49.4 (In this study)
PAN+SBA-15+BYK W-9010	5.72:1	50.1 (In this study)
PAN nanofibers	1:1	8.4 (In this study)

The adsorption results of NR on all adsorbents used in this study, except pristine PAN nanofibers are quite impressive as compared to the adsorption results of NR on different adsorbents in literature. Therefore the purpose of maximum adsorption of pollutants like NR dye from PAN+SBA-15 and PAN+SBA-15+BYK W-9010 composite nanofibers is achieved at neutral pH and room temperature.

4.3.4 Effect of pH

NR adsorption on 30 µM concentration (selected randomly) was studied at different pH of 3, 5, 7 and 9 and impact is displayed in figure IV.16 and table IV.15.

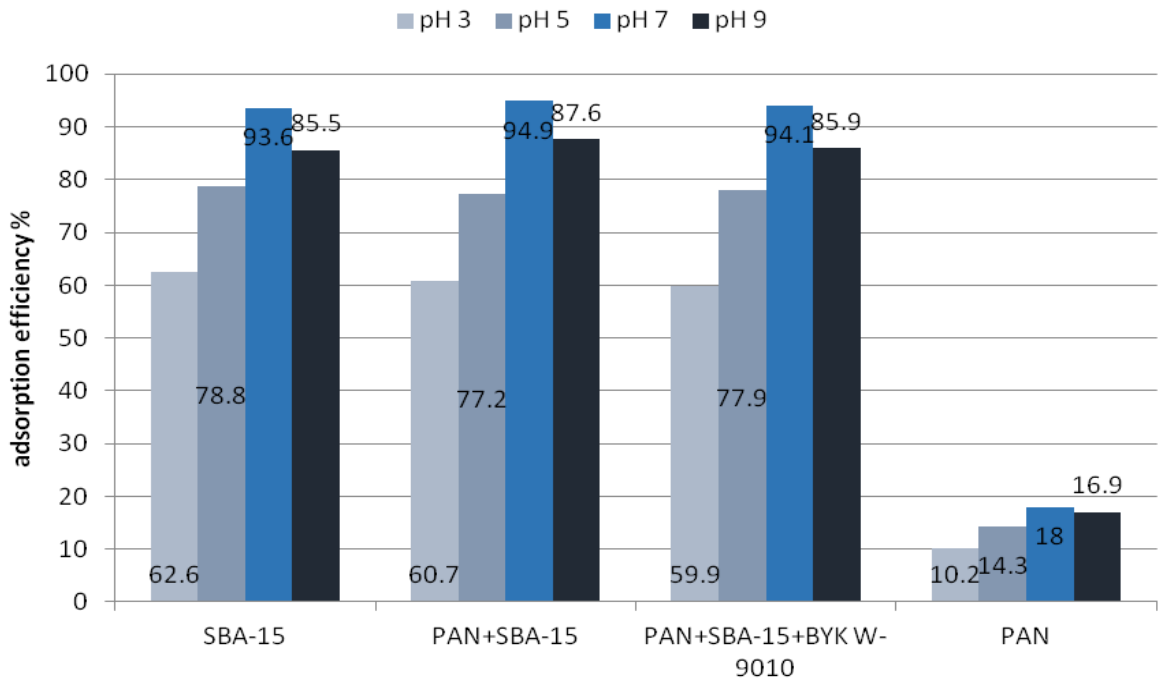


Figure IV.16: NR adsorption efficiency at different pH (30µM and room temperature)

Table IV.15: NR adsorbed quantity (mg/g) at different pH on different adsorbents (30 µM, room temperature)

pH	SBA-15	PAN+SBA-15 nanofibers	PAN+SBA-15+BYK W-9010 nanofibers	PAN nanofibers
3	19.7	19.4	18.8	3.4
5	24.8	24.7	24.4	4.8
7	29.4	30.4	29.5	6
9	26.9	28	26.9	5.7

Figure IV.16 and table IV.15 explain the effect of pH on adsorption % of NR dye using SBA-15 (having zeta potential -40 mV at neutral pH), PAN (having zeta potential -12.5 mV at neutral pH) and PAN+SBA-15 composite nanofibers. With the increase in pH, the adsorption of NR dye is increased and is the highest at pH 7. In basic and neutral environment, strong electrostatic attractive forces exist between the negatively charged surface of SBA-15 and positively charged surface of NR, leading to enhanced adsorption [3]. Above pH 7 a little decrease in adsorption of NR is observed, at that point coverage of surface of adsorbents is significantly affected by the potential of interfacial regions. Because the accumulation of NR cations in the interfacial region causes the development of a positive charge, that reduces further adsorption of NR cations [219].

As described above that SBA-15 has high zeta potential value of -40 mV as compared to pristine PAN having -12.5 mV, therefore NR dye molecules are more attracted towards SBA-15 due to very strong electrostatic attractive forces. So SBA-15 and PAN+SBA-15 composite nanofibers have very high adsorption rate of NR, whereas pristine PAN has very low [5, 216].

4.3.5 Effect of temperature

The adsorption efficiency of different adsorbents for NR at temperature 20, 35 and 50 ^{o}C and pH 7 are shown in figure IV.17, whereas figure IV.18 explains the plot of LnK_L versus 1/T.

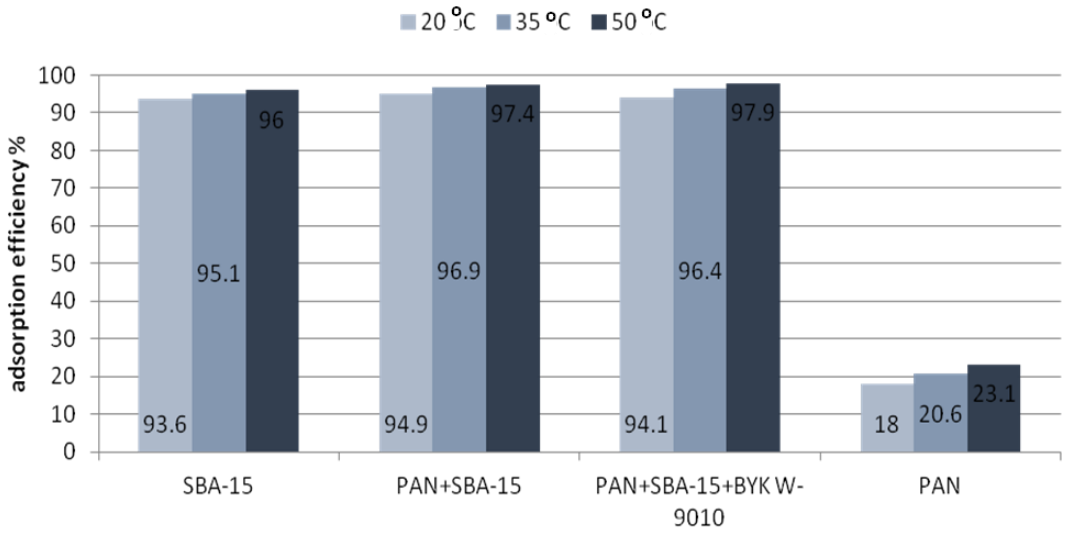


Figure IV.17: NR adsorption efficiency at 20, 35 and 50 ^{o}C on all adsorbents (30 µM and pH 7)

Figure IV.17 shows the effect of temperature increase on adsorption percentage of NR dye over all the used adsorbents. With increase in temperature from 20 to 35 ^{o}C and then to 50 ^{o}C, the adsorption efficiency of NR increased from 93.3 to 96% for SBA-15, from 94.9 to 97.4% for PAN+SBA-15 composite nanofibers, from 94.1 to 97.9% for PAN+SBA-5+BYK W-9010 composite nanofibers and from 18 to 23.1% for pristine PAN nanofibers. This increase in adsorption efficiency is not very significant as small increase was observed and reason behind this increment is increase in kinetic energy of dye molecules which enhanced the mobility of dye molecules to penetrate on the available active sites of the adsorbent molecules [3].

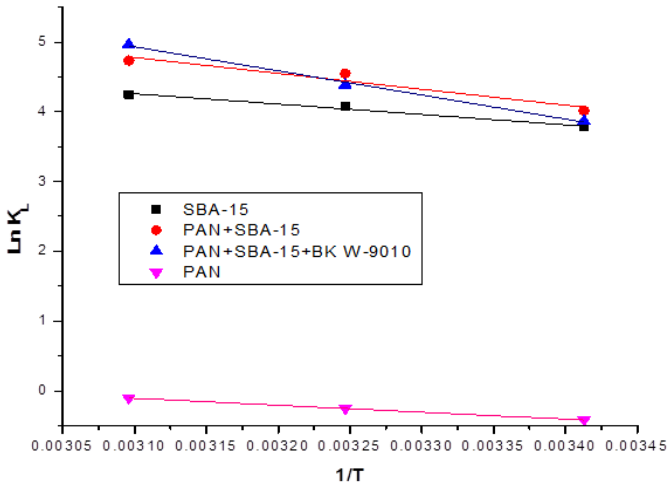


Figure IV.18: Plot for evaluating thermodynamic parameters of NR on all adsorbents

Table IV.16 describes the thermodynamic properties of NR adsorption on different adsorbents.

Table IV.16: Thermodynamic properties of NR adsorption on different adsorbents

Adsorbent	Temperature (K)	K_L (L/g)	Δ G° (KJ/mol)	Δ H° (KJ/mol	Δ S° (J/K. mol)	R^2
SBA-15	293	43.	-9.2	12.4	73.7	0.98
	308	58.6	-10.4			
	323	70.1	-11.4			
PAN+SBA-15	293	55.5	-9.8	18.9	98.5	0.9
	308	94.4	-11.6			
	323	113.7	-12.7			
PAN+SBA-15+BYK	293	47.8	-9.4	28.8	130.2	0.993
	308	80.5	-11.2			
	323	143.4	-13.3			
PAN	293	0.7	1	8.3	24.8	0.999
	308	0.8	0.7			
	323	0.9	0.3			

The negative values of ΔG^o in the case of SBA-15 and PAN+SBA-15 composite nanofibers (table table IV.16) confirmed that dye uptake process is spontaneous in nature, whereas for PAN nanofibers positive values of Gibbs free energy depicts that dye process is non-spontaneous (additional energy required for reaction to occur) [3, 6]. Positive values of ΔH^o for all adsorbents, suggested that adsorption of NR dye is an endothermic reaction, which meant that increase in

temperature increased the adsorption capacity [3, 6]. Positive values of ΔS^o revealed the increase in randomness at the solid-solution interface all through the adsorption of NR used on the active sites of all used adsorbents [3, 6].

4.3.6 Batch screening test of Neutral red (NR)

Neutral red is a weak cationic dye having pKa 6.8 and was selected for adsorption on different adsorbents used earlier. The screening results of four adsorbents of Neutral Red, including SBA-15 particles, pristine PAN nanofibers, PAN+ SBA-15 nanofibers with and without dispersing agent at pH 7 and room temperature are shown in figure IV.19.

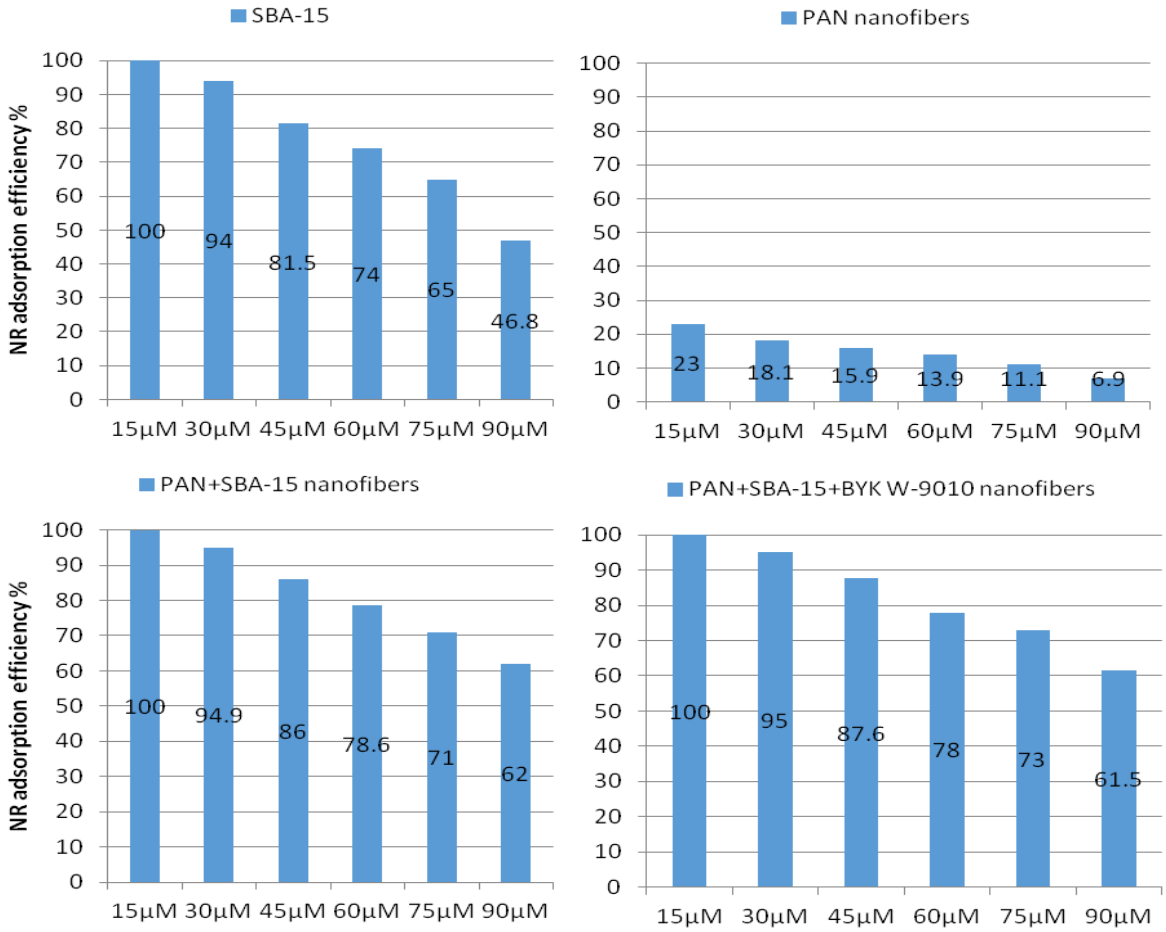


Figure IV.19: NR adsorption efficiency on all used adsorbents at equilibrium (pH 7, room temperature)

As per selection criteria (section 2.1.4), SBA-15 particles and PAN+SBA-15 composite nanofibers were categorized into highly efficient adsorbents ≥90%, whereas pristine PAN

nanofibers are inefficient ≤40%. Pristine PAN nanofibers demonstrated as not adsorbent for NR adsorption, but as silica particles were added, composite nanofibers adsorption increased to similar as adsorption of silica particles. Therefore, highly efficient composite nanofibers for treatment of NR wastewater were successfully prepared. NR adsorption process of 15 µM concentration on all the adsorbents at equilibrium, neutral pH and room temperature displayed in figure IV.20.

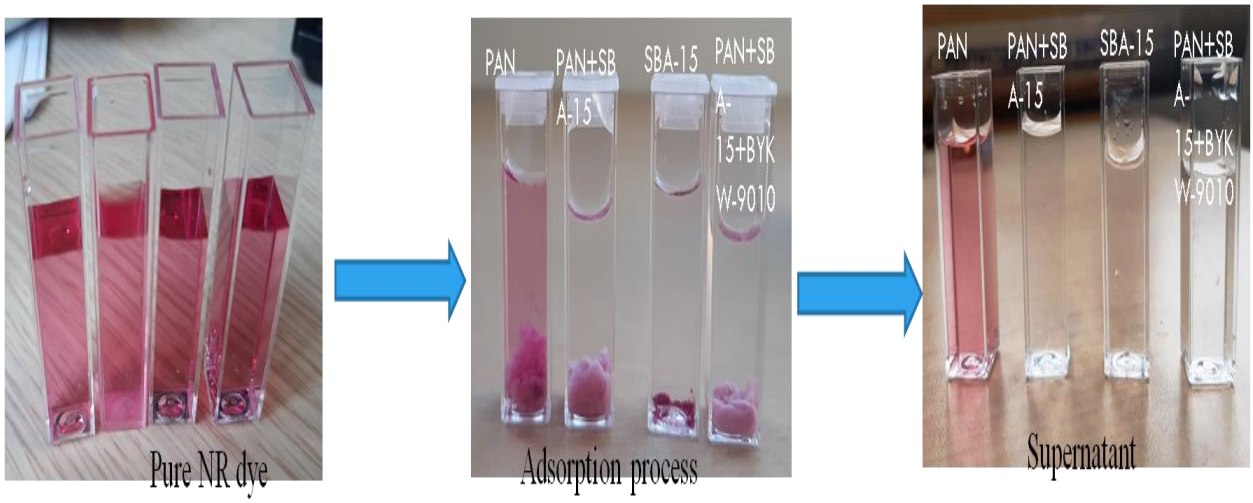


Figure IV.20: NR adsorption on all adsorbent at equilibrium (15 µM, pH 7, room temperature)

4.3.7 Conclusion

NR dye is weak cationic dye having pKa of 6.8 and screening test explained that except pristine PAN nanofibers, other adsorbents including SBA-15 and PAN+SBA-15 composite nanofibers have excellent adsorption behavior due to presence of high charge of -40 mV on SBA-15 as compared to PAN that has just -12.5 mV at pH 7. The adsorption results showed that pseudo 1st order kinetic model and Langmuir isotherm model better describe it and explain that adsorption is monolayer homogenous and physisorption takes place on active sites of adsorbents. Increase in pH of the solution, increased the adsorption due to electrostatic forces of attraction. Increase in dye concentration increased adsorption quantity, initially very rapid till 45µM and then slowly till 75µM and after remained constant due to saturation of active sites. The slightly temperature impact is in direct relation with adsorption of NR on all adsorbents due to increase in kinetic energy of adsorbates to penetrate onto available active sites of adsorbents and the adsorption process is physisorption on all adsorbents. The main purpose of preparing PAN+SBA-15

composite nanofibers was maximum adsorption of NR dye from wastewater and achieved as there is huge difference of NR adsorption on pristine PAN and PAN composite nanofibers.

4.4 Congo Red (CR)

Congo Red (CR) is an anionic dye with 696.66 g/mol molecular weight and structural formula is mentioned in figure IV.21.

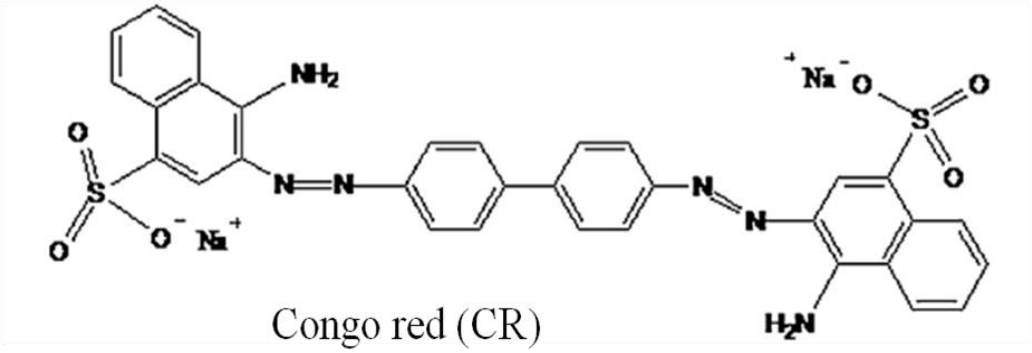


Figure IV.21: Chemical formula of Congo Red (CR)

CR dye is mostly used in textile, cosmetics, printing, dyeing, food coloring and paper-making industries [3, 8].

4.4.1 Effect of concentration

The initial concentration effect of CR dye adsorption at equilibrium (7.5 to 45 µM= 275 minutes for each solution concentration) on SBA-15, PAN nanofibers and PAN+SBA-15 composite nanofibers was studied at room temperature and at neutral pH (figure IV.22).

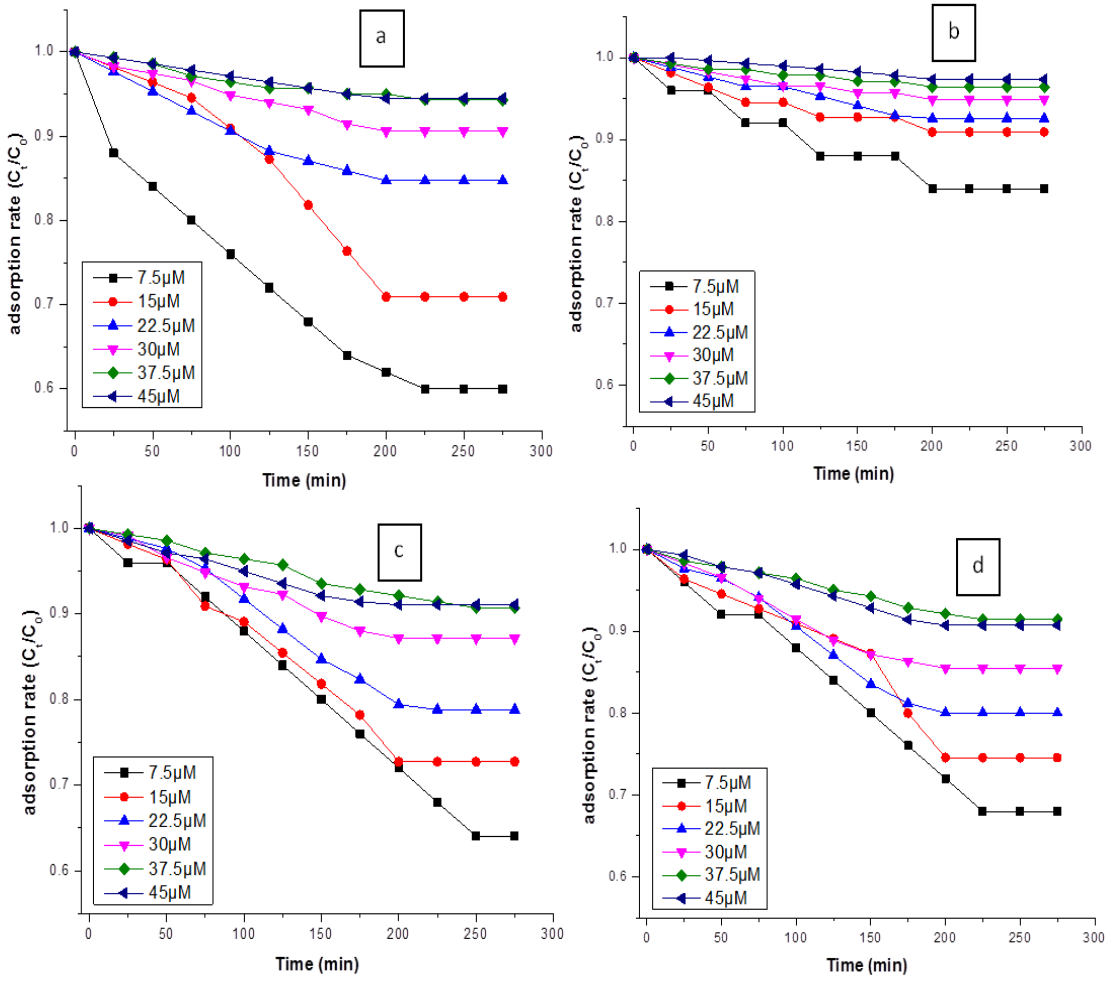


Figure IV.22: Adsorption rate of different concentrations of CR on SBA-15 (a), PAN nanofibers (b), PAN+SBA-15 nanofibers (c) and PAN+SBA-15+BYK nanofibers (d) (at pH 7, room temperature)

It is observed that adsorption rate of CR is far less than for MB and NR due to repulsive electrostatic forces between adsorbate and adsorbent. By increasing the initial concentration of CR the adsorption rate of adsorbate is decreased due to the saturation of sites where dye molecules could be deposited. Figure IV.23 describes the adsorbed quantity of CR on different adsorbents at neutral pH.

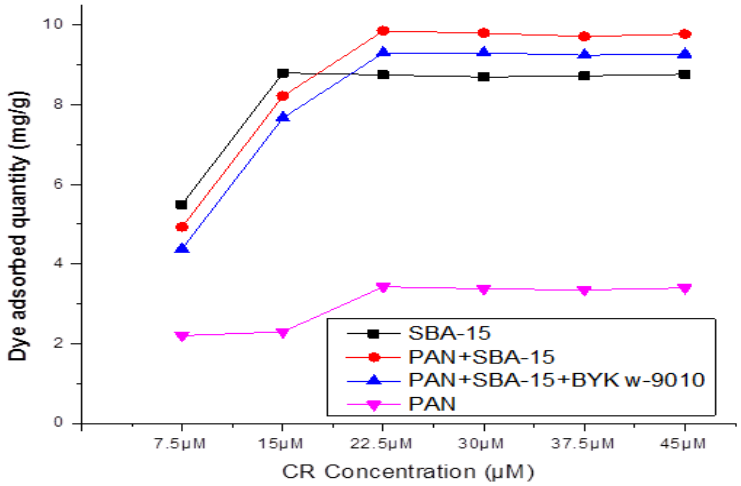


Figure IV.23: CR adsorbed quantity (mg/g) on different adsorbents

It is observed from figure IV.23 that adsorbed quantity increases with the increasing initial concentration of dye till 22.5µM (except SBA-15 that is saturated at 15 µM) and after, adsorbed quantity remained constant due to saturation of active sites.

4.4.2 Adsorption kinetics

Adsorption kinetics is desirable, as it provides information about the mechanism of adsorption, which is important for the efficiency of the process. For this purpose a mother solution of 45µM was prepared and followed by daughter solutions of 7.5, 15, 22.5, 30 and 37.5µM. The plots of pseudo 1st and 2nd order kinetic models of CR on SBA-15, PAN nanofibers and PAN+SBA-15 composite nanofibers with and without dispersing agent at room temperature and neutral pH are displayed in figure IV.24.

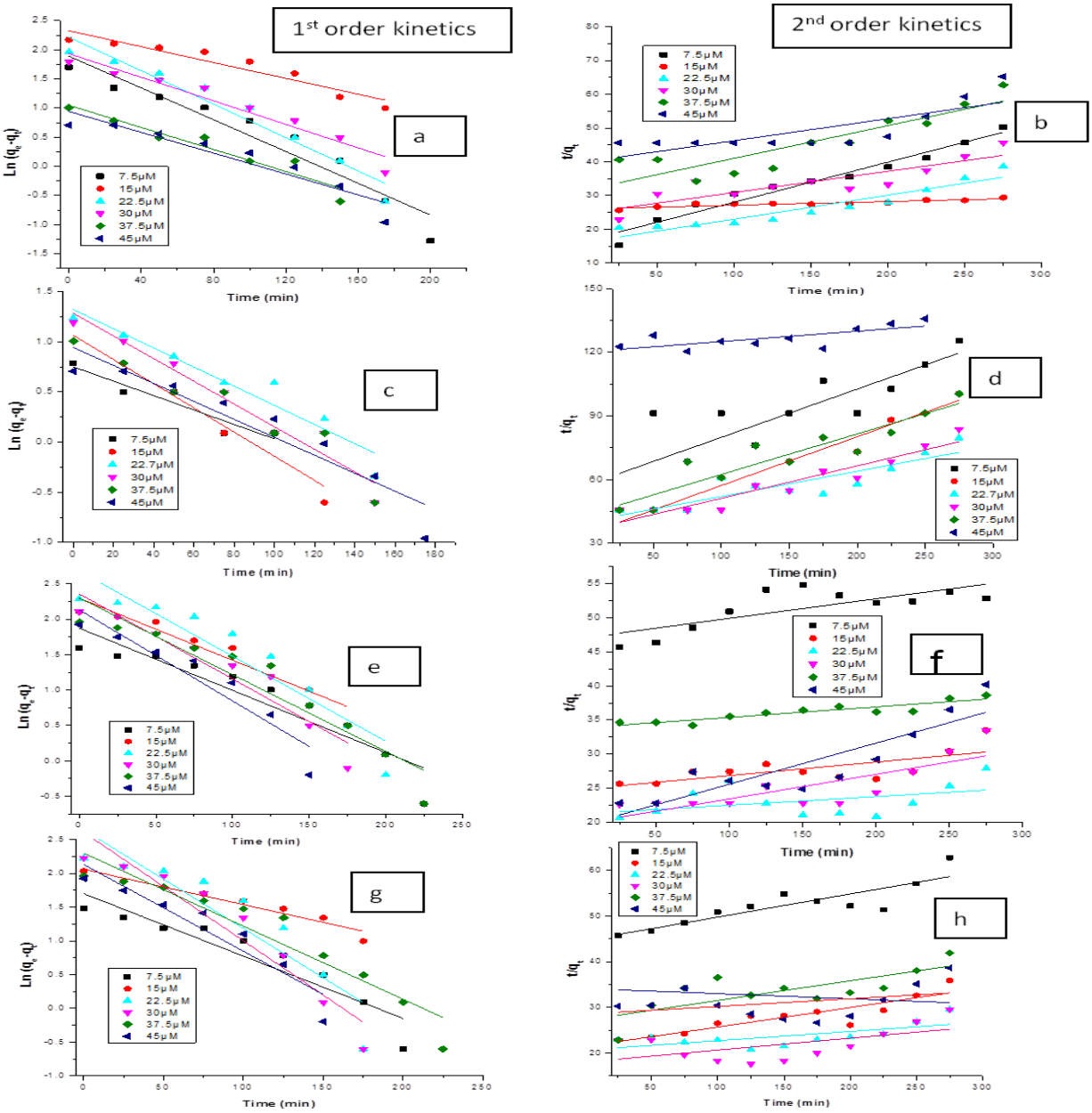


Figure IV.24: CR kinetics models of pseudo 1st and 2nd order on SBA-15 (a, b), PAN nanofibers (c, d), PAN+SBA-15 nanofibers (e, f) and PAN+SBA-15+BYK W-9010 nanofibers (g, h) at pH 7 and room temperature

The parameters values of both kinetic models and their correlation coefficients (R^2) were obtained by plotting graphs $Ln(q_e-q_t)$ versus t and t/q_t versus t for 1st and 2nd order kinetics respectively and are mentioned in table IV.17 for SBA-15, table IV.18 for PAN nanofibers, table IV.19 for PAN+SBA-15 nanofibers and table IV.20 for PAN+SBA-15+BYK W-9010 nanofibers.

Table IV.17: Pseudo 1st and 2nd order kinetics values of CR adsorption on SBA-15 particles

CR Conc.	Pseudo 1st order kinetics			q_e exp**	Pseudo 2nd order kinetics		
	q_e cal.* mg/g	K_1 min^{-1}	R^2	mg/g	q_e cal.* mg/g	K_2 g/min.mg	R^2
7.5µM	6.6	0.07×10^{-3}	0.92	**5.5**	6.3	0.1×10^{-3}	0.96
15µM	10.3	0.04×10^{-3}	0.89	**8.8**	12.3	0.25×10^{-3}	0.79
22.5µM	8.3	0.09×10^{-3}	0.95	**8.75**	10.9	0.47×10^{-3}	0.81
30µM	7.8	0.06×10^{-3}	0.94	**8.7**	11.3	0.59×10^{-3}	0.73
37.5µM	8.1	0.06×10^{-3}	0.97	**8.73**	10.3	0.3×10^{-3}	0.77
45µM	7.5	0.07×10^{-3}	0.88	**8.77**	15.4	0.11×10^{-3}	0.58

*** q_e calculated** obtained by Pseudo 1st and 2nd order kinetics equations (15 and 16)
****q_e experimental** data determined by adsorption curves from spectrophotometer

Table IV.18: Pseudo 1st and 2nd order kinetics values of CR adsorption on PAN nanofibers

CR Conc.	Pseudo 1st order kinetics			q_e exp**	Pseudo 2nd order kinetics		
	q_e cal.* mg/g	K_1 min^{-1}	R^2	mg/g	q_e cal.* mg/g	K_2 g/min.mg	R^2
7.5µM	2.8	0.05×10^{-3}	0.91	**2.2**	4.41	0.9×10^{-3}	0.69
15µM	2.7	0.06×10^{-3}	0.93	**2.3**	2.92	3.4×10^{-3}	0.94
22.5µM	2.9	0.06×10^{-3}	0.93	**3.43**	3.125	2.95×10^{-3}	0.93
30µM	3.6	0.06×10^{-3}	0.96	**3.38**	3.97	1.76×10^{-3}	0.89
37.5µM	3.85	0.05×10^{-3}	0.94	**3.35**	5.26	0.84×10^{-3}	0.85
45µM	2.56	0.05×10^{-3}	0.88	**3.4**	18.18	0.025×10^{-3}	0.52

*** q_e calculated** obtained by Pseudo 1st and 2nd order kinetics equations (15 and 16)
****q_e experimental** data determined by adsorption curves from spectrophotometer

Table IV.19: Pseudo 1st & 2nd order kinetics values of CR adsorption on PAN+SBA-15 nanofibers

CR Conc.	Pseudo 1st order kinetics			q_e exp**	Pseudo 2nd order kinetics		
	q_e cal.* mg/g	K_1 min^{-1}	R^2	mg/g	q_e cal.* mg/g	K_2 g/min.mg	R^2
7.5µM	6.5	0.11×10^{-3}	0.87	**4.93**	11.3	1.2×10^{-3}	0.53
15µM	9.9	0.05×10^{-3}	0.91	**8.22**	17.6	0.13×10^{-3}	0.45
22.5µM	12.1	0.07×10^{-3}	0.87	**9.86**	17.2	0.17×10^{-3}	0.52
30µM	8.9	0.07×10^{-3}	0.9	**9.8**	15.2	0.22×10^{-3}	0.62
37.5µM	8.8	0.06×10^{-3}	0.9	**9.72**	12.8	0.18×10^{-3}	0.82

45µM	8.42	0.09×10^{-3}	0.85	**9.78**	13.5	0.46×10^{-3}	0.76

*** q_e calculated** obtained by Pseudo 1st and 2nd order kinetics equations (15 and 16)
****q_e experimental** data determined by adsorption curves from spectrophotometer

Table IV.20: Pseudo 1st & 2nd order kinetics of CR adsorption on PAN+SBA-15+BYK W-9010 nanofibers

CR Conc.	Pseudo 1st order kinetics			q_e exp**	Pseudo 2nd order kinetics		
	q_e cal.* mg/g	K_1 min^{-1}	R^2	mg/g	q_e cal.* mg/g	K_2 g/min.mg	R^2
7.5µM	5.48	0.04×10^{-3}	0.86	**4.38**	10.17	2.2×10^{-3}	0.74
15µM	7.87	0.03×10^{-3}	0.94	**7.67**	12.11	0.32×10^{-3}	0.79
22.5µM	11.14	0.07×10^{-3}	0.89	**9.31**	26.32	0.07×10^{-3}	0.41
30µM	10.59	0.09×10^{-3}	0.91	**9.31**	25.65	0.09×10^{-3}	0.46
37.5µM	11.1	0.06×10^{-3}	0.86	**9.25**	18.87	0.01×10^{-3}	0.51
45µM	11.3	0.06×10^{-3}	0.89	**9.27**	44.85	0.018×10^{-3}	0.19

*** q_e calculated** obtained by Pseudo 1st and 2nd order kinetics equations (15 and 16)
****q_e experimental** data obtained by adsorption curves from spectrophotometer

The results displayed in all kinetics tables of different adsorbents of CR explained that second order model does not seem to be good for modeling the kinetics of the whole adsorption process and the regression coefficients (R^2) are less than those obtained from the first order kinetics. The results also explained that the equilibrium adsorption (q_e calculated) from the pseudo 1st order kinetics is close to the experimental data (q_e experimental) suggesting the better application of the first order kinetics resulted in physisorption adsorption.

4.4.3 Adsorption isotherm

The equilibrium adsorption isotherm is of importance in the design of adsorption system. Two adsorption isotherms were selected for CR adsorption including Langmuir isotherm (equation 12) and Freundlich isotherm (equation 14). The plots of Langmuir and Freundlich isotherms and their results for CR adsorption at room temperature are displayed in figure IV.25 and table IV.21 respectively.

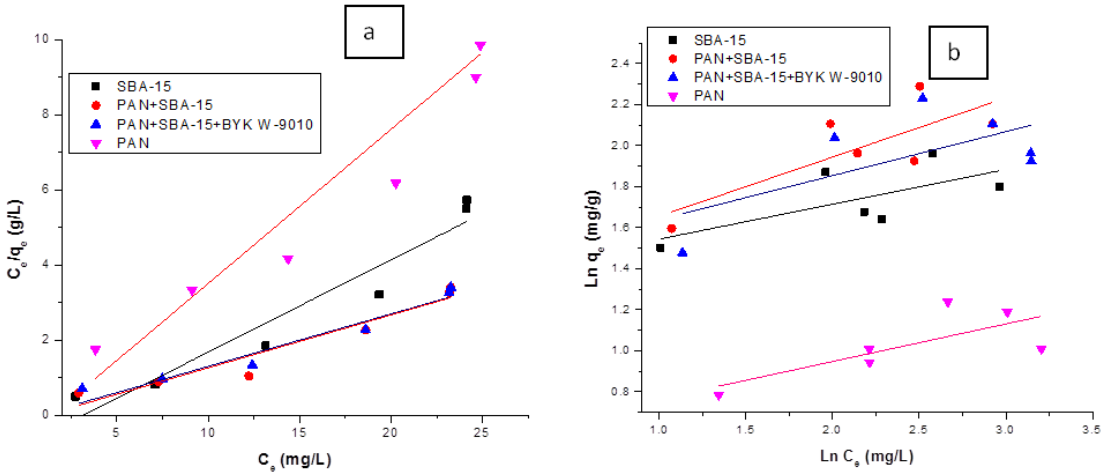


Figure IV.25: CR plots of Langmuir (a) and Freundlich (b) isotherms on different adsorbents at pH 7 and room temperature

Table IV.21: Langmuir and Freundlich isotherm data with actual value of adsorbed quantity (at pH 7 and room temperature)

S No.	Langmuir isotherm				q_e act.**	Freundlich isotherm		
	$q_{e\ max.}$ mg/g	K_L (L/mg)	R_L	R^2	mg/g	1/n	K_f mg/g	R^2
1*	7.3	1	0.18	0.84	**8.76**	0.17	23.4	0.32
2*	8.3	1.25	0.15	0.94	**9.86**	0.29	20.4	0.51
3*	8.2	1.27	0.146	0.94	**9.31**	0.34	15.1	0.62
4*	4	1.071	0.17	0.92	**3.43**	0.11	11.2	0.44

1*= SBA-15 2*= PAN+SBA-15 3*= PAN+SBA-15+BYK 4*= PAN nanofibers
** q_e actual= actual adsorbed quantity of CR (data obtained from curves of spectrophotometer)

All the parameters including Freundlich constants, linear regression, actual adsorbed quantity, $q_{e\ max}$ etc, obtained by Langmuir and Freundlich isotherm models are listed in table IV.21. The results of CR adsorption revealed that correlation coefficient R^2 values for Langmuir isotherm model are higher (in the range of 0.84 - 0.94) as compared to Freundlich isotherm which are very low and scattered (0.32 - 0.62), therefore Langmuir model better describes the adsorption behavior of CR on used adsorbents. The well fitting of equilibrium data in the Langmuir isotherm expression also confirms the monolayer coverage of CR on adsorbents which is homogeneous in adsorption affinity. It is also observed that calculated values $q_{e\ max}$ for all used adsorbents are in agreement with the actual values $q_{e\ act}$. The dimensionless constant separation factor R_L is evaluated between 0 and 1 indicating a favorable adsorption process for CR. 1/n obtained values

derived from Freundlich isotherm are less than 1 which explains the adsorption is linear and favorable [3,5,6]. In table IV.22, the maximum monolayer adsorption of CR on different adsorbent mentioned in literature is compared with the adsorption of CR in this study.

Table IV.22: Comparison of maximum adsorption of CR onto various adsorbents (pH =7, room temperature)

Adsorbents	**Adsorbent: adsorbate (mg/mL)**	**Adsorbed quantity q_m (mg/g)**
Amide-Calixarene/PAN nanofibers	1:2.1	35 [50]
Ester-Calixarene/PAN nanofibers	1:2.1	23 [50]
Calixarene/PAN nanofibers	1:2.1	19 [50]
PAN nanofibers	1:4	4 [8]
SBA-15	1:1	8.8 (In this study)
PAN+SBA-15	5.72:1	9.9 (In this study)
PAN+SBA-15+BYK W-9010	5.72:1	9.3 (In this study)
PAN nanofibers	4.72:1	3.4 (In this study)

The adsorption results of CR on all adsorbents used in this study are compared with the adsorbents used in literature and it is concluded that adsorbents of this study are not as effective as in literature for the adsorption of CR due to the repulsive electrostatic forces on adsorbents and adsorbates. Therefore adsorbents of this study cannot be used for effective adsorption of CR dye in wastewater.

4.4.3 Effect of pH

pH of the adsorbate solution significantly affects the adsorption process due to its effect on the surface charge of the adsorbent. The effect of pH on adsorption of CR dye on SBA-15, PAN and PAN+SBA-15 nanofibers was investigated at initial concentration of 15µM (randomly selected) at room temperature. The results of adsorption are displayed in figure IV.26 and adsorbed quantities are mentioned in table IV.23.

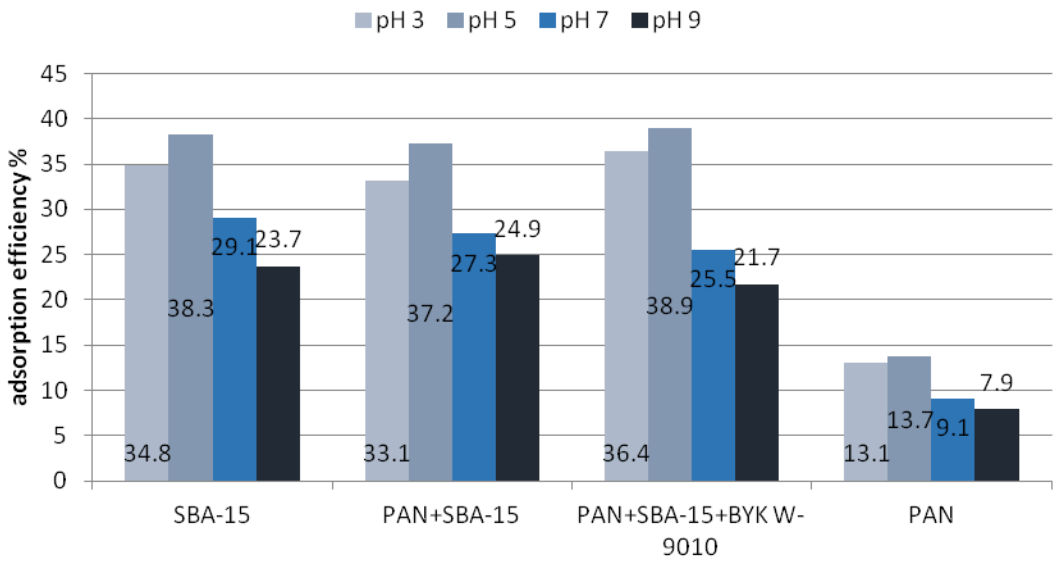


Figure IV.26: pH impact on CR adsorption at equilibrium on different adsorbents (15µM and room temperature)

Table IV.23: CR adsorbed quantity (mg/g) at different pH on different adsorbents (15µM and room temperature)

pH	SBA-15	PAN+SBA-15 nanofibers	PAN+SBA-15+BYK W-9010 nanofibers	PAN nanofibers
3	10.5	10	11	3.1
5	11.5	11.2	11.7	3.3
7	8.8	8.2	7.7	2.2
9	7.1	7.5	6.5	1.9

The data in table IV.23 shows that in acidic medium, CR adsorption is maximum because of presence of attractive electrostatic forces between negatively charged anionic dye and increase of positive charge on adsorbents due to acidic pH. Whereas as the pH increases from neutral to basic medium, it results in reduction of adsorption due to repulsive electrostatic forces [3, 8]. It is also suggested that two primary amines ($-NH_2$) attached to the two naphthalene rings of the Congo red molecule, can be protonated at the initial pH 6 and have stronger basicity which resulted in the attraction between the protonated amino groups of Congo red molecule and negatively charged adsorbent surface, that results in more adsorption in acidic conditions [227].

4.4.5 Effect of temperature

The adsorption efficiency of CR on different adsorbents at temperature 20, 35 and 50 ^{o}C , neutral pH and 15µM concentration is displayed in figure IV.27, whereas figure IV.28 explains the plot of LnK_L versus 1/T.

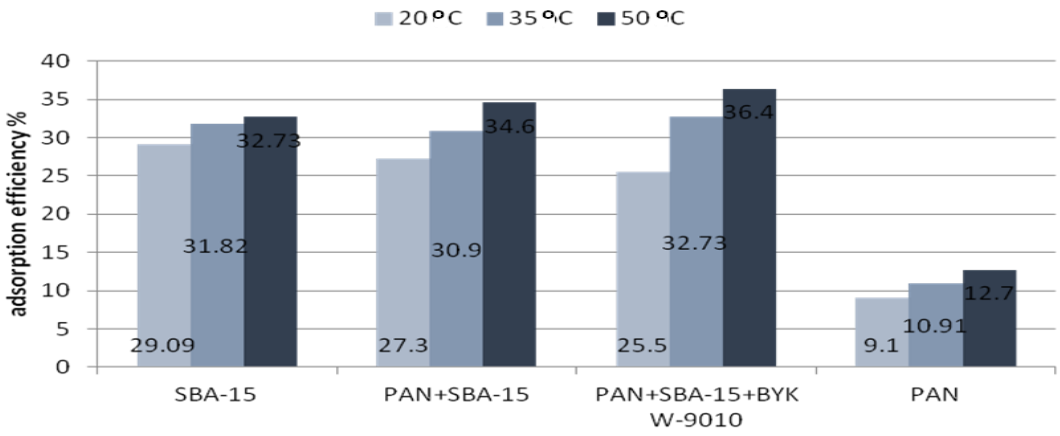


Figure IV.27: CR adsorption efficiency at equilibrium on 20, 35 and 50 ^{o}C (15µM and pH 7)

Figure IV.27 explained the effect of temperature increase on adsorption percentage of CR dye over all the used adsorbents. With increase in temperature from 20 to 35 and then 50 oC, the adsorption efficiency of CR increased from 29.1 to 31.8 and 32.7% for SBA-15, 27.3 to 30.9 and 34.6% for PAN+SBA-15 composite nanofibers, from 25.5 to 32.7 and 36.4% for PAN+SBA-5+BYK W-9010 composite nanofibers and from 9.1 to 10.9 and 12.7% for pristine PAN nanofibers. This increase in adsorption is due to increase in kinetic energy of dye molecules which enhanced the mobility of dye molecules to penetrate onto the available active sites of the adsorbents molecules [3]. Impact of thermodynamic parameters on the adsorption of CR dye is displayed in figure IV.28 and their data is explained in table IV.24.

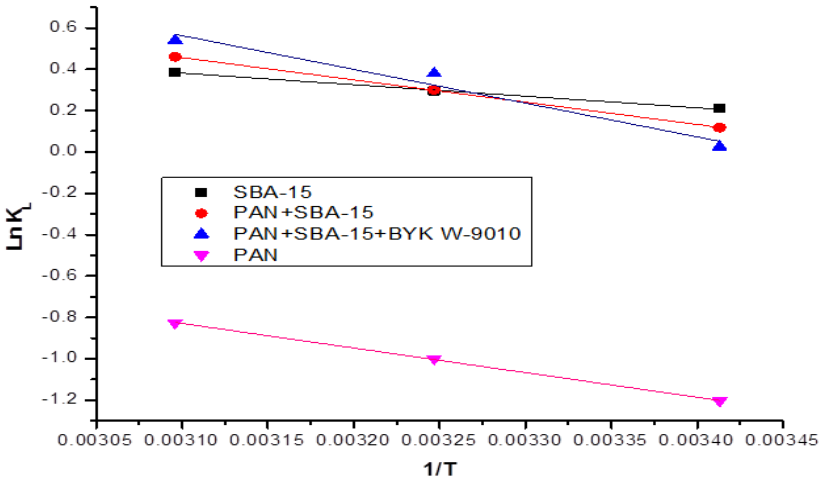


Figure IV.28: Plot for evaluating thermodynamic parameters of CR adsorption on all adsorbents

Table IV.24: Thermodynamic properties of CR adsorption on different adsorbents (15µM and pH 7)

Adsorbent	Temperature (K°)	K_L	ΔG° (KJ/mol)	ΔH° (KJ/mol)	ΔS° (J/K. mol)	R^2
SBA-15	293	1.2	-0.5	4.6	17.5	0.996
	308	1.3	-0.7			
	323	1.5	-1.1			
PAN+SBA-15	293	1.1	-0.3	9	31.6	0.999
	308	1.3	-0.8			
	323	1.6	-1.24			
PAN+SBA-15+BYK	293	1.1	-0.1	13.6	46.7	0.94
	308	1.5	-1			
	323	1.7	-1.4			
PAN	293	0.3	2.9	9.9	23.8	0.999
	308	0.4	2.6			
	323	0.4	2.2			

The results of Gibbs free energy change (ΔG°), enthalpy change (ΔH°) and entropy change (ΔS°) are described in table IV.24 and these results were measured by equation 8, 9 and plot between LnK_L versus 1/T. The negative values of ΔG° for Congo red dye adsorption on SBA-15 and PAN+SBA-15 composite nanofibers on various temperatures show that adsorption process is spontaneous and thermodynamically favorable except adsorption on pristine PAN nanofibers [3,

5]. Positive values of ΔH^o indicate that adsorption of CR on all adsorbents is endothermic, which means rise in temperature leads to higher adsorption capacity of adsorbents. As the values of ΔH^o <25 KJ/mol, therefore the adsorption of CR is physisorption in this study. Positive values of ΔS^o reveal the energy gain and increase randomness at the solid/solution interface during adsorption process [3, 5].

4.4.6 Batch screening test

Congo red (CR) is a strong anionic dye having pKa 4 and was selected to check the adsorption behavior on SBA-15 particles, PAN nanofibers and PAN+SBA-15 composite nanofibers. The batch screening test was performed to evaluate the efficiency of CR on selected adsorbents at neutral pH and room temperature, which is displayed in figure IV.29.

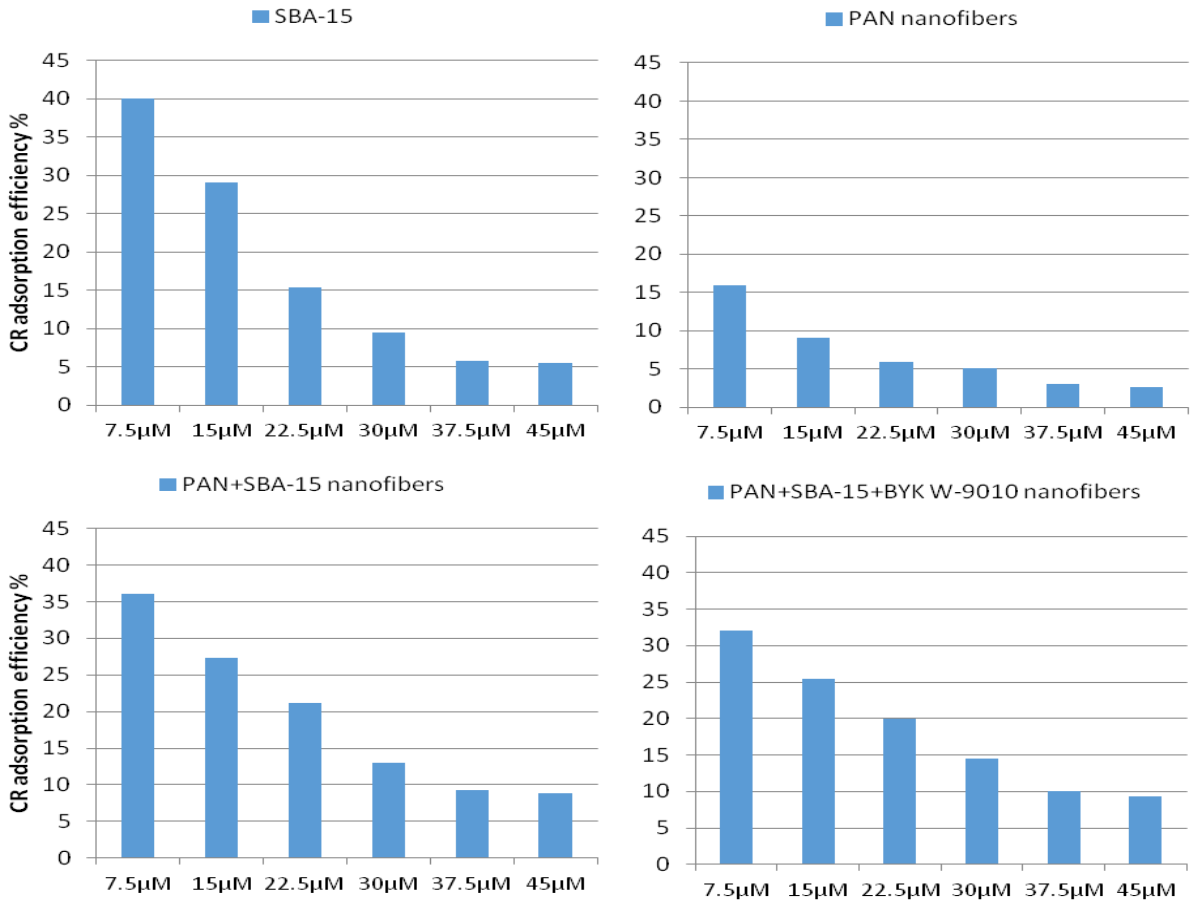


Figure IV.29: CR screening test adsorption efficiency on different adsorbents (pH 7, room temperature)

As per screening test selection criteria, the adsorption of CR at silica particles and composite nanofibers is very small in the range of ≤40%, even at very low concentration, therefore these adsorbents are categorized as inefficient. If pristine PAN nanofibers were discussed for screening test, their adsorption is almost negligible ≤16%. Therefore all the above used adsorbents are not applicable for the adsorption of CR, because the adsorbents are negatively charged and CR is also anionic dye, which is not suitable for this adsorption process. The adsorption process of 7.5 µM CR dye on all adsorbent at equilibrium, neutral pH and room temperature is displayed in figure IV. 30.

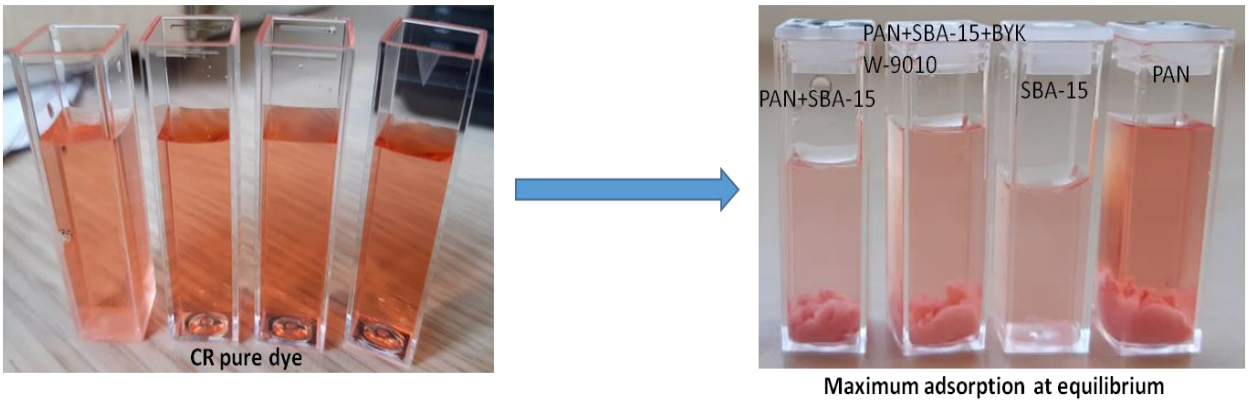


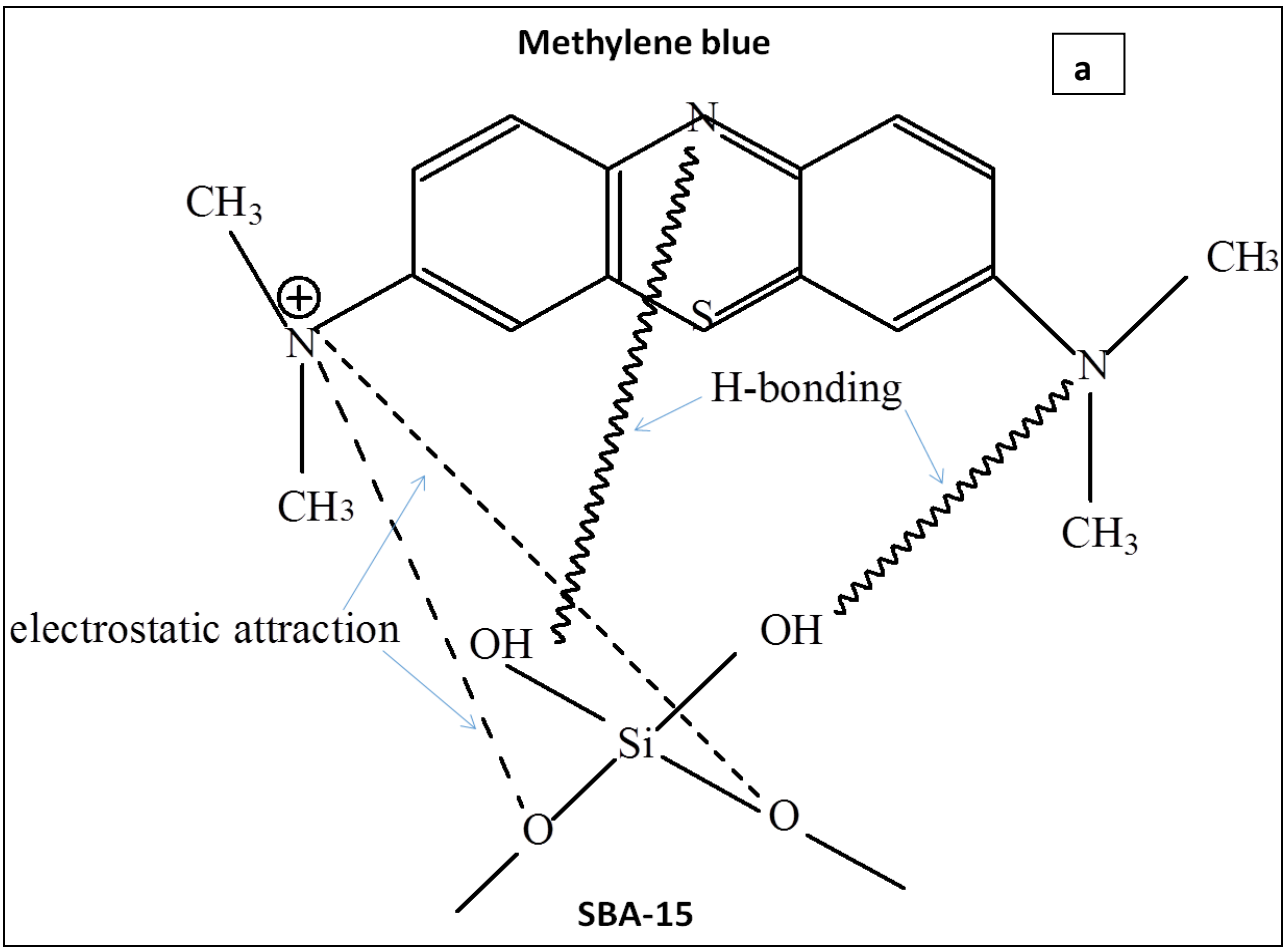
Figure IV.30: CR adsorption on all adsorbents at equilibrium (7.5 µM, pH 7 and room temperature)

4.4.7 Conclusion

Congo red is an anionic dye having pKa of 4. Adsorption efficiency of CR on all used adsorbents was observed below 40%, therefore all used adsorbents are not suitable for treatment of CR polluted water because of electrostatic repulsive forces of anionic dye and adsorbents having negative charge. Kinetics of CR dye showed the pseudo 1st order kinetics and Langmuir isotherm is better fitted resulted in monolayer homogenous adsorption. CR dye adsorption increased by decreasing pH due to increase in attractive forces. Increase in temperature also increased the adsorption due to increase in molecules mobility to penetrate into the available active sites on adsorbents surface.

4.5 Adsorption mechanisms of MB, NR and CR dyes

The screening test results showed that adsorption of MB on SBA-15, PAN nanofibers and PAN+SBA-15 composite nanofibers was very good and adsorption of NR dye was also quite efficient on all adsorbents except PAN nanofibers because MB is strong cationic dye having pKa 3.8 whereas NR is a weak cationic dye having pKa 6.8 therefore MB made strong interaction with PAN nanofibers as compared to NR. Whereas CR dye was an anionic dye having pKa 4 and had adsorption efficiency ≤40% on all the adsorbents therefore it was screened as inefficient adsorbate due to electrostatic repulsive forces (schematic diagram is shown at IV.31).



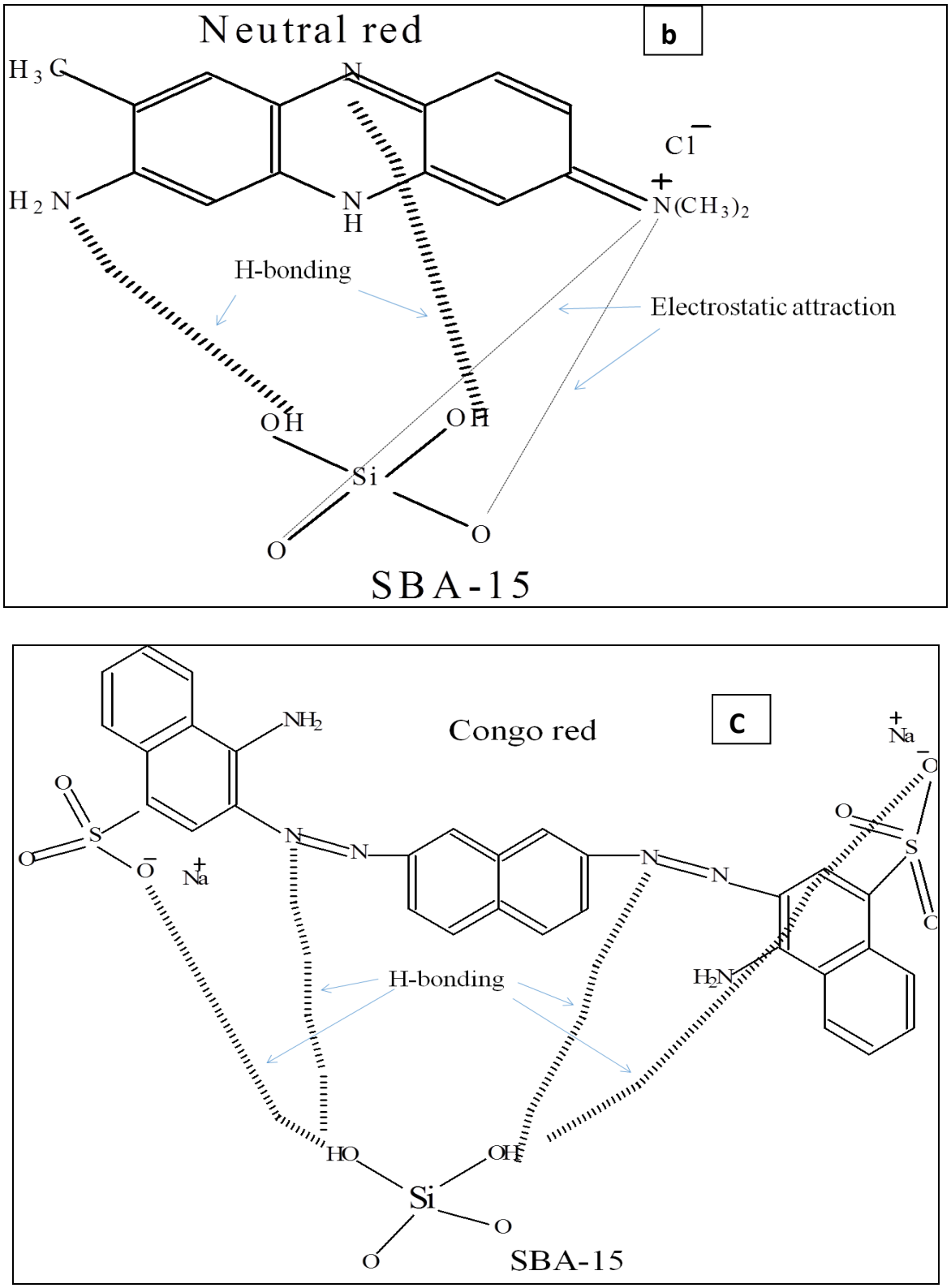


Figure IV.31:Possible interactions between (a) MB and SBA-15, (b) NR and SBA-15, (c) CR and SBA-15

In the case of MB, the calculated values of pseudo 1st order including $q_{calculated}$ were far different from $q_{experimental}$ values and correlation coefficient R^2 were also less than pseudo 2nd order kinetics therefore pseudo 2nd order described MB adsorption well whereas in the case of NR and CR, pseudo 1st order kinetics better explained the adsorption kinetics on all adsorbents. The adsorption of MB, NR and CR on all used adsorbents is better described by Langmuir isotherm models where R^2 values are higher and closer to 1 as compared to Freundlich model. This suggested that the adsorption of MB, NR and CR is monolayer on the homogenous adsorbents surface and the adsorption mechanism was assumed to be physisorption. The closeness of $q_{experiment}$ and $q_{calculated}$ values also confirmed the applicability of Langmuir model. Freundlich isotherm model explained that the value of 1/n was below 1 in all adsorbate/adsorbent cases and the favorability of the process measured by separation factor R_L was also found to be less than 1, therefore the adsorption processes of all adsorbate/adsorbents were favorable. pH was one major controlling parameter for dyes adsorption from fluid phase. When MB, NR and CR dyes were dissolved in aqueous solutions, they exist as cations or anions according to their chemistry. Being an ionic species, the extent of their bindings at all adsorbents was affected by the charges on adsorbent surface, which was controlled by the pH of solution. The adsorption of MB and NR was small at low pH and increased at high pH. This is because excessive positive charges are present at low pH, those charges will repel the cations of MB and NR for active binding sites. Moreover, at high pH, the adsorbent became negatively charged due to decrease in positive charge at the solid/liquid interface and this resulted in high adsorption of MB and NR. On the other hand, in the case of CR, the adsorption increased by decreasing solution pH due to increase in positive charges.

Study revealed that adsorbed quantities of MB, NR and CR increased when concentration of dyes increased from 15µM to 45 µM, from 15µM to 75 µM and from 7.5µM to 22.5 µM, respectively. This was probably due to a high mass transfer driving forces which made the previously inaccessible adsorbent sites for dye adsorption available [5]. Whereas after increasing more dyes concentrations dye removal efficiency remained constant, which was expected because of the coverage of active binding sites on adsorbents. Thermodynamic analysis was undertaken to check the role of temperature on MB, NR and CR adsorption on all used adsorbents. The negative values of ΔG^o for all dyes on all adsorbents except pristine PAN nanofibers at various temperatures represented that adsorption process was spontaneous and thermodynamically favorable. It was also observed that by increasing temperature, ΔG^o values decreased. The large q_e

values at higher temperature and negative ΔG^o values further confirmed that MB, NR and CR were easily adsorbed (except PAN nanofibers for CR and NR) at higher temperature and there is no energy barrier in adsorption at higher temperatures. The positive values of ΔH^o indicated that adsorption of MB, NR and CR on all adsorbents was endothermic, which meant higher adsorption at high temperature. Whereas the positive values of ΔS^o revealed the energy gained and increased randomness at solid/solution interface during adsorption process.

4.6 Desorption study of MB, NR and CR with recyclability of adsorbents

An efficient adsorbent should possess qualities like: high adsorption capacities, fast adsorption and as well as excellent desorption capacity. Therefore, to determine the reusability of all the adsorbents including SBA-15 particles, pristine PAN nanofibers and PAN+SBA-15 composite nanofibers with and without dispersing agent for MB, NR and CR, five simultaneously desorption-adsorption cycles were performed (desorption at pH 2, 7 and 10 whereas re-adsorption at neutral pH). The results of MB, NR and CR desorption-adsorption on all adsorbents and different pH described above, are displayed in figure IV.28, IV.29 and IV.30 respectively.

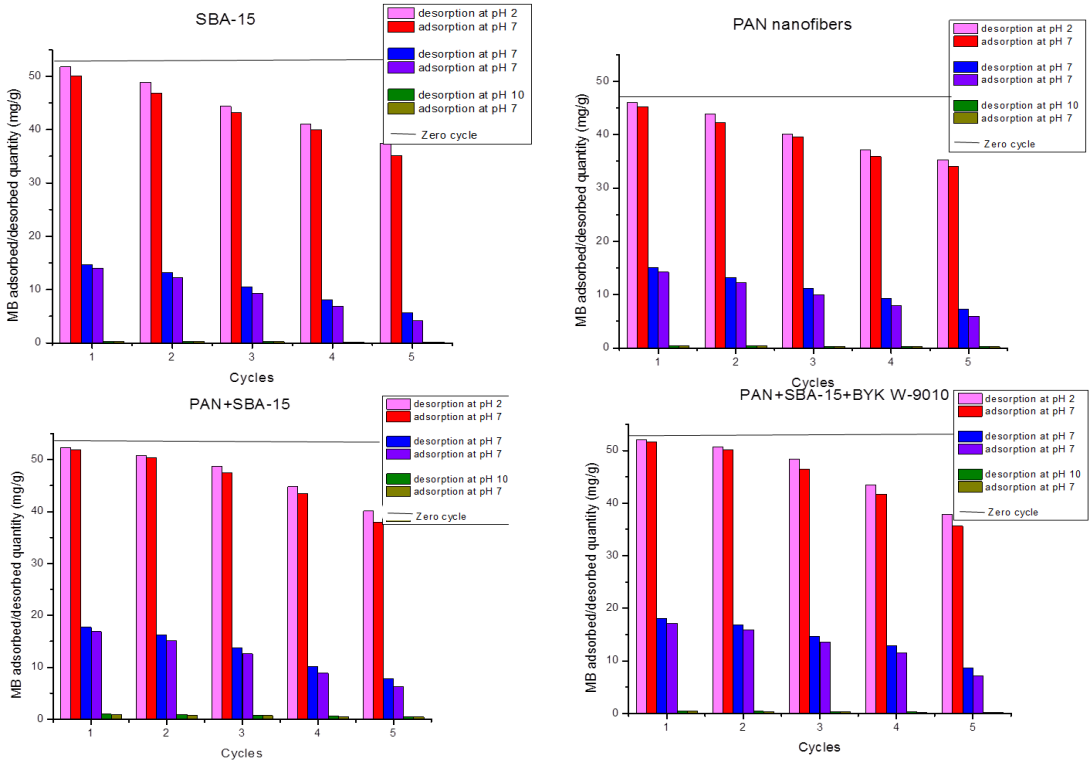


Figure IV.28: MB adsorption (pH 7)/desorption (pH 2, 7, 10) at SBA-15, PAN, PAN+SBA-15 and PAN+SBA-15+BYK W-9010 (30 µM and room temperature)

The horizontal black line in above figure shows the maximum adsorbed quantity of dye (mg/g) before the desorption-adsorption process which is 52.5, 46.8, 53 and 52.7 mg/g for SBA-15, PAN, PAN+SBA-15 and PAN+SBA-15+BYK W-9010 nanofibers, respectively. Results in figure IV.28 explained that for MB, the maximum desorption was observed at pH 2 for all adsorbents, which reduced later at neutral pH 7 and at basic pH 10, desorption was minimum. This phenomenon was due to the presence of opposite charges of dye molecule and adsorbents surface [6]. Whereas, in the case of re-adsorption at neutral pH, maximum adsorption was observed for adsorbents, desorbed at pH 2 due to availability of maximum active sites, less re-adsorption for samples desorbed at neutral pH and almost negligible re-adsorption was observed for adsorbents desorbed at pH 10 which is due to less available sites on adsorbents as very small dye removal was observed during desorption at pH 7 and 10.

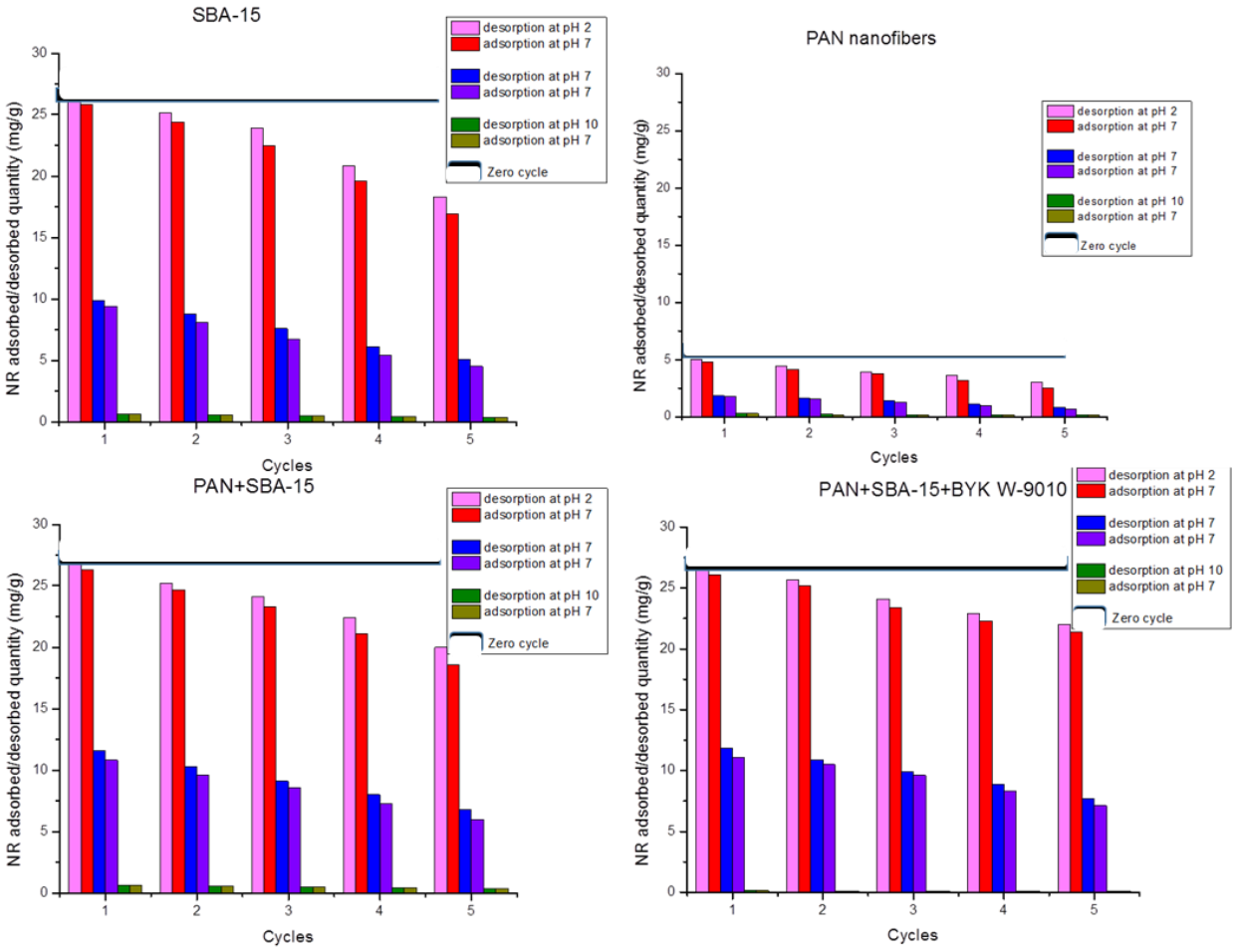


Figure IV.29: NR adsorption (pH 7)/desorption (pH 2, 7, 10) at SBA-15, PAN, PAN+SBA-15 and PAN+SBA-15+BYK W-9010 (30 µM and room temperature)

Maximum adsorbed quantities of NR dye at zero cycle shown as black bar in above figure are 26.9, 5.2, 27.3 and 27.1 mg/g for SBA-15, PAN, PAN+SBA-15 and PAN+SBA-15+BYK W-9010 nanofibers respectively. NR is a weak cationic dye and showed maximum desorption at low pH of 2 due to opposite electrostatic repulsive forces and minimum desorption at high pH 10 due to attractive forces. Similarly, maximum re-adsorption was observed at neutral pH for the samples desorbed at pH 2 because of maximum availability of free active sites due to desorption and re-adsorption was less on samples desorbed at high pH 7 and 10, as there were less free sites because of less desorption [6].

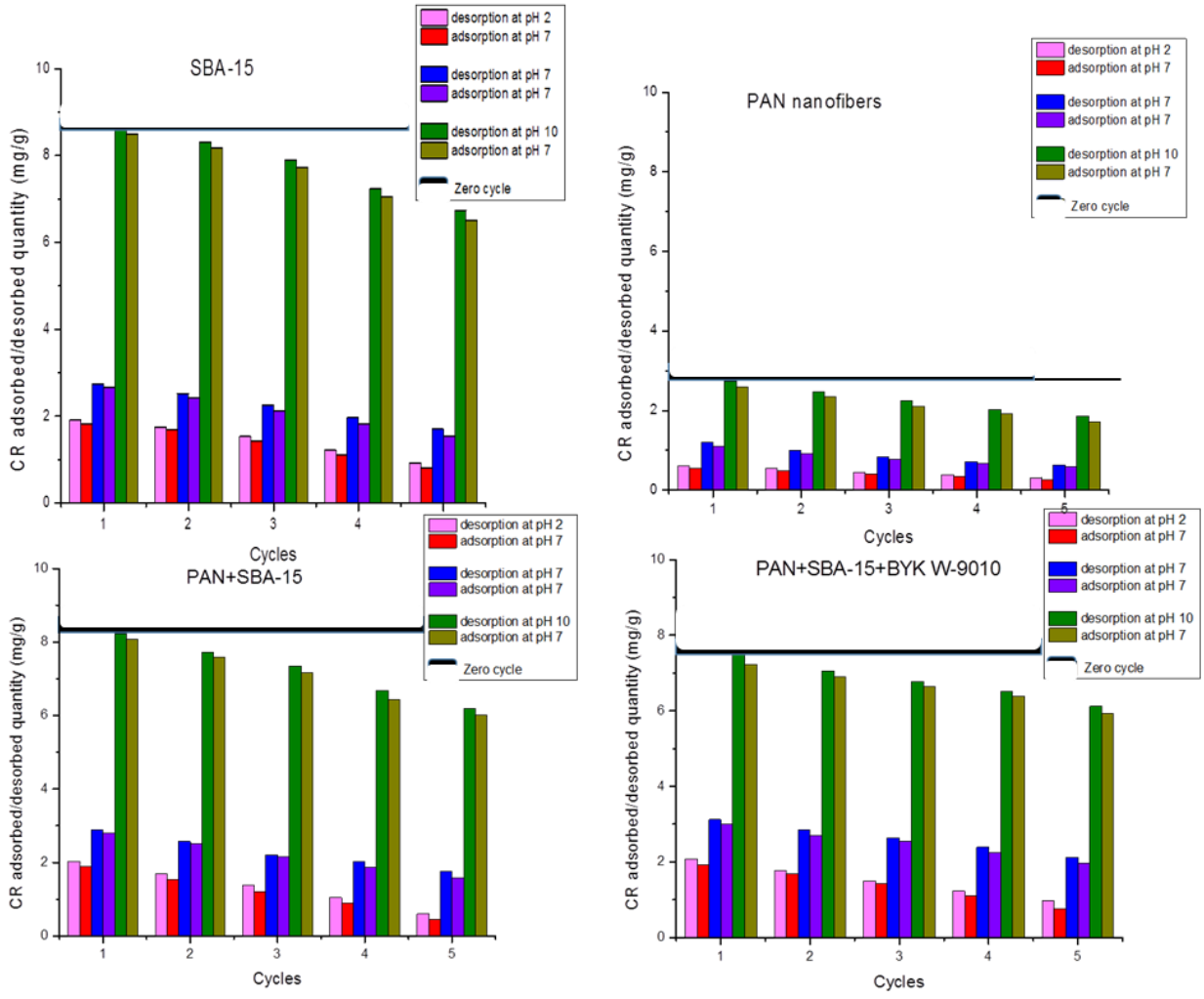


Figure IV.30: CR adsorption (pH 7)/desorption (pH 2, 7, 10) at SBA-15, PAN, PAN+SBA-15 and PAN+SBA-15+BYK W-9010 (15 µM and room temperature)

In Figure IV.30 maximum adsorbed quantities at equilibrium of CR dye at zero cycle (black bar) are 8.76, 2.74, 8.21 and 7.67 mg/g for SBA-15, PAN, PAN+SBA-15 and PAN+SBA-15+BYK W-9010 respectively at neutral pH, room temperature and 15µM concentration. As CR is anionic dye therefore it's desorption is maximum at higher pH 10 due to opposite repulsive forces and least in the region of acidic pH 2. As maximum desorption was observed at basic pH therefore maximum free active sites are also available at this basic pH and maximum re-adsorption was observed for these samples at neutral pH and least desorption was calculated at acidic pH 2 therefore very small free available sites were available here therefore small re-adsorption was observed for these adsorbents at neutral pH [6].

4.7 FTIR analysis of adsorbates/adsorbents

FTIR spectrum of pure PAN powder is taken as reference and mentioned in figure IV.31. The bands of PAN can be assigned as follows: 2941 and 2870 cm^{-1} C-H stretching vibration in C-H_2 and C-H_3 groups, 2243 cm^{-1} stretching vibration of C≡N, 1629 cm^{-1} stretching vibration in C=C, 1452 cm^{-1} bending vibration of C-H_3 and CH_2 groups, 1374 cm^{-1} bending vibration of CH_3 symmetric in CCH_3, 1225 cm^{-1} stretching vibration of C-H, 1070 cm^{-1} bending vibration of C-N and 535 cm^{-1} twisting vibration of C=O and band at 793 cm-1 is due to =C-H bond formation [206, 209, 210, 211, 212].

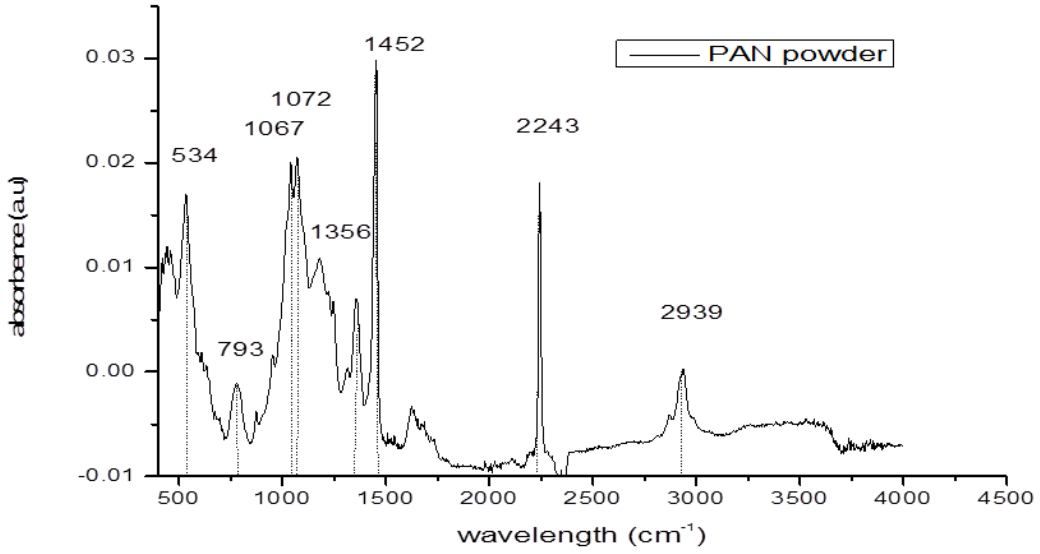


Figure IV.31: FTIR spectrum of pure PAN

Figure IV.32 describes the FTIR spectrum of pure SBA-15 particles as a reference. The characteristics bands at 1083, 800 and 458 cm^{-1} are corresponding to the stretching, bending and out of plane of Si-O bonds respectively. Whereas bands at 939 cm^{-1} is for Si-OH stretching, 1630 cm^{-1} for C-O bending, 2357 cm^{-1} for Si-C stretching and 3444 cm^{-1} for –OH stretching. [211, 212].

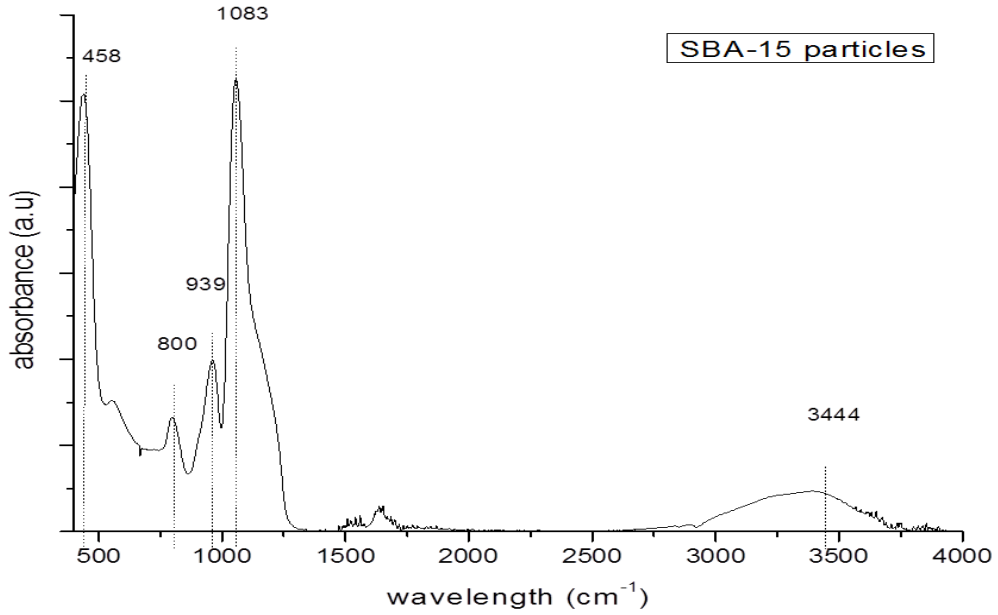


Figure IV.32: FTIR spectra of pure SBA-15 particles

Figure IV.33 and IV.34 shows the FTIR spectrum of PAN+SBA-15 composite nanofibers with and without dispersing agent.

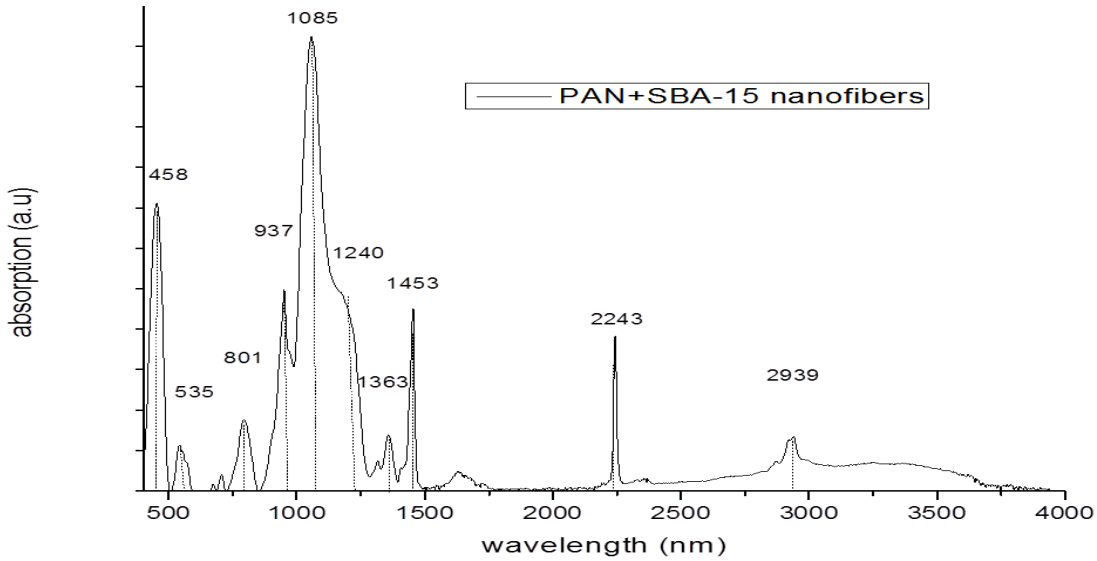


Figure IV.33: FTIR spectra of PAN+SBA-15 nanofibers

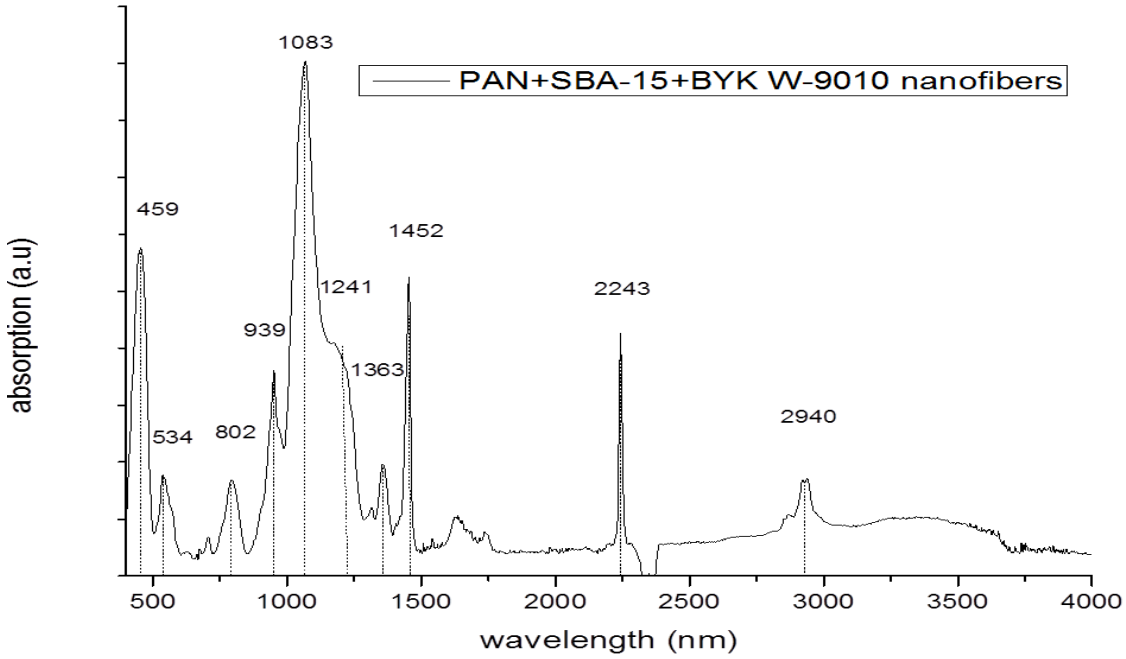


Figure IV.34: FTIR spectrum of PAN+SBA-15+BYK W-9010 nanofibers

Above two figures present the FTIR spectrums of PAN/SBA-15 composite nanofibers with and without dispersing agent named BYK W-9010. The bands close to 458 cm^{-1}, 801 cm^{-1} and 1083 cm^{-1} in both samples corresponds to the stretching, bending and out of plane Si-O bonds respectively. The peak close to 939 cm^{-1} is the result of Si-OH stretching in both samples. The peaks of PAN are assigned as follows: close to 535 cm^{-1} for C=O twisting vibration, 1241 cm^{-1} for stretching vibration of C-N, 1452 cm^{-1} scissor vibration of C-H in $C-H_2$, 2242 cm^{-1} stretching vibration of saturated nitrile group C≡N and 2940 cm^{-1} stretching vibration of C-H and 1363 cm^{-1} bending vibration of CH_3 symmetric to CCH_3 . The results of bands of both samples are also identical, because the quantity of dispersing agent was very small no band of P-OH in the range of 2300-2100 cm^{-1} and 2700-2560 cm^{-1} and no band of P=O at 1680 cm^{-1} were detected [206, 209, 210, 211, 212].

FTIR spectrum of pure MB dye and MB dye after adsorption on PAN nanofibers, on SBA-15 particles, on PAN+SBA-15 and on PAN+SBA-15+BYK W-9010 composite nanofibers are compared in figure IV.35. The bands at 1660 and 1334 cm^{-1} corresponds to $C_{het} = N^+ (CH_3)_2$ stretching vibration and stretching vibration of C-N terminal saturated dimethylamino groups of dye. There are also C-H bending and C-S-C vibrations of MB^+ heterocyclic at 814 cm^{-1}, 852 cm^{-1},1136 cm^{-1} and 1066 cm^{-1} respectively. Bending vibrations of C-H is found at 1487cm^{-1}. Some

bands of MB are detected on PAN nanofibers and SBA-15 particles, which include 814 cm^{-1}, 1334 cm^{-1}, 1487 cm^{-1}. The fourth and fifth part of figure displays the presence of MB on PAN+SBA-15 composite nanofibers with and without dispersing agent and these bands are almost similar as described above. There is no band of BYK W-9010 detected *because the quantity of dispersing agent was very small and no band of P-OH in the range of 2300-2100 cm^{-1} and 2700-2560 cm^{-1} and no band of P=O at 1680 cm^{-1} were detected [211, 213, 215, 223, 226]. FTIR spectra proved the adsorbance of MB on all adsorbents.*

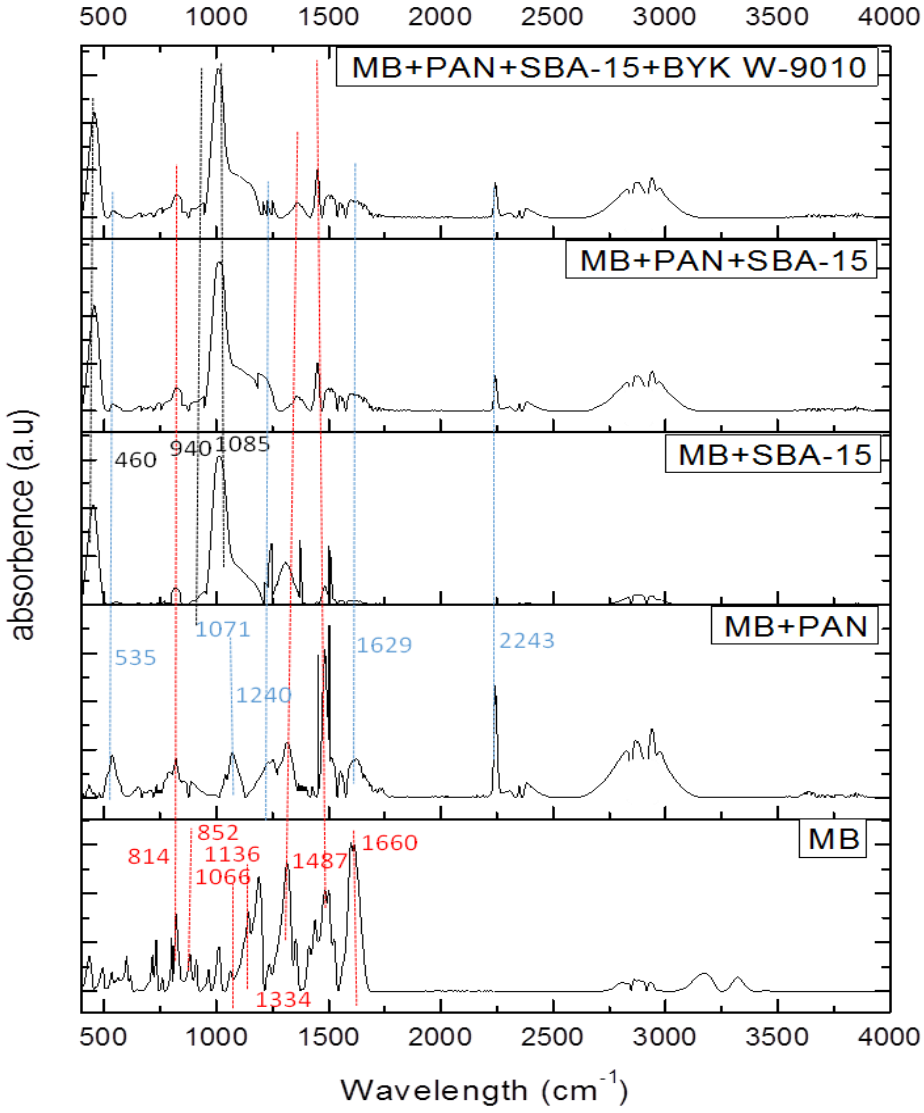


Figure IV.35: FTIR Spectra of MB, PAN+MB, SBA-15+MB, PAN+SBA-15+MB and PAN+SBA-15+BYK W-9010+MB

Figure IV.36 presents the spectrum of NR dye and presence of NR on pristine PAN, on SBA-15 particles and on composite nanofibers with and without dispersing agent. In the case of pure NR, a less intense band at 2855 cm^{-1} is assigned to symmetrical aliphatic carbon -CH_2 and a weak band near 434 cm^{-1} corresponds to NR dye. Peaks at 1326 cm^{-1} and 884 cm^{-1} for the –C=C-H in plane –C-H bend and 820 cm^{-1} for ring vibration. A band at 1202 cm^{-1} for –C-N confirms the heterocyclic nature of NR with bands at 3334 cm^{-1} and 1619 cm^{-1} representing –N-H stretching in amide and band at 2939 cm^{-1} is CH asymmetric in CH_2. After adsorption, NR groups at 884, 1326 and 1619 cm^{-1} are present on all adsorbents used in this study. Whereas NR band at 820 cm^{-1} is present only on composite nanofibers. No group of BYK W-9010 is detected due to its small quantity [211, 213, 215, 224]. Therefore it is concluded that NR is adsorbed at all adsorbents.

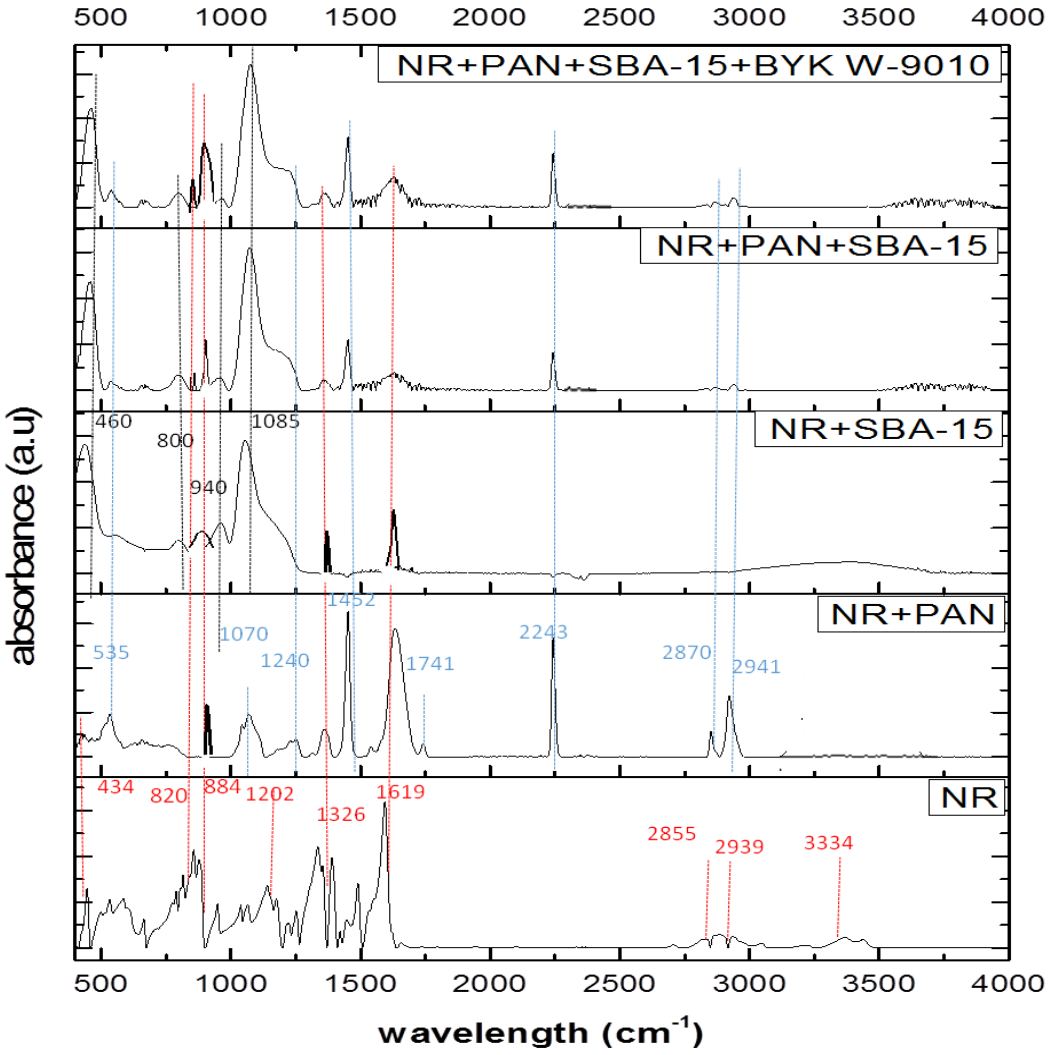


Figure IV.36: FTIR spectra of pure NR dye, PAN+NR, SBA-15+NR, PAN+SBA-15+NR and PAN+SBA-15+BYK W-9010+NR

Figure IV.37 describes the spectrum of pure CR and its adsorption on pristine PAN nanofibers, SBA-15 particles and PAN+SBA-15 composite nanofibers. The infrared spectrum of diazo CR is at 1612 cm^{-1} and the asymmetry stretching vibration of S-O(SO_3-H) group appearance is detected at 1196 cm^{-1} and 1336 cm^{-1} to NO_2.

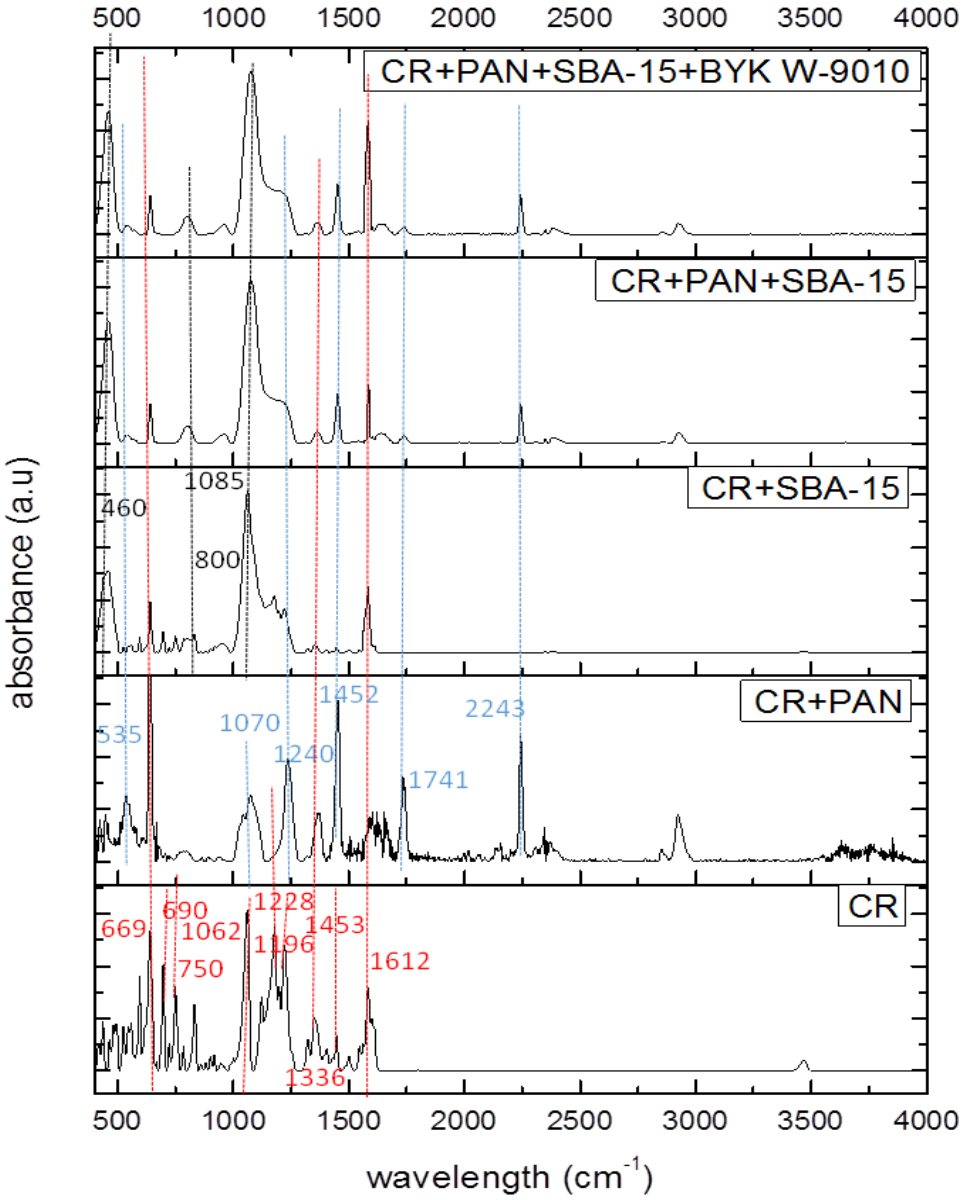


Figure IV.37: FTIR spectra of pure CR, PAN+CR, SBA-15+CR, PAN+SBA-15+CR and PAN+SBA-15+BYK W-9010+CR

Bands at 669 cm^{-1} are due to SO_3^-, 690 cm^{-1} due to C-N is functional groups of CR, at 750 and 1453 cm^{-1} due to N-H bending. In addition bands at 1062 and 1228 cm^{-1} represent primary aromatic amines with C-N. Three bands of CR 669 and 1336 and 1612 cm^{-1} were detected on all

adsorbents while band at 750 cm^{-1} is also detected on pristine PAN and SBA-15 samples. [211, 213, 215, 223, 225, 226].

4.8 Conclusion

The adsorption of dyes like MB, NR and CR onto SBA-15, pristine PAN nanofibers and PAN +SBA-15 composite nanofibers has been demonstrated. In the case of MB, all the used adsorbents even pure PAN nanofibers have very good adsorption behavior, because of high cationic ability made it possible to attach on all adsorbent including pristine PAN nanofibers. Whereas for NR that is a weak cationic dye the maximum adsorption was observed on SBA-15 and PAN+SBA-15 composite nanofibers due to their high negative charge on SiO_2 surface that causes electrostatic attraction. On the other hand, CR is a strong anionic dye and it showed very small adsorption due to repulsive forces of dye molecule and adsorbents. The results showed that for MB, pseudo 2^{nd} order kinetic is better fitted, whereas adsorption of NR and CR is better described by pseudo 1^{st} order kinetics and physisorption. Langmuir isotherm model explains adsorption of all three dyes by monolayer homogenous adsorption behavior as R^2 values are greater than Freundlich isotherm model values and q_e calculated values are also close to q_e experimental values whereas K_L and R_L values show that adsorption behavior is favorable. For more precisely differentiate the monolayer and multilayer portions of adsorbed dyes on adsorbent surface, SIPS isotherm model would be applied in future study which explains the quantities of both regimes of adsorbate on adsorbent. The pH impacted strongly the adsorption of MB, NR and CR dyes on all used adsorbents. As MB and NR are cationic in nature, therefore their adsorption increases by increasing pH and CR being an anionic dye has reverse effect. This phenomenon is due to increase in electrostatic attractive forces towards higher pH for cationic dyes and lower pH for anionic dye. Initial concentration of dyes also impacts on their adsorption. For MB, adsorption increases by increasing concentration till 45µM, for NR till 75µM and for CR 22.5µM and then remained almost constant, which is due to saturation of active sites. The increased solution temperature causes the increase in adsorption of all used dyes on all used adsorbents which is due to enhanced mobility of dye molecules to penetrate into active sites of adsorbents. All the adsorbents show recycling ability at different pH, according to nature of dye.

Conclusion and future prospects

In this work a nonwoven filler-loaded PAN nanofibers composite was produced via needleless electrospinning. Ordered mesoporous silica SBA-15 sub-micron particles were used as filler due to their high porosity, high specific surface area and pore volume.

There were some aggregates of SBA-15 observed on the surface of composite nanofibers which made the nanofibers surface non-uniform, therefore to remove these aggregates, 1wt% (w.r.t wt of SBA-15) dispersing agents were successfully incorporated in PAN+SBA-15/DMSO solution. Three different dispersing agents BYK W-9010, W-980 and W-966 were used at different concentrations of 0.5, 1, 1.5 and 2wt% w.r.t weight of SBA-15 and 1wt% of BYK W-9010 was best optimized for better deagglomeration of SBA-15. Prior to electrospinning, the viscosity of 5 to 12wt% of pure PAN, PAN+SBA-15 and PAN+SBA-15+BYK W-9010 solutions (PAN: SBA-15 5:1 and 1wt% of BYK W-9010 w.r.t weight of SBA-15) was measured and 8 and 10wt% of PAN and PAN+SBA-15 solutions were selected for electrospinning. Nanofibers at 8 and 10wt% of PAN concentrations were obtained but at 6wt% of PAN there was just electrospraying due to low viscosity. In process parameters, voltage of 30, 50 and 70 kV and 12.5, 15 and 20cm wire to collector distances were selected whereas 33±2 relative humidity % and 20±2 ^{o}C were fixed for whole electrospinning process. The electrospinning parameters were optimized on the basis of standard deviation (SD) and coefficient of variation % (CV %) of nanofibers diameters determined by SEM analysis of pristine PAN and composite nanofibers with and without dispersing agent. The optimized parameters are 8wt% of PAN and 1.7wt% of SBA-15 at 30, 50 kV and 12.5, 15 and 20 cm electrode distance. Composite nanofibers obtained with dispersing agent have very small aggregation and silica particles are uniformly spread over the surface of PAN nanofibers and their SD and CV% are also quite less as compared to composite nanofibers without dispersing agent. The TGA realized on composite nanofibers have shown that composite nanofibers without and with BYK W-9010 contain 15.7 wt% and 16.7 wt% of SBA-15, respectively. The S_{BET} of these composite nanofibers is 69 m^2/g and indicates that 45 % of the porosity is accessible. In the presence of BYK W-9010, S_{BET} is higher with 98.5 m^2/g that corresponds to 64 % of accessible porosity of SBA-15 particles embedded in PAN nanowebs. The higher pore accessibility may be relied to the deagglomeration effect due to the dispersing agent. The presence of silica particles in PAN favors the fast dehydrogenation and imparts a high thermal stability to PAN therefore composite nanofibers can be used for adsorption of dyes at

different temperatures. PAN nanofibers and PAN+SBA-15 composite nanofibers with and without dispersing agent were analyzed by EDX and some aggregates of PAN and SBA-15 were observed. Tensile strength results of nanofibers showed that incorporation of SBA-15 in PAN nanofibers increased the strength of composite nanofibers due to interfacial interaction between silica particles and PAN matrix whereas imparting of dispersing agent reduced the tensile strength.

The main objective of this work was to produce nonwoven web for wastewater treatment. MB gave excellent results of adsorption on all used adsorbents including pristine PAN nanofibers whereas NR had very good adsorption on SBA-15 particles and composite nanofibers but very small adsorption at PAN nanofibers, because of electrostatic attractive forces of negatively charged silica particles and positive group of NR dye. But in the case of CR a very small adsorption was observed due to repulsive forces adsorbate and adsorbent. It was observed that adsorption of MB followed pseudo 2^{nd} order kinetic model and the adsorption was chemisorption due to its strong cationic behavior and negatively charged adsorbents, whereas in the case of NR and CR, pseudo 1^{st} order kinetics model was better fitted and the adsorption process was physisorption, indeed NR was weak cationic and CR anionic dye. Langmuir isotherm model was better fitted for all used dyes on all adsorbents which explained a monolayer homogenous adsorption on active sites. pH has great impact on adsorption of dyes, as in the case of cationic dyes, adsorption increases by increasing the pH and for anionic dye, adsorption increases by decreasing pH. This phenomenon is due to increase in electrostatic attraction forces in basic and acidic conditions. Initial concentration of dye has great impact on adsorption, as initially increased in dye concentration increased the adsorption and after specific high concentration, adsorption remained constant which is due to the saturation of active sites. In the case of MB, adsorption increased till 45µM, for NR till 75µM and for CR till 22.5µM and then remained constant. Adsorption is dependent to temperature for all used dyes and MB, NR and CR dyes adsorption process is endothermic. The increase in adsorption capacity was due to the penetration of dye molecules across the external boundary layer and through the internal pores of adsorbents with increasing temperature. Desorption process was completed on all the adsorbents at different pH 2, 7 and 10, then all samples were re-adsorbed successfully at neutral pH for all used dyes and the desorption and re-adsorption efficiency was reduced in each cycle.

Therefore, it can be concluded that a successful PAN+SBA-15 composite nanofibers mat was prepared in which incorporation of 1wt% of dispersing agent resulted in better deagglomeration of silica particles with increase in S_{BET} from 68.7 to 98.5 m^2/g and also increase in accessible porosity of SBA-15 particles embedde in PAN nanowebs from 45 to 64%, respectively. This composite nanofibers mat is quite effective for the adsorption of NR dye as it can reach 100% adsorption (at some concentrations) whereas in the case of MB adsorption, the composite nanofibers behave almost similar as pristine PAN nanofibers because MB is strong cationic dye therefore it is adsorbed on PAN nanofibers so it is not much effective. On the other hand, CR dye is anionic dye and it is not adsorbed effectively on any adsorbents, which are also negatively charged.

In this study PAN+SBA-15 composite nanofibers have shown good potential for adsorption of cationic dyes due to electrostatic force of attraction but in future these composites could be used for adsorption of anionic dyes also by grafting amino ($-NH_2$) functional groups to the surface of composite nanofibers as amino functional group has a large adsorption capacity and strong affinity for anionic dyes. Amino ($-NH_2$) functional group can be grafted on silica particles using 3-aminopropyltrimethoxysilane. The efficiency of PAN+SBA-15 composite nanofibers for cationic dyes can be further increased by adding carboxylic (-COOH) groups on the surface of SBA-15. As carboxylic group can increase negativity on the surface of composite nanofibers. Another way to increase the dye adsorption capacity of composite nanofibers, by further increasing ordered mesoporous silica content with increasing the concentration of dispersing agent in same weight ratio of SBA-15 that will result in high accessibility of porosity. PAN+SBA-15 composite nanofibers can also be used as promising adsorbents for the removal of different pharmaceuticals (carbamazepine, diclofenic, ibuprofen, ketoprofen etc) from industrial waste water where high level concentrations of pharmaceuticals can be observed. Whether the adsorption of pharmaceuticals is on individual basis or on mixture basic, composite nanofibers can be effective in both cases. In the beginning of this study it was planned to check the efficiency of composite nanofibers in batch equilibrium and continuous flow adsorption processes. But due to closure of lab in the wake of COVID-19 worldwide, continuous flow adsorption process remained unexecuted that was an integral part of this study. Indeed, the shaping of composite membrane for continuous/batch adsorption is still a question that have to

be solved in future. Therefore, designing a batch/continuous entrapment for the treatment of effluents of ionic dyes will be analyzed in future to complete this research work.

References

[1] A. A. sabri, T. M. Albayati, R. A. Alazawi, Synthesis of ordered mesoporous SBA-15 and its adsorption of Methylene blue *Korean J. Chem. Eng*., **32**(9), 1835-1841 (2015)

[2] I. A. W. Tan, A. L. Ahmad, B.H. Hameed, Adsorption of basic dye using activated carbon prepared from oil palm shell: batch and fixed bed studies *Desalination* **225** 13-28 (2008)

[3] H. Chaudhuri, S Dash, A. Sarkar, Synthesis and use of SBA-15 adsorbent for dye-loaded waste water treatment *J. Environ. Chem. Eng.* 3 2866-2874 (2015)

[4] J. S. Shameran, Removal of basic dyes from aqueous solution by chloroacetic acid modified ferula communis based adsorbents: Thermodynamic and kinetic studies, Thesis MSc *Eastern Mediterranean university Cyprus* 1-2 (2014)

[5] C. H. Chih, K. P. Chang, H. D. Ou, Y. C. Chiang, C. F. Wang, Adsorption of cationic dyes onto mesoporous silica *Microporous and Mesoporous Mater.* **141** 102-109 (2011)

[6] B. M. Thamer, H. el-Hamshary, S.S Al-Deyab, M. H. El-Newehy, Functionalized electrospun carbon nanofibers for removal of cationic dye *Arab. J. Chem.* **12**, 747-759 (2019)

[7] M. Faccini, G. Borja, M. Boerrigter, D. Morillo, S. Martinez, Electrospun carbon nanofibers membranes for filtration of nanoparticles from water, *J. Nanomater.* **10**, 1155 (2015)

[8] S. A. Jadoo, J. A. Naser, Adsorption thermodynamic study of Congo red dye on electrospun nanofibers mat of Polyacrylonitrile *Glob. Pharma Technol.* **11(7)** 401-411 (2019)

[9] S. M. H. Gardazi, Cost Effective Adsorption Technique for Removal of Cationic Dyes from Textile Wastewater *PhD Thesis* COMSATS Institute of Information Technology Pakistan (2016)

[10] S. Ramakrishna, K. Fujihara, W.E. Teo, T. C. Lim, Z. Ma, An Introduction to Electrospinning and Nanofibers: *World Scientific*, 2005

[11] S. Almuhamed, N. Khenoussi, M. Bonne, L. Schacher, B. Lebeau, D. Adolphe, J. Brendle, Electrospinning of PAN nanofibers incorporating SBA-15 type ordered mesoporous silica particles, *European Polymer Journal* **54** 71-78 (2014)

[12] A. Nazir, Modelling and optimization of electrospun materials for technical application, *PhD Thesis*, University of haute Alsace France, 1-2 (2016)

[13] H. Niu and T. Lin, Fiber generators in needleless electrospinning *J. Nanomater.* **2012** p. 1-14 (2012)

[14] V. Pillay, C. Dott, Y. E. Choonara, C. Tyagi, L. Tomar, P. Kumar, V. M. K. Ndesendo, L. C. d. Toit, A Review of the Effect of Processing Variables on the Fabrication of Electrospun Nanofibers for Drug Delivery Applications, *J. Nanomater.* **2013**, p. 1-22, (2013)

[15] N. Rahmat, A. Z. Abdullah, A. Mohamed, A review: mesoporous Santa Barbara amorphous-15 types, synthesis and its applications towards biorefinery production *Am. J. Appl. Sci.* **7(12)** 1579 (2010)

[16] S. Almuhamed, Study and development of nonwovens made of electrospun composite nanofibers *PhD Thesis* University of Haute Alsace France, 2-3 (2015)

[17] J. Vamyazal, Review: The use constructed wetlands with horizontal sub-surface flow for various types of wastewater *Ecol. Eng.* 35 1–17 (2009)

[18] D. A. Yaseen, M. Scholz, Textile dye wastewater characteristics and constituents of synthetic effluents: a critical review *Int. J. Environ. Sci. Technol.* 16 1193–1226 (2019)

[19] V. K. Gupta, Suhas, Application of low-cost adsorbents for dye removal- A review *J. Environ. Manage.* 90 2313-2342 (2009)

[20] H. Benaissa, Effect of temperature on Methylene blue sorption from aqueous solutions by almond peel: experimental studies and modeling *Thirteen international water technology conference, IWTC 13 Hurghada Egypt* 377 (2009)

[21] Q. Y. Sun, L. Z. Yang, The adsorption of basic dyes from aqueous solution of modified peat-resin particle *Water Res.* 37 1535-1544 (2003)

[22] D. Ramesh, B. Goutam, S. Saini, Adsorption of Methylene blue using green pea peels (Pisum sativum): A cost effective option for dye based waste water treatment *Biotechnol. Bioprocess Eng.* 17 862-874 (2012)

[23] P. S. Kumar, S. Ramalingam, K. Sathishkumar, Removal of Methylene blue dye from aqueous solution by activated carbon prepared from cashew nut shell as a new low cost adsorbent *Korean J Chem Eng* **28** 149-155 (2011)

[24] V. Vadivelan, K. Vasanth, Equilibrium, kinetics, mechanism and process design for sorption of Methylene blue onto rice husk *J. Colloid Interface Sci.* **286** 90-100 (2005)

[25] K. K. Vasanth, V. Ramamurthi, S. Sivanesan, Modeling and mechanism involved during the sorption of Methylene blue onto fly ash *J. Colloid Interface Sci.* **284** 14-21 (2005)

[26] G. Dipa, G. B. Krishna, Adsorption of Methylene blue on kaolinite *Appl. Clay Sci.* **20(6)** 295-300 (2002)

[27] M. Anuradha, B. Malvika, The flocculation performance of tamarindus mucilage in relation to removal of vat and direct dyes *Bioresour. Technol.* **97(8)** 1055-1059 (2006)

[28] I. H. Faisal, Y. Kazuo, N. Fumiyuki, F. Kensuke, Removal of structurally different dyes in submerged membrane fungi reactor-biosorption/PAC-adsorption, membrane retention and biodegradation *J. Membr. Sci.* **325(1)** 395-403 (2008)

[29] M. Rafatullah, S. Othman, H. Rokiah, A. Anees, Adsorption of Methylene blue on low cost adsorbents: A review *J. Hazard. Mater.* **177(1-3)** 70-80 (2010)

[30] K. Sarayu, S. Sandhya, Aerobic biodegradation pathway for remazol orange by pseudomonas aeruginosa *Appl. Biochem. Biotechnol.* **160** 1241-1253 (2009)

[31] K. Sarayu, Sandhya S, Current technologies for biological treatment of textile waste water-A review. *Biochem. Biotechnol.***167** 645-661 (2012)

[32] M. Bilal, J. A. Shah, T. Ashfaq, S. M. H. Gardazi, A. A. Tahir, A. Pervez, Q. Mehmood Waste biomass adsorbents for copper removal from industrial waste water-A *J. Hazard. Mater.* **263** 322-333 (2013)

[33] V. K. Gupta, T. A. Saleh, Sorption of pollutants by porous carbon, carbon nanotubes and fullerene- An overview *Environ. Sci. Pollut. Res.* **20** 2828-2843 (2013)

[34] X. Yuan, S. P. Zhuo, W. Xing, H. Y. Cui, X. D. Dai, X. M. Liu, Z. F. Yan, Aqueous dye adsorption on ordered mesoporous carbons *J. Colloid Interface Sci.* **310** 83-89 (2007)

[35] V. M. Paula, C. S. Pablo, Adsorption of reactive dyes on titania-silica mesoporous materials *J. Colloid Interface Sci.* **299** 305-320 (2006)

[36] W. Shaobin, L. Huiting, X. Longya, Application of zeolite MCM-22 for basic dye removal from waste water *J. Colloid Interface Sci.* **295** 71-78 (2006)

[37] I. A. W. Tan, A. L. Ahmad, B. H. Hameed, Adsorption of basic dye using activated carbon prepared from oil palm shell: batch and fixed bed studies *Desalination* **225** 13-28 (2007)

[38] A. S. Anaam, M. A. Talib, A. A. Raghad, Synthesis of ordered mesoporous SBA-15 and its adsorption of Methylene blue *Korean J Chem Eng* **32(9)** 1835-1841 (2015)

[39] I. G. Ji, W. Bin, M. Z. Guang, P. Y. Chun, G. N. Cheng, Y. N. Qiu, J. Z. Wen, L. Yi, Removal of cationic dyes from aqueous solution using magnetic multi wall carbon nanotubes as adsorbent *Journal of Hazardous Materials* **164** 1517-1522 (2009)

[40] M. T. Badar, E. H. Hany, S. A. Salem, H. E. Mohamed, Functionalized electrospun carbon nanofibers for removal of cationic dye *Arab. J. Chem.* **12** 747-759 (2019)

[41] L. Shengbiao, J. Zhigang, L. Ziyu, L. Yanhua, Z. Rongsun, Synthesis and characterization of mesoporous carbon nanofibers and its adsorption for dye in waste water *Adv Powder Technol.* **27** 591-598 (2016)

[42] B. Rasim, M. Nishil, Z. Masuduz, M. Gagan, M. B. Richard, C. T. Kam, Cellulose nanocrystals as promising adsorbents for the removal of cationic dyes *Cellulose* **21** 1655-1665 (2014)

[43] R. Dod, G. Banerjee, S. Saini, Adsorption of Methylene blue using green pea peels (pisum sativum): A cost effective option for dye based waste water treatment *Biotechnol. Bioprocess Eng.* **17** 862-874 (2012)

[44] K. Y. Foo, B. H. Hameed, Insights into the modeling of adsorption isotherm systems *Chem. Eng. J.* **156** 2-10 (2010)

[45] M. A. Talib, M. D. Aidan, Purification of aniline and nitrosubstituted aniline contaminants from aqueous solution using beta zeolite *Bulg. J. Sci. Educ.* **23(1)** 105 (2014)

[46] A. A. Zeid, A review: Fundamental aspects of silicate mesoporous materials *Materials* **5(12)** 2874-2902 (2012)

[47] R. Brayner, The toxicological impact of nanoparticles *Nano Today* 3(1-2) 48-55 (2008)

[48]W. Liu, S. Adanur, Properties of electrospun polyacrylonitrile membranes and chemically-activated carbon nanofibers *Text. Res. J.* **80(2)** 124-134 (2009)

[49] K. Yoon, K. Kim, X. Wang, D. Fang, B. S. Hsiao, B. Chu, High flux ultrafiltration membranes based on electrospun nanofibrous PAN scaffolds and chitosan coating *Polymer* **47** 2434-2441 (2006)

[50] M. Chen, C. Wang, W. Fang, J. Wang, W. Zhang, G. Jin, G. Diao, Electrospinning of Calixarene-functionalized polyacrylonitrile nanofibers membranes and application as an adsorbent and catalyst support *Langmuir* **29** 11858-11867 (2013)

[51] S. A. Jadoo, J. A. Naseer Adsorption optimization of Congo red dye onto electrospun nanofibers of polyacrylonitrile functionalized with Fe_3O_4 nanoparticles *Mater. Sci. Eng.* **928** 052024 (2020)

[52] A. Aluigi, F. Rombaldoni, C. Tonetti, L. Jannoke, Study of Methylene blue adsorption on keratin nanofibrous membranes *J. Hazard. Mater.* **268** 156-165 (2014)

[53] J. Cheng, C. Zhan, J. Wu, Z. Cui, J. Si, Q. Wang, X. Peng, L. S. Turang, Highly efficient removal of methylene blue dye from an aqueous solution using cellulose acetate nanofibrous membranes modified by polydopamine *ACS Omega* **5** 5389-5400 (2020)

[54] L. Y. Yeo, J. R. Friend, Electrospinning carbon nanotube polymer composite nanofibers *J. Exp. Nanosci.* **1** 177-209 (2006)

[55] L. Wannatong, A. Sirivat, P. Supaphol, Effects of solvents on electrospun polymeric fibers: preliminary study on polystyrene *Polym. Int.* **53** 1851-1859 (2004)

[56] L. Zhang, A. Aboagye, A. Kelkar, C. Lai, H. Fong, A review: carbon nanofibers from electrospun polyacrylonitrile and their applications *J. Mater. Sci.* **49** 463-480 (2014)

[57] Z. Li, C. Wang, Effects of working parameters on electrospinning in; One Dimensional Nanostructures: *Springer* 15-28 (2013)

[58] J. Doshi, D. H. Reneker, Electrospinning process and applications of electrospun fibers," in Industry Applications Society Annual Meeting *Conference Record of the 1993 IEEE* 1698-1703 (1993)

[59] A. Yarin, E. Zussman, Upward needleless electrospinning of multiple nanofibers *Polymer*. **45** 2977-2980 (2004)

[60] D. Rodoplu, M. Mutlu, Effects of electrospinning setup and process parameters on nanofiber morphology intended for the modification of quartz crystal microbalance surfaces *J. Eng. Fibers Fabr.* **7** 118-123 (2012)

[61] B. Lu, Y. Wang, Y. Liu, H. Duan, J. Zhou, Z. Zhang, Superhigh-Throughput Needleless Electrospinning Using a Rotary Cone as Spinneret *Small* **6** 1612- 1616 (2010)

[62] H. Niu, T. Lin, X. Wang, Needleless Electrospinning: Developments and Performances," in Nanofibers – Production, Properties and Functional Applications*: INTECH Open Access Publisher* 17-36 (2011)

[63] N. Lavielle, A. Hebruad, P. C. Mendoza, A. Ferrand, J. N. Benkinrane, G. Schlatter, Structuring and modeling of electrospun nanofibers: effect of electrical and topographical local properties of micro-patterned collectors *Macromolecular Material engineering* **297** 958-68 (2012)

[64] J. M. Deitzel, J. D. Kleinmeyer, J. K. Hirvonen, T. N. Beck, Controlled deposition of electrospun poly(ethylene oxide) fibers *Polymer* **42** 8163-70 (2001)

[65] D. H. Reneker, A. L. Yarin, H. Fong, S. Koombhongse, Bending instabilities of electrically charged liquid jets of polymer solutions in electrospinning *Int. J. Appl. Phys.* **87** 4531-47 (2000)

[66] D. H. Reneker, A. L. Yarin, Electrospinning jets and polymer nanofibers *Polymer* **49** 2387-425 (2008)

[67] G. C. Rutledge, S. V. Fridrikh, Formation of fibers by electrospinning *Adv. Drug Deliv. Rev.* **59** 1384-91(2007)

[68] D. S. Katti, K. W. Robinson, F. K. Ko, and C. T. Laurencin, Bioresorbable nanofiber- based systems for wound healing and drug delivery: Optimization of fabrication parameters *J. Biomed. Mater. Res. Part B Appl. Biomater.* **70** 286-296 (2004)

[69] P. Supaphol, C. Mit-Uppatham, M. Nithitanakul, Ultrafine electrospun polyamide-6 fibers: Effect of emitting electrode polarity on morphology and average fiber diameter *J. Polym. Sci. B Polym. Phys.* **43** 3699- 3712 (2005)

[70] W. Wei, J. T. Yeh, P. Li, M. R. Li, W. Li, X. L. Wang, Effect of nonsolvent on morphologies of polyamide 6 electrospun fibers *J. Appl. Polym. Sci.* **118** 3005-3012 (2010)

[71] K. Nasouri, A. M. Shoushtari, A. Kaflou, Investigation of polyacrylonitrile electrospun nanofibers morphology as a function of polymer concentration, viscosity and Berry number *Micro Nano Lett. IET* **7** 423-426 (2012)

[72] C. Mituppatham, M. Nithitanakul, P. Supaphol, Ultrafine electrospun polyamide 6 fibers: effect of solution conditions on morphology and average fiber diameter *Macromol. Chem. Phys.* **205** 2327-2338 (2004)

[73] P. Kebarle, M. Peschke, On the mechanism by which the charged droplets produced by electrospray lead to gas phase ions *Anal. Chim. Acta*. **406** 11-35 (2000)

[74] L. Tong, W. Hongxia, W. Huimin, W. Xungai, Effects of polymer concentration and cationic surfactant on the morphology of electrospun Polyacrylonitrile nanofibers *J Mater Sci Technol* . **21(1)** 9-12 (2005)

[75] M. K. Pilehrood, P. Heikkila, A. Harlin, Preparation of carbon nanotubes embedded in Polyacrylonitrile (PAN) nanofibers composites by electrospraying process *Autex Res. J.* **12** 1-6 (2012)

[76] P. Brown, K. Stevens, Nanofibers and Nanotechnology in Textiles *(Woodhead Publishing)* 93-94 (2007)

[77] R. G. Lebel, D. A. I. Goring, Density, viscosity, refractive index and hygroscopicity of mixtures of water and Dimethyl Sulphoxide *J. Chem. Eng. Data* **7(1)** 100-101 (1962)

[78] G. M. Matthew, L. W. Garth, H. C. Ralph, E. L. Timothy, Correlation of solution rheology with electrospun fiber formation of linear and branched polyester *Macromolecules* **37** 1760-67 (2004)

[79] N. Khenoussia, A. H. Hekmatia, B. E. Dreana, L. Schachera, D. Adolphe, Rheology study of polymer solutions for electrostatic nanofibers spinning, *Congres Francais de Mecanique* 1-6 (2009)

[80] L. Huang, K. Nagapudi, R. P. Apkarian, E. L. Chaikof, Engineered collagen-PEO nanofibers and fabrics *J. Biomater. Sci. Polym. Ed*. **12** 979-93 (2001)

[81] T. Lin, H. Wang, H. Wang, X. Wang, Effects of polymer concentration and cationic surfactant on the morphology of electrospun polyacrylonitrile nanofibres *J. Mater Sci Technol* . **21** 1-4 (2005)

[82] W. K. Son, J. H. Youk, T. S. Lee, W. H. Park, The effects of solution properties and polyelectrolyte on electrospinning of ultrafine poly(ethylene oxide) fibers *Polymer* **45** 2959-2966 (2004)

[83] H. Fong, I. Chun, D. H. Reneker, Beaded nanofibers formed during electrospinning *Polymer* **40** 4585-4592 (1999)

[84] A. K. Haghi, M. Akbari, Trends in electrospinning of natural nanofibers *phys. stat. sol. (a)* **204(6)** 1830–1834 (2007)

[85] C. J. Luo, M. Nangrejo, M. Edirisinghe, A novel method of selecting solvents for polymer electrospinning, *Polymer* **51** 1654-62 (2000)

[86] T. J. Sill, H. A. von Recum, Electrospinning: Applications in drug delivery and tissue engineering *Biomaterials* **29** 1989-2006 (2008)

[87] L. Wannatong, A. Sirivat, P. Supaphol, Effects of solvents on electrospun polymeric fibers: preliminary study on polystyrene *Polym. Int.* **53** 1851-1859 (2004)

[88] P. K. Baumgarten, Electrostatic spinning of acrylic microfibers *J. Colloid Interface Sci.* **36** 71-79 (1971)

[89] A. G. Sener, A. S. Altay, F. Altay, Effect of voltage on morphology of electrospun nanofibers," in Electrical and Electronics Engineering (ELECO), *7th International Conference* I-324-I-328 (2011)

[90] Y. Li, Z. Huang, Y. Lǔ, Electrospinning of nylon-6, 66, 1010 terpolymer *Eur. Polym. J.* **42** 1696-1704 (2006)

[91] J. Zeleny, The role of surface instability in electrical discharges from drops of alcohol and water in air at atmospheric pressure *J Franklin Inst.* **219** 659-675 (1935)

[92] X. Zong, K. Kim, D. Fang, S. Ran, B. S. Hsiao, B. Chu, Structure and process relationship of electrospun bioabsorbable nanofiber membranes *Polymer* **43** 4403-4412 (2002)

[93] S. Megelski, J. S. Stephens, D. B. Chase, J. F. Rabolt, Micro- and Nanostructured Surface Morphology on Electrospun Polymer Fibers *Macromolecules* **35** 8456-8466 (2002)

[94] P. Heikkila, A. Harlin, Electrospinning of polyacrylonitrile (PAN) solution: Effect of conductive additive and filler on the process *Express polm. Lett.* **3** 437-45 (2009)

[95] E. Atabey, S. Wei, X. Zhang, H. Gu, X. Yan, Y. Huang, L. Shao, Q. He, J. Zhu, L. Sun, A. S. Kucknoor, A. Wang, Z. Guo, Fluorescent electrospun polyvinyl alcohol/CdSe@ZnS nanocomposites fibers *J. Compos. Mater.* **47** 3175-85 (2013)

[96] S. Fridrikh, J. Yu, M. Brenner, G. Rutledge, Controlling the fiber diameter during electrospinning, *Phys. Rev. Lett.* **90** 144502-1 144502-4 (2003)

[97] R. Jalili, M. Morshed, S. A. Hosseini, The effects of operating parameters on the morphology of electrospun polyacrylonitrile nanofibers *Iran. Polym. J.* 2005 **14** 1074-81

[98] N. Okutan, P. Terzi, F. Altay, Affecting parameters on electrospinning process and characterization of electrospun gelatin nanofibers *Food Hydrocoll.* **39** 19-26 (2014)

[99] T. Jarusuwannapoom, W. Hongrojjanawiwat, S. Jitjaicham, L. Wannatong, M. Nithitanakul, C. Pattamaprom, P. Koombhongse, R. Rangkupan, P. Supaphol, Effect of solvents on electrospinnability of polystyrene solutions and morphological appearance of resulting electrospun polystyrene fibers *Eur. Polym. J.* **41** 409-21 (2005)

[100] V. Beachley, X. Wen, Effect of electrospinning parameters on nanofibers diameter and length *Mater. Sci. Eng. C* **29** 663-68 (2009)

[101] Y. Ahn, S. Park, G. Kim, Y. Hwang, C. Lee, H. Shin, Development of high efficiency nanofilters made of nanofibers *Curr Appl Phys.* **6** 1030- 1035 (2006)

[102] M. Naraghi, S. Arshad, I. Chasiotis, Molecular orientation and mechanical property size effects in electrospun polyacrylonitrile nanofibers *Polymer* **52** 1612-1618 (2011)

[103] A. Kirecci, U. Ozkoc, H. I. Icoglu, Determination of optimal production parameters for polyacrylonitrile nanofibers *J. appl. Polym. Sci.* **124** 4961-8 (2012)

[104] T. Wang, S. Kumar, Electrospinning of polyacrylonitrile nanofibers *J. appl. Polym. Sci.* **102** 1023-29 (2006)

[105] Z. Guo, S. Wei, D. Zhang, Electrospun polyacrylonitrile nanocomposites fibers reinforced with magnetic particles *Materials research society proceeding* **1240** (Material research society) WW 10-06 (2010)

[106] H. I. Icoglu, R. T. Ogulata, Effect of ambient parameters on morphology of electrospun polyetherimide (PEI) fibers *Tekst. ve Konfeksiyon.* **23** 313-318 (2013)

[107] E. S. Medeiros, L. H. C. Mattoso, R. D. Offeman, D. F. Wood, W. J. Orts, Effect of relative humidity on the morphology of electrospun polymer fibers, *Can. J. Chem.* **86** 590-9 (2008)

[108] S. N. Arshad, High strength carbon nanofibers derived from electrospun polyacrylonitrile, *M S thesis* 2011 (Urbana, Illinois USA: University of Illinois at Urbana-Champaign)

[109] S. D. Vrieze, T. V. Camp, A. Nelvig, B. Hagstrom, P. Westbroek, K. D. Clerck, The effect of temperature and humidity on electrospinning *J. Mater. Sci.* **44** 1357-62 (2008)

[110] Y. Zhang, B. Su, J. Venugopal, S. Ramakrishna, C. Lim, Biomimetic and bioactive nanofibrous scaffolds from electrospun composite nanofibers, *Int. J. Nanomedicine* **2** 623–638 (2007)

[111] J. Ayutsede, M. Gandhi, S. Sukigara, M. Micklus, H.-E. Chen, F. Ko, Regeneration of Bombyx mori silk by electrospinning. Part 3: characterization of electrospun nonwoven mat *Polymer* **46** 1625-1634 (2005)

[112] X. Zhuang, B. Cheng, W. Kang, X. Xu, Electrospun chitosan/gelatin nanofibers containing silver nanoparticles *Carbohydr. Polym* **82** 524-527 (2010)

[113] G. E. Wnek, M. E. Carr, D. G. Simpson, G. L. Bowlin, Electrospinning of nanofibers fibrinogen structures *Nano Lett.* **3** 213-216 (2003)

[114] X. Xu, M. Zhou, Antimicrobial gelatin nanofibers containing silver nanoparticles *Fibers Polym.* **9** 685-690 (2008)

[115] L. Fagundes, T. Sousa, A. Sousa, V. Silva, E. Sousa, SBA-15-collagen hybrid material for drug delivery applications *J. Non-Cryst. Solids* **352** 3496-3501 (2006)

[116] C. P. Barnes, M. J. Smith, G. L. Bowlin, S. A. Sell, T. Tang, J. A. Matthews, Feasibility of electrospinning the globular proteins hemoglobin and myoglobin, *Biomaterials* **27(5)** 724–734 (2006)

[117] M. R. Karim, H. W. Lee, R. Kim, B. C. Ji, J. W. Cho, T. W. Son, Preparation and characterization of electrospun pullulan/montmorillonite nanofiber mats in aqueous solution *Carbohydr. Polym.* **78** 336-342 (2009)

[118] R. Nirmala, H.-M. Park, R. Navamathavan, H.-S. Kang, M. H. El-Newehy, H. Y. Kim, Lecithin blended polyamide-6 high aspect ratio nanofiber scaffolds via electrospinning for human osteoblast cell culture *Mater. Sci. Eng. C*. **31** 486-493 (2011)

[119] L. Kong, G. R. Ziegler, Role of molecular entanglements in starch fiber formation by electrospinning *Biomacromolecules* **13** 2247-2253 (2012)

[120] L. M. Guerrini, M. C. Branciforti, T. Canova, R. E. S. Bretas, Electrospinning and characterization of polyamide 66 nanofibers with different molecular weights *Mater. Res.* **12** 181-190 (2009)

[121] H. Hou, J. J. Ge, J. Zeng, Q. Li, D. H. Reneker, A. Greiner, Electrospun polyacrylonitrile nanofibers containing a high concentration of well-aligned multiwall carbon nanotubes *Chem. Mater.* **17** 967-973 (2005)

[122] B. Ding, M. Yamazaki, S. Shiratori, Electrospun fibrous polyacrylic acid membrane-based gas sensors *Sens. Actuators B Chem.* **106** 477- 483 (2005)

[123] N. Kattamuri, C. Sung, Uniform polycarbonate nanofibers produced by electrospinning *Macromolecules* **3** 425-428 (2004)

[124] S. Moon, J. Choi, R. J. Farris, Preparation of aligned polyetherimide fiber by electrospinning *J. Appl. Polym. Sci.* **109** 691-694 (2008)

[125] M. S. Khil, D. I. Cha, H. Y. Kim, I. S. Kim, N. Bhattarai, Electrospun nanofibrous polyurethane membrane as wound dressing *J. Biomed. Mater. Res. Part B Appl. Biomater.* **67** 675-679 (2003)

[126] M. Jannesari, J. Varshosaz, M. Morshed, M. Zamani, Composite poly (vinyl alcohol)/poly (vinyl acetate) electrospun nanofibrous mats as a novel wound dressing matrix for controlled release of drugs *Int. J. Nanomedicine* **6** 993-1003 (2011)

[127] H. Zhu, S. Qiu, W. Jiang, D. Wu, C. Zhang, Evaluation of electrospun polyvinyl chloride/polystyrene fibers as sorbent materials for oil spill cleanup *Environ. Sci. Technol.* **45** 4527-4531 (2011)

[128] R. Gopal, S. Kaur, C. Y. Feng, C. Chan, S. Ramakrishna, S. Tabe, Electrospun nanofibrous polysulfone membranes as pre-filters: Particulate removal *J. Membr. Sci.* **289** 210-219 (2007)

[129] S. Imaizumi, H. Matsumoto, K. Suzuki, M. Minagawa, M. Kimura, A. Tanioka, Phenolic resin-based carbon thin fibers prepared by electrospinning: additive effects of poly (vinyl butyral) and electrolytes *Polymer journal* **41** 1124-1128 (2009)

[130] C. Yang, Z. Jia, Z. Guan, L. Wang, Polyvinylidene fluoride membrane by novel electrospinning system for separator of Li-ion batteries *J. Power Sources* **189** 716-720 (2009)

[131] C. Chen, L. Wang, Y. Huang, Electrospinning of thermo-regulating ultrafine fibers based on polyethylene glycol/cellulose acetate composite *Polymer* **48** 5202-5207 (2007)

[132] C. Luo, E. Stride, M. Edirisinghe, Mapping the influence of solubility and dielectric constant on electrospinning polycaprolactone solutions *Macromolecules* **45** 4669-4680 (2012)

[133] A. G. Mikos, M. D. Lyman, L. E. Freed, R. Langer, Wetting of poly (L-lactic acid) and poly (DL-lactic-co-glycolic acid) foams for tissue culture *Biomaterials* **15** 55-58 (1994)

[134] S. Nataraj, K. Yang, T. Aminabhavi, Polyacrylonitrile-based nanofibers-- a state of-the-art review *Prog. Polym. Sci.* **37** 487-513 (2012)

[135] T. Maitra, S. Sharma, A. Srivastava, Y.-K. Cho, M. Madou, and A. Sharma, Improved graphitization and electrical conductivity of suspended carbon nanofibers derived from carbon nanotube/polyacrylonitrile composites by directed electrospinning *Carbon* **50** 1753-1761 (2012)

[136] M. S. A. Rahaman, A. F. Ismail, A. Mustafa, A review of heat treatment on polyacrylonitrile fiber *Polym. Degrad. Stab.* **92** 1421-1432 (2007)

[137] P. Morgan, Carbon Fibers and Their Composites: *CRC Press*, 2005

[138] H. R. Jung, D. H. Ju, W. J. Lee, X. Zhang, R. Kotek, Electrospun hydrophilic fumed silica/polyacrylonitrile nanofiber-based composite electrolyte membranes, *Electrochimica Acta*, **54** 3630-3637 (2009)

[139] L. Chuilin, Z. Ganji, Y. Zhongren, C. Gui, Z. Lifeng, V. Ahmad, W. Ying, Z. Lei, L. Jie, F. Hao, Investigation of post-spinning stretching process on morphological, structural and mechanical properties of electrospun polyacrylonitrile copolymer nanofibers *Polymer* **52(2)** 519-528 (2011)

[140] F. Sheng, P. C. Jyh, T. W. Wen, Electrospun polyacrylonitrile nanofibrous membranes for lipase immobilization *J. Mol. Catal. B Enzym.* **47(3-4)** 117-124 (2007)

[141] J. H. He, Y.Q. Wan, J.Y. Yu, Effect of concentration on electrospun polyacrylonitrile (PAN) nanofibers *Fibers Polym.* **9** 140-142 (2008)

[142] X. H. Qin, E. L. Yang, N. Li, S. Y. Wang, Effect of different salts on electrospinning of polyacrylonitrile (PAN) polymer solution *J. Appl. Polym. Sci.* **103** 3865-3870 (2007)

[143] M. Wu, Q. Wang, K. Li, Y. Wu, H. Liu, Optimization of stabilization conditions for electrospun polyacrylonitrile nanofibers *POLYM DEGRAD STABIL* **97** 1511-1519 (2012)

[144] S. N. Arshad, M. Naraghi, I. Chasiotis, Strong carbon nanofibers from electrospun polyacrylonitrile *Carbon* **49** 1710-1719 (2011)

[145] H. Hou, J. J. Ge, J. Zeng, Q. Li, D. H. Reneker, A. Greiner, Electrospun polyacrylonitrile nanofibers containing a high concentration of well-aligned multiwall carbon nanotubes *Chem. Mater.* **17** 967-973 (2005)

[146] R. Houtz, ""Orlon" Acrylic Fiber: Chemistry and Properties *Text. Res. J.* **20** 786-801 (1950)

[147] N. Grassie, J. N. Hay, I. C. McNeill, Coloration in acrylonitrile and methacrylonitrile polymers *J. Polym. Sci.* **31** 205-206 (1958)

[148] N. Grassie, J. Hay, Thermal coloration and insolubilization in polyacrylonitrile *J. Polym. Sci.* **56** 189-202 (1962)

[149] J. Schurz, Discoloration effects in acrylonitrile polymers *J. Polym. Sci.* **28** 438-439 (1958)

[150] S. Dalton, F. Heatley, P. M. Budd, Thermal stabilization of polyacrylonitrile fibers, *Polymer* **40** 5531-5543 (1999)

[151] Y. Yang, F. Simeon, T. A. Hatton, G. C. Rutledge, Polyacrylonitrile-based electrospun carbon paper for electrode applications *J. Appl. Polym. Sci.* **124** 3861-3870 (2012)

[152] B. O. Donnet JB, Encyclopedia of Physical Science and Technology," **2**, ed: New York: *Acedamic Press Inc* (1987)

[153] I. H. Chen, C. C. Wang, C. Y. Chen, Fabrication and structural characterization of polyacrylonitrile and carbon nanofibers containing plasma-modified carbon nanotubes by electrospinning *J. Phys. Chem. C.* **114** 13532-13539 (2010)

[154] Z. Zhou, C. Lai, L. Zhang, Y. Qian, H. Hou, D. H. Reneker, Development of carbon nanofibers from aligned electrospun polyacrylonitrile nanofiber bundles and characterization of their microstructural, electrical, and mechanical properties *Polymer* **50** 2999-3006 (2009)

[155] L. Zhang, Y. L. Hsieh, Carbon nanofibers with nanoporosity and hollow channels from binary polyacrylonitrile systems *Eur. Polym. J.* **45** 47-56 (2009)

[156] T. H. Ko, The influence of pyrolysis on physical properties and microstructure of modified PAN fibers during carbonization *J. Appl. Polym. Sci*, **43** 589-600 (1991)

[157] T. H. Ko, L. C. Huang, The influence of cobaltous chloride modification on physical properties and microstructure of modified PAN fiber during carbonization *J. Appl. Polym. Sci.* 70 2409-2415 (1998)

[158] G. C. Han, A. N. Bradley, V. G. Prabhakar, L. Yaodong, K. G. Kishor, G. K. Manjeshwar, M. L. Kevin, G. Sushanta, P. Chandrani, G. Lucille, S. Korhan, C. Ioannais, K. Satish, High strength and high modulus carbon fibers *Carbon* **93** 81-87 (2015)

[159] H. Liu, J. Kameoka, D. A. Czaplewski, H. G. Craighead, Polymeric nanowire chemical sensor *Nano Lett.* **4** 671-675 (2004)

[160] N. J. Pinto, A. T. J. Jr, A. G. Macdiarmid, C. H. Mueller, N. Theofylaktos, D. C. Robinson, F. A. Miranda, Electrospun polyaniline/polyethylene oxide nanofibers field effect transistor, *Appl. Phys. Lett.* **83** 4244-46 (2003)

[161] Y. Chou, C. Shao, X. Li, C. Su, H. Xu, M. Zhang, BiOCl nano sheets immobilized on electrospun polyacrylonitrile nanofibers with high photo catalytic activity and reusable property *Appl. Surf. Sci.* **285** 509-516 (2013)

[162] L. Ji, X. Zhang, Ultrafine polyacrylonitrile/silica composite fibers via electrospinning *Mater. Lett.* **62** 2161-2164 (2008)

[163] C. Drew, X. Liu, D. Ziegler, X. Wang, F. F. Bruno, J. Whitten, L. A. Samuelson, J. Kumar, Metal oxide-coated polymer nanofibers *Nano letters* **3** 143-147 (2003)

[164] Z. M. Liu, Z. K. Xu, J. Q. Wang, J. Wu, J. J. Fu, Surface modification of polypropylene microfiltration membranes by graft polymerization of N-vinyl-2-pyrrolidone *Eur. Polym. J.* **40** 2077-87 (2004)

[165] J. P. Chen, C. H. Su, Surface modification of electrospun PLLA nanofibers by plasma treatment and cationized gelatin immobilization for cartilage tissue engineering *Acta Biomater.* **7** 234-243 (2011)

[166] J. E. Oliveira, V. P. Scagion, V. Grassi, D. S. Correa, L. H. C. Mattoso, Modification of electrospun nylon nanofibers using layer-by-layer films for application in flow injection electronic tongue: Detection of paraoxon pesticide in corn crop *Sens actuators B Chem* **171-172** 249-255 (2012)

[167] S. Demirci, A. Celebioglu, T. Uyar, Surface modification of electrospun cellulose acetate nanofibers via RAFT polymerization for DNA adsorption *Carbohydr. Polym.***113** 200-207(2014)

[168] J. Chen, Z. Li, D. Chao, W. Zhang, C. Wang, Synthesis of size-tunable metal nanoparticles based on polyacrylonitrile nanofibers enabled by electrospinning and microwave irradiation *Mater. Lette.* **62** 692-94 (2008)

[169] L. Chen, S. Hong, X. Zhou, Z. Zhou, H. Hou, Novel Pd-carrying composite carbon nanofibers based on polyacrylonitrile as a catalyst for Sonogashira coupling reaction *Catal. Commun*. **9** 2221-2225 (2008)

[170] C. Su, Y. Tong, M. Zhang, Y. Zhang, C. Shao, TiO_2 nanoparticles immobilized on polyacrylonitrile nanofibers mats: a flexible and recyclable photocatalyst for phenol degradation *RSC Adv.* **3** 7503-7512 (2013)

[171] H. Yu, Z. Jiao, H. Hu, G. Lu, J. Ye, Y. Bi, Fabrication of Ag_3PO_4–PAN composite nanofibers for photo catalytic applications *CrystEngComm* **15** 4802-4805 (2013)

[172] D. Zhang, A. B. Karki, D. Rutman, D. P. Young, A. Wang, D. Cocke, Electrospun polyacrylonitrile nanocomposite fibers reinforced with Fe_3O_4 nanoparticles: fabrication and property analysis *Polymer* **50** 4189-4198 (2009)

[173] L. Ji, Z. Lin, A. J. Medford, X. Zhang, Porous carbon nanofibers from electrospun polyacrylonitrile/SiO2 composites as an energy storage material *Carbon* **47** 3346-3354 (2009)

[174] Y. Chen, Z. Lu, L. Zhou, Y.-W. Mai, and H. Huang, In situ formation of hollow graphitic carbon nano spheres in electrospun amorphous carbon nanofibers for high performance Li-based batteries *Nanoscale* **4** 6800-6805 (2012)

[175] G. N. Sichani, M. Morshed, M. Amirnasr, D. Abedi, In situ preparation, electrospinning, and characterization of polyacrylonitrile nanofibers containing silver nanoparticles *J. Appl. Polym. Sci.* **116** 1021-1029 (2010)

[176] B. H. Kim, K. S. Yang, H. G. Woo, Thin, bendable electrodes consisting of porous carbon nanofibers via the electrospinning of polyacrylonitrile containing tetraethoxy orthosilicate for super capacitor *Electrochem. commun.* **13** 1042-1046 (2011)

[177] Q. Yu, D. Yang, D. Teng, X. Yang, S. Ryu, Reticular Sn nanoparticle-dispersed PAN-based carbon nanofibers for anode material in rechargeable lithium-ion batteries *Electrochem. commun*. **12** 1187-1190 (2010)

[178] Z. Yang, G. Du, Q. Meng, Z. Guo, X. Yu, Z. Chen, Synthesis of uniform TiO_2@ carbon composite nanofibers as anode for lithium ion batteries with enhanced electrochemical performance *J. Mater. Chem.* **22** 5848-5854 (2012)

[179] S. Nataraj, B. Kim, M. dela Cruz, J. Ferraris, T. Aminabhavi, K. Yang, Free standing thin webs of porous carbon nanofibers of polyacrylonitrile containing ironoxide by electrospinning *Mater. Lett.* **63** 218-220 (2009)

[180] Z. Liu, C. Zhou, B. Zheng, L. Qian, Y. Mo, F. Luo, In situ synthesis of gold nanoparticles on porous polyacrylonitrile nanofibers for sensing applications *Analyst* **136** 4545-4551 (2011)

[181] W. Wang, Z. Li, X. Xu, B. Dong, H. Zhang, Z. Wang, Au-Doped Polyacrylonitrile–Polyaniline Core–Shell Electrospun Nanofibers Having High Field Effect Mobilities *Small* **7** 597-600 (2011)

[182] Z. Dongyuan, F. Jianglin, H. Qisheng, M. Nicholas, F. H. Glenn, C. F. Bradley, S. D. Galen, Triblock Copolymer Syntheses of Mesoporous Silica with Periodic 50 to 300 Angstrom Pores *Science* **279**(5350): 548–52 (1998)

[183] R. O. Lopez, I. J. Perez-Hermosillo, J. M. Esparza-Schulz, A. Cervantes-Uribe, A. Dominguez-Ortiz, SBA-15 materials, calcinations temperature influence on textural properties and total silanol ratio *Adsorption* **21** 659-669 (2015)

[184] D. Zhao, J. Feng, Q. Huo, N. Melosh, G. H. Fredrickson, B. F. Chmelka, G. D. Stucky, Triblock copolymer synthesis of mesoporous silica with periodic 50 to 300 angstrom pores *Science* **279** 548-552 (1998)

[185] J. L. Blin, M. I. Clerc, Mechanism of self-assembly in the synthesis of silica mesoporous materials: *in situ* studies by X-ray and neutron scattering *Chem. Soc. Rev.* **42** 4071 (2013)

[186] M. I. Clerc, I. Grillo, A. Y. Khodakov, D. Durand, Vladimir L. Zholobenko, New insights into the initial steps of the formation of SBA-15materials:an *in situ* small angle neutron scattering investigation, *Chem. Commun.* 834-836 (2007)

[187] V. K. Ambili, S. Sugunan**,** Studies on catalysis by ordered mesoporous SBA-15 materials modified with transition metals *International Conference on Material* (2011)

[188] Y. Belmoujahid, M. Bonne, Y. Schdeller, D. Schleich, Y. Grohens, B. Lebeau, Thermal conductivity of monolithic assemblies of SBA-15 ordered Mesoporous silica particles *Micropor. Mesopor. Mat.* **201** 124-133 (2015)

[189] N. Wang, Y. Si, G. Sun, M. El-Newehy, S. S. Al-Deyab, B. Ding, Multilevel structured polyacrylonitrile/silica nanofibrous membranes for high performance air filtration *Sep. Purif. Technol* **126** 44-51 (2014)

[190] B. Song, C. Wu, J. Chang, Controllable delivery of hydrophilic and hydrophobic drugs from electrospun poly(lactic-co-glycolic acid)/mesoporous silica nanoparticles composite mats *J. biomed. Mater. Res. B appl. Biomater*. **100B** 2178-86 (2012)

[191] A. Dastbaz, A. R. Keshtkar, Adsorption of Th4+, U6+, Cd2+ and Ni2+ from aqueous solution by a novel modified polyacrylonitrile composite nanofibers adsorbent prepared by electrospinning *Appl. Surf. Sci.* **293** 336-44 (2014)

[192] Soltec Soluzioni Technologieche 2010 The principles of ultrasonic cleaning *www.soltec.it*

[193] C. Gregory, N. Liudmila, P. Sabine, How efficiently combine sonochemistry and clay science? *Applied clay science* **119** 191-201 (2016)

[194] Y. Wang, J. Wu, F. Wei, A treatment method to give separated multi-walled carbon nanotubes with high purity, high crystallization and a large aspect ratio *Carbon* **41** 2939-48 (2003)

[195] A. Montazeri, M. Chitasazzadeh, Effect of sonication parameters on the mechanical properties of multi walled carbon nanotubes/epoxy composites *Mater. Des.* **56** 500-8 (2014)

[196] J. Hilding, E. A. Grulke, Z. G. Zhang, F. Lockwood, Dispersion of carbon nanotubes in liquids *J. dispers. Sci. technol.* 1-41(2003)

[197] R. D. Brooker, M. J. Green, H. Fan, A. N. G. Parra-Vasquez, N. Behabtu, C. C.Young, R. H. Hauge, H. K. Schmidt, R. E. Smalley, W. F. Hwang, M. Pasquali, High shear treatment of single walled carbon nanotubes-suspension solution as a pre-processing technique for the assembly of fibers and films *Proc. Inst. Mech.eng. part N J. nanoeng. Nanosyst.* **222** 101-9 (2008)

[198] M. S. Trano, V. C. Moore, M. K. Miller, M. J. Allen, E. H. Haroz, C. Kittrell, R. H. Hauge, R. E. Smalley, The role of surfactant adsorption during ultrasonication in the dispersion of single walled carbon nanotubes *J. nanosci. Nanotechnol.* **3** 81-6 (2003)

[199] E. Youngho, S. Byoung, Solubility parameter-based analysis of polyacrylonitrile solutions in N, N-Dimethyl formamide and Dimethyl sulphoxide *Polymer* **03** 047 (2014)

[200] M.G. McKee, G.L. Wilkes, R.H. Colby, T.E. Long, Correlations of Solution Rheology with Electrospun Fiber Formation of Linear and Branched Polyesters, Macromolecules 37 1760–1767 (2004)

[201] M. Thommes, K. Kaneko, A. V. Neimark, J.P. Olivier, F. Rodriguez-Reinoso, J. Rouquerol, K.S.W. Sing, Physisorption of gases, with special reference to the evaluation of surface area and pore size distribution (IUPAC Technical Report), 2015

[202] H. X. Huang, J. J. Zhang, Effect of filler-filler and polymer-filler interactions on rheological and mechanical properties of HDPE-wood composites *J. Appl. Polym. Sci.* 2806-2812 (2009)

[203] R. Rošic, J. Pelipenko, P. Kocbek, S. Baumgartner, M. Bešter-Rogač, J. Kristl, The role of rheology of polymer solutions in predicting nanofiber formation by electrospinning, *Eur. Polym. J.* **48** 1374–1384 (2012)

[204] N. Grassie, R. McGuchan, Pyrolysis of polyacrylonitrile and related polymers—I. Thermal analysis of polyacrylonitrile, *Eur. Polym. J.* **6** 1277–1291 (1970)

[205] V.O. Goracheva, T.K. Mikhailova, S.G. Fedorkina, N.F. Konnova, M.T. Azarova, A.A. Konkin, Thermographic and thermogravimetric analysis of the thermal behaviour of polyacrylonitrile fibres, *Fiber Chem.* **1** 496–498 (1974)

[206] J. Thomas, A. Micheal, A. Charles, The thermal degradation of polyacrylonitrile *Polym. Degrad. Stab.***58** 193-202 (1997)

[207] Q. Ouyang, L. Cheng, H. Wang, K. Li, Mechanism and kinetics of the stabilization reactions of itaconic acid-modified polyacrylonitrile, *Polym. Degrad. Stab.* **93** 1415–1421(2008)

[208] Q. Gao, H. Zhu, W.-J. Luo, S. Wang, C.-G. Zhou, Preparation, characterization, and adsorption evaluation of chitosan-functionalized mesoporous composites, *Microporous Mesoporous Mater.* **193** 15–26 (2014)

[209] R. E.Farsani, S. Raissi, A. Shokuhfar, A. Sedghi, FT-IR study of stablized PAN fibers for fabrication of carbon fibers *Int. J. Mech. Mechatron. Eng.* **3(2)** 161-164 (2009)

[210] W.S. Khan, M. Ceylan, A. Jabarrania, L. Saeednia, R. Asmatulu, Chemical and thermal investigations of electrospun polyacrylonitrile nanofibers incorporated with various nanoscale inclusions *Int. J. Therm. Eng.* **3(4)** 1375-1390 (2017)

[211] H.F. Moafi, A.F. Shojaie, M.A. Zanjanchi, Photoactive polyacrylonitrile fibers coated by nano-sized titanium dioxide: synthesis, characterization, thermal investigation *J. Chil. Chem. Soc* **56(1)** 610-615 (2011)

[212] B. Shokri, M.A. Firouzjah, H. I. Hosseini, FTIR analysis of silicone dioxide thin film deposited by metal organic based PECVD *Materials* **12** 1-4 (2019)

[213] S. Benkhaya, S. M. Rabet, A. El-Harfi, A review on classifications, recent synthesis and applications of textile dyes *Inorg. Chem. Commun.* **115** 1-35 (2020)

[214] J. A. Kiernan, Classification and naming of dyes, stains and fluorochromes *Biotech. Histochem* **76(5-6)** 261–278 (2001)

[215] P. R. Ginimuge, S. D. Jyothi, Methylene Blue: Revisted *J Anaesthesiol Clin Pharmacol* **26(4)**:517-20 (2010)

[216] F.Azeez, E. A. Hetlani, M. Arafa, M. Madkour, The effect of surface charge on photocatalytic degradation of methylene blue dye using chargeabletitania nanoparticles *Scientific Report* **8** 1-9 (2018)

[217] D. Cho, S. Lee, M. W. Frey, Characterizing zeta potential of functional nanofibers in a microfluidic device *J. Colloid Interface Sci.***372** 252-260 (2012)

[218] N. Pourizza, T. Naghdi, Removal and separation of Neutral red from water samples by adsorption on acid-treated sawdust *Fresenius Environ. Bull.* **20** 3076-3080 (2011)

[219] P.Luo, Y. Zhao, B. Zhang, J. Liu, Y. Yang, J. Liu, Study on the adsorption of Neutral red from aqueous solution onto halloysite nanotubes *Water Res.* **44** 1489-1497 (2010)

[220] S. Coruh, F. Geyikci, S. Elevli, Adsorption of Neutral red dyefrom an aqueous solution onto natural sepiolite using full factorial design *Clays Clay Miner.* **59(6)** 617-625 (2011)

[221] F.P. de Freitas, L. Carvalho, A. Carneiro, M. Magalhaes, M. Xisto, W. Canal, Adsorption

of Neutral red dye by chitosan and activated carbon composite films *Heliyon* **7** e07629 (2021)

[223] O. V. Ovchinnikov, A. V. Evtukhova, T. S. Kondratenko, M. S. Smirnov, V. Y. Khokhlov, O. V. Erina, Manifestation of intermolecular interactions in FTIR spectra of methylene blue molecules, *Vib. Spectrosc.* **86** 181-189 (2016)

[224] J.Si, X. C. Li, B. K. Cui, Decolorization of heterocycle dye Neutral red by white-rot fungus perenniporia subacida, *Desalination Water Treat.***52** 5594-5604 (2014)

[225] S. Chakraborty, B. Basak, S. Dutta, B. Bhunia, A. Dey, Decolorization and biodegradation of Congo red dye by anovel white rot fungus alternaria alternata CMERI F6 *Bioresour. Technol.***147** 662-666 (2013)

[226] A. Bartosova, L. Blinova, M. Sirotiak, A. Michalikova, Usage of FTIR-ATR as Non-Destructive analysis of selected toxic dyes *Sciendo* **25(40)** 103-111 (2017)

[227] R.Rehman, A. Abbas, S. Murtaza, T. Mahmud, W. Zaman, M. Salman, U. Shafique, Comparitive removal of congo red dyefrom water by adsorption on Grewia asiatica leaves, Raphanus sativus peels and activated charcoal *J. Chem.Soc.Pak* **34(1)** 112-119 (2012)

[228] D. A. Yaseen, M. Scholz, Textile dye wastewater characterstics and constituents of synthetic effuelents: a critical review, *International Journal of Environmental Science and Technology* (2019) 16: 1193-1226